

This work is protected by copyright and other intellectual property rights and duplication or sale of all or part is not permitted, except that material may be duplicated by you for research, private study, criticism/review or educational purposes. Electronic or print copies are for your own personal, non-commercial use and shall not be passed to any other individual. No quotation may be published without proper acknowledgement. For any other use, or to quote extensively from the work, permission must be obtained from the copyright holder/s.

The relative dominance of allo-controls and local-scale
sedimentary processes upon preserved successions of
aeolian-marine margins

Sarah Louise Cross

Master of Philosophy

October 2022

Keele University

Abstract

The sedimentology, controls and efficiency of central erg environments are well-constrained, however marginal relationships are less understood and often under-represented. The Moab Member of the Curtis Formation is a well-exposed, laterally continuous example of the preserved sediments of an aeolian erg system deposited along a marine margin. It comprises the Upper Jurassic deposits found on the Colorado Plateau, a 380,000km² area in the Four Corners region of the Western United States. The Moab Member provides an excellent opportunity to study the controls upon aeolian dune fields with increasing proximity to the coastal marine margin. Lateral relationships within the Curtis Formation preserve spatial interactions between systems, temporal interactions are represented by the vertical transition from the Moab Member into the overlying Summerville Formation. This work provides an understanding and analysis of both the sequence-stratigraphical scale and the element scale interactions between dune and contemporaneous sedimentary deposition.

Results from fieldwork carried out in the Canyonlands Section of the Colorado Plateau provided extensive data in the form of sedimentary logs, Spectral Gamma Ray (SGR) data and drone photogrammetry. The collation of these individual data sets enabled a basin wide analysis and the construction of sedimentary models providing a context for the deposition of the Moab Member and its contemporaneous environments.

The results identify a significant change in the sedimentology and geometry of the erg system towards the marine margin. Establishing the morphologies of this system and its interactions with the surrounding environments enabled the identification of 'pulses' linked to small scale sea-level fluctuations. When

considered within the wider framework of basin sea-level fluctuations identified from shallow marine deposits, which preserved allocyclic signals, these smaller scale events provide a more in-depth characterisation of sequence stratigraphy in the area and hence document the behaviour of the aeolian-marine margin through a transgressive-regressive cycle.

Acknowledgements

I would firstly like to thank my supervisor Dr Stuart Clarke for his invaluable help, and patience in the face of zoom calls, emails and ‘the new normal’. I would also like to thank my colleague Dr Ross Pettigrew for his assistance in the field and unwavering support throughout the writing process as well. Furthermore, I would like to extend my thanks to Dr Valentin Zuchuat for his proof-reading and expertise. Finally, many thanks to my family and to Reece, who stayed with me 24:7 (by government mandate) and kept me going every step of the way.

Contents

Chapter 1: Introduction.....	1
1.1.1 Aims & Objectives	3
1.1.2 Fieldwork Location	5
1.2 Geological Setting	7
1.2.1 Geological Development of the North American Cordillera	7
1.2.2 Palaeozoic Tectonics	9
1.2.3 Mesozoic Tectonics.....	11
1.2.4 Post-Laramide Tectonics	15
1.3 Evolution of the Colorado Plateau and the Paradox Basin	17

1.3.1 Stratigraphy of the Paradox Basin	19
1.4 Evolution of the Curtis Basin	21
1.4.1 Stratigraphy of the Curtis Basin	23
1.4.2 The Glen Canyon Group.....	24
1.4.3 The San Rafael Group.....	25
1.4.4 Morrison Formation.....	31
1.5 Summary.....	33
Chapter 2: Processes, Landforms and Environments.....	35
2.1 Aeolian Systems.....	35
2.1.1 Creation of the Aeolian System	36
2.1.2 Accumulation within the Aeolian System	41
2.1.3 Preservation of the Aeolian System.....	49
2.1.4 The Role of Climate & Controlling Factors.....	57
2.2 Coastal Plain Environments	60
2.2.1 Sabkha	61
2.3 Tide Dominated Marine Margins	66
2.3.1 Subtidal Flat.....	67
2.3.2 Intertidal Flat.....	67
2.3.3 Supratidal Flat.....	67
2.4 Coastal Plain Deposits	68
2.5 Summary.....	71
Chapter 3: Lithofacies of the Entrada/Curtis/Summerville Formations.....	73

3.1 Wind-Blown Facies	77
3.1.1 Planar Cross-Stratified Sandstone- Sxs.....	77
3.1.2 Trough Cross-Stratified Sandstone- Stxs.....	79
3.1.3 Planar Bedded Sandstone- Sfpd.....	81
3.2 Poned Water Facies	82
3.2.1 Undulose Sandstone-Sdun	82
3.2.2 Undulose Sandstone with Ripple Laminations-Surpl	83
3.2.3 Structureless Sandstone- Scs.....	85
3.2.4 Parallel Laminated Siltstone- Sspl	86
3.2.5 Parallel Laminated Siltstone with evaporites- Ssepl.....	87
3.3 Palaeosol Facies	88
3.3.1 Ferrallitic Gleysol- Fegl	88
3.3.2 Parallel Laminated Oxisol- Oxpl.....	90
3.3.3 Saline Soil with Sulphate Reduction- Sasr	91
3.4 Shallow Water Facies	92
3.4.1 Parallel Laminated Inverse Graded Siltstone- Ssgpl.....	92
3.4.2 Parallel Laminated Sandstone- Spl.....	94
3.4.3 Ripple Laminated Sandstone- Srpl	95
3.4.4 Wavy Bedded Sandstone- Swb	96
3.4.5 Flaser Bedded Sandstone- Sfb	96
3.4.6 Herringbone Cross-stratified Sandstone- Sxhc	96
3.5 Facies Associations of the Entrada/Curtis/Summerville Formations.....	97

3.5.1 Sinuous-crested Aeolian Dune Association- SinD	98
3.5.2 Straight-crested Aeolian Dune Association- StrD	99
3.5.3 Sand sheet Association- SanS	101
3.5.4 Damp Interdune Association-DInD	102
3.5.5 Wet Interdune Association-WInD.....	103
3.5.6 Supratidal Flat- SupTF.....	103
3.5.7 Intertidal Mud Flat- IMF.....	105
3.5.8 Intertidal Mixed Flat- IMSF.....	105
3.5.9 Intertidal Sand Flat- ISF.....	106
3.5.10 Subtidal Flat- SBF.....	107
3.6 Assemblages of the Entrada/ Curtis/ Summerville Formations	110
3.6.1 Wet Aeolian Dune Field- CWDF	110
3.6.2 Coastal Dry Aeolian Dune Field- CDDF.....	113
3.6.3 Coastal Plain- COPL.....	116
3.6.4 Tide Dominated Marine Margin (TDMM)	118
3.7 Summary.....	120
Chapter 4: Quantifying Dune Geometry on an Aeolian-Marine Margin.....	121
4.1 Background.....	122
4.1.1 Principles of UAV Photogrammetry	122
4.1.2 Use of UAV Photogrammetry within Preserved Aeolian Successions	127
4.2 Methods	129
4.3 Results	132

4.3.1 Locality 1- Bartlett Wash	132
4.3.2 Locality 2a- Lone Mesa	141
4.3.3 Locality 2b- Dubinky Well.....	150
4.3.4 Locality 3- Duma Point Transition	157
4.4 Summary	165
Chapter 5: Spectral Gamma-Ray Characterisation of an Aeolian-Marine Margin	167
5.1 Background	167
5.1.1 Principles of Spectral Gamma Ray	168
5.1.2 Facies Cross-plot Analysis.....	171
5.1.3 Log Motifs & Trends.....	174
5.1.4 Application of SGR in Geological Interpretations	175
5.2 Methods.....	178
5.2.1 Spectral Gamma Ray Field Techniques.....	178
5.2.2 Cross-plots and Statistical Analysis	179
5.2.3 Spectral Gamma-ray Logs	179
5.3 Identification of Facies from K:Th Cross-Plots.....	180
5.3.1 Results	185
5.3.2 Interpretation.....	195
5.3.3 Discussion.....	201
5.4 Peak Correlation.....	203
5.4.1 Results	203

5.4.2 Interpretation.....	212
5.4.3 Discussion	212
5.5 Log Motifs.....	216
5.5.1 Results.....	216
5.5.2 Interpretation.....	217
5.5.3 Discussion	219
5.6 Summary.....	222
Chapter 6: Application of Spectral Gamma-Ray upon Aeolian-Marine Margins..	224
6.1 Interpretation	225
6.1.1 Reconstructing the Aeolian-Marine Margin.....	225
6.1.2 Spatial and Temporal Evolution of the Dune Field.....	228
6.1.3 Cyclicity of the Curtis Formation	231
6.2 Discussion	234
6.3 Summary.....	235
Chapter 7: Discussion of Allocyclic and Local-scale Sedimentary Processes upon an Aeolian-Marine Margin.....	236
7.1 Allocyclic vs Autocyclic Processes	236
7.2 Characterising the Aeolian-Marine Margin	238
7.3 Sequence Stratigraphy and Global Context	240
Chapter 8: Conclusions and Further Work.....	242
8.1 Research Aims.....	242
8.1.1 Establish local-scale interactions of contemporaneous aeolian and marine margins.....	242

8.1.2 Identify significant bounding surfaces traceable within proximal deposits and their distal counterparts.....	243
8.1.3 Reconstruct an aeolian-marine margin and identify sea-level fluctuations upon it.	243
8.2 Summary of Findings.....	244
8.3 Future Work.....	245
8.3.1 Provenance of the Moab Member- Reworked Entrada dunes?	245
8.3.2 Supersurfaces and Sequence Stratigraphy.....	246
8.3.3 A Closer Look at the Summerville Formation.....	247
Chapter 9: References	249

List of Figures and Tables

Figure 1.1.1- Tectonic features surrounding the Colorado Plateau in the Four Corners region of the USA.

Figure 1.1.2- Locality map of the six main sites visited by this study. The most easterly locality is Bartlett Wash, the most westerly is the San Rafael Swell. Figure 1.1.3- Satellite image of the four corners region of the USA with a map showing the same location within the wider United States.

Figure 1.1.4- Localities of the drone surveys at localities 2-4. Locality 1- Bartlett Wash was excluded due to proximity to the Canyonlands airport (shown). 5

Figure 1.2- From right to left: Stratigraphic column drawn from the initial work on the Curtis Basin

sediments by Gilluly and Reeside (1928) This work placed the Carmel, Entrada, Curtis, and Summerville formations correctly within the Upper Jurassic but extended the Morrison well into the Cretaceous. Further work from the 1950s identified the end of the Morrison as the boundary between Jurassic and Cretaceous deposits. The modern stratigraphic column (modified from Zuchuat *et al.*, 2019) shows the complex relationships between the Entrada, Curtis, and Summerville formations from Central Utah to Northern New Mexico. 6

- Figure 1.3- The evolution of the Colorado Plateau throughout geological history starting with the Proterozoic and continuing to the modern-day. Although the environments are transitional the representation for the end of each of the periods have been selected here to provide a summary that best fits the environment of deposition for each period (After Blakey & Ranney, 2008). 8**
- Figure 1.4.1- The Grenville orogenic cycle. Precambrian tectonic activity leading to the deposition, tilting and erosion of the Grand Canyon Supergroup, resulting in its modern-day preservation and distribution across within the Colorado Plateau (After Spencer *et al.*, 2015). Figure 1.4.2- Palaeogeographic reconstruction of continental landmasses at the end of the Grenville orogenic cycle (~900 Ma) 9**
- Figure 1.5.1- Evolution of the passive margin setting defining the tectonic activity for the Cambrian Period to Mississippian Epoch (After Blakey & Ranney 2008). Figure 1.5.2- Position of the continental landmasses in the early Cambrian when rifting and high sea-levels allowed for extensive continental shelf environments. 10**
- Figure 1.6.1- Subduction cycle in the Western United States, continental collision, thrusting, uplift and sediment infill of basins leading to the shallow marine grading into continental deposits of the Paradox Formation (After Dickinson, 2004). Figure 1.6.2- Position of the continental landmasses within the super-continent Pangaea at the start of the Devonian. 12**
- Figure 1.7.1- Tectonic evolution of the North American Cordillera from the formation of the Cretaceous Sevier Belt to the modern-day Rocky Mountains and the San Andreas Fault (After Ducker *et al.*, 2001). Figure 1.7.2- Position of the continental landmasses during the Cretaceous Period. 16**
- Figure 1.8- A summary of the major geological events and environments on the Colorado Plateau on a geological time scale. White represents periods of erosion, displayed in the rock record by major unconformities. Yellow displays mainly continental deposition and blue mainly marine deposition. Not all events are shown. The periods are in accordance with the most recent figure released by the International Commission on Stratigraphy (v 2020/03). (After Blakey & Ranney, 2008). 17**
- Figure 1.9.1- Key geographical features within the Paradox basin during the deposition of the Paradox formation in the Permian Period. The main uplift features are shown in addition to the position of the modern-day Colorado Plateau. Figure 1.9.2- Key geographical features of the Hoskinnini basin that formed at the start of the Triassic Period, replacing the deposition environment of the Paradox**

basin. This basin was home to the extensive floodplains and fluvial systems of the Moenkopi and Chinle formations (Modified after Fillmore, 2010).	19
Figure 1.10- Cross-section of the Paradox basin from Southwest to Northeast across the Utah-Colorado border. The diagram shows the transition from the basement rock of the Uncompaghre highlands into the alluvial fans and then into the characteristic evaporites and carbonates of the Paradox Formation (Modified after Fillmore, 2010).	21
Figure 1.11.1- Key features of the Colorado Plateau affecting deposition in the Middle Jurassic. Including, the Uncompaghre highlands and the Nevadan Orogenic Belt, the main sources of sediment supply and the Utah-Idaho Trough that formed in response to lithosphere loading of the nearby mountain belt. Figure 1.11.2- The first incursion of a Jurassic Sea resulted in the deposition of the Carmel Formation with the Page Sandstone deposited as along its south-eastern margin. Figure 1.11.3- The southward transgression of the Sundance Sea created the aeolian-marine margin of the Curtis-Entrada deposits. Figure 1.11.4- As the Curtis Sea regressed another aeolian-marine margin forms from the Middle Curtis-Moab Member, surrounded by the coastal plain of the Summerville Formation.	22
Figure 1.12- Summary of the stratigraphic units of the San Rafael Group, including the Entrada, Curtis and Summerville Formations as investigated by this study.	33
Figure 2.1- Modes of grain transport occurring in terrestrial aeolian systems, suspension particles are most affected by a threshold capacity and velocity of the transporting winds. Grains that are too large for entrainment are therefore transported via saltation or reptation.	37
Figure 2.2- Changes in available sediment through time expressed in terms of different sedimentary environments (After Jagger, 2003).	39
Figure 2.3-Comparison between the accommodation space in marine systems versus aeolian systems. This is important for the principles of sequence stratigraphy as discussed above (After Jagger, 2003).	40
Figure 2.4- The role of subsidence in the deposition and preservation of aeolian sediments up succession. Note the relationship between water table and aeolian sediment budget, peak sediment availability occurs when the water table is at its lowest, as described above in dry aeolian vs. wet aeolian systems (After Mountney & Thompson, 2002).	41

Figure 2.5- Scatter plot of grain-size against wavelength for aeolian bedforms. There are no transitional forms between the three groups A, B, C, which correspond to ripples, dunes and draa (After Wilson, 1972).	42
Figure 2.6- Cross-section of an aeolian dune form (After McDonald and Anderson, 1996).	44
Figure 2.7- The most comprehensive classification of dune-forms currently within the literature, with illustrations demonstrating the various morphologies and their dominant wind-directions (After Cousins 2020, Fryberger et al., 1966).	46
Figure 2.8- Illustration of the types of stratification visible at ripple scale within an aeolian succession (After Hunter 1977).	50
Figure 2.9- Types of stratification as 3-D models and as horizontal and vertical cross-sections (After Rubin & Carter, 1987).	51
Figure 2.10- Interactions between dunes and interdunes at the surfaces and the geometries preserved in the subsurface (After Pettigrew 2019, Jagger 2014).	53
Figure 2.11- Stages of super-surface development within a preserved aeolian succession (After Wakefield 2010, Loope 1985).	55
Figure 2.12- Plant or tree root preserved within the Moab Member of the Curtis Formation, the white ring is sediment that has been bleached by organic acid circulating between the root and the sediment itself, the root itself is not preserved and is instead represented by the smaller dark circle in the center.	56
Figure 2.13- Interactions of climate and subsidence in sediment supply and preserved deposits within the principal depositional environments. Supersurfaces created by changes in accumulation can be regarded as sequences and linked to drying upwards cycles as shown (After Howell & Mountney, 1997).	59
Figure 2.14- Varying environments in which continental sabkhas can be found, transitioning from alluvial fans to saltpans (After Warren, 2016).	62
Figure 2.15- Theoretical environments in which sabkha can develop (above), and the relationships between these environments in a typical transitional setting (below) (After Handford 1981, Warren 1989).	65
Figure 2.16- Environments of deposition within a tidal flat system, including the subtidal, intertidal, and supratidal zones within a tide-dominated shallow marine setting (From Desjardins <i>et al.</i> , 2012).	66

- Figure 2.17- Idealised facies for a tidal flat succession (After Desjardins *et al.*, 2012) 67
- Figure 2.18- Classification of palaeosols based on their most prominent feature arranged into a flow chart that allows identification on an 'if not that, then this' basis (After Mack *et al.*, 1993). 68
- Figure 2.19- Most common subordinate modifiers for palaeosols, these can be used before the classification to describe one or more features that are not the most prominent within the palaeosol itself. 69
- Figure 3.1.1- Locality map of the study area within South-eastern Utah, showing the positions of each of the localities at which sedimentary logs were taken. Figure 3.1.2-The relative position of the study area within the four corners region of the United States of America. 74
- Figure 3.2.1- Planar cross-stratification within units 1 & 2 of the facies Sxs, separated by an index surface. Figure 3.2.2- Planar cross stratification within dune package 3 of the facies Sxs. Figure 3.2.3- Outcrop view of units 1 & 2 within facies Sxs at the Lone Mesa Locality. Figure 3.2.4- Outcrop view of units 1 & 2 within facies Sxs at the Bartlett Wash locality. Figure 3.2.5- Rhizolith within Facies Sxs at the Lone Mesa Locality. Figure 3.2.6- Weathered Rhizolith within facies Sxs at the Bartlett Wash Locality. Figure 3.2.7- Planar cross-bedding and differential bleaching within unit 3 at Lone Mesa. Figure 3.2.8- Rhizoliths along foresets of facies Sxs at the Lone Mesa Locality. 78
- Figure 3.3.1- Prominent grainfall/ grainflow strata forming cross-bedding within the dune form of Stxs. The tops are truncated, whilst the base remains asymptotic. HB pencil for scale. Figure 3.3.2- Trough cross-stratification within a 2m thick unit of Stxs. Figure 3.3.3- Sample of the sedimentary log taken at Bartlett Wash showing occurrence of the Stxs facies. Figure 3.3.4- Relative thickness of the units within the Stxs facies interbedded with those of Sdun. 80
- Figure 3.4.1- Sample of the sedimentary log taken at the Lone Mesa Locality, showing the facies Sfpd and the overlying units. Figure 3.4.2- Outcrop view of the Sfpd facies at the Lone Mesa Locality. 81
- Figure 3.5.1-Outcrop scale view of a unit of Sdun as it is most commonly found, between units of Stxs at the Lone Mesa locality Figure 3.5.2- Units of Sdun interbedded with units of Stxs at Bartlett Wash (Locality 1) Figure 3.5.3- Outcrop scale view of figure 3.5.2, note that the interbedded units of Sdun become thinner and more frequent upwards. 83
- Figure 3.6.1- Mud drapes within facies Surpl at the San Rafael Swell (Locality 5), they occur sporadically and are usually isolated Figure 3.6.2-An additional example of the mud drapes within Sumd at Duma Point Transition 3 (Locality 3). Figure 3.6.3- Symmetrical round-crested ripples within facies

Surpl at the Duma Point Transition 1 locality. Figure 3.6.4- Undulose bedding and symmetrical ripples within Surpl at Duma Point Transition1.	84
Figure 3.7.1- Unit of facies Scs approximately 60cm in height, with the first 40cm appearing structureless.	
Figure 3.7.2- ‘zoomed out’ view of the Scs unit, the base may also contain some load casts at Duma Point Transition 1 (Locality 4).	85
Figure 3.8.1- Parallel laminations within the Sspl facies as found at all localities overlying the planar cross-bedded sandstones (Sxs). Figure 3.8.2- Representation of the poorly consolidated nature of Sspl leading to large mound-like structures.	86
Figure 3.9.1-Parallel Laminated siltstone beds interlaced with satin spar gypsum at the San Rafael Swell	
Figure 3.9.2- Isolated nodule of gypsum occurring within beds of Sspl at the San Rafael Swell (Locality 5).	87
Figure 3.10.1- The informally named ‘popcorn facies’ characterised by red-brown mottles within a pale cream matrix, typical of a ferrallitic gleysol. Figure 3.10.2-oxidation of iron minerals during palaeosol formation leads to concretions of the minerals gathering in lower units.	89
Figure 3.11.1-The most distal expression of the facies Oexpl at Duma Point Transition 1 (Locality 4), the purple colour is characteristic of the oxidized iron minerals Figure 3.11.2- Characteristic yellow, green, and purple striping that defines a parallel laminated oxisol at Lone Mesa (Locality 2) Figure 3.11.3- The most proximal expression of Oexpl, featuring the purple, green and yellow banding at Bartlett Wash (Locality 1).	90
Figure 3.12.1-Yellow staining within unit’s underneath Sasr, including the thin yellow bed and gley horizon that I visible above. Figure 3.12.2- Strong yellow bed rich in sulphate minerals, overlain by a blue grey gley horizon at Lone Mesa (Locality 2) Figure 3.12.3- Close-up of the yellow staining caused by sulphate leaching, unique to Lone Mesa.	91
Figure 3.13.1-Cliff face formed of facies Ssgpl that has been weathered to appear columnar, note the characteristic grey colour of the unit when compared with the overlying coarser grained pink unit Spl. Figure 3.13.2-Closer view of the Ssgpl facies, beds can appear discontinuous, but this is likely to be a weathering feature than a depositional one. Figure 3.13.3- Outcrop scale view of Ssgpl and its overlying facies at the San Rafael Swell (Locality 5).	93

- Figure 3.14.1- Characteristically pink unit of Spl that directly overlies the Ssgpl facies at the San Rafael Swell locality. Figure 3.14.2- Closer view of the Spl facies, parallel laminated sandstones are an unusual facies and appear only at this locality. 94**
- Figure 3.15.1-Bed of facies Srpl, featuring cross-laminated peak-crested ripples. Although this bed is only ~30cm thick, it can occur frequently in a succession, often interbedded with Mpl. Figure 3.15.2- Edited image of figure 3.15.1 highlighting the ripple crests and internal structure of the ripples. 95**
- Figure 3.16.1-Bed ~30cm thick demonstrating textbook herringbone cross-stratification features bi-directional foresets with mud drapes separating them. The mud drapes have since been eroded away leaving the oval shaped depressions. Figure 3.16.2- Edited image of figure 3.16.1 highlighting the internal structure of the unit and the clear herringbone features. 97**
- Figure 3.17.1- Field photo of the WDA, showing facies Stxs and Sdun. Figure 3.18.2- Aerial field photo showing the interbedding of Stxs and Sdun. Figure 3.18.3- Field photo taken at Bartlett Fault of the Bartlett Wash (Jedi-3D) outcrop. Figure 3.18.4- Numbered environments on the sedimentary log as identified within Figures 3.18.1, 3.18.2 & 3.18.3 1) Compound Aeolian Dune Association, 2) Damp Interdune Association, 3) Wet Interdune Association. The sedimentary log has been colour coded by facies, facies association and assemblage, with the red vertical bar representing the whole wet interdune assemblage. Figure 3.18.5- 3D depositional model showing the interaction between facies and associations within a wet aeolian dune system. 112**
- Figure 3.18.1- Field photo of the CDA at Dubinky Well showing the dry aeolian system overlying the wet aeolian system. Figure 3.19.2 Field photo of the CDA taken at Bartlett Fault. Figure 3.19.3- Field photo of the low-angle bedding within Sxs at Bartlett Fault. Figure 3.19.4 Sedimentary log with numbered environments showing the relationships between different cosets and associations within the assemblage. 1) Coset 1, 2) Coset 2, 3) Coset 3, 4) Cosets 4 & 5 5) Palaeosol & Coastal Plain. The sedimentary log has been colour coded by facies, facies association and assemblage, with the red vertical bar representing the wet interdune assemblage and the yellow bar representing the coastal dry aeolian assemblage. Figure 3.19.5- Depositional environment of CDA showing the interactions between the facies and associations described above, supported by field photos of the preserved succession. 115**
- Figure 3.19.1- Field photo of the COPL assemblage overlying the coastal dry aeolian dune system at Bartlett Wash (Jedi 3D). Figure 3.20.2- Field photo of the COPL overlying the TISF assemblage at the**

San Rafael Swell. Figure 3.20.3- Field photo showing the gypsum morphologies visible within Ssepl/COPL at the San Rafael Swell. Figure 3.20.4- Sedimentary log with numbered environments showing the relationships between different associations within the assemblage. 1) Underlying aeolian dunes 2) parallel laminated silts of the coastal plain, 3) marginal marine sabkha. The sedimentary log has been colour coded by facies, facies association and assemblage, with the purple vertical bar representing the coastal plain assemblage. Figure 3.20.5- Depositional environment for the coastal plain assemblage showing the interaction between facies and environments described above, supported by field photos and sedimentary logs of the preserved succession. 117

Figure 3.20.1- Field photo of the whole tidally influenced shoreface succession at the San Rafael Swell from the sub-tidal mud flat through to the intertidal mud flat. Figure 3.21.2- Field photo of the intertidal sand flat deposits overlying the subtidal mud flat deposits within the TISF, note the unique columnar weathering pattern. Figure 3.21.3- Sedimentary log with numbered environments showing the relationships between different associations within the assemblage. 1) Subtidal Mud Flat 1, 2) Subtidal Mud Flat transition 3) Intertidal Sand Flat, 4) Intertidal Mixed Flat. Sedimentary log has been colour coded by facies, facies association and assemblage, with the dark blue vertical bar representing the tidally influenced shoreface assemblage. Figure 3.21.4- Depositional environment model for the tidally influenced shoreface assemblage showing the interactions between facies and associations described above, supported by field photos and sedimentary logs of the preserved succession. 119

Figure 4.1- Graphic demonstrating the three stabilisation directions of UAV's that must be considered when flying and capturing footage. 124

Figure 4.2- Overlapping field of view for a camera attached to a UAV, increasing darkness representing an increase in the number of cameras viewing that point. 124

Figure 4.3-Panel showing the positions of photos taken by the UAV at the Duma Point locality, compared to the outcrop, note the distinct horizontal lines parallel to the outcrop at almost identical angles, to minimise the potential for error when composing the photogrammetric models. 125

Figure 4.4-Workflow for producing a photo-realistic 3D model from UAV aerial photographs, using Agisoft Photoscan software 127

Figure 4.5.1- Location map showing the relative position of Utah within the United States of America.

Figure 4.5.2- Position of the study area within the state of Utah. Figure 4.5.3- Lateral extent of

Bartlett Wash (Jedi 3D) with lithostratigraphic labels. Figure 4.5.4- Position of the Bartlett Wash locality relative to neighboring landmarks such as Moab Airport. Figure 4.5.5- Google earth screenshot demonstrating the parallax errors from satellite surveys. Figure 4.5.6- True appearance of the Bartlett Wash (Jedi 3D) outcrop taken at Bartlett Fault in the field. 133

Figure 4.6- Relationship between maximum grainflow thickness and potential slip-face height of preserved dunes. Black dots are those obtained from field studies by Kocurek & Dott (1983), the lines represent average measurements taken from dunes in the field work for this study. 136

Figure 4.7.1- Field photo of the Bartlett Fault locality taken from Bartlett Wash (Jedi 3D) including the 4 index surfaces terminating upon the Moab Fault. Figure 4.7.2- Field photo of Bartlett Fault with a section highlighted to emphasise bounding surface relationships. Figure 4.7.3- Outcrop photo of Bartlett Wash (Jedi 3D) with the genetic packages highlighted by colour moving up the succession. 137

Figure 4.8.1- Field photograph of the aeolian succession at Bartlett Fault with the key index surfaces and genetic packages highlighted. Figure 4.8.2- Field photograph of the aeolian succession at Bartlett Wash (Jedi 3D) with the same correlatable index surfaces and genetic packages highlighted. Figure 4.8.3- Photograph of an outcrop at the Bartlett Fault locality, a section has been highlighted and the bounding surface relationships shown. Figure 4.8.4- Snapshot of genetic package 3 with bounding surfaces shown. Figure 4.8.5- Snapshot of a set genetic package 3 with foreset relationships shown. Figure 4.8.6- Field photograph of genetic package 1 at Bartlett Fault Figure 4.8.7- Sedimentary log taken at Bartlett Fault showing the identified index surfaces and genetic packages. 138

Figure 4.9.1- The position of Utah within the United States of America. Figure 4.9.2- Location of the study area within the state of Utah. Figure 4.9.3- Google Earth photo of the outcrop showing lithostratigraphic unit names, scale references foreground measurement. Figure 4.9.4- Position of the outcrop relative to the nearest landmark, State Route 313. Figure 4.9.5- Field photograph of the outcrop, red dot marks the reference point common to all photographs as above. Figure 4.9.6- Field photograph of the planar cross-bedded aeolian succession at the Lone Mesa locality. 142

Figure 4.10.1- Snapshot from VRGS showing GP3 to scale with a representative foreset thickness measurement. Figure 4.10.2- Snapshot from VRGS showing GP4 to scale with a representative foreset thickness measurement. Figure 4.10.3- Panel diagram showing the dune measurements for each unit from the drone photogrammetric model. Each arrow shows one representative grainflow

thickness from each unit, which can then be compared with the virtual scale to give an estimation for grainflow thicknesses. Figure 4.10.4-Snapshot from VRGS showing GP1 to scale with a representative foreset thickness measurement. Figure 10.4.5-Snapshot from VRGS showing GP2 to scale with a representative foreset thickness measurement. 145

Figure 4.11.1- Interpretation of the Lone Mesa outcrop, processed within VRGS, showing the key index surfaces that divide the outcrop into genetic packages. Figure 4.11.2- Virtual outcrop model of the Lone Mesa outcrop with a section highlighted to further demonstrate the relationships between index surfaces. In addition, areas of differential bleaching have been highlighted. Figure 4.11.3- Complete outcrop view of Lone Mesa, taken from VRGS with the genetic packages shown, WIA refers to the underlying wet interdune deposits, whilst COPL refers to the overlying coastal plain. 147

Figure 4.12- Graph representing the linear relationship between maximum grainflow thickness and potential slip-face height of preserved dunes. Black dots are those obtained from field studies by Kocurek & Dott (1983), the lines represent average measurements taken from dunes in the field work for this study. 148

Figure 4.13.1-The position of Utah within the United States of America. Figure 4.13.2- Location of the study area within the state of Utah. Figure 4.13.3- Google Earth photo of the outcrop showing lithostratigraphic unit names, scale references foreground measurement. Figure 4.13.4- Position of the outcrop relative to the nearest landmark, the Secret Spire Safari Rte. Figure 4.13.5- Field photograph of the outcrop with lithostratigraphic units, red dot marks the reference point common to all photographs as above. Figure 4.13.6- Field photograph of the planar cross-bedded aeolian succession at Dubinky Well. 151

Figure 4.14- Graph representing the linear relationship between maximum grainflow thickness and potential slip-face height of preserved dunes. Black dots are those obtained from field studies by Kocurek & Dott (1983), the lines represent average measurements taken from dunes in the field work for this study. 153

Figure 4.15.1- Snapshot from VRGS showing GP3 to scale with a representative foreset thickness measurement. Figure 4.15.2- Snapshot from VRGS showing the overlying coastal plain with a representative foreset thickness measurement. Figure 4.15.3- Panel diagram showing the dune measurements for each unit from the drone photogrammetric model. Each arrow shows one

representative grainflow thickness from each unit, which can then be compared with the virtual scale to give an estimation for grainflow thicknesses. Figure 4.15.4-Snapshot from VRGS showing GP1 to scale with a representative foreset thickness measurement. Figure 4.15.5-Snapshot from VRGS showing GP2 to scale with a representative foreset thickness measurement. 154

Figure 4.16.1-Interpretation of the Dubinky Well outcrop, processed within VRGS, showing the key index surfaces that divide the outcrop into genetic packages. Figure 4.16.2- Virtual outcrop model of the Dubinky Well outcrop with a section highlighted to further demonstrate the relationships between index surfaces. In addition, areas of differential bleaching have been highlighted. Figure 4.16.3- Complete outcrop view of Dubinky Well, taken from VRGS with the genetic packages shown, WIA refers to the underlying wet interdune deposits, whilst COPL refers to the overlying coastal plain. 155

Figure 4.17.1-The position of Utah within the United States of America. Figure 4.17.2- Location of the study area within the state of Utah. Figure 4.17.3- Google Earth photo of the outcrop showing lithostratigraphic unit names, scale references foreground measurement. Figure 4.17.4- Position of the outcrop relative to the nearest landmark, the Crystal Geyser Safari Route. Figure 4.17.5- Field photograph of the outcrop including lithostratigraphic units, red dot marks the reference point common to all photographs as above. 158

Figure 4.18- Graph representing the linear relationship between maximum grainflow thickness and potential slip-face height of preserved dunes. Black dots are those obtained from field studies by Kocurek & Dott (1983), the lines represent average measurements taken from dunes in the field work for this study. 161

Figure 4.19.1-Interpretation of the Duma Point Transition 3 outcrop, processed within VRGS, showing the key index surfaces that divide the outcrop into genetic packages. Figure 4.19.2- Virtual outcrop model of the Duma Point outcrop with a section highlighted to demonstrate the relationships between index surfaces further. The diagonal features shown are likely to be post-depositional fracturing of the sandstone. Figure 4.19.3- Complete outcrop view of Duma Point, taken from VRGS with the genetic packages shown. WIA refers to the underlying wet interdune deposits, whilst COPL refers to the overlying coastal plain. 162

Figure 4.20.1-Field photo of the coastal plain deposits at Duma Point Transition 3. Figure 4.20.2- Field photo of burrowing within the coastal plain deposits at Duma Point Transition 3. Figure 4.20.3-

Panel diagram showing the dune measurements for each unit from the drone photogrammetric model. Each arrow shows one representative grainflow thickness from each unit, which can then be compared with the virtual scale to give an estimation for grainflow thicknesses. Figure 4.20.4-Snapshot from VRGS showing TS1 and GP1 to scale with a representative foreset thickness measurement. Figure 4.20.5-Snapshot from VRGS showing GP1 to scale with a representative foreset thickness measurement. 163

Figure 5.1- Gamma Ray spectra of the most prominent naturally occurring radioisotopes, potassium-40, thorium-232 and Uranium-238. Spectral Gamma Ray detectors use these peaks as their controls values with which to distinguish and present levels of the elements within the rock (After Cripps & McCann, 2000). 169

Figure 5.2-The effects of spectrometer positioning on outcrop SGR measurements. Blue represents the expected measuring volume of the tool which is reduced for a convex profile (A), increased for concave (B), diluted for thin bed readings (C) or concentrated when placed on the bedding plane (D) (After, Svendsen & Hartley, 2001). 170

Figure 5.3- Positions of the spectrometer were chosen based on the most effective angle for measurement as outlined by Svendsen & Hartley, 2001. 170

Figure 5.4-Log motifs identifiable within spectral gamma-ray logs of preserved successions. Bell-shaped motifs imply retrograding sets and therefore transgression, cylinder motifs, aggradation, and funnel-shaped motifs progradation and hence regression (After Martinius *et al.*, 2002). 175

Figure 5.5-Summary of spectral gamma ray data obtained from localities 1-5, visualised as the total amount of each element (total counts), and the amount of each element (U,Th & K) against height. 181

Figure 5.6- Ratio between potassium and thorium isotopes found at Locality 2a Lone Mesa by a handheld spectral gamma ray tool. The trendlines for each association have been added showing the equation of the line and the coefficient of determination (r^2). 182

Figure 5.7- Ratio between potassium and thorium isotopes found at Locality 1. Bartlett Fault logged by a handheld spectral gamma ray tool. The trendlines for each association have been added showing the equation of the line and the coefficient of determination (r^2). 182

- Figure 5.8-Ratio between potassium and thorium isotopes found at Locality 4 Duma Point Transition 1 logged by a handheld spectral gamma ray tool. The trendlines for each association have been added showing the equation of the line and the coefficient of determination (r^2). 183
- Figure 5.9- Ratio between potassium and thorium isotopes found at Locality 3 Duma Point Transition 3 logged by a handheld spectral gamma ray tool. The trendlines for each association have been added showing the equation of the line and the coefficient of determination (r^2). 183
- Figure 5.10-Ratio between potassium and thorium isotopes found at Locality 5-San Rafael Swell logged by a handheld spectral gamma ray tool. The trendlines for each association have been added showing the equation of the line and the coefficient of determination (r^2). 184
- Figure 5.11.1- K:Th cross-plot for trough cross-bedded aeolian dunes, note the clustering in the lower left-hand corner. Figure 5.11.2- K:Th cross-plot for planar bedded aeolian dune facies. Figure 5.11.3- K:Th cross-plot for the undulose bedded sandstone facies, which has a more linear trend compared with the facies in 5.11.1. Figure 5.11.4- K:Th cross-plot for parallel laminated siltstones. 187
- Figure 5.12- K:Th cross-plot for the planar cross-bedded sandstone facies with distinct clustering in the lower left-hand corner. Figure 5.12.2- K:Th cross-plot for the saline soil palaeosol facies. Any results gained from this graph is insignificant and should be discounted as there are only two data points. Figure 5.12.3- K:Th cross-plot for the ferrallitic gleysol palaeosol facies. Figure 5.12.4- Facies K:Th cross-plot for the parallel laminated oxisol facies. 190
- Figure 5.13.1- K:Th cross-plot for the undulose ripple laminated sandstone facies. Figure 5.13.2- K:Th cross-plot for the massive sandstone with load cast facies. Figure 5.13.3- K:Th cross-plot for parallel laminate siltstone (same diagram as 5.11.4, added here for comparison to similar coastal plain facies). Figure 5.13.4- K:Th cross-plot for the parallel laminated siltstone with evaporites facies. 192
- Figure 5.14.1- K:Th cross-plot for the inverse graded parallel laminated siltstone facies. Figure 5.14.2- K:Th cross-plot for the parallel laminated sandstone facies. Figure 5.14.3- K:Th cross-plot for the ripple laminated sandstone facies. Figure 5.14.4- K:Th cross-plot for the herringbone cross-stratified sandstone facies. 194
- Figure 5.15- Clustering and trends of the broad scale depositional environments within a thorium-potassium cross-plot. Estimated areas have been obtained from the average values of potassium and thorium for each facies attributed to the depositional environment. Aeolian environments produce a distinct cluster in the lower left corner of the graph, interdune environments create two

separate linear trends that could be explained by the difference in aqueous influence between damp and wet interdunes. The palaeosol facies occupies an incredibly linear are in the center of the graph. Coastal and tidal environments both create a cluster in the center of the graph spreading over a wide data range. 196

Figure 5.16- Comparative box plot showing the total gamma ray values at each locality for sandstones within different depositional environments i.e., cross-stratified aeolian sandstones (Sxs), coastal plain sandstones (Scs) and sub-aqueous/tidal sandstones (Srpl). 198

Figure 5.17- Log correlation across the West to East transect from the San Rafael Swell (Locality 5) to Bartlett Wash (Locality 1) based on the sedimentology alone. 205

Figure 5.18- Thorium-Uranium logs separated by locality with individual bounding surfaces highlighted and annotated. Each surface has been identified by the relative proportions of thorium and uranium and compared with the relative position of bounding surfaces in the sedimentary logs, where a key surface is present but does not correlate with any surface previously identified by this study a (★) has been used. 207

Figure 5.19- From left to right, the total counts logs, sedimentary logs, simplified and annotated sedimentary logs demonstrating the relative proportions of measured thorium levels in ppm and the measured potassium levels by % for each locality. Within the Th/K ratio surfaces have been identified corresponding to previously identified surfaces, where a peak has been identified that cannot be correlated but is of interest a (★) has been used. 209

Figure 5.20- Uranium and Potassium logs separated by locality with individual bounding surfaces highlighted and annotated. Each surface has been identified by the relative proportions of uranium and potassium and compared with the relative position of bounding surfaces in the sedimentary logs, where a key surface is present but does not correlate with any surface previously identified by this study a (★) has been used. 211

Figure 5.21- Correlation of the surfaces TS1, TS2, TS3, TS4 and TS5 east to west across the study area, starting with Locality 1- Bartlett Wash in the East and ending with Locality 5- San Rafael Swell in the west. The relative distances in km have been shown between each of the localities in addition to their position on a map of the study area (bottom right-hand corner). For ease of correlation

simplified sedimentary logs have been used as opposed to the detailed logs found in figures 5.17, 5.18, 5.19 & 5.20. 215

Figure 5.22- Log motifs and annotations for the total count logs, at each locality in parts per million.

These logs are correlated with their respective sedimentary logs to emphasise any trends in depositional environment. AGCY- Aggrading cylinder motif, SEFL- serrated funnel motif, SEBL- serrated bell motif. 218

Figure 6.1- 3D environment reconstructions showing the transition between depositional environments upon an aeolian-marine margin in the Jurassic Period. The diagrams go in chronological order from the bottom to the top, with the topmost diagram representing the modern-day environment, with the relative positions of the localities, the town of Green River and Moab Airport. T1-T6 refer to individual time-points and not necessarily to the surfaces described above (TS1-TS5). The approximate age for the deposits has been given between 160Ma and 152Ma placing the deposits of the Moab Member within the Oxfordian Age. 227

Figure 6.2- 3D diagrams representing the behaviour of the aeolian dune field at the time of deposition of genetic packages 1-5 and during periods of non-deposition represented by the surfaces TS1-TS5, working chronologically upwards from the bottom to the top. Significant features of each unit have been annotated and a description of changes in the dune field can be found in the right hand column. 230

Figure 6.3- Locality map and sequence stratigraphy of the study area, from Bartlett Wash in the East to the San Rafael Swell in the west. The key environments have been colour coded with the aeolian dunes further broken down into classifications based on size, as identified in Chapter 4. The key surfaces traceable across each of the localities have been shown as well as their main identifiers such as rhizoliths. 233

Chapter 1: Introduction

Aeolian successions comprise vast and seemingly homogeneous deposits, documenting millions of years of geological time, recorded within both the preserved successions and by the unconformities that separate them. Aeolian environments interacting with neighbouring fluvial, lacustrine, and marine margins are subject to both allogenic and autogenic forcing, and produce complex interbedded successions of aeolian, alluvial, lacustrine, coastal, and shallow marine deposits (Mountney and Jagger, 2004; Rodriguez-Lopez, 2008; Zuchuat et al., 2019a; Priddy and Clarke, 2020; 2021; Pettigrew et al., 2020; 2021).

Continental erg systems have been studied extensively (e.g., Bagnold, 1941; Wilson, 1972; Hunter, 1977; Porter, 1986; Peterson, 1988; Clemmensen and Blakey, 1989; Kocurek, 1991; Crabaugh and Kocurek, 1993; Carr-Crabaugh and Kocurek 1998; Jerram et al., 2000; Mountney and Thompson, 2002; Mountney, 2012; Kok et al., 2012; Rodríguez-López et al., 2014; Pettigrew et al., 2018; Mesquita et al., 2021; Yu et al., 2021) and are known to deposit and preserve high porosity and high permeability clastic reservoir sands (Taggart et al., 2010; Scorgie et al., 2021). However, marginal relationships between erg systems and surrounding contemporaneous marine environments are generally less well-understood, and often perhaps under-represented in the literature (Rodriguez-Lopez et al., 2013; Rodriguez-Lopez et al., 2014). A detailed study on the interaction between continental depositional processes and oscillatory/tidal currents has the potential to improve the predictive power of depositional and sediment-dispersal models of targeted basins. This is especially important as mudstones and other tidally-influenced or marginal fine-grained facies often represent non-reservoir lithologies (Chandler, 1987; Chandler et al., 1989;

Svendsen et al., 2007; Henares et al., 2014, Heidsieck et al., 2020), which may directly influence fluid migration pathways in the subsurface.

The Entrada-Curtis-Summerville succession exposed in South-eastern Utah provides an excellent opportunity to document the interactions and evolution of an arid coastal erg system and provide detail at both the element scale and the basin scale. The Curtis-Summerville formations were deposited in what is thought to have been a narrow Oxfordian seaway that extended from the Sundance Sea (Kreisa and Moila, 1986; Caputo and Prior, 1991; Wilcox and Currie, 2008; Zuchuat et al., 2018 and references therein), in which tidal resonance temporarily developed during periods of optimal conditions. During such resonant episodes, autogenic processes have the potential to overprint the stratigraphic signature of autocyclic processes (Zuchuat *et al.*, 2019a). Determining sea-level fluctuations in the neighbouring aeolian dunes is therefore crucial to establishing aeolian-marine margin interaction within the study area in the Jurassic Period.

The Moab Member of the Curtis Formation is a perfect example of such a complex palaeoenvironmental setting, and illustrates the potential implications associated with correlating tide-dominated shallow-marine sediments and dry aeolian successions. Therefore, to investigate the complexities within such environments, this study aims to: (i) better characterise facies interactions and depositional processes at both local and regional scales (ii) correlate significant bounding surfaces within marine successions of the basin and their proximal counterparts., and; (iii) decipher sea-level fluctuations across an aeolian-shallow marine margin, ultimately reconstructing the Entrada-Curtis-Summerville aeolian-marine margin through detailed models.

1.1.1 Aims & Objectives

This project aims to improve our knowledge of complex marginal interactions between aeolian and shallow marine environments. This study uses high-resolution drone photogrammetry to characterise preserved aeolian successions and spectral gamma-ray to highlight key surfaces correlatable across the margin. The three main aims addressed in this thesis are as follows.

Aim 1: Characterise facies interactions and depositional processes at both local and regional scales

This study uses sedimentary logging to describe successions of aeolian, coastal and shallow marine environments upon the modern-day Colorado Plateau.

Logging in an east to west transect across a palaeo aeolian-marine margin provides a comprehensive and detailed picture of facies interactions. Scaling these interactions up at association and assemblage scale builds a local and regional picture of changes in environment.

In addition to sedimentary logging, the data obtained from high-resolution drone photogrammetry describes changes in dune height and sediment supply within the aeolian deposits of the study area. Documenting the responses to sea-level fluctuations and changes in sediment supply seeks to establish the local-scale changes to the dune field whilst comparing any significant changes to signals in the nearby shallow marine deposits.

Aim 2: Correlate significant bounding surfaces within marine successions of the basin and their proximal counterparts.

Spectral gamma-ray (SGR) logging and subsequent analysis allows the identification of several significant peaks at different scales attributable to events

happening within the depositional environment. Large-scale surfaces, visible within aeolian, coastal and marine deposits, represent a significant change in environment or a substantial time gap/ unconformity, i.e., allocyclic signals. Small-scale surfaces indicate bounding surfaces within aeolian successions related to more localised changes in the water table, sediment supply or wind dynamics.

Aim 3: Decipher sea-level fluctuations across an aeolian-shallow marine margin

Combining sedimentary, drone and SGR data highlights both spatial and temporal changes on the palaeo-margin. Sedimentary logging enables a facies analysis of the deposits, dividing preserved successions into facies representative of depositional environments. This is supported by 'gamma-facies', an analysis of K:Th cross-plots that defines the relative clay composition of the deposits and attributes them to a general depositional environment. Once the depositional environments have been established, shifts in these environments can be identified using further SGR analysis such as potassium, thorium and uranium logs and varying ratios of the above. Using log trends and motifs, the changes in the environment at each locality through time can be inferred.

Finally, all the techniques and analysis mentioned above combined, produce an over-arching story of deposition upon an aeolian-marine margin, including eustatically driven sea-level changes affecting the entire margin and local-scale, and more minor, sea-level fluctuations. These are likely to be driven by autocyclic factors that affect the small-scale interactions between the aeolian, coastal and shallow marine environments.

1.1.2 Fieldwork Location

The areas around Green River and Moab in South-eastern Utah (Figure 1) contain the best-exposed examples of a complete aeolian-marine margin preserved in the Entrada-Curtis-Summerville formations of the Curtis basin. The Colorado Plateau, upon which the formations can be found, spans 386,000 km² across Arizona, Utah, Colorado, and New Mexico (Figure 1). At the time of deposition, the environment would have been that of a restricted marine environment bound by the highlands to the east and the west. This optimal physiographical condition created a narrow inland sea within which sediments of the Curtis Formation (Figure 1.2) was deposited immediately adjacent to an ever-expanding coastal plain and a restricted dune field.

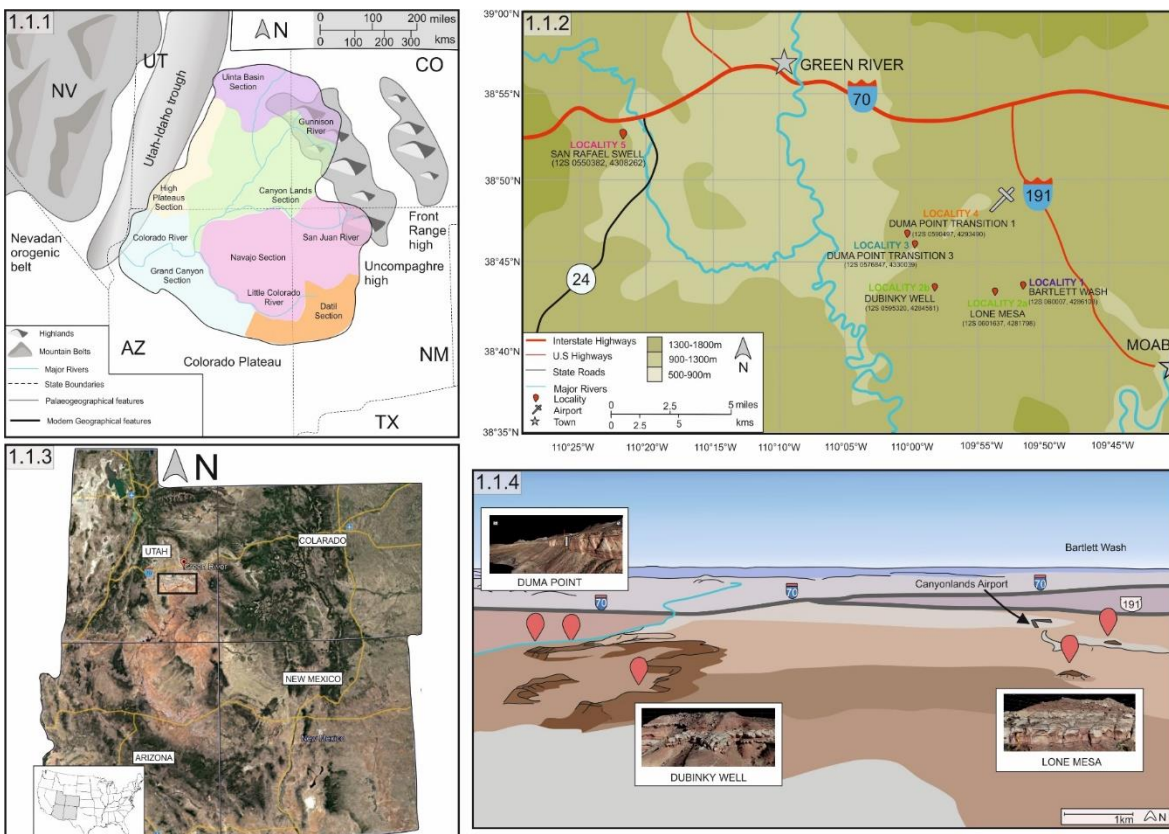


Figure 1.1.1- Tectonic features surrounding the Colorado Plateau in the Four Corners region of the USA. Figure 1.1.2- Locality map of the six main sites visited by this study. The most easterly locality is Bartlett Wash, the most westerly is the San Rafael Swell. Figure 1.1.3- Satellite image of the four corners region of the USA with a map showing the same location within the wider United States. Figure 1.1.4- Localities of the drone surveys at localities 2-4. Locality 1- Bartlett Wash was excluded due to proximity to the Canyonlands airport (shown).

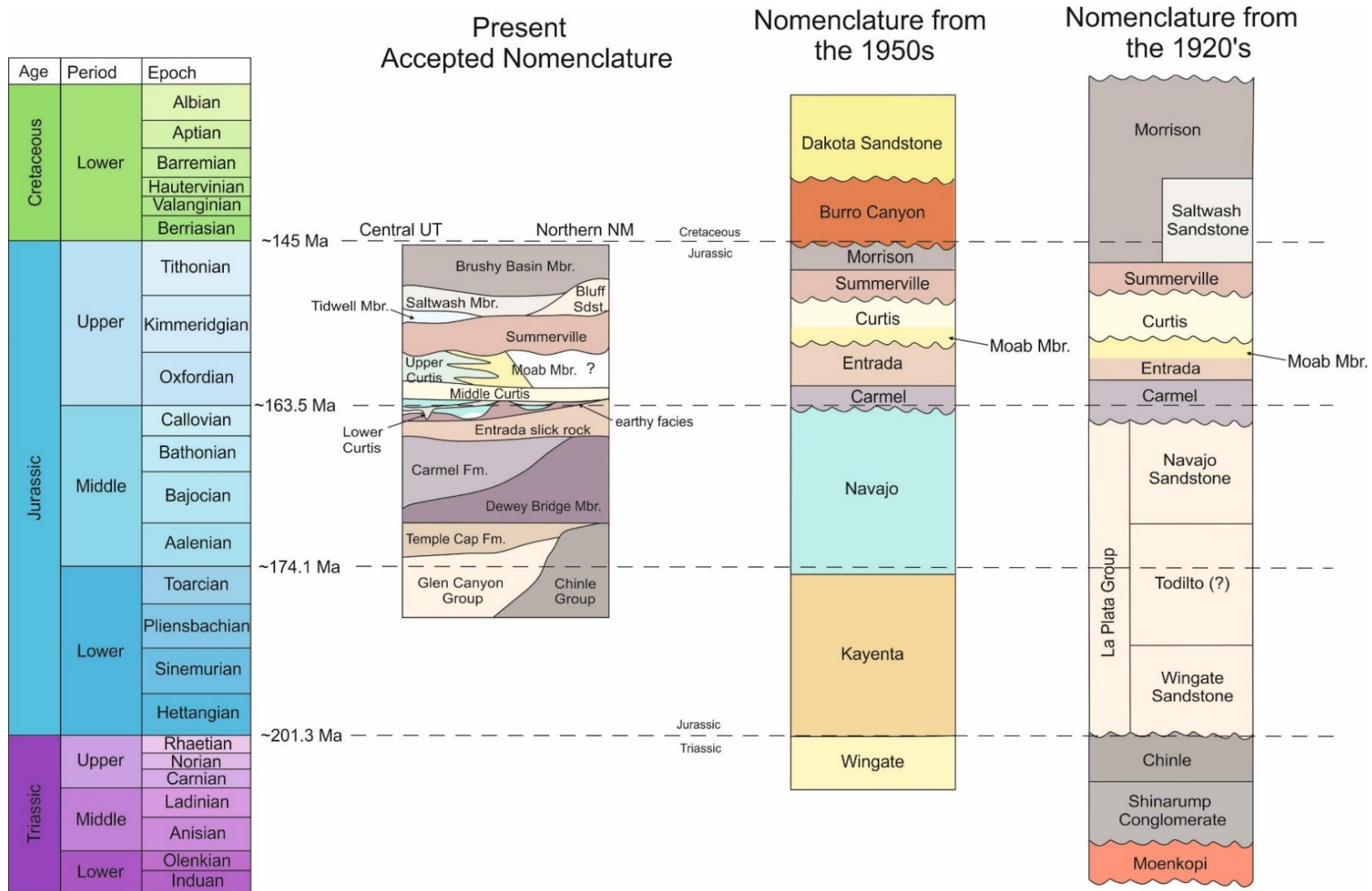


Figure 1.2- From right to left: Stratigraphic column drawn from the initial work on the Curtis Basin sediments by Gilluly and Reeside (1928) This work placed the Carmel, Entrada, Curtis, and Summerville formations correctly within the Upper Jurassic but extended the Morrison well into the Cretaceous. Further work from the 1950s identified the end of the Morrison as the boundary between Jurassic and Cretaceous deposits. The modern stratigraphic column (modified from Zuchuat *et al.*, 2019) shows the complex relationships between the Entrada, Curtis, and Summerville formations from Central Utah to Northern New Mexico.

1.2 Geological Setting

The aeolian and coastal margin sediments of the Jurassic Entrada, Curtis and Summerville formations are found on the Colorado Plateau: an elevated area that covers 386,000km² in the Four Corners Region of the Western USA (Figure 1). Many of the preserved successions for these formations are best exposed between the towns of Green River and Moab, at Duma Point, Bartlett Wash and the San Rafael Swell (Figure 1).

1.2.1 Geological Development of the North American Cordillera

The North American Cordillera is an extensive mountain range forming the western mountain system of the modern United States. The Cordillera, from the Gulf of Alaska to the Gulf of California, is approximately 5000km long (Dickinson *et al.*, 1986). The Cordillera accounts for only 20% of the total length of the Circum-Pacific Orogenic belt, the active tectonic region that was responsible for the construction of the North American Cordillera and consequent events forming the Colorado Plateau (Dickinson, 2004). Precambrian and Palaeozoic deposition within the modern-day Four Corners Region (Figure 1) occurred predominantly within the shallow marine environment, depositing a range of marine clastics and carbonate sediments. Throughout geological time this region continued to be affected by deposition, both continental and shallow-marine, erosion and even periods of volcanism. The interplay of these depositional processes creates unique preserved stratigraphy from the Proterozoic right up until the modern Quaternary (Figure 1.3).

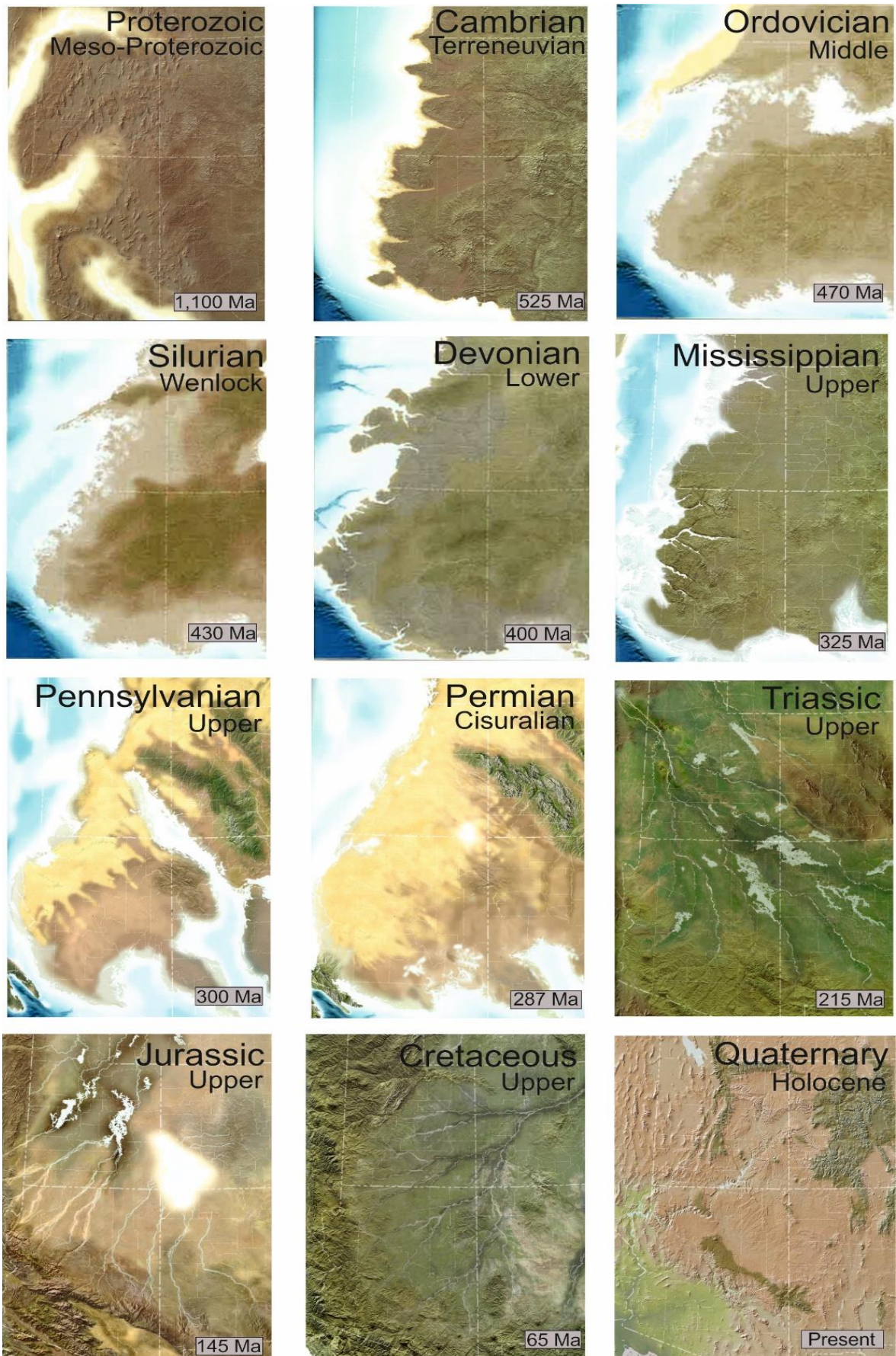


Figure 1.3- The evolution of the Colorado Plateau throughout geological history starting with the Proterozoic and continuing to the modern-day. Although the environments are transitional the representation for the end of each of the periods have been selected here to provide a summary that best fits the environment of deposition for each period (After Blakey & Ranney, 2008).

1.2.2 Palaeozoic Tectonics

Exposures of Palaeozoic deposits within the Colorado Plateau outcrop within the most incised areas along the Colorado River and within the Grand Canyon.

Precambrian Basement

Understanding Jurassic sediments on the Colorado Plateau and their formation must first begin with the basement upon which the rocks rest. The formation of the basement rocks of the Colorado Plateau began in the Archean with the oldest surviving rocks preserved in the area being The Grand Canyon Supergroup. This Supergroup consists of two groups, the Unkar and Chuar groups, separated into the Nankoweap Formation and the Sixtymile Formation, respectively.

Neoproterozoic tectonic collision formed basins attributed to the deposition of the Grand Canyon Supergroup (Blakey & Ranney, 2008) (Figure 1.4).

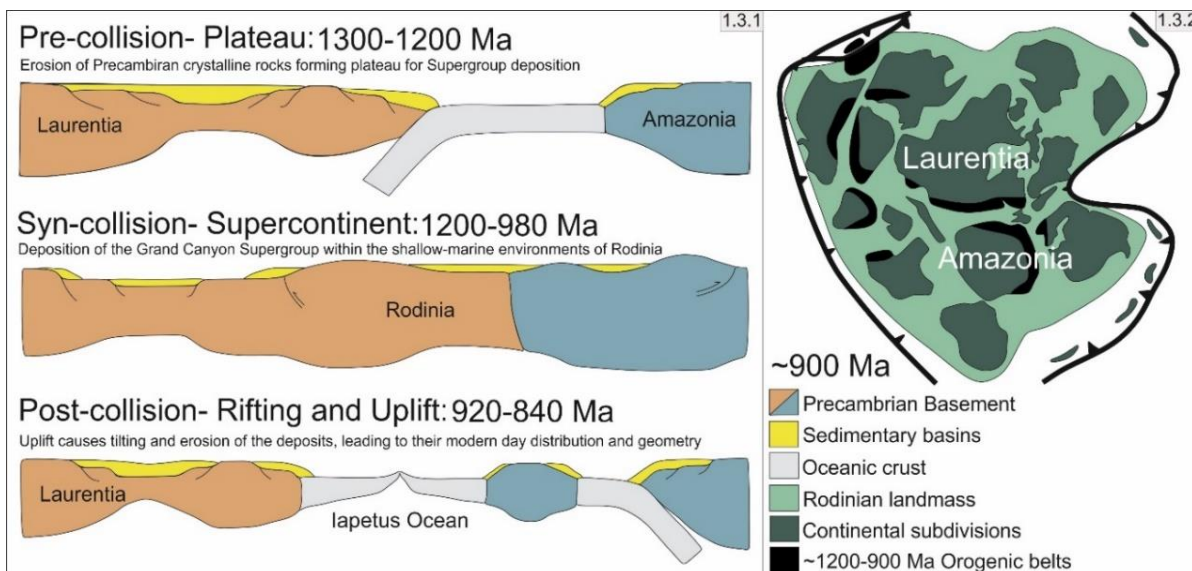


Figure 1.4.1- The Grenville orogenic cycle. Precambrian tectonic activity leading to the deposition, tilting and erosion of the Grand Canyon Supergroup, resulting in its modern-day preservation and distribution across within the Colorado Plateau (After Spencer *et al.*, 2015). Figure 1.4.2- Palaeogeographic reconstruction of continental landmasses at the end of the Grenville orogenic cycle (~900 Ma)

Cambrian to Mississippian Shallow Marine Shelf

Following the Grenville Orogeny and the break-up of Rodinia, modern-day western North America became a passive continental margin (Figure 1.5). The Wasatch Line is a structural lineament underpinning significant tectonic activity upon the plateau and is linked to this margin development. The feature itself is approximately 400km long and runs south-south-west from southern Idaho through northern Utah, terminating in central Utah. Parts of this lineament are still active today, with the activity of the remaining parts a key influence throughout the depositional history of the area (Stokes, 1976). Sediments from the middle Palaeozoic Era (Cambrian Period to Mississippian Period) were deposited upon a broad continental shelf subject to many small-scale transgressions throughout the Cambrian Period. Sandstones were deposited variably upon the surviving Precambrian crystalline deposits and the Grand Canyon Supergroup leading to a 1,255-million-year gap in the depositional record known as the Rodinian Break-up Unconformity (Li, Zhang & Powell, 1995, Marshak *et al.*, 2017).

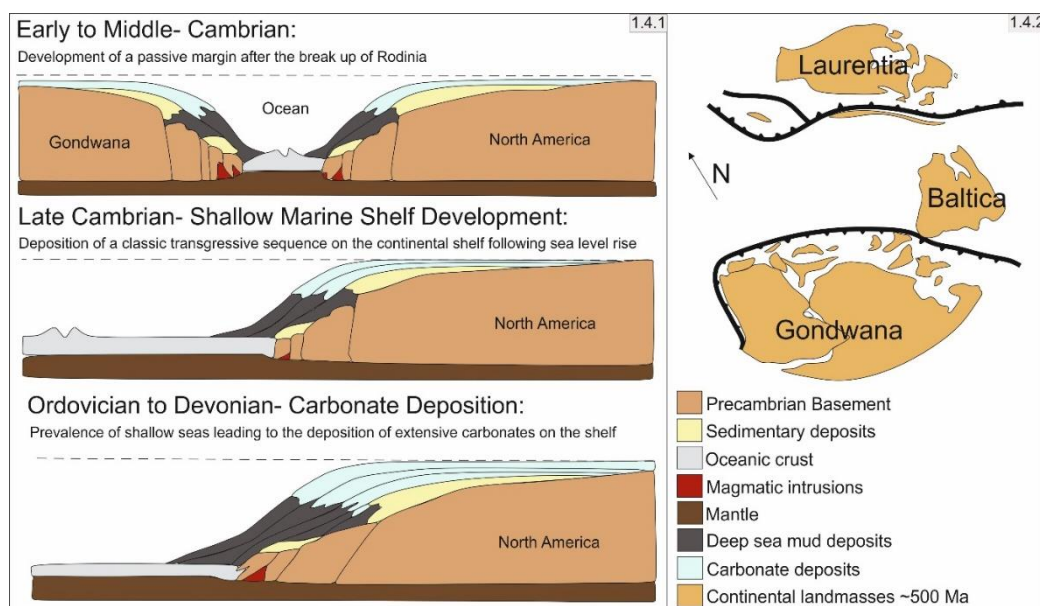


Figure 1.5.1- Evolution of the passive margin setting defining the tectonic activity for the Cambrian Period to Mississippian Epoch (After Blakey & Ranney 2008). Figure 1.5.2- Position of the continental landmasses in the early Cambrian when rifting and high sea-levels allowed for extensive continental shelf environments.

Pennsylvanian and Permian Uplift

Late Palaeozoic deposits mark the formation of the supercontinent Pangaea: a large scale amalgamation of continents, the origins of which stretch back to the Neoproterozoic and reach its furthest extent at the end of the Triassic Period (Wang *et al.*, 2021). This immense landmass had a notable impact on ocean circulation and climatic conditions within western North America (Fillmore, 2010). The initial influence of this continental amalgamation occurred in the Carboniferous Period with the rise of the Ancestral Rocky Mountains. In addition to the formation of the mountain belt, the uplift was also responsible for the creation of a foreland basin named the Paradox Basin (Baker *et al.*, 1933). Throughout the Pennsylvanian Period, there was significant tectonic unrest relating to the rise of the Ancestral Rockies and the Uncompaghre Highlands, the westernmost expression of these mountain ranges (Fillmore, 2010). The highlands occupied most of western Colorado, extending southwards along the modern-day Utah-Colorado border and into northern New Mexico. To the southwest of this mountainous extent lay the Paradox basin (Figure 1.6), marked by a series of large-scale reverse thrust faults (Frahme & Vaughn, 1983).

1.2.3 Mesozoic Tectonics

The break-up of the supercontinent Pangaea inevitably featured extensive rifting and tectonics; however, this affected western North America minimally as it was far removed from any tectonic boundaries at the time (Fillmore, 2010).

Triassic Erosion

The previously extensive Uncompaghre highlands were subject to dramatic erosion throughout the Triassic Period. They provided a substantial sediment supply to the Paradox Basin and created an extensive drainage basin into which fluvial systems could expand and later be preserved as the Chinle and Moenkopi formations. During this time, there was a new mountain-building event - the Sonoma Orogeny - whose epicentre was probably located in modern-day central Nevada. The collision of volcanic islands with the western coast of the continent resulted in uplift that continued throughout both the Triassic and Jurassic Periods, steadily moving the locus of deformation eastwards. It also reversed the drainage direction of the landscape and, critically, shut off any potential moisture arising from the sea to the west and hence causing the extreme aridity characteristic of the Colorado Plateau in the Jurassic Period (Fillmore, 2010).

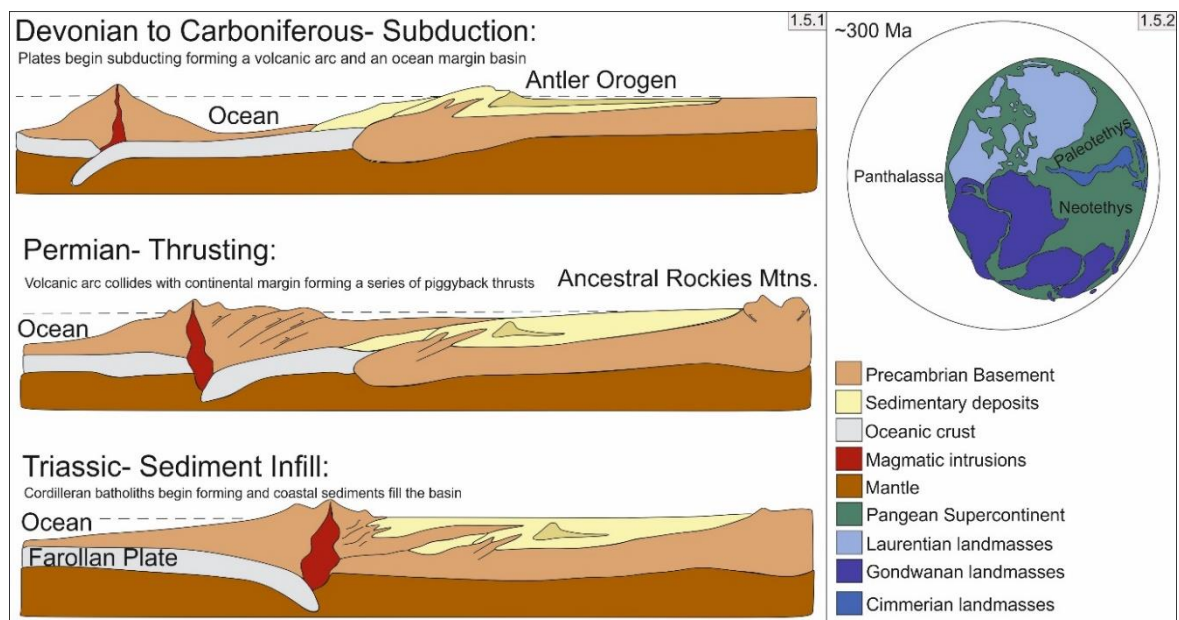


Figure 1.6.1- Subduction cycle in the Western United States, continental collision, thrusting, uplift and sediment infill of basins leading to the shallow marine grading into continental deposits of the Paradox Formation (After Dickinson, 2004). Figure 1.6.2- Position of the continental landmasses within the super-continent Pangaea at the start of the Devonian.

Jurassic Basin and Range

The persistently arid conditions of the Triassic continued through into the Jurassic climate of the western United States. The continental plate maintained buoyancy from residual heat whilst drifting westward towards oceanic plates, leading to a continued uplift period (Fillmore, 2010). Throughout this period, the largest sand seas, or ergs, ever to have been deposited on the surface of the planet, existed. Jurassic tectonic influence can be attributed to two main orogenic events, the Nevadan Orogeny and the Elko Orogeny (Thorman & Peterson, 2003). The Elko Orogeny is not recognised as a global event due to its previous association with the Sevier Orogeny but has since been determined to be an entirely separate event (Thorman & Peterson, 2003, Thorman & Sandberg, 2020). A foredeep basin extending along the leading edge of the Elko orogenic belt resulted in the deposition of sediments that thicken westward towards the Colorado Plateau Basin and Range border (Thorman & Peterson, 2003). The dating of cross-cutting relationships enables this event to be placed within the Early Jurassic Period (Thorman *et al.*, 2020).

Cretaceous Tectonics

After the unexpected period of quiescence at the end of the Jurassic Period, tectonic activity renewed with vigour throughout the Cretaceous Period. As the Curtis Sea regressed the flat coastal plain it left behind was inundated with the fluvial systems and lakes of the Morrison Formation.

The main tectonic events occurring throughout the Cretaceous Period are the Sevier and Laramide orogenies. Within the Western United States, the physical representation of the Sevier Orogeny can be found within the Sevier Belt, defined as "a linear group of closely spaced thrust faults and related folds that extends

from Las Vegas, Nevada and up to the Idaho State Line" (Armstrong, 1968). The leading edge of the thrusting is linked with the modern-day position of the Wasatch Line terminating on the edge of the plateau. Therefore, the sediments on the plateau were subjected to a downward force produced by differential loading of the crust in response to westward thickening (Fillmore, 2010). The Sevier Orogeny's overarching impact in the Cretaceous can be broken down into two main categories: thrusting, deformation and mountain building in the west, and subsidence, transgression, and foreland basin creation in the east (Blakey & Ranney, 2008).

The Laramide Orogeny took place between 70 and 40 million years ago and was responsible for the uplift that formed the modern-day Rocky Mountains. This event is considered an extension of the Sevier in modern literature (Copeland *et al.*, 2017). The Laramide is attributed to the northward movement of the Tertiary thrusting centre (Figure 1.7). The angle of subduction during the Elko, Nevadan and Sevier Orogenies was approximately 45-60°. For the duration of the Laramide, it may have decreased to just 25° or even less (Copeland *et al.*, 2017). This is an unusual angle for subducting plates; however, it may explain the formation of the Rocky Mountains so far from an active plate boundary (Blakey & Ranney, 2008). The physical representation of this can be found on the Colorado Plateau as laccolith mountains puncturing the landscape. These were formed as a direct consequence of increased volcanism along the boundaries (Figure 1.7). Like the Uncompaghre Uplift, mountain belt development driven by the Elko and Sevier orogenies occurring in modern-day Nevada led to an increase in sedimentation, which moved sediment en-masse directly from the highlands into the basin below. Relatively high tectonic activity throughout this period led to volcanism on the plateau. The evidence for this can be found in the Jurassic and

Cretaceous sediments, where volcanic ash erupted during this comparatively tumultuous time, formed lithified layers within preserved sediment, providing valuable and correlatable time surfaces (Stewart *et al.*, 1986).

1.2.4 Post-Laramide Tectonics

Tectonic activity upon the Colorado Plateau in the Cenozoic era is dominated by uplift and fluvial erosion, transforming the landscape into the canyonlands we see today.

Tertiary Uplift and Quaternary Erosion

An eastward shift of the Laramide orogenic belt resulted in high-relief landscapes interjected by relatively small basins. Upon the Colorado Plateau, this change in activity resulted in monoclines such as the San Rafael Swell (Fillmore, 2010). This process allowed for enhanced erosion, by contrast to the periods of deposition experienced on the plateau previously. The most significant depositional features of the Tertiary are the intrusive igneous landforms such as the La Sal Mountains and the Colorado River drainage system, which is still active today.

There is clear evidence that uplift must have occurred to achieve the incised canyons visible within the Colorado Plateau today. However, there is some debate as to whether this uplift occurred during the Early or Late Tertiary, and even further debated is the cause of this uplift (Crow *et al.*, 2019). Recent research has established that multiple periods of uplift offer the most viable solution, explaining the well-established erosion of the Grand Canyon despite a relatively young Colorado River system (5 Ma or younger). There was likely a component of uplift immediately following the Laramide Orogeny (80-50 Ma) and another component during the Oligocene (5 Ma) (Crow *et al.*, 2019). Further activity on the North

American Cordillera was mainly a result of global climate changes. Tertiary glaciation dominated the northern hemisphere paving the way for massive fluvial systems fuelled by glacial melt that carved the typical trough features and dramatic canyon landscapes that can be seen today (Blakey & Ranney, 2008, Figure 1.8).

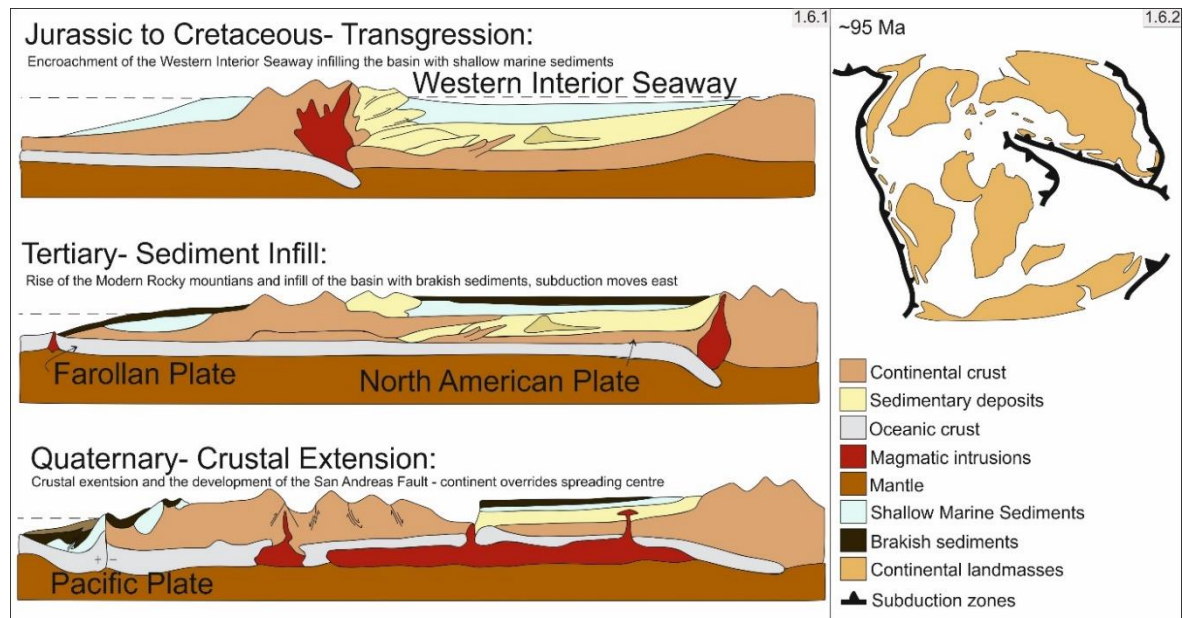


Figure 1.7.1- Tectonic evolution of the North American Cordillera from the formation of the Cretaceous Sevier Belt to the modern-day Rocky Mountains and the San Andreas Fault (After Ducker *et al.*, 2001). Figure 1.7.2- Position of the continental landmasses during the Cretaceous Period.

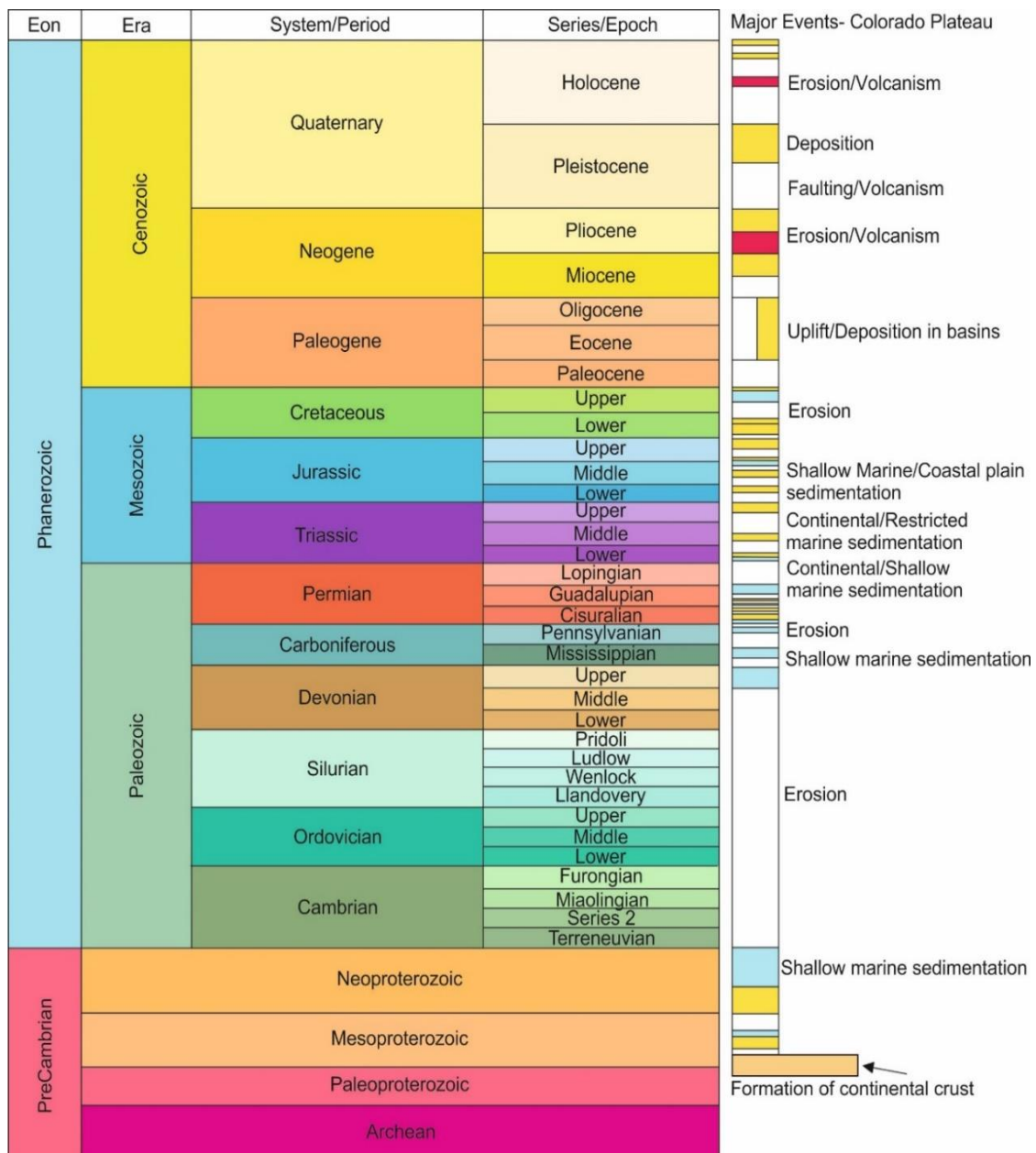


Figure 1.8- A summary of the major geological events and environments on the Colorado Plateau on a geological time scale. White represents periods of erosion, displayed in the rock record by major unconformities. Yellow displays mainly continental deposition and blue mainly marine deposition. Not all events are shown. The periods are in accordance with the most recent figure released by the International Commission on Stratigraphy (v 2020/03). (After Blakey & Ranney, 2008).

1.3 Evolution of the Colorado Plateau and the Paradox Basin

As described above, the evolution of the Colorado Plateau is directly related to the tectonic activity of the North American Cordillera. Throughout geological history, the environment on the plateau fluctuates, alternating between continental, shallow-marine and even volcanic periods of deposition (Figure 1.8).

Tectonic activity following the unconformity that separates the Mississippian deposits from the overlying Pennsylvanian deposits, resulted in the uplift of the Uncompaghre highlands and their corresponding basin, the Paradox Basin. The evolution of the Paradox Basin and the Jurassic Curtis Basin are palaeogeographically closely related to the evolution of the Colorado Plateau (Figure 1.9). The Paradox Basin is a foreland basin defined by the lateral extent of the salts that form the initial fill portion of its stratigraphy, termed the Paradox Formation. The depositional basin itself formed parallel to the Uncompaghre uplift and currently occupies an area of approximately 28,500 km². Due to its unique locality surrounded by highlands on almost all sides, the Paradox Basin was a restricted environment promoting the cyclic deposition of evaporites, shallow marine and carbonate sediments (Foos 1999, Trudgill, 2011).

The climatic changes from warm swamps to arid deserts that mark the distinction between the Pennsylvanian and Permian periods in other parts of the world are largely indistinguishable within the Paradox Basin. Due to its already arid climate, there were no changes to the depositional environment save those already resulting from the regular cycles of sea-level rise and fall. The Uncompaghre highlands continued to rise and be eroded by a network of alluvial fans and fluvial systems carrying sediments into the neighbouring lowlands. Towards the end of the Permian, decreasing sediment thicknesses evidence decreasing tectonic activity in the Ancestral Rockies, the Uncompaghre highlands, and the Paradox Basin. By the end of the Permian, tectonic activity had subsided entirely, and erosive forces dominated, reducing the Precambrian rocks to a plain within 80 million years (Fillmore, 2010). The Permian-Triassic unconformity separate the deposits of the Paradox Basin and the overlying Moenkopi Formation. The depositional environment during this time was an extensive coastal plain with the

Sonoma highlands to the west, driving subsidence and replacing the Paradox Basin with the Hoskinnini Basin (Fillmore, 2010) (Figure 1.9).

Early Mesozoic tectonic activity reactivated several of the deep-seated basement faults in the area, creating up to twenty foreland basins, controlled by the differential loading and hence flexure of the crust. This continued crustal loading caused further widespread movement of the Paradox salts that have persisted since their original deposition (Blakey & Ranney, 2008).

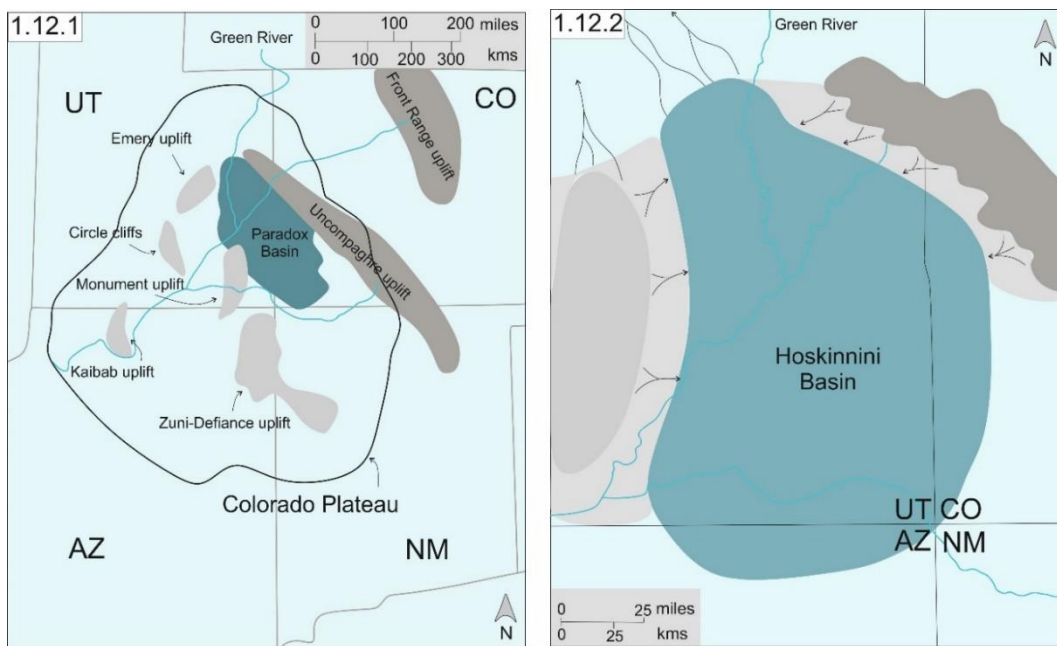


Figure 1.9.1- Key geographical features within the Paradox basin during the deposition of the Paradox formation in the Permian Period. The main uplift features are shown in addition to the position of the modern-day Colorado Plateau. Figure 1.9.2- Key geographical features of the Hoskinnini basin that formed at the start of the Triassic Period, replacing the deposition environment of the Paradox basin. This basin was home to the extensive floodplains and fluvial systems of the Moenkopi and Chinle formations (Modified after Fillmore, 2010).

1.3.1 Stratigraphy of the Paradox Basin

Extensive evaporites are the most well-known sediments within the Paradox Basin and were formed due to periodic inundation of the sea. As the sea level subsequently fell, however, surrounding highlands such as the Uncompaghe, Monument, Emery and Zuni-Defiance prevented the sea level from completely subsiding and promoted the formation of extensive salts (Figure 1.10).

The stratigraphy of the Paradox Basin is controlled by local tectonics, which influences topography, sediment supply and post-depositional movement. The Paradox Basin lies in the modern-day Canyonlands Section of the Colorado Plateau.

Pennsylvanian deposition within the Paradox Basin was highly variable. In the northeast, along the boundary with the Uncompaghre highlands, the stratigraphy comprises 5,500m of coarse sandstone and conglomerates. Moving southwest into Utah, these deposits grade into 2,000m of deep-water evaporites and finally into 300m of shallow-water carbonates (Fillmore, 2010) (Figure 1.10). A characteristic feature of these deposits is their uniform cyclicity. The Paradox Formation was deposited within the Early Pennsylvanian Period and comprised twenty-three cycles, marking a sea-level change (Condon, 1997, Jordan *et al.*, 2012). Whether the sea level was at low-stand, transgression, at high-stand or regressing is crucial to the type of stratigraphy that was deposited. During transgression and when the sea level was high, deposition dominated the rim of the basin, thriving in the warm, shallow marine environment. However, as the sea level fell, the limestone would migrate to a more distal part of the basin and be overlain by coastal mudstones. These characteristic cycles of limestones, mudstones and salts produced from restricted 'pools' are some of the most easily recognisable cyclic successions in the world (Raup & Hite, 1992). The Cutler Group comprises various coeval environments attributed to different formations in the proximal and distal parts of the Paradox Basin. Distal coeval aeolian deposits of the Cedar Mesa Sandstone can be found overlain by the continental fluvial Organ Rock Formation. As the Permian progressed, the climate became increasingly arid, however, as the continent remained only just above sea level, even a small fluctuation would result in flooding (Blakey & Ranney, 2008).

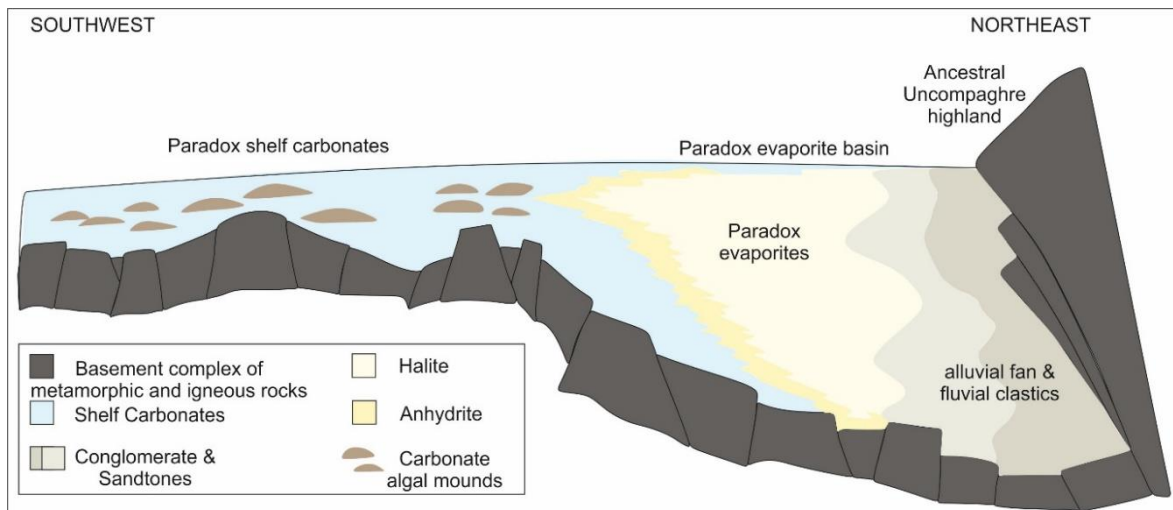


Figure 1.10- Cross-section of the Paradox basin from Southwest to Northeast across the Utah-Colorado border. The diagram shows the transition from the basement rock of the Uncompaghre highlands into the alluvial fans and then into the characteristic evaporites and carbonates of the Paradox Formation (Modified after Fillmore, 2010).

1.4 Evolution of the Curtis Basin

The effects of the Sonoma Orogeny on the Colorado Plateau until this point were limited, as a sea separated the locus of deformation and the modern-day Four Corners region. However, this sea retreated during the Jurassic, leaving the coastal plain exposed to the effects of this nearby orogeny. The overlapping Sonoma and Elko Orogenies produced two distinct types of mountains, volcanic and compressional, that will hereafter be combined and referred to as the Nevadan orogenic belt.

This increased activity along the western deformational margin provided a substantial sediment supply resulting in the westward thickening of sediment. Preserved deposits of Jurassic sediment upon the Colorado Plateau have a distinctly asymmetrical geometry. They thicken westward and thin eastward, implying they likely formed adjacent to the mountain belt forming in Nevada at the time (Thorman & Peterson, 2003). Thickness patterns within the Carmel Formations reveal the eastward migration of the mountain front into Western Utah during the Middle and Upper Jurassic Epochs (Bjerrum & Dorsey, 1995, Figure

1.11). This was followed by a sudden quiescence that halted tectonic activity and subsidence in the Jurassic Period until its renewal in the Cretaceous Period.

Subsidence from the Nevadan orogenic belt caused rapid subsidence upon the Colorado Plateau, initiating the inundation of the Sundance Sea into this region.

The Sundance Sea had previously occupied an area north of modern-day Utah but had extended down in a finger-like incursion in response to the tectonic activity in the area. This incursion is distinguished as the Curtis Sea, and the area into which it flooded is referred to as the Curtis Basin (Figure 1.11).

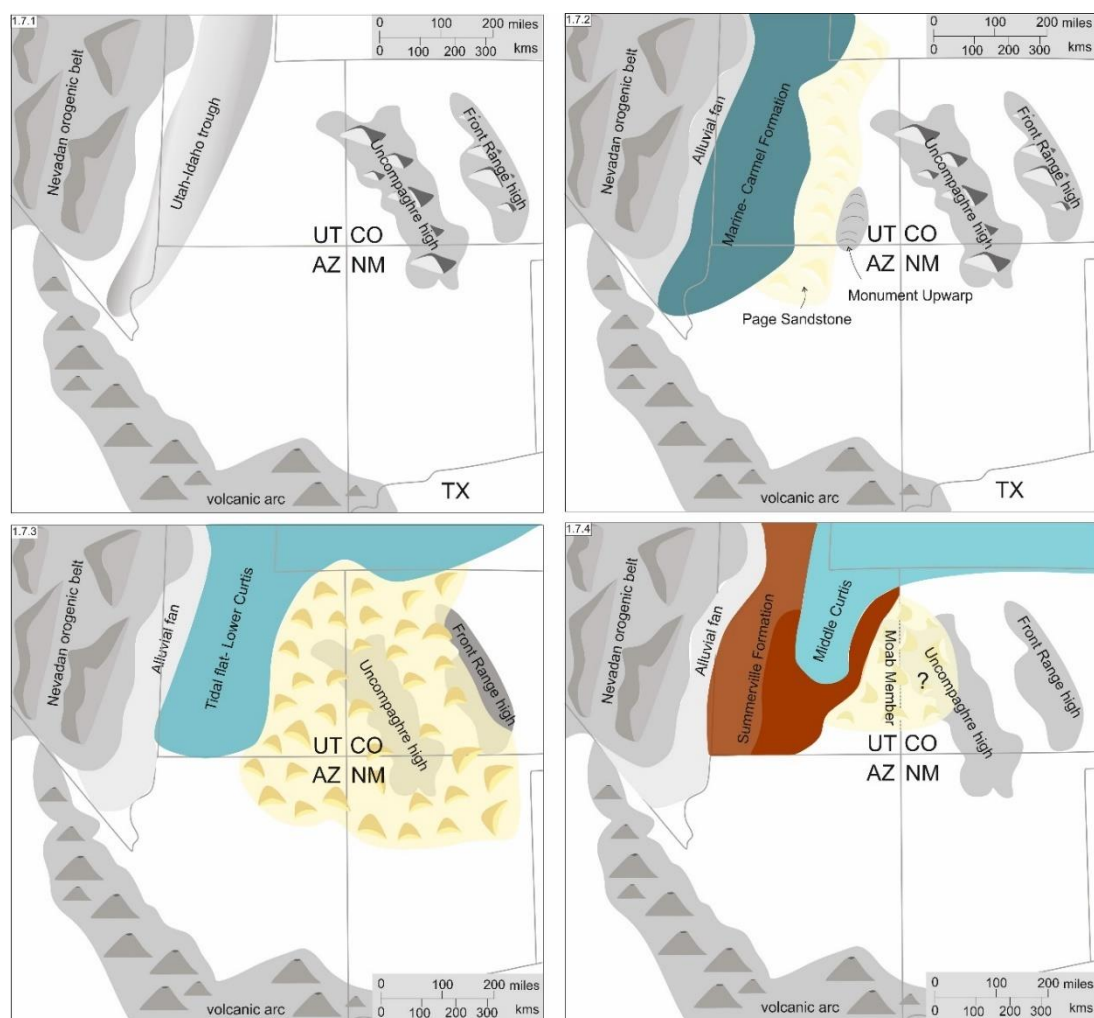


Figure 1.11.1- Key features of the Colorado Plateau affecting deposition in the Middle Jurassic. Including, the Uncompaghre highlands and the Nevadan Orogenic Belt, the main sources of sediment supply and the Utah-Idaho Trough that formed in response to lithosphere loading of the nearby mountain belt. Figure 1.11.2- The first incursion of a Jurassic Sea resulted in the deposition of the Carmel Formation with the Page Sandstone deposited as along its south-eastern margin. Figure 1.11.3- The southward transgression of the Sundance Sea created the aeolian-marine margin of the Curtis-Entrada deposits. Figure 1.11.4- As the Curtis Sea regressed another aeolian-marine margin forms from the Middle Curtis-Moab Member, surrounded by the coastal plain of the Summerville Formation.

The Curtis Basin is unique in that the dimensions of the basin (800 by 150km) made it subject to tidal resonance during periods of transgression. The morphology of the basin, which corresponded to an odd multiple of a quarter of the tidal wavelength, provided ideal conditions for the overprinting of allocyclic processes by tidal interference (Zuchuat *et al.*, 2019). Further deposition within the Jurassic Period is controlled almost exclusively by fluctuations in the Curtis Sea and the relative response of the basin.

1.4.1 Stratigraphy of the Curtis Basin

Triassic and Jurassic deposits comprise some of the largest sand seas and fluvial systems that have ever covered the surface of the planet. The Moenkopi and Chinle formations were deposited within complex river systems and contained many well-preserved ripple marks and mud cracks (Stewart *et al.*, 1972). They formed on a vast plain that existed during the Triassic Period, where even the slightest rise in sea level could cause inundation (Banham & Mountney, 2013).

The Jurassic Period brought severe drought and arid conditions to the basin leading to the deposition of the Wingate and Navajo sandstones, the most extensive aeolian deposits found anywhere on Earth. As the Sundance Sea encroached, the extremely arid environments of these immense sand seas alleviated into a shallow marine coastal environment with neighbouring aeolian dune fields, maintained by the substantial sediment supply from local orogenies (Massare *et al.*, 2014, Danise *et al.*, 2020). Within this environment, the marine Carmel and the aeolian Page Sandstone were deposited. Sea-level begins to rise, flooding the Page Sandstone and widening the narrow sea-way, depositing the sabkhas of the Dewey Bridge Member. However, a subsequent regression

returned the Colorado Plateau once again to an arid aeolian environment with localised influence from the local water table, depositing the Entrada Sandstone.

A transgressive event separated Entrada deposits from the overlying Curtis Formation. This transgression of the Curtis Sea was likely to be gradual throughout Entrada deposition. However, a sudden event caused the sea to flood and then rapidly regress, bringing the aeolian dunes of the Moab Member, which formed along the south-eastern edge of the marine margin. The expansion of the coastal plain, a decrease in subsidence and sediment supply, and the Curtis Sea retraction northward caused the eventual shutdown of the Moab Member dunes and the expansion of the coastal Summerville Formation (Fillmore, 2010).

1.4.2 The Glen Canyon Group

The units within this group comprise the Late Triassic and Early Jurassic sediments of the Colorado Plateau, a mix of aeolian and fluvial systems that form the Wingate sandstone, the Moenave Formation, the fluvial Kayenta Formation, and the Navajo sandstone. The Temple Cap through to the Summerville formations thicken towards the west; however, contemporaneous deposits are not found in the Basin and Range Province. Therefore, it can be hypothesised that a period of uplift eroded the surrounding stratigraphy, leaving depositional evidence only in central and South-eastern Utah (Thorman & Peterson, 2003).

Wingate/ Moenave Formation

The Wingate sandstone and the Moenave ephemeral fluvial system are closely related, laterally equivalent and intertongue in South-western Utah. The change in sedimentological characteristics upward through the unit, known as the lithofacies gradient, as identified by Tanner & Lucas (2007), shows a north-south transition

from the erg margin (distal) to erg interior (proximal). The climate of the time was seasonally arid due to an abundance of burrowing and vegetation but a relative lack of preserved aridisols and evaporites. (Tanner & Lucas, 2007).

Kayenta Formation

The Kayenta Formation consists of more fluvial sandstones that developed within a sandy braided system. The sedimentology of the succession can be separated into two environments. Deposits from the north of the basin are characteristic of sandy low-sinuosity fluvial systems, which exhibit perennial to intermittent discharge indicators. The southern basin displays intermittent to ephemeral fluvial systems with extensive floodplain deposition, which transitions into an aeolian dune and sandsheet/ interdune deposition (Luttrell, 1993).

Navajo Formation

The Navajo Formation deposits represent some of the largest dune and draa deposits that have ever covered the surface of the planet. The deposits are characterised by transverse south-easterly moving dunes and draa that grade into peripheral interdunes. These interdunes were initially fluvially flooded but later became damp, encouraging the growth of algae, secreting thin limestone beds, no more than 3m thick (Sansom, 1992).

1.4.3 The San Rafael Group

Relative sea-level fluctuations throughout the Jurassic period created a range of deposits, demonstrating the complex relationships between shallow marine settings and neighbouring aeolian dune fields. Tidal environments contain a complex variety of facies, and the Upper Jurassic Curtis-Summerville formations are no exception. They comprise part of the San Rafael Group: nine

Transgressive-Regressive (T-R) sequences that display a thinning upwards trend (Zuchuat *et al.*, 2019). Using conceptual ideas formed within the framework of sequence stratigraphy, the sequences identify four main intervals. They relate to the regression and transgression of the Sundance and Curtis ephemeral seas. (Zuchuat *et al.*, 2018). The Pre-Curtis Sea Transgression forms the base of the cycle; a slight sea-level rise causing the deposition of the Entrada Sandstone Formation within a wet aeolian environment (Crabaugh & Kocurek, 1993). Overlying the Entrada is the Moab Member of the Curtis Formation, which contains recognisable cycles correlatable with regional deposits. As the transition between formations occurs, there is evidence of an early transgression of the Curtis Sea (Zuchuat *et al.*, 2019). Lower Curtis deposits contain conglomerates and mudstones and are found only in the most distal regions but are contemporaneous with neighbouring wet interdune and coastal sabkha sediments of the Entrada Sandstone. Middle Curtis deposits range from marine to aeolian (Moab Mbr.). In the more proximal realm, this aeolian system directly underlies the Summerville, which is interpreted as a coastal plain.

The San Rafael Group contains the formations and members upon which this study focuses and will be described in more detail in this section. The base is marked by the J1 unconformity, found at the top of the Navajo Formation. However, the characteristic formations within this group can vary, moving upwards in stratigraphy depending on the basin's position (Figure 1.12).

Temple Cap Formation

In Southwestern Utah, the Navajo Formation is unconformably overlain by the Temple Cap Formation, the top of which also is represented by an unconformity titled the J2 (Doelling *et al.*, 2013). The members of this formation include the Manganese Wash Member, the Sinawava Member, the White Throne Member,

and the Esplin Point Member, as defined by Sprinkel *et al.* (2011). However, the J2 unconformity and the Temple Cap Formation itself are not present within the study area of this project as it merges with the J1 around the Canyonlands region of Utah, at the last recorded outcrop of the Temple Cap sandstone.

The Temple Cap Formation is Middle Jurassic (Aalenian) in age. In South-eastern Utah, this period is marked by the J1/J2 unconformity, overlain by the Dewey Bridge Member. This unconformity is defined by Fossen (2010), who acknowledges its previous position as a member of the Entrada Sandstone, but here identifies it as the sabkha equivalent of the marine Carmel Formation that can be found in South-western and Central Utah. The facies consist of interbedded poorly sorted fine-grained sandstone and siltstone at the base and a massive fine-grained unit referred to as the Upper Dewey Bridge Sandstone at the top (Fossen, 2010). The boundary between the two units is contorted and deformed, the origin of which is unknown with several hypotheses presented. One such hypothesis was described by Alvarez *et al.*, 1998, who suggested the deformation could be due to impact shaking, creating the lumpy and contorted bedding. The Carmel Formation is the marine equivalent of this Member that outcrops further north of the study area, forming the smallest of the 'flat iron' structures at the San Rafael Swell.

Entrada Sandstone- Slick-Rock Member

The Entrada Sandstone is Callovian in age and represents a further extensive dune field that spanned most of Utah in the Jurassic period (ref). It contains exceptionally well-preserved cross-bedding, grainfall/grainflow structures and differential bleaching. The Entrada is split into two main members, the Slick Rock Member and the informally-named 'earthy facies'. The whole system has been

categorised as 'wet aeolian', meaning that the water table was close to the surface at the time of deposition leading to frequent interdune facies (Crabaugh & Kocurek, 1993). There are several coastal dunes, sabkha and shallow marine beds that occasionally interbed with the aeolian dune facies of the Entrada, indicating a nearby shallow water source (Crabaugh & Kocurek, 1993). The interdune deposits characteristically have a darker red colour than the lighter dune facies; this is further evidence for fluid flow post-depositionally, causing bleaching of the foresets (Crabaugh & Kocurek, 1993).

Entrada Sandstone- earthy facies

In contrast to the Slick-Rock Member, which is laterally extensive and maintains a more or less constant thickness of approximately 150m, the earthy facies thickness varies from the proximal to distal realms. Closest to the San Rafael Swell, the earthy facies is the thickest, comprising about 15m of mottled, very fine-grained sands and silts that contains little evidence of fossils. Sometimes referred to as 'red-beds', they were previously interpreted as sub- to supra-tidal marine-influenced sediments (Valenza, 2016). Linking these beds to the underlying aeolian dune system, an idea of sea-level changes can begin to be formed, narrowing down the depositional environment to an interfingering fluvial terminal splay and inland sabkha system (Valenza, 2016). Towards Moab, the earthy facies thins dramatically and becomes more parallel laminated. The top of the unit is marked by the J3 surface, found in South-eastern Utah, between Green River and Moab.

Curtis Formation- Moab Member

Work on the Moab Member of the Curtis Formation is limited and can often be confusing, with stratigraphic position and depositional environment previously

dictated by the author's preference. The relative position of the Moab Member has been contested in the literature; this study follows the nomenclature as defined by Zuchuat *et al.* (2018, 2019), who define the Moab Member as the lateral equivalent of the marine middle Curtis Formation, overlain by the Summerville, the top of which is marked by the Tidwell Member at the base of the Morrison. The J3 “unconformity” is a regional composite and diachronous transgressive surface that marks the boundary between the Entrada and the base of the Curtis Formation. Above that surface, the Moab Member can be split into five individual dune packets that mark the lateral equivalence of the middle Curtis Formation as discussed below. Zuchuat *et al.* 2019, hypothesise that each of the dune packets represents humid-arid climate fluctuations and can be interpreted as sequences due to the presence of intertidal deposits towards the western extent and rhizolith horizons towards the modern-day Utah-Colorado border. The boundaries between the aeolian dune packages within the Moab Member of the Curtis Formation and the lower, middle, and upper units indicates an overprinting of the allocyclic controls on the basin by the local autocyclic, tidal processes. The primary evidence for this is in the size of the basin, as dictated by the modern-day extent of the Curtis deposits, which suggest a basin at least 800km in length and 150km in width. This provided ideal conditions for tidal resonance, which could have overprinted the tectonically influenced large-scale transgressions and regressions within the marine Curtis units that is clear within the proximal continental equivalents (Sztano & Boer, 1995).

Curtis Formation- lower, middle & upper

In the most distal part of the basin, the Curtis Formation can reach up to 100m thick and consists of marine sediments that can be split into three characteristic units, informally referred to as the lower, middle, and upper Curtis (Zuchuat *et al.*,

2019). Early work on the Curtis identifies a pinch out in the south and the west that dictates the maximum transgression of the Curtis Sea (Guilluly & Reeside Jr., 1928). Further work in the 1980s focused on the sedimentary structures and the presence of sigmoidal bundles around the San Rafael Swell. This work was carried out by Kreisa & Moila (1986), who established in detail the cyclic variability and, therefore, the tidal influence upon sedimentary deposition. This was followed by Caputo & Pryor's (1991) work to determine the tide and wave-influenced facies for the entirety of the Jurassic succession. They established that the varying sandstone and mudstone facies of the lower and middle Curtis units represent periodic incursions resulting in changes in water depth, energy, and sediment supply across sub-tidal to inter-tidal environments. The heavily rippled silt facies of the upper Curtis indicate a change to the more restricted and hypersaline environment present throughout the deposition of the Summerville.

Work on the sequence stratigraphy of the Curtis Formation has been well documented regarding the distal deposits along the San Rafael Swell (Wilcox & Currie 2008, Sleveland 2016, Zuchuat *et al.*, 2018, Zuchuat *et al.*, 2019, Zuchuat *et al.*, 2019). The Entrada Sandstone transition through the Curtis and Summerville formations represents one complete, transgressive-regressive sequence. Extensive sedimentary logging and documentation of local scale sedimentary features identified several depositional environments and sequence stratigraphic surfaces.

The J-3 "unconformity" marks the lower boundary of the sequence; this occurs at the top of the Entrada Sandstone and represents a period of erosion before and during the transgression of the Curtis Formation. Due to the tidal resonance of the basin, the Maximum Flooding Surface is regionally traceable and defines the base of the middle Curtis (Zuchuat *et al.*, 2018, 2019). The region then underwent local

scale regression as sediment supply outpaced rising sea level, depositing coastal plain facies and intertidal facies contemporaneously. The sequence is then bounded by another erosional surface, the J-5 “unconformity” which defines the base of the Morrison Formation (Holland and Wright, 2020).

Summerville Formation

There has been relatively little work done on the Summerville Formation. The first mention within published literature offered little description of the lithology and briefly described the bounding unconformity as "a conspicuous plane of discordance" (Baker *et al.*, 1927). In further work, they go on to describe the unit as thin-bedded red and white very-fine grained sandstones and maroon shales (Baker *et al.*, 1936). In modern literature, the depositional environment has been identified as a coastal plain. Whilst still a very brief description, it does provide the basis for more detailed interpretations such as sabkha, supratidal or hypersaline marine, wave-dominated deltaic and lacustrine (Anderson, 1992). Recent work by Zuchuat *et al.* (2018) provides the most accurate description of the Summerville as supratidal sabkha that in some areas occurred contemporaneously with the Curtis Formation, forming the coastal plain equivalent of the Upper Curtis marine deposits.

1.4.4 Morrison Formation

At the top of the Summerville is the J-5 surface, previously defined as an unconformity (Pipiringos & O’Sullivan, 1978) representing a bounding surface of the transgressive/regressive sequences present throughout the San Rafael Group (Holland & Wright, 2020). The Morrison Formation is split into three members, the Tidwell Member, the Salt Wash Member, and the Brushy Basin Member. In South-eastern Utah, the uppermost visible member of the Jurassic sediments is

the Salt Wash, providing an excellent characteristic boundary that can be easily identified across the region. The Tidwell is characterised in the Green River area by a thin layer of grey/green shales that are not laterally extensive. The Salt Wash Member is more defined and consists of approximately 80m of fluvial channels. The Brushy Basin Member is not present in South-eastern Utah and therefore not

recognisable in the study area; however, it has been identified as a lacustrine environment (Hintze & Kowallis, 2009).

1.5 Summary

This chapter addresses the study's aims and objectives and provides a comprehensive background for the evolution of the North American Cordillera, the

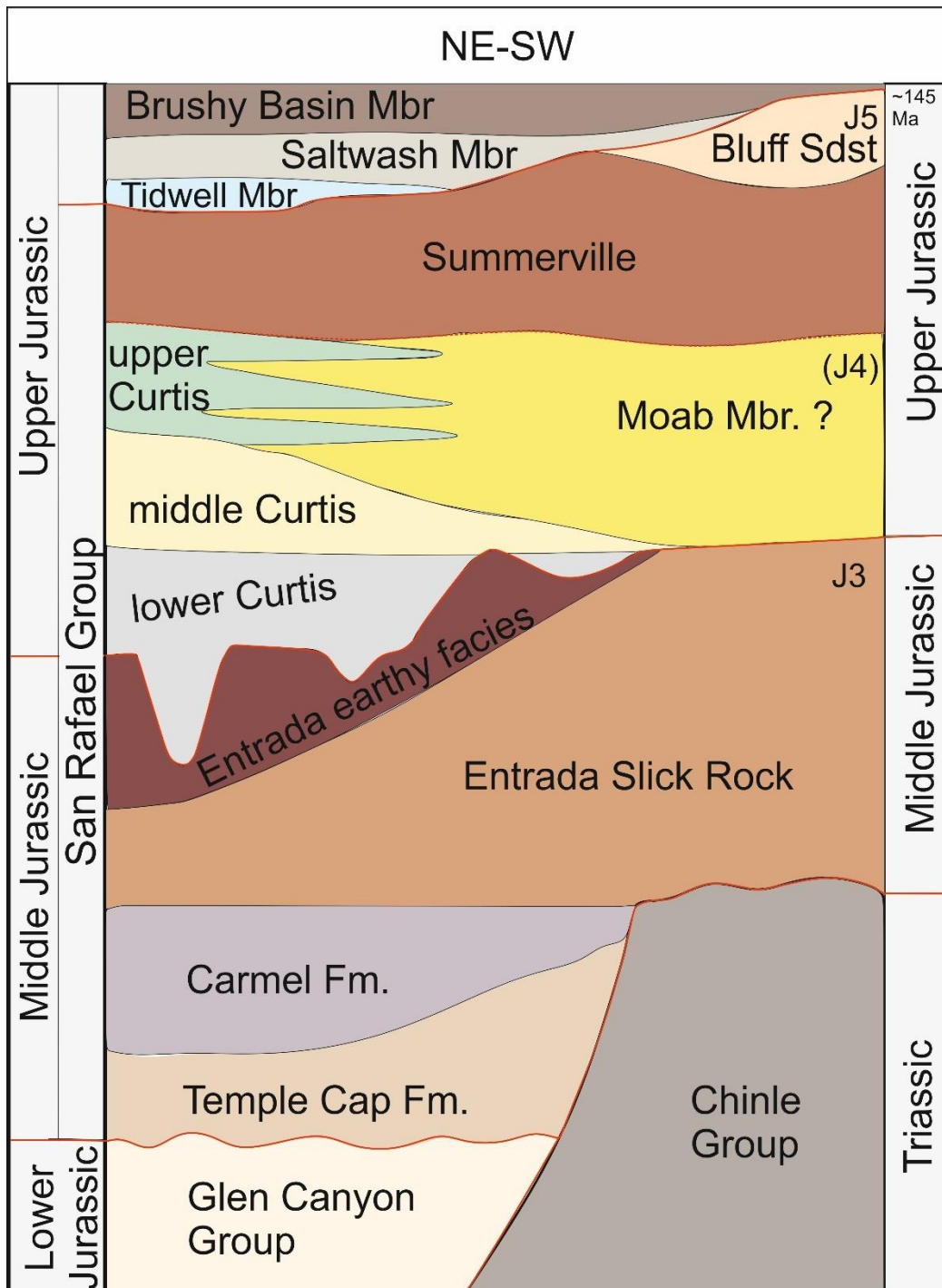


Figure 1.12- Summary of the stratigraphic units of the San Rafael Group, including the Entrada, Curtis and Summerville Formations as investigated by this study.

Colorado Plateau and the Curtis Basin. The aims include establishing local-scale interactions and significant bounding surfaces upon an aeolian-marine margin, to reconstruct the margin and document sea-level fluctuations upon it. This will be addressed by completing both statistical and geophysical analysis, critical to establishing environmental interactions upon the margin. The Middle and Upper Jurassic deposits of the Entrada Sandstone, Curtis Formation, and Summerville Formation in South-eastern Utah provide an opportunity to achieve this study's aims.

This succession was deposited within the Curtis Basin, a foreland basin that produced westward-thickening shallow marine, coastal and aeolian deposits preserved upon the modern-day Colorado Plateau. Prior to the coastal environment found in the Upper Jurassic Epoch, the area underwent a long history of fluctuating sea level, climate change and tectonics.

Chapter 2: Processes, Landforms and Environments

As the defined lithostratigraphy and previously studied deposits of the Colorado Plateau show, the dominant environments influencing the preservation of the Entrada-Curtis-Summerville succession are an aeolian system and a neighbouring shallow marine coastal margin. This chapter will detail the processes, landforms and depositional environments present within both of these systems and their interactions. This literature review will therefore provide a comprehensive summary of the features, facies and cyclicity as reference later in this study.

2.1 Aeolian Systems

Originating from the Latin “Æolus”, meaning “god of the winds”, or something which is “changeable, shifting, varied”, aeolian processes refer to the erosion, transport and deposition of materials via the wind. This can occur in any environment in which wind is the dominant transport process, and a threshold wind velocity and grain size have been met.

Some of the most characteristic landforms within the rock record can be found within aeolian environments. From kilometre-scale dune fields to centimetre-scale ripples, the variety of bedforms formed by aeolian processes, and the signature that they leave behind preserved in the rock record, are critical to establishing palaeo-environments and climates. The preserved expression of aeolian sediments varies considerably, both spatially and temporally. In addition to sedimentological diversity between proximal and distal successions, Palaeozoic, Mesozoic and Cenozoic aeolian systems all contain unique and characteristic aeolian strata (Rodríguez-López *et al.*, 2014).

Three main stages lead to the aeolian deposits visible within rock formations on the earth's surface today. These are described by Kocurek (1999) as the creation

of the dune field via the construction of a sand sea, accumulation of strata and finally, the preservation of the accumulated strata. This section will outline the current research into the processes, landforms, and structures formed within aeolian environments. Key terminology will be defined as per the most widely accepted uses, and these terms will be used to describe many concepts throughout this thesis.

2.1.1 Creation of the Aeolian System

The initial creation and sediment state of an aeolian system is controlled by three main factors, 1) sediment supply, 2) sediment availability, and 3) accommodation space available for deposition and consequently preservation of aeolian sediments (Kocurek & Lancaster 1999). Sediment supply defines the source material used either contemporaneously or with some delay within the aeolian system. However, sediment supply is not a reliable quantifier of how much sediment is used within the system as sediment availability; how much of the sediment is susceptible to transport, is also an essential factor. This transport capacity itself is mainly established through the wind, such that the velocity and sediment capacity can be used to determine the actual transport rate (Kocurek & Lancaster, 1999).

Sediment Supply

As with all processes occurring on the surface of the planet, aeolian processes are controlled by the laws of physics. This means that dunes and other related strata formed by the movement of grains by wind are defined by a threshold grain size and wind velocity (Bagnold, 1941). The size of the particles is the most significant controlling factor upon transport and formation (Kok *et al.*, 2012). As wind speed increases, particles of 100µm in diameter move via fluid drag. As wind speed increases, larger sand grains begin to move via saltation (Bagnold 1941, Shao

2008), the 'bouncing' of grains along a surface after the Latin *salto*, to leap or spring (Kok *et al.*, 2012). Particles with a diameter less than 100 μ m have cohesive forces too strong to be subject to aerodynamics and are therefore entered into short or long-term suspension due to ejection via the larger saltated particles (Shao 2008, Kok *et al.*, 2012). Grains of 500 μ m in diameter are also no longer transported via saltation, but due to their large inertia, they move by short 'bouncing' (reptation) and rolling or sliding (creep), and these particles account for a large percentage of wind-blown sediment transport (Durán *et al.*, 2011, Kok *et al.*, 2012) (Figure 2.1).

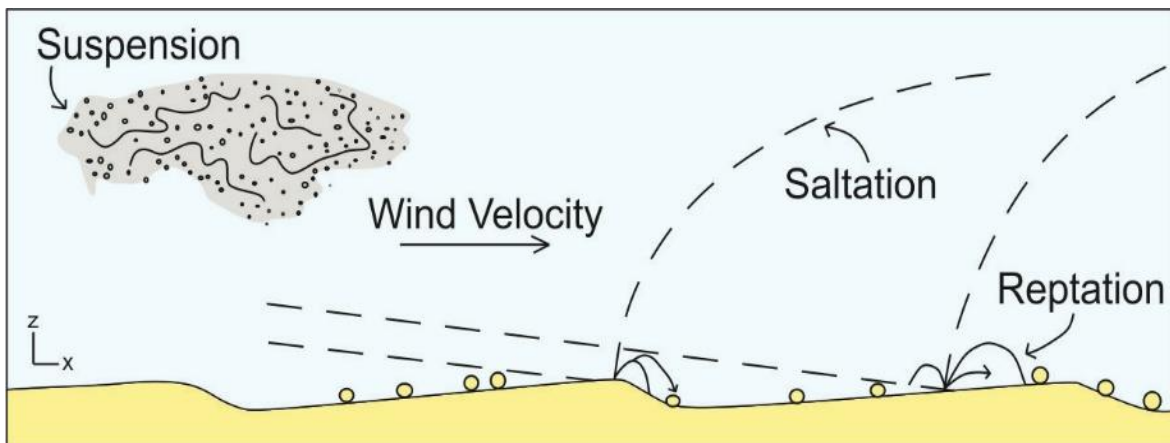


Figure 2.1- Modes of grain transport occurring in terrestrial aeolian systems, suspension particles are most affected by a threshold capacity and velocity of the transporting winds. Grains that are too large for entrainment are therefore transported via saltation or reptation.

Sediment Availability

The sediment availability of an aeolian system is determined by the sediment influx (Q_i), its output (Q_o) and the ratio between these factors. Whether the sediment budget is positive or negative can be established using the following equations.

For a positive sediment budget- $Q_i > Q_o$

For a neutral sediment budget- $Q_i = Q_o$

For a negative sediment budget- $Q_i < Q_o$

A positive sediment budget will result in accumulation; a neutral budget will produce a bypass supersurface, and a negative budget an erosive surface (Kocurek, 1988). The development of dunes and supersurfaces is key to the application of sequence stratigraphy within an aeolian system. The relative importance of the bounding supersurfaces and the processes that control them are identified differently within wet and dry aeolian systems. Dry aeolian systems are defined as “those in which the water table and its capillary fringe is significantly below the surface of deposition such that they have no demonstrable effect on the substrate” (Kocurek & Havholm, 1993). In addition, no stabilisation can occur, meaning that theoretically, all the sediment in the system is available. Within this environment, the development of supersurfaces is solely controlled by aerodynamics and the movement of wind-blown sand over interdune surfaces (Figure 2.2). The Upper Jurassic Entrada Sandstone in South-eastern Utah is an example of a wet aeolian system. These are defined by the water table and its capillary fringe existing at or close to the depositional surface (Crabaugh & Kocurek, 1993). In contrast to dry aeolian systems, accumulation, bypass and erosion are controlled exclusively by the position of the water table. A rise in the water table will promote deposition and accumulation, whereas a static or falling one will induce bypass or erosion, respectively (Figure 2.2, Kocurek & Havholm, 1993).

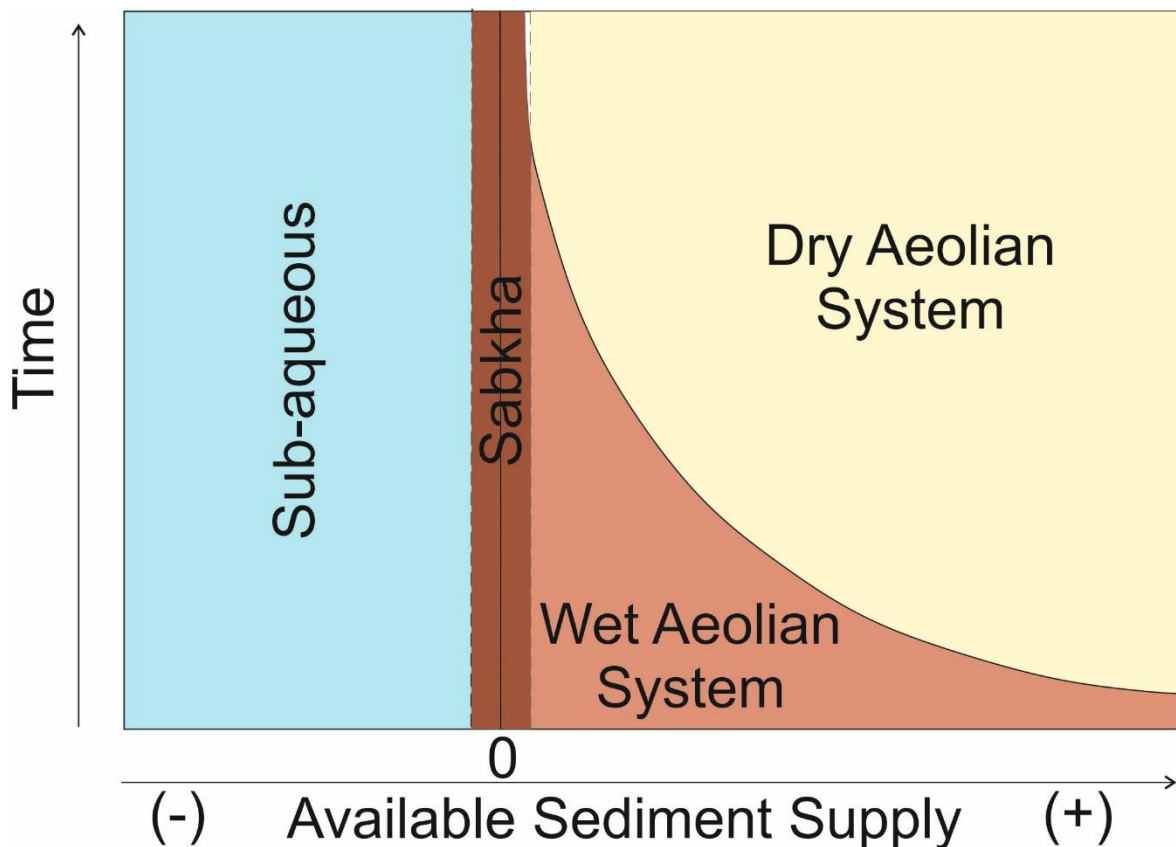


Figure 2.2- Changes in available sediment through time expressed in terms of different sedimentary environments (After Jagger, 2003).

Accommodation

The limit to the space in which sediment can be deposited is defined by the volume of air in the atmosphere and can, therefore, be observed to be theoretically infinite (Figure 2.3). In reality, the accommodation space is controlled by the parts of the lower atmosphere that have a significant enough air density and wind capacity with which to transport sediment. Sedimentation in the shallow marine realm is controlled by accommodation space and sediment supply. This relationship provides a base or equilibrium level marking the surface that separates erosional and depositional processes within a basin (Van Wagoner *et al.*, 1988).

The principal mechanism that defines the creation of accommodation space is subsidence. Subsidence can occur for a number of reasons, most commonly,

tectonism, sediment loading or sediment compaction. The magnitude of these factors also influences the changes in the rate of subsidence within a basin, that itself has a direct impact on the preservation of aeolian bedforms (Mountney et al., 1999). The most critical environmental change that occurs as a result of a change in subsidence is a change in the water table. This could occur for two reasons, (1) local subsidence resulting in a forced rise in the water table or (2) an absolute change in the water table related to a regional climatic shift (Mountney & Thompson, 2002). The accumulation and preservation of aeolian sediments is dependent on the maintenance of an overall positive sediment budget (Kocurek & Havholm, 1993). This ensures preservation of the climbing dunes and the maintenance of their size as they migrate (Rubin & Hunter, 1982, Mountney & Thompson, 2002). Therefore, the relationship between the rate of subsidence, the relative water table and the resultant depositional surface is therefore complex but critical in controlling the nature of the preserved stratigraphic record (Mountney & Thompson, 2002).

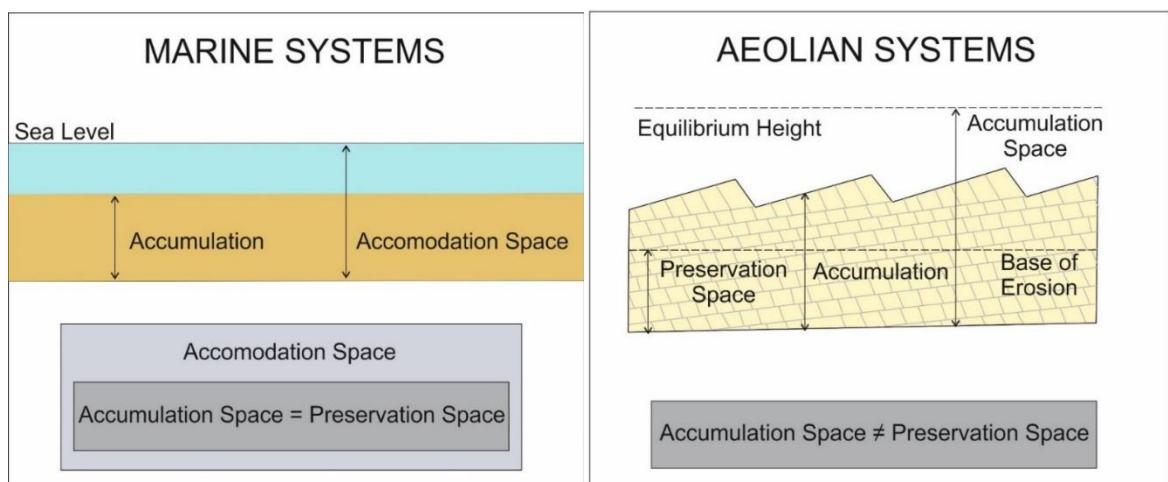


Figure 2.3-Comparison between the accommodation space in marine systems versus aeolian systems. This is important for the principles of sequence stratigraphy as discussed above (After Jagger, 2003).

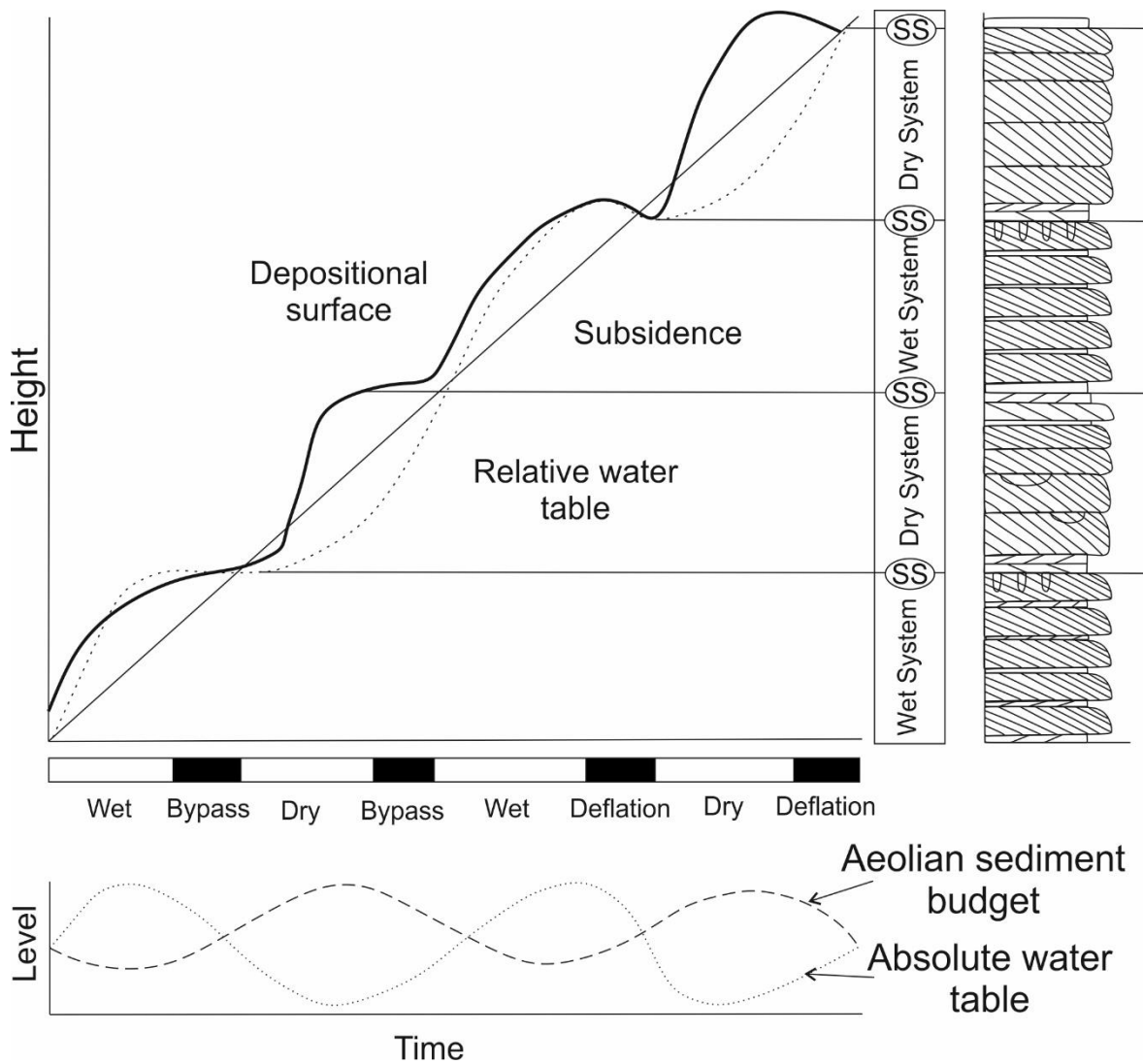


Figure 2.4- The role of subsidence in the deposition and preservation of aeolian sediments up succession. Note the relationship between water table and aeolian sediment budget, peak sediment availability occurs when the water table is at its lowest, as described above in dry aeolian vs. wet aeolian systems (After Mountney & Thompson, 2002).

2.1.2 Accumulation within the Aeolian System

Mechanisms for dune climb and accumulation can vary greatly between dry aeolian systems and wet aeolian systems (Kocurek & Havholm 1993, Crabaugh & Kocurek 1993, Mountney, 2011). In dry systems accumulation is typically controlled by the angle of climb, the trajectory of climb and the component of lateral bedform migration over time (Mountney, 2011). In wet aeolian systems there is an additional component dictated by the position of the water table in relation to the surface of deposition. The accumulation determined by these

factors therefore produces variable bedforms and structures that are characteristic of an aeolian system and will be described in more detail below.

If conditions relating to the sediment supply, sediment availability and accommodation space are met, as described above, then aeolian bedforms will accumulate upon the depositional surface. When combined with a sufficient sediment supply and threshold wind speed this produces several bedforms that are identifiable up to kilometres scale within the rock record. A bedform can be defined as “a regularly repeated pattern which forms on a solid surface because of the shearing action of a fluid” (Wilson, 1972). To differentiate between sands deposited in an aeolian setting and those in the marine realm, distinctions between bedforms can be made. These separate structures into three categories based on size, which, when plotted on a graph of wavelength vs grainsize, show distinct classes with no overlap between the fields (Wilson 1972, Figure 2.4). Ripples, dunes and draa coexist together in quasi-equilibrium and not as a transitional system, such that ripples reach a maximum height and width and hence do not become dunes (Figure 2.5).

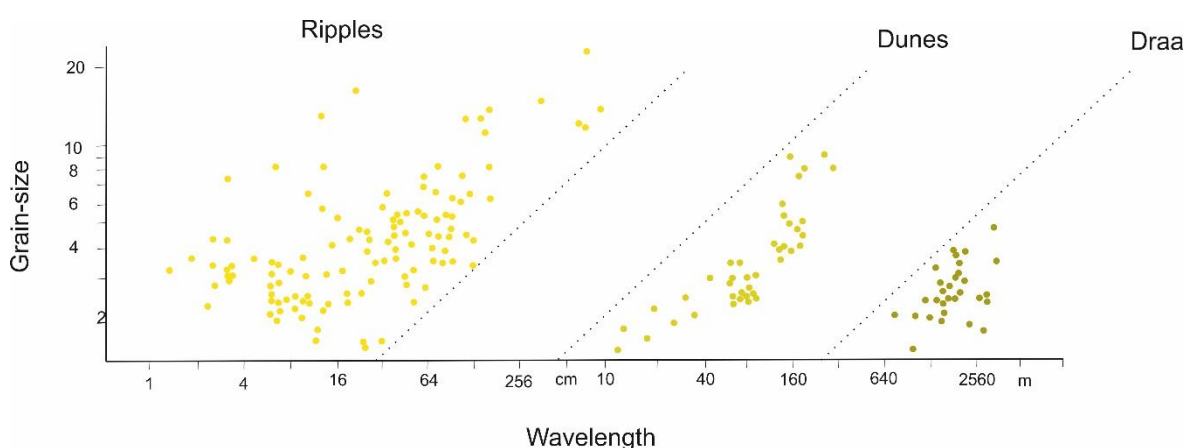


Figure 2.5- Scatter plot of grain-size against wavelength for aeolian bedforms. There are no transitional forms between the three groups A, B, C, which correspond to ripples, dunes and draa (After Wilson, 1972).

Grainfall and Grainflow

The mechanisms of grainfall and grainflow are the most identifiable and characteristic feature representing accumulation within an aeolian bedform; they are an incredibly useful tool in the field when establishing the depositional environment (Figure 2.6). Grainfall/grainflow strata and stratification occur as a result of the three main types of deposition on dunes: 1) ripple migration, 2) fallout upon the lee slope, 3) lee slope avalanches (Hunter 1977). Grainfall deposits are represented by millimetre thick laminae, comprising very fine-grained sand, and are deposited due to fallout on the lee slope of dunes. This occurs due to the decrease in velocity and hence the load capacity of the wind as it moves over the dune crest. Wind dynamics also control the mechanics of grainflow, most readily impacting smaller grain sizes that are of the minimum radius with which the force of the wind can lift and transport it. When experimental tests were carried out to determine the exact behaviour of grainflow, it was established that the depositional bedforms reached a maximum angle at which there was slope failure, and the flow began to migrate down-slope (McDonald & Anderson, 1996). These tests also determined that grainflow thickness is controlled by the size of the dune such that, for dunes whose length equals the natural run-out length of a grainflow, a minimum flow thickness will be reached. However, for dunes of greater length, the grain flows are likely to merge, leading to the slope failure of a much larger mass and hence a thicker grainflow deposit (McDonald & Anderson, 1996).

It is important to note that the relationship between maximum slope height and slope failure is not consistent and therefore extrapolating this information from foreset thickness should be taken as an estimation (Kocurek & Dott, 1983). In the Jurassic deposits of Utah, one relevant influence on grainflow is dinosaur tracks, that may trigger and deform grainflows on dune slip faces (Loope, 2006).

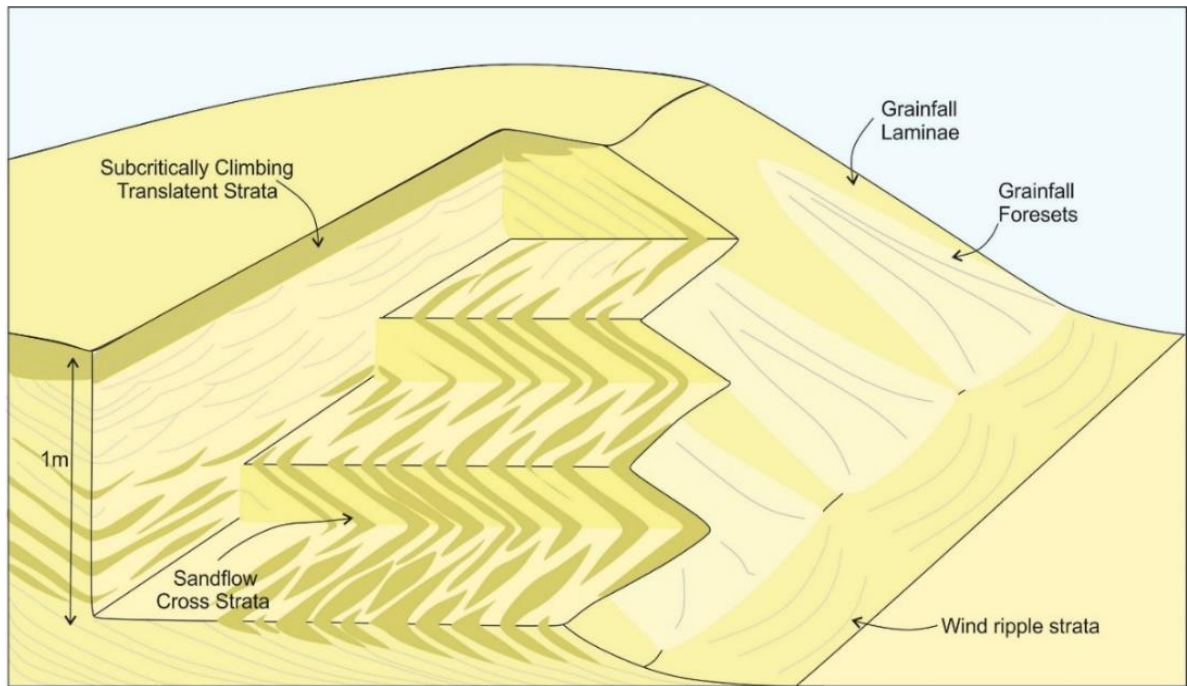


Figure 2.6- Cross-section of an aeolian dune form (After McDonald and Anderson, 1996).

Ripples

Ripples are small-scale aeolian structures that form regular patterns of ridges and troughs within a wind-blown sand environment. They have an average wavelength of between 0.5cm-20cm and most typically propagate transverse to the prevailing wind direction. Another characteristic feature is that the ridge crests of ripple forms, similar to that of dune forms, are almost invariably coarser than the troughs. This allows a distinction between ripples that form subaqueously and those that form in an aeolian environment, termed ballistic ripples. The principal transport method responsible for the formation of ballistic ripples is saltation. Small depressions are generated from the oblique collision of saltating particles upon the surface of a sand bed. As the particles collide, a chain reaction is initiated in which more particles are thrown into suspension, and larger grains are subject to reptation, moving forward several grain diameters as a result of impact (Kok *et al.*, 2012). The asymmetric profile (gentle windward slope and steep lee slope) caused

by the creation of the small depressions leads to the stoss slope receiving more impacts than the lee-side. This promotes growth and provides a mechanism for the windward transportation of the ripples (Leeder, 2011). If this pattern continues under steady conditions, the ripple forms will reach a 'fully developed state', transverse to the wind direction (Seppälä & Lindé, 1978). The bimodal grainsize that is observable within preserved successions containing ballistic ripples is caused by the concentration of fine sand and silt particles within troughs and the migration of coarser-grained crests over these. In contrast to subaqueous ripples, no cross-lamination is visible within the ballistic ripples. Less bombardment and avalanches result in differential accretion on the lee side of the dune hence the lack of internal structure (Leeder, 2011).

Dunes

Dune bedforms are larger in scale and can be anywhere between 3m-600m in wavelength and 10cm-100m in height (Nichols, 2009). By contrast to ripple forms, dunes are large enough to be impacted by hydrodynamic instability; however, unlike ripples, they require a starting mass that creates an anomaly in an otherwise planar profile, leading to the natural flow pattern of the wind being offset (Kok *et al.*, 2012). A differential pressure forms on the stoss side of the dune, which forces the material to move along the slope and down the lee side, creating a variety of characteristic geometries. As eddy currents form in the shadow of the dune at any scale, there is no limitation on the scale at which the dune can form, and scale is instead controlled by the starting mass with which the hydrodynamic instability stemmed from in addition to the available sediment supply. This promotes a strong variance in the scale of dunes and their morphology such that the shape of dunes is not necessarily controlled by the starting shape but rather their size (Kok *et al.*, 2012). The classification of these dune forms is somewhat

complex, and there currently is no single scheme that fully encompasses the vast array of environments within which dune forms can be found (Wiggs, 2019). The initial classification distinguishes between ‘free’ and ‘anchored’ dunes, defining mobile and stabilised by vegetation, respectively. Further distinction divides dune forms by the most prominent dune types found within desert environments. However, this is not a comprehensive list, as there are often more complex morphologies interacting. The dominant dune-type is dictated by wind variability and sand availability; low variability and supply lead to more simplistic dune-forms such as barchans, whereas bi-directionality leads to star and network dunes (Wasson & Hyde, 1993).

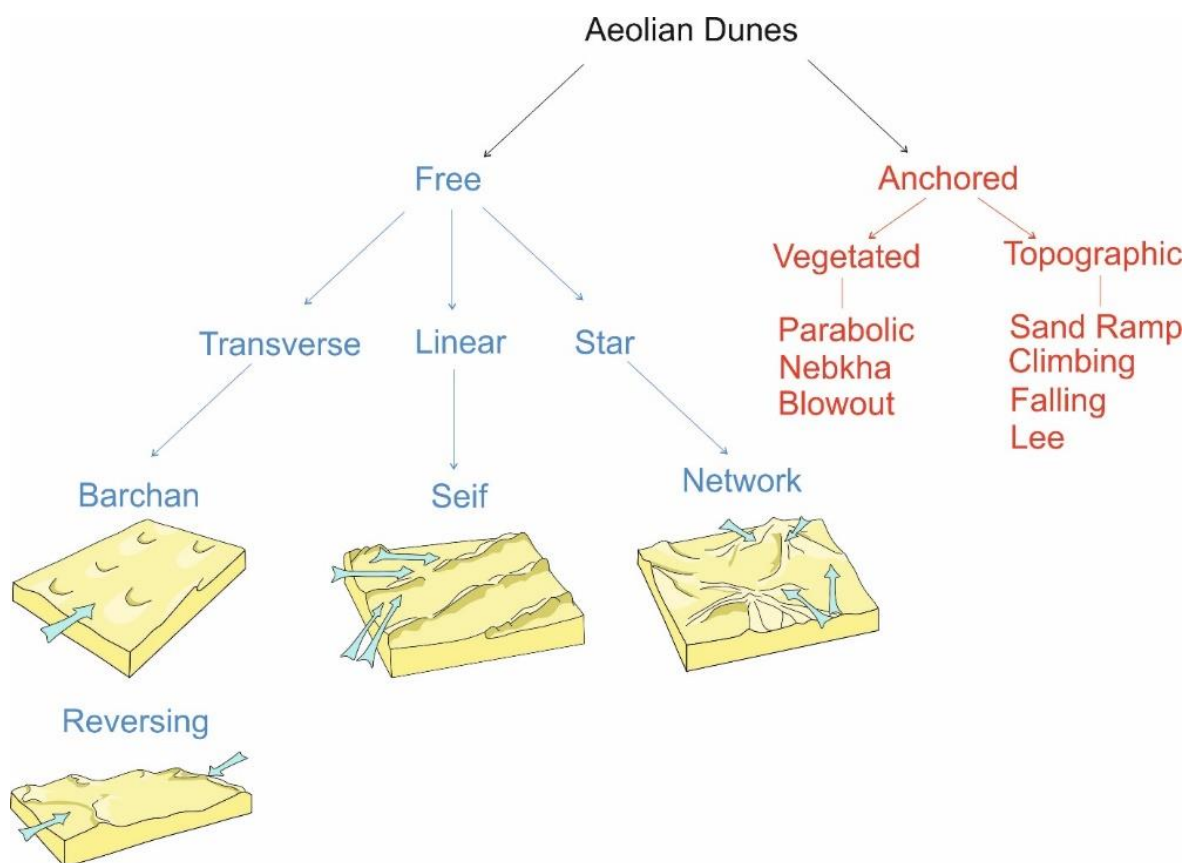


Figure 2.7- The most comprehensive classification of dune-forms currently within the literature, with illustrations demonstrating the various morphologies and their dominant wind-directions (After Cousins 2020, Fryberger et al., 1966).

Draa

In aerial view, some dune-like features can be picked out that appear to be on the kilometres scale and are entirely separate from the dunes superimposed upon them. These structures form the same morphologies as dunes; however, in contrast to grainfall and grain flow patterns on the lee slopes, draa structures often have dunes on their stoss slope and a single slip face on the lee slope. Evidence shows that draa will only be absent in areas where there has not been sufficient time for nucleation to occur or if the sand cover is too thin to promote significant landform development. In areas where more than 10,000 years have passed, and the sand thickness was consistently above 3m, draa would be present within most erg systems (Wilson, 1972).

When considered 'dunes but on a larger scale', the classification of draa can be divided into three categories (McKee, 1979).

- 1) Simple: single or bifurcated ridges with narrow crests, with no secondary or superimposed bedforms.
- 2) Compound: linear ridges that have superimposed bedforms of the same morphological type, which may intersect or spread obliquely from the main ridge.
- 3) Complex: narrow or broad linear ridges where the superimposed bedforms are of different morphology.

Sandsheets

Sand sheets often mark the transitional relationships between aeolian ergs and their surrounding environments. Within the rock record, they can account for significant accumulations of low angle, often rippled or undulating stratification, formed by the lack of slip faces on the dune forms themselves. The limiting factors

that promote sandsheet formation as opposed to dune formation are as follows (Kocurek & Neilson, 1986).

- 1) A high water table- introducing water into the dune system increases the wind velocity required to move individual sand grains as a result of capillary water tension. Increasing the water table at the same rate as the supply of sediment to the basin leads to a constant limit to the amount of dry sand available for dune formation and hence promotes the creation of sand sheets.
- 2) Surface cementation or binding- Limits the availability of dry sand through adhesion structures on the dune surface. This mechanism is prevalent in coastal marine/ sabkha environments.
- 3) Periodic flooding- Regions at or below sea level and have a particularly flat topography are often subject to seasonal inundation. The increase in water run-off across the system leads to the denudation of dune forms into large expanses of sandsheet.
- 4) A significant coarse-grained sediment population- In addition to capillary tension, the size of grains also impacts the minimum wind velocity required for movement, i.e., the larger the grains, the greater the wind speed required.
- 5) Vegetation- Extensive rooting has the potential to stabilise dune fields, whilst vast amounts of bushes and grasses can lower wind speeds near the dune surface, promoting small dune forms that ultimately fail and flow into sheets.

Interdunes

Two main geometries are prevalent within an aeolian interdune system. Firstly, an elongate interdunal geometry is likely to arise from a rising water table

encroaching into a sand sea (Handford 1981, Mountney and Thompson 2002). Secondly, new research has identified that the edges of many active sand seas are likely to contain sheet-like aeolian sabkhas where deflation is limited by the position of the water table, exposing large expanses of erosional sandflats, which can promote aeolian sabkha development within the continental interior (Ginau *et al.*, 2012, Warren 2016). These end-member scenarios are directly controlled by the sinuosity of the bedforms.

Dry interdunes are distinguishable from dune forms and from the other types of interdunes by parallel laminated sands that have wind ripples superimposed upon them. Damp interdunes often feature discontinuous ripple laminated beds. There may also be evidence of life, as the shallow water and stable surface provide an ideal platform for rooting desert shrubs. The prevalence of damp/ wet interdune strata within an aeolian system, more specifically, sandwiched between climbing dune forms, leads to the description of the system as a 'wet aeolian system', a perfect example of which is the Jurassic Entrada Sandstone in South-eastern Utah (Crabaugh & Kocurek, 1993).

2.1.3 Preservation of the Aeolian System

For an aeolian succession to be preserved, it must develop below the regional baseline of erosion. Dune accumulation can occur above the line of erosion; however, preservation potential is then lowered. This can only be reversed if the level of the water table changes or there is increased subsidence (Kocurek & Havholm, 1993). The creation of the aeolian system and the processes of accumulation as described above, can lead to a variety of preserved structures. Climbing bedforms produce cross-bedded sets bound by set bounding surfaces, stacked into cosets that are then bound by super surfaces, extending beyond

outcrop scale. The interactions between sets, cosets and the preserved morphologies produce the aeolian rock record that is visible today.

Stratification

Ripples, dunes and draa each preserve a unique morphology within the rock record, often referred to as stratification. At the smallest scale there are (approximately) six types of recognisable strata, planebed laminae, rippleform laminae, ripple-foreset cross laminae, climbing translantent strata, grainfall laminae, and sand flow cross-strata. These types of stratification are largely influenced by the any of climb of the rippleform within a dynamic aeolian system. Where the angle of climb is less than the angle of the stoss slope, subcritical climb will occur, where equal critical climb will occur, and where the angle of climb is greater than the angle of the stoss slope the ripples will supercritically climb. Each of these outcomes will produce a different preserved type of stratification (Figure 2.8, Hunter 1977).

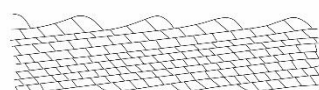
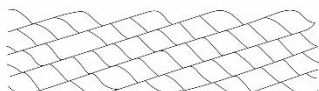
		Translatent strata	Rippleform laminae	
Angle of ripple climb (a) relative to inclination of ripple stoss slope (B)	Subcritical	 Subcritically climbing translantent strata	Incomplete rippleform laminae (ripple-foreset crosslaminae)	 Truncated ripple-foreset crosslaminae
	Critical	 Critically climbing translantent strata		 Complete ripple-foreset crosslaminae
	Supercritical	 Supercritically climbing translantent strata	 Complete rippleform laminae	

Figure 2.8- Illustration of the types of stratification visible at ripple scale within an aeolian succession (After Hunter 1977).

The descriptive terms of cross-bedding and trough cross-bedding were introduced in the 1950s and were used to determine the layering and structure within sedimentary rocks. Cross-bedding or cross-stratification is used to denote the arrangement of such layers at one or more angles to the bedding. This led to the classification of stratification into three categories (McKee & Weir, 1953). Simple cross-stratification defines cross-bedding in which the bases of the sets are non-erosional. Planar cross-stratification refers to cross-bedding in which the lower bounding surfaces of the sets are erosive, trough cross-stratification to cross-bedding where the lower bounding surface of the sets present as curved surfaces of erosion.

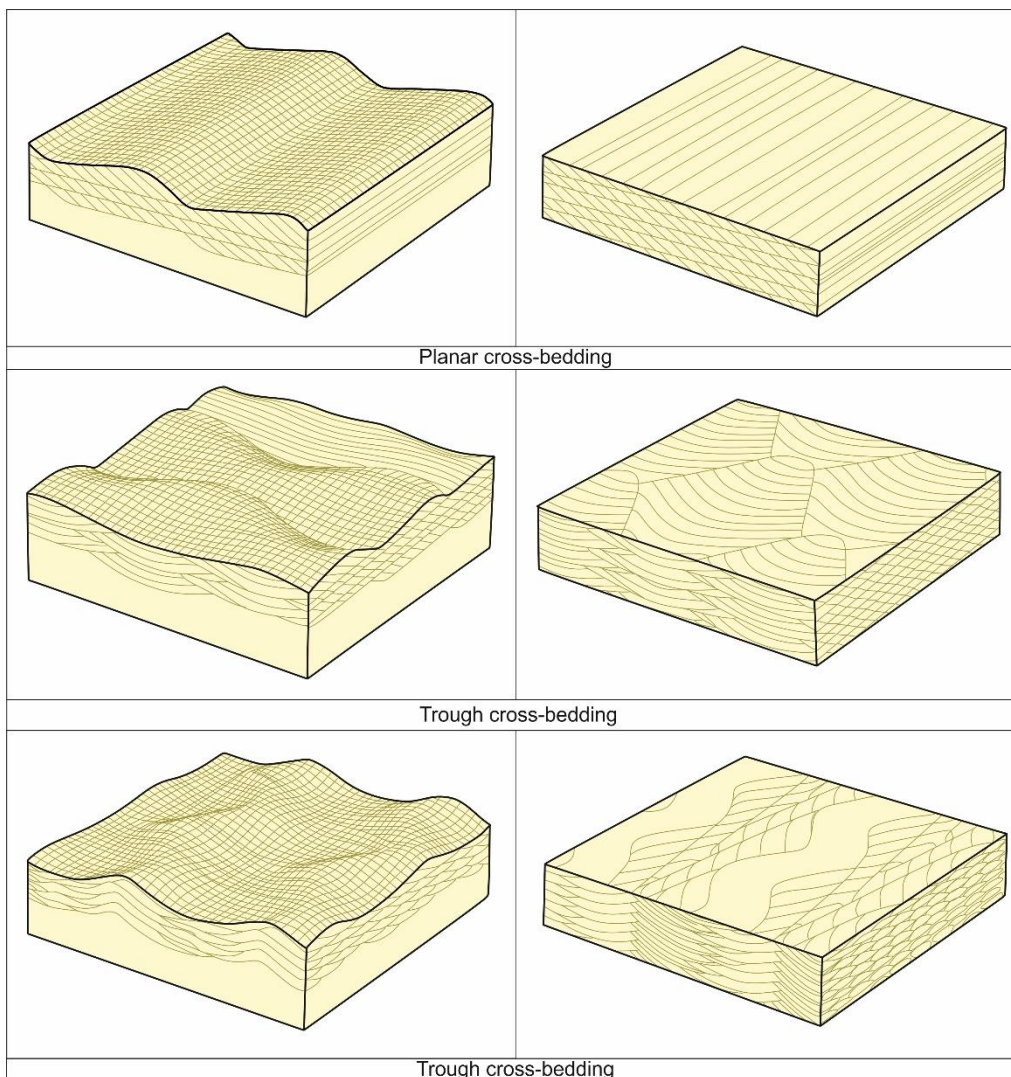


Figure 2.9- Types of stratification as 3-D models and as horizontal and vertical cross-sections (After Rubin & Carter, 1987).

Bounding Surfaces

Dune, interdune relationships and marginal interactions produce bounding surfaces, which are the most visible part of the aeolian system in a preserved succession. Bounding surfaces can be found at all scales representing a different sedimentological characteristic at each. The slopes of grainflows that make up the previously described cross-stratification are referred to as foreset bounding surfaces, this term can be applied to the smallest of boundaries between foresets (Allaby, 2013). Depending on the type of dune climb, i.e., sub-critical, critical, and super-critical, the top and base of the foresets may be asymptotic. The point at which this asymptote is truncated by a surface above and below is known as a set bounding surface. The layer of sediment found between two bounding surfaces is a set. If a number of these sets are preserved within a succession, this is known as a coset, providing they share the same features such as grainsize and set thickness (Allaby, 2013). An alternative to foreset is the term 'cross-set'; this describes any preserved cross-stratification between two bounding surfaces. These terms can be used interchangeably. In circumstances where the bedform that produced the cross set is preserved and forms the top bounding surface, the term 'form set' can be used. It is important to note that these bounding surfaces can be found on a millimetre scale; however, beds are hereafter referred to as laminae, and cross-stratification then becomes cross-lamination.

These interactions and their bounding surfaces are summarised below (Figure 2.10). Note the introduction of the term reactivation surface, this here refers to a supersurface that has been preserved by bypass or deflation has occurred within a dune field, followed by a renewal of sediment supply that has caused the dunes to begin migrating and crucially preserving, once again (Figure 2.10, Figure 2.11).

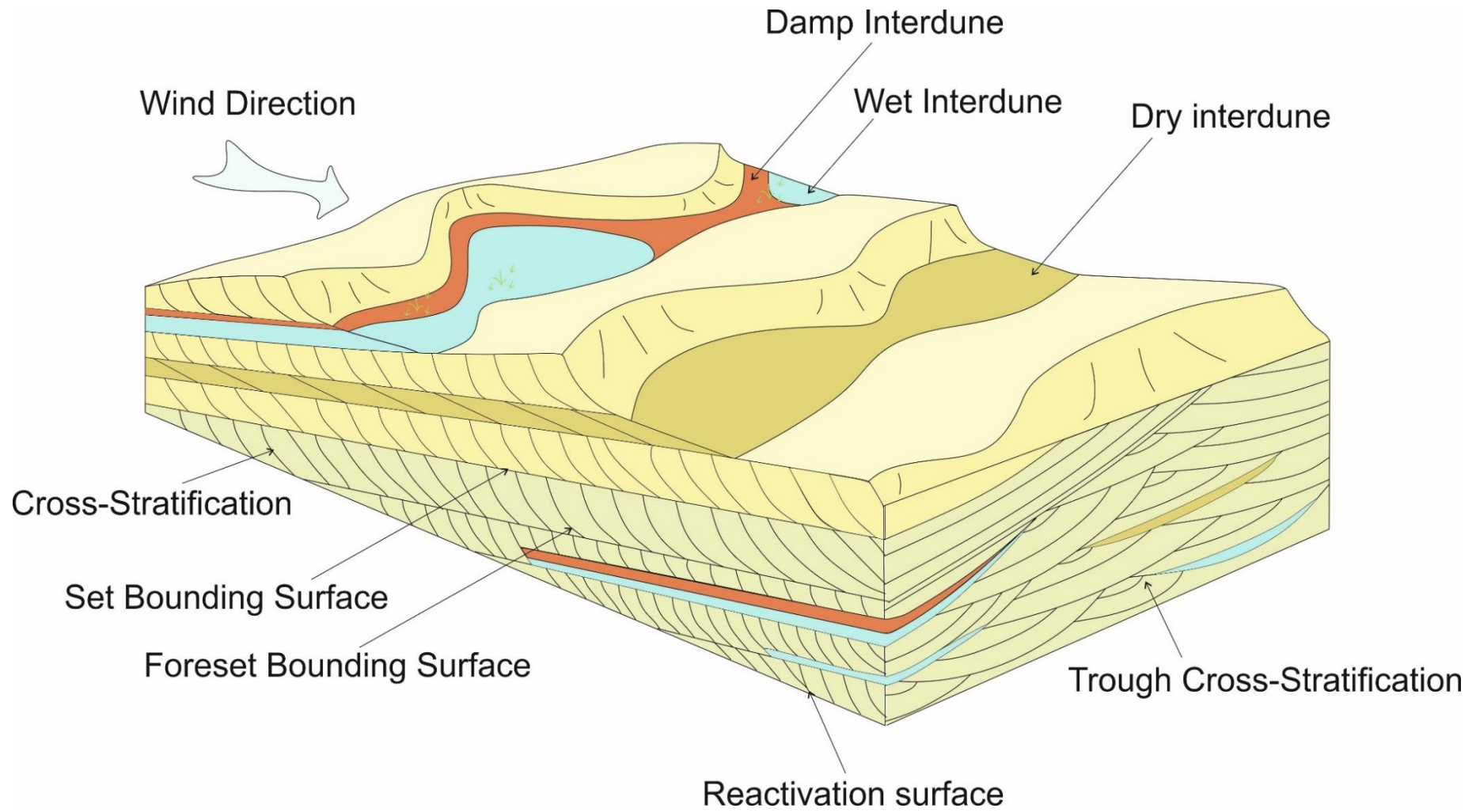


Figure 2.10- Interactions between dunes and interdunes at the surfaces and the geometries preserved in the subsurface (After Pettigrew 2019, Jagger 2014).

In addition to the smaller scale bounding surfaces, a number of large-scale surfaces can be identified that can occur basin-wide and represent significant changes, both environmental and geographical, within the erg system. These are known as super surfaces, of which there are three main categories (Kocurek, 1988). Firstly, bypass surfaces are brought about by changes in sediment supply, leading to the lack of accumulation of dune forms. Secondly, deflation and flooding surfaces: the termination of dunes as a result of fluctuating sea levels or global climate change. The last category of supersurface is formed by the migration of the ergs, a decrease in sediment supply or a change in wind direction, causing re-deposition with a new orientation (Figure 2.11).

Regarding the aeolian system, bounding surfaces can most easily be established via a change in sediment flux. A change from a positive sediment flux (dune accumulation) to negative sediment flux (dune depletion) will lead to erosional or deflation super-surfaces that therefore bound dune accumulation. These packages of accumulation and their respective bounding surfaces form the building blocks of aeolian sequence stratigraphy, in the same way as parasequences and chronostratigraphic surfaces do in the marine realm. Whether the aeolian system is dry, damp, or wet impacts the position and cause of bounding surfaces within the succession (Kocurek & Havholm 1993). In a dry system, the supersurface is closely related to the overall aerodynamic conditions in the system, i.e., wind speed controls the accumulation potential of the dune system. Within damp or wet systems, the sediment flux is related to the position of the water table as well as the aerodynamics. A drop in the water table allows for a greater amount of sediment to be available for transport and hence the accumulation of dune forms. A rising water table has the reverse effect, binding more sediment and hence decreasing the amount available for transport (Mountney, 2006). As a result, the

angle of climb of the dunes decreases and the dune field begins to diminish.

Supersurfaces in the succession at this point mark the highest point of the water table during times of peak humidity (Mountney, 2012).

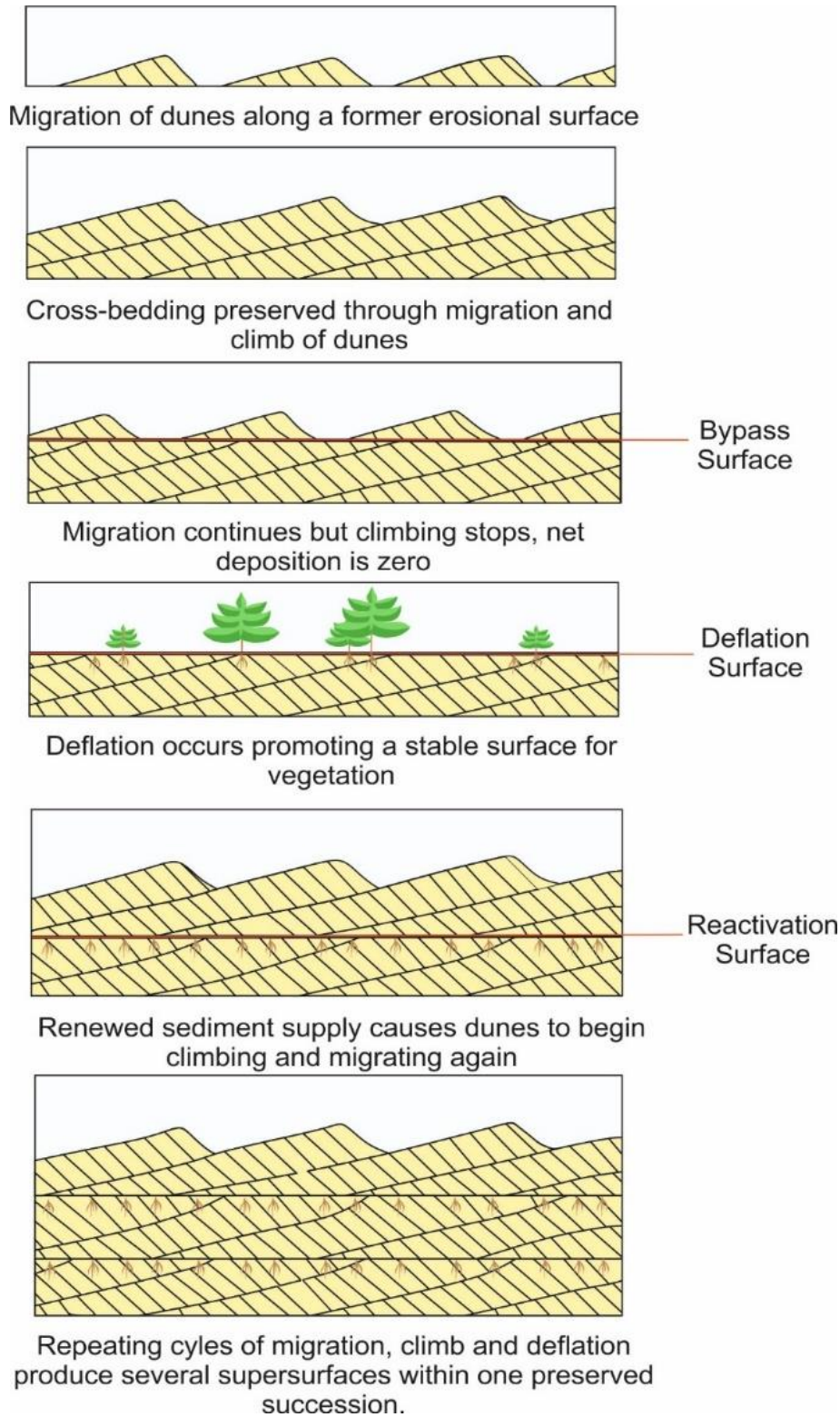


Figure 2.11- Stages of super-surface development within a preserved aeolian succession (After Wakefield 2010, Loope 1985).

Non-aeolian Structures

In addition to structures such as ripples, cross-bedding and erosive surfaces, aeolian successions can also contain many key features that are not directly caused by wind or wind-related processes and are instead caused by a range of chemical, physical, and biological processes. Chemical changes in the atmosphere can cause increased erosion, as can increased amounts of subsidence due to tectonic movement. Arguably the most recognisable non-aeolian structures, however, are biological in nature. These can include things such as trace fossils, evidence of burrowing or algal mats, and rhizoliths (Figure 2.11, Loope, 1988).

Interdunes can also preserve some atypical structures not commonly found within a dry aeolian system. These can include subaqueous ripples, wavy laminae and soft-sediment deformation through adhesion warts, bioturbation, and desiccation cracks.



Figure 2.12- Plant or tree root preserved within the Moab Member of the Curtis Formation, the white ring is sediment that has been bleached by organic acid circulating between the root and the sediment itself, the root itself is not preserved and is instead represented by the smaller dark circle in the center.

2.1.4 The Role of Climate & Controlling Factors

Sequence stratigraphy is defined as “the study of rock relationships within a chronostratigraphic framework of repetitive, genetically related strata, bounded by surfaces of erosion or non-deposition, or their correlative unconformities” (Van Wagoner *et al.*, 1988). In simpler terms, it is the relationship between cyclic successions deposited either during transgression or regression, or in cases where no deposition occurred, or the deposits have been eroded the relationship between the erosive and unconformable boundaries. The concepts and principles of sequence stratigraphy are crucial to the understanding of climate cyclicity within successions. It is most effective within the marine realm, due to easily recognisable flooding, regression and clinothem bounding surfaces, however, by using different characteristics and horizons that indicate sea-level fluctuations, the principles can also be applied in the continental realm.

The principles of sequence stratigraphy were first developed by Sloss (1963) and was built upon by further authors (Mitchum *et al.*, 1977, Vail 1987, Posamentier *et al.*, 1988) until the Exxon team (Van Wagoner *et al.*, 1988) pioneered the standard model for sequence stratigraphy, referred to as the “Exxon Model”. More recent work has endeavoured to standardise the terminology within sequence stratigraphy (Catuneanu 2017, 2019, 2019), quantify trends within parasequences (Ainsworth *et al.*, 2018), and even take the principles of sequence stratigraphy to the extra-terrestrial realm (Barker & Bhattacharya 2018).

It is known that the relative sea level and climate allo-controls are somewhat related through a complex system of feedback loops (Shanley & McCabe, 1994). Therefore, it is not entirely without reason to suggest that the two can be regarded in the same way with respect to influences upon an inland basin versus a shallow-

marine shoreface. In the same way that as sea level falls, the rate of sediment supply outpaces the rate of creation of accommodation space (sediments prograde), as the climate becomes drier, the position of the water table no longer rises quickly enough to match sediment supply, promoting the development of dunes. By contrast, a drop in sea level causes shallow marine sediments to retrograde, whereas a wetter climate in an aeolian setting promotes the growth of sand sheets. It can, therefore, be established that some facies and geometries can be just as representative of the environment within an inland basin, completely unaffected by sea level, as they can in a marine realm (Clemmensen et al 1989, Galloway 1989).

Aeolian Sequence Stratigraphy

The same allocyclic control apply in aeolian systems as in marine environments, as discussed these are climate, tectonism, eustasy and sediment supply (Mountney et al., 1999). Each of these factors have a distinct influence deposition and preservation of deposits and their bounding surfaces. From this it can be suggested that aeolian sequences and supersurfaces correspond to sea-level fluctuations and could be correlated with global eustatic cycles as in the marine realm (Talbot 1985, Kocurek 1984, 1988, Crabaugh & Kocurek 1993, Galloway et al., 1996). Critical to this hypothesis is the definition of an aeolian supersurface as the end of an accumulation event. A change in sediment flux alters accumulation within a dune field, hence a unit bound by a supersurface represents a basic unit bound by a change in conditions above and below, parallel with the definition of a 'genetic stratigraphic sequence' (Galloway 1989, Pye 1993).

The complexities of these controlling factors, however, make confidently identifying sequence stratigraphical boundaries and units within aeolian successions challenging. If the position of the water table is a component of

relative sea-level in the study area (which it is likely to be in a tidally dominated marine margin), then inferring water table behaviour in the rock record will provide an indication of sea-level fluctuations. Any wider inferences however would not be possible as sea-level rise (or fall) related to tectonism or eustasy are almost impossible to distinguish between (Havholm et al., 1993, Havholm & Kocurek 1994). A number of other problems associated with correlating arid aeolian successions within a sequence stratigraphic context are described by Howell & Moutney (1997).

With the introduction of spectral gamma ray logging, it has been possible to correlate across a basin with a range of environments. George & Berry (1993, 1994) highlight that in complex desert lake sequences, drying upward cycles are often subjective, however, it is possible to identify changes in environment through the occurrence of peaks in the gamma log.

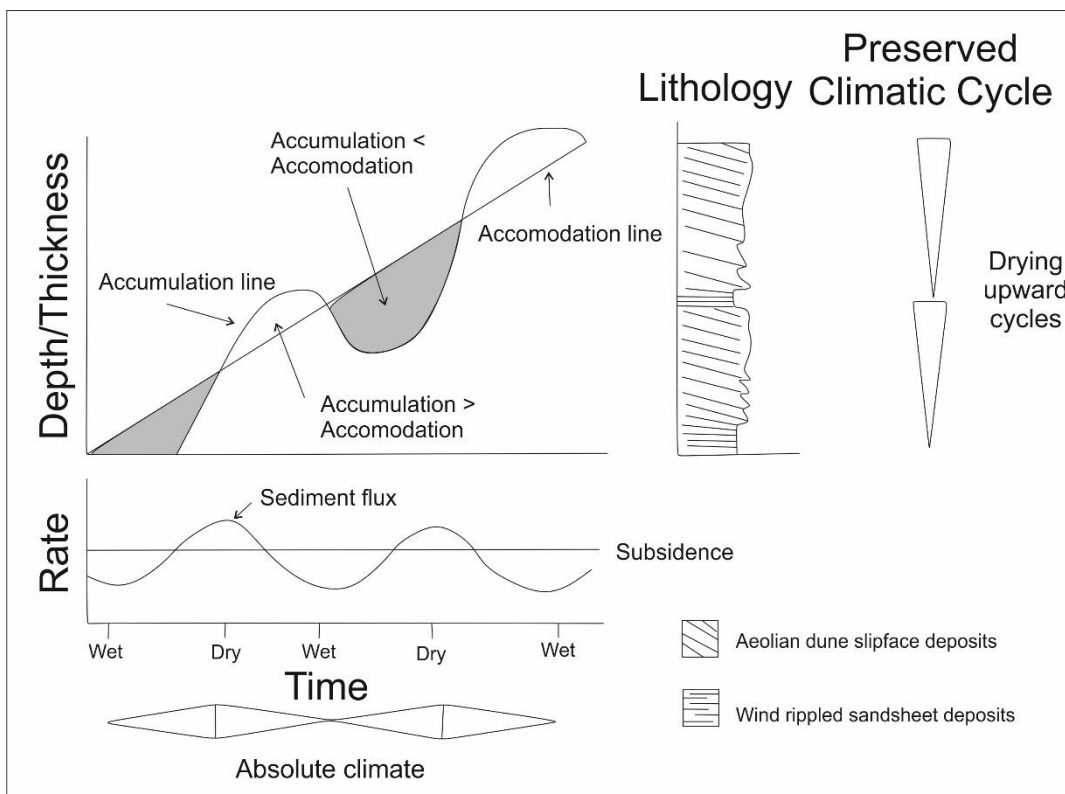


Figure 2.13- Interactions of climate and subsidence in sediment supply and preserved deposits within the principal depositional environments. Supersurfaces created by changes in accumulation can be regarded as sequences and linked to drying upwards cycles as shown (After Howell & Moutney, 1997).

2.2 Coastal Plain Environments

“Amongst the landforms which geographers have occasion frequently to describe, none suffers more from the unsatisfactory condition of geographic terminology than do the various types of plains of deposition” (Johnson, 1916). Unfortunately, this statement is still partially true today, with a coastal plain being described as “a flat, low-lying region of land adjacent to a seacoast”. This broad definition, geologically speaking, can contain various facies and environments, including sabkhas, lagoons, channel systems, palaeosols, and evaporitic pools.

Coastal environments represent the transition from the continental realm to the marine realm. They can be characterised by various features, each unique to the depositional environment and its contemporaneous settings. By contrast to the aeolian processes and landforms described above, coastal processes are poorly understood, and the environment is often used as a sweeping statement to describe a range of sub-environments. Most common within the coastal region of an aeolian marine margin are sabkha, tidal flat and lagoonal environments. In addition to the preserved facies along the coast, there are often partially vegetated palaeosols representing sub-aerial sections largely unaffected by tidal processes.

Current research documents the occurrence of sabkhas and tidal flats within modern successions using case studies such as Shark Bay, Western Australia (Logan & Cebulski 1970, Logan 1974, Ferguson & Skyring 1995, Jahnert & Collins, 2013) and within preserved successions such as the Permian deposits of the Texas Panhandle (Handford 1981, Handford 1991, Warren 1991, Andreason 1992).

2.2.1 Sabkha

The term sabkha is used to define a region of continental salt flats with an equilibrium geomorphological surface in which evaporites are formed above the capillary fringe of a shallow water table (Warren, 1991). Sabkha environments can be found within three dominant settings: marginal-marine, continental, and aeolian interdune (Handford, 1981). The transition between these environments, notably between coastal and continental sabkhas, can often occur with no noticeable changes in lithology or morphology such that the classification of sabkhas can be considered a continuum (Warren 1989). Depositional environments can be shallow-subaqueous; however, sub-aerial muds characterise the large majority of deposits.

Aeolian Sabkha

Aeolian interdune sabkhas represent the wet or damp environments that allow for shallow water pooling, the concentration of solutes, and evaporite formation between migrating dunes. They exclusively form in damp or wet aeolian systems, which are characterised as those in which the water table or its capillary fringe is at or near the accretionary surface. Expanses of interdune sabkhas develop between dune-forms as deflationary basins, whereby sedimentation occurs mostly as a mixture of wind lag and suspension settlement (Handford, 1981). In addition to providing sediment, wind processes can also modify interdune sabkhas during active periods by developing scattered dunes and adhesion ripples upon the surface.

Aeolian dominated sabkhas can be further categorised based on their evaporite to siliciclastic matrix ratio. If there is relatively little evidence of preserved capillary salts, then the sabkha can be classified as detritally-dominated or wet-aeolian.

However, if capillary salts are abundant, it is referred to as chemically-dominated or saline-aeolian.

Fluvio-Lacustrine Sabkha

Within entirely continental environments, sabkhas preserved within the rock record are dominated either by fluvial or lacustrine processes. Continental sabkhas are defined as part of a playa mud-flat complex in which the capillary fringe intersects the landscape (Warren, 2016). The transition between the highland continental and the saline basin floor takes place gradually from alluvial fan/ ephemeral stream/ floodplains to sand flats, dry mud-flats, saline mud-flats and finally saline pans (Figure 2.14). Saline lakes contain mud-flats, sabkhas and saline pans within three individual settings, an alluvial fan-ephemeral saline lake setting, an ephemeral stream or dune field–ephemeral saline lake or a perennial stream floodplain–perennial saline lake setting. Although these environments form

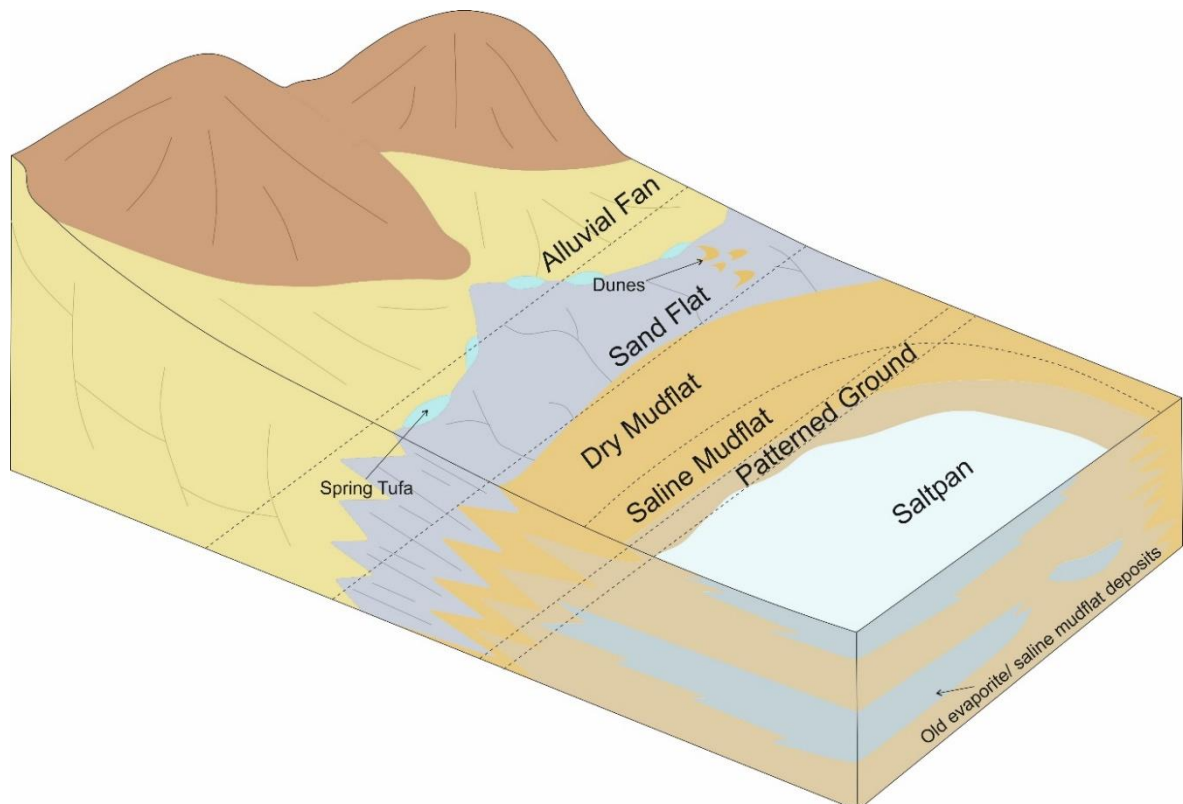


Figure 2.14- Varying environments in which continental sabkhas can be found, transitioning from alluvial fans to salt pans (After Warren, 2016).

individually, a change in climate, tectonics or other allo-controls can cause a transition from one to another.

Marginal-marine Sabkha

Marginal-marine sabkhas can be found forming narrow belts along arid margins. By using modern analogues such as the coasts of the Arabian Gulf, Australia and North Africa, the facies found in such an environment can be classified into supratidal, intertidal, or subtidal based on their position along the shoreline. Facies found within the subtidal region of a marginal-marine sabkha can be further separated into those that develop via open marine sedimentation and those that form in restricted environments such as lagoons (Warren, 2016). Within the open marine setting, the termination of shallow drainage channels, flanked by tidal ebb deltas, bring an influx of sediment that often contains a high percentage of organic material. Along the landward side of barrier islands, lagoons form, which connects to open marine water via a channel system, and rarely receive any freshwater input from another source, especially along an aeolian/ marine margin.

Intertidal deposits often overlap with those classified as subtidal as a result of a transitional environment. Such that upper lagoonal terrace facies within a subtidal environment can often be confused with the lowermost intertidal cemented flats (Warren, 2016). In modern successions such as the sabkhas of the Arabian Gulf, intertidal facies are geologically characterised by the occurrence of algal mats. However, this may not be true for palaeo-successions. Instead, they may be dominated by a 'mush' that may be cross-cut by euhedral or lenticular gypsum.

Lower, middle and upper supratidal environments are dictated by their distance from the high water line, such that the tidal influence, predictably, decreases with distance inland. Lower supratidal regions span approximately 2.5km in width and

are flooded perhaps once or twice a month. This leads to the development of lagoonal muds and small gypsum crystals. The middle supratidal realm is flooded less frequently, with a notable transition from small lenticular gypsum to nodular and laminate gypsum occurring within a matrix of reworked aeolian sediment (Wilson *et al.*, 2013). Finally, upper supratidal sediments mark the top of the capillary fringe, whereby flooding occurs sporadically, every four to five years. Within this environment, the lithology is characterised by 'chicken-wire' anhydrite and widespread displacive calcium sulphate growth (Lokier, 2012).

The development and expansion of coastal sabkhas are often bi-directional. Carbonate ramps, microbial mats and other sub-tidal features can extend seaward, but crucially the system can also expand landward via deflation of the neighbouring dune field (Kirkham & Evans, 2019) (Figure 2.15).

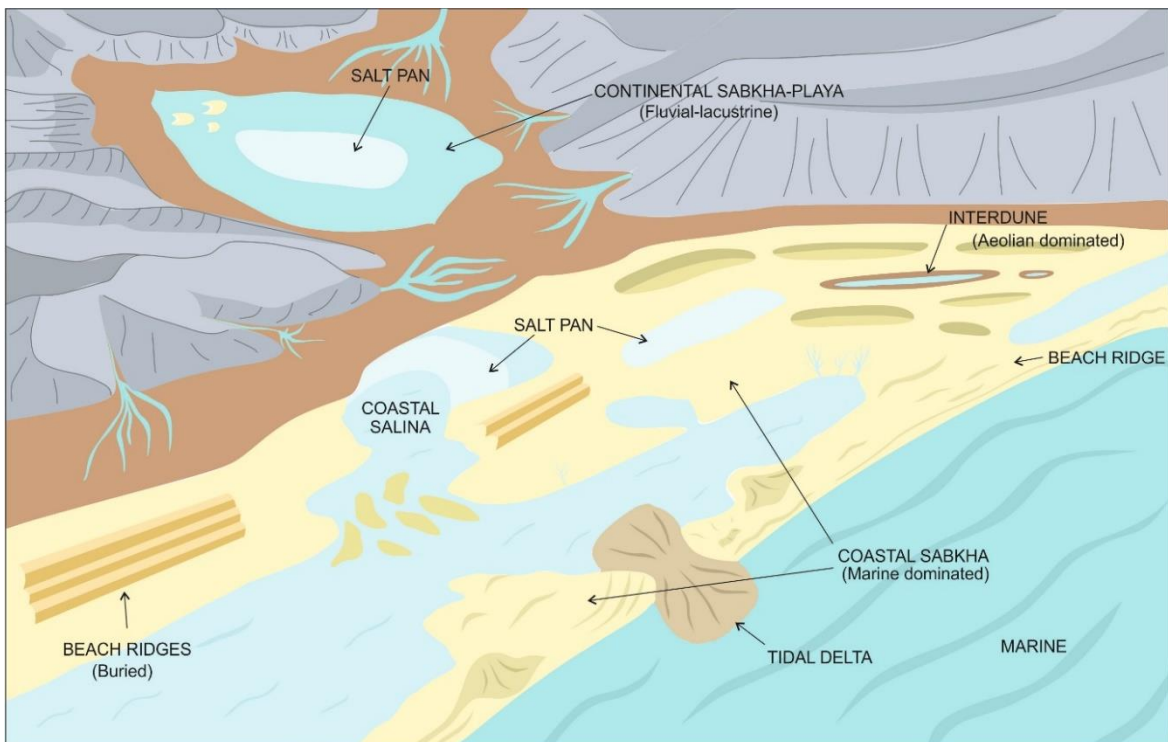
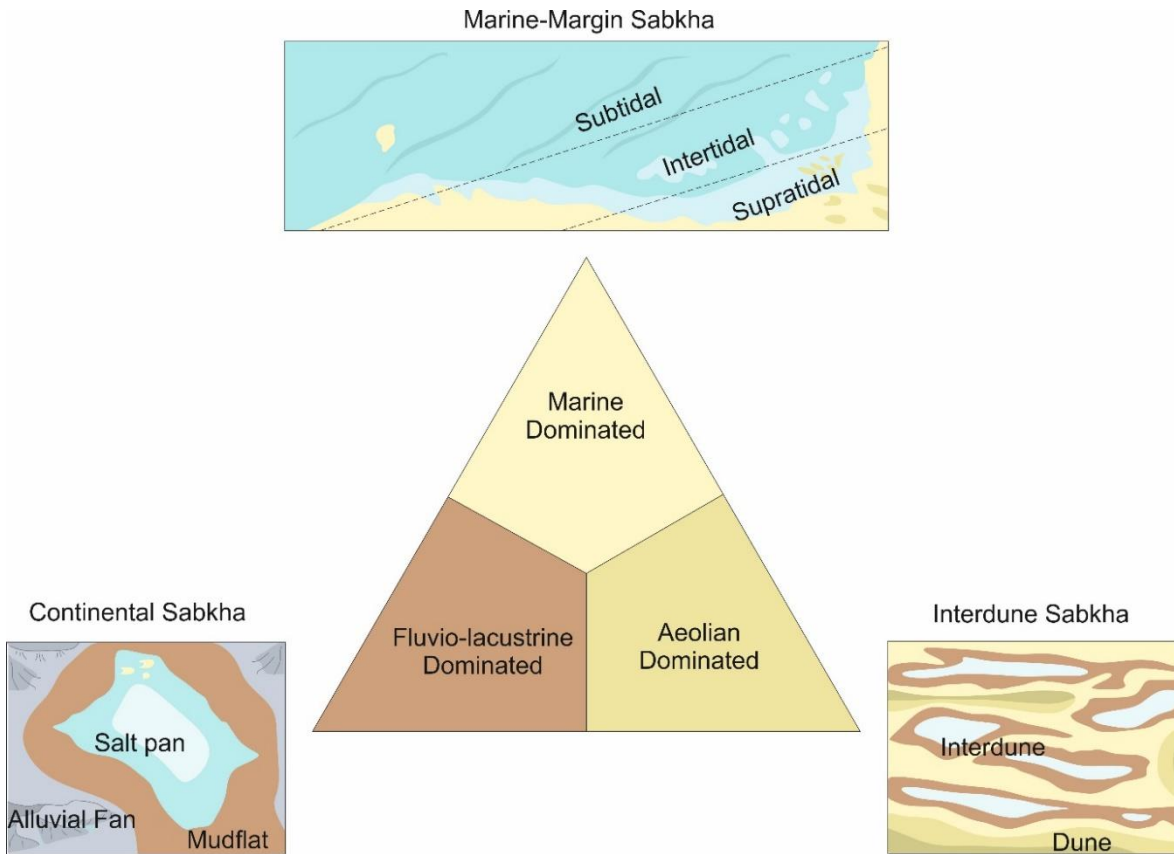


Figure 2.15- Theoretical environments in which sabkha can develop (above), and the relationships between these environments in a typical transitional setting (below) (After Handford 1981, Warren 1989).

2.3 Tide Dominated Marine Margins

Similarly, to marginal marine sabkhas, tidal flats can be categorised into sub-, inter-, or supra-tidal based on the relative influence of local sea level. Such that sub-tidal environments can be found below the water level, inter-tidal, sub-aerially with frequent inundation, and supra-tidal only sporadically influenced by tidal activity. Tidal flats are broadly described as 'sandy to muddy or marshy flats emerging during low tide and submerging during high tide'. Terminology for these regions is somewhat ambiguous within the literature. Some use zonation, i.e., the intertidal zone refers to the whole tidal flat, and others using terminology that implies a separate environment for each zone, i.e., sub-, inter-, and supra-tidal flat (Figure 2.16).

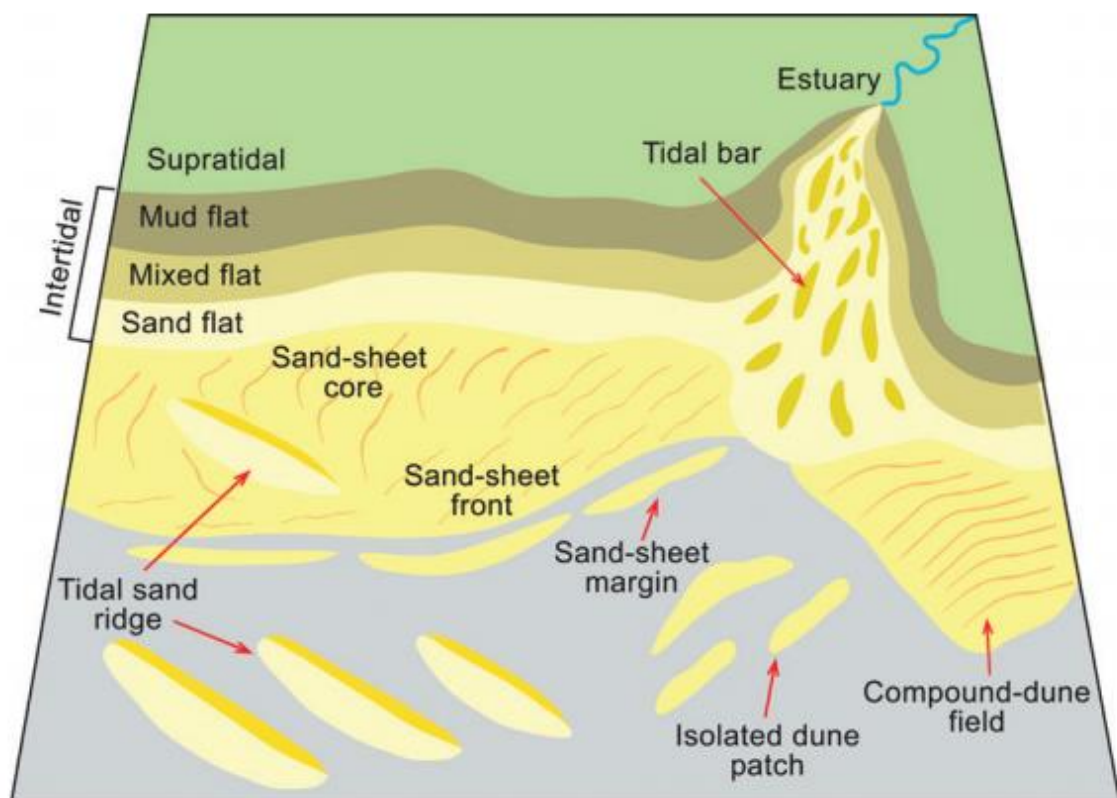


Figure 2.16- Environments of deposition within a tidal flat system, including the subtidal, intertidal, and supratidal zones within a tide-dominated shallow marine setting (From Desjardins *et al.*, 2012).

2.3.1 Subtidal Flat

Existing below the waterline, the subtidal region of a tidal flat comprises mostly subtidal sand bars and shoals with extensive tidal channels that expand seaward (Reineck & Singh, 1980). This is the tidal flat region with the greatest preservation potential due to the high proportion of channel infill and tidal point bars (Weimer *et al.*, 1982). In contrast to wave-influenced shorelines, tidal flats demonstrate a 'coarsening seaward' trend, whereby the grainsize increases with proximity to the shoreline and below the sea level.

2.3.2 Intertidal Flat

The intertidal zone hosts the majority of the tidal flat environment and is mainly unvegetated. The tidal range largely determines the sediments and characteristics of this zone, typically mixed flat facies. These are heterolithic successions of interbedded muds and sands that contain tidal features such as ripple laminated sandstones, parallel-laminated mudstones and flaser bedding.

2.3.3 Supratidal Flat

The upper regions of tidal flats are dominated by mud-flats, formed by the fallout of suspended sediment. The sedimentology in such areas is characterised by parallel laminated or massive mudstones, lenticular siltstones, or occasionally fine-grained sandstone (Desjardins *et al.*, 2012). In arid climates, supratidal flats lack vegetation. However, in areas where there is a greater amount of humidity, mangroves can often develop over the top of existing mud-flats.

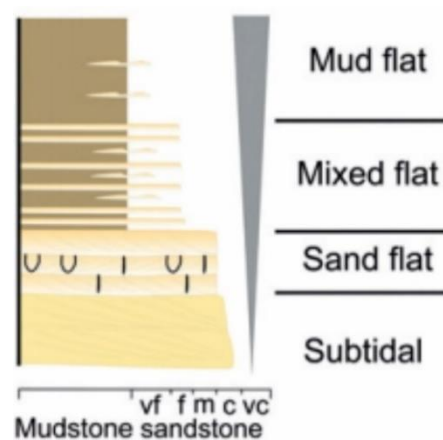


Figure 2.17- Idealised facies for a tidal flat succession (After Desjardins *et al.*, 2012)

2.4 Coastal Plain Deposits

Deposition within a coastal plain can produce a range of facies and features. Most typically these are very fine grained sands or silts found within a transitional system of sub-, inter- and supra-tidal flats. Slightly more complex however, are the variable deposits that can be classified as palaeosols, these will be discussed in more detail below.

Palaeosols

Palaeosols are defined as soils that formed on landscapes of the past (Yaalon, 1971). They often represent time periods much greater than the amount of preserved sediment would suggest, i.e., a preserved palaeosol could form a bed just 5cm thick but represent a time period of 1000 years (Kraus, 1999). The classification of ancient soils is complex and somewhat disputed in the literature, with several 'all-encompassing' classifications existing and in use (Mack *et al.* 1993, Nettleton *et al.* 2000, Duchaufour 2012). One of the main reasons for this is that a number of essential features of modern soils that allow for its classification are often not preserved during burial and secondary alteration. Nevertheless,

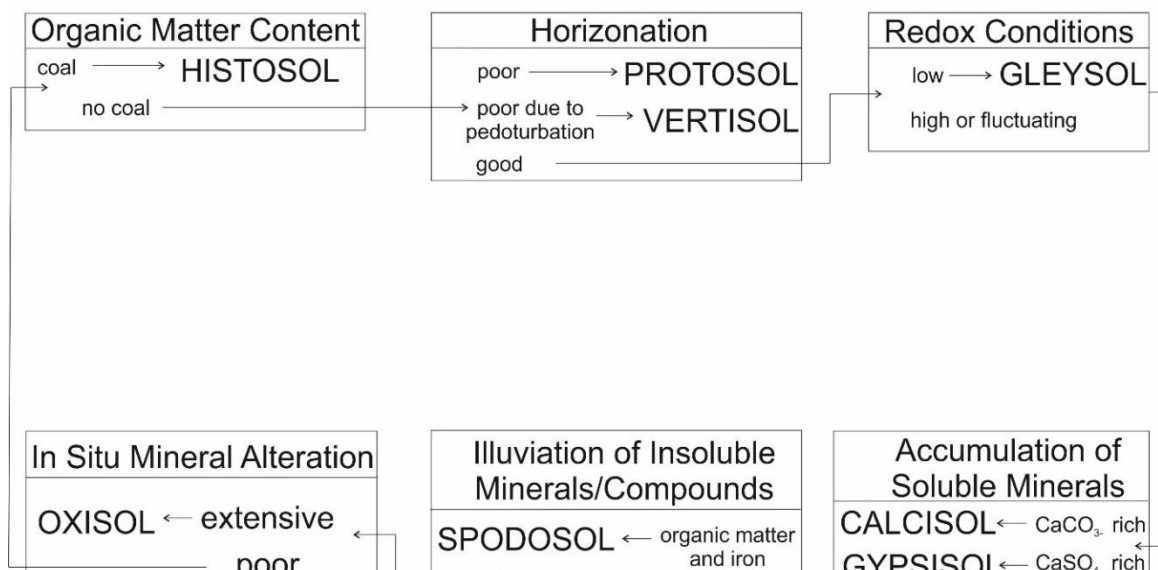


Figure 2.18- Classification of palaeosols based on their most prominent feature arranged into a flow chart that allows identification on an 'if not that, then this' basis (After Mack *et al.*, 1993).

determination of the type of palaeosol based on its most prominent feature has proven to be the most effective way of classifying ancient soil horizons and will hence be used for the remainder of this report (Mack *et al.*, 1993) (Figure 2.18).

Subordinate Modifiers

In conjunction with the classifications above, palaeosols can be further categorised based on secondary or even tertiary features using subordinate modifiers. This allows for a more detailed description without over-complicating the classification scheme, which would be easy, given the diverse nature of both relict and buried palaeosols. A list of the most common subordinate modifiers and their identifying features can be found below (Figure 2.19).

COMMON SUBORDINATE MODIFIERS OF PALAESOLS	
Albic	Presence of eluvial horizon
Allophanic	Presence of allophane or other amorphous Si and Al Compounds
Argillic	Presence of illuvial clay
Calcic	Presence of pedogenic carbonate
Carbonaceous	Presence of dark organic matter but not coal
Concretionary	Presence of glaebules with a concentric fabric
	Presence of iron oxides
Ferric	Subsurface horizon that was hard at the time of soil formation
Fragic	Evidence of periodic waterlogging
	Presence of vadose gypsum or anhydrite
Gleyed	Presence of glaebules with an undifferentiated internal fabric
Gypsic	Presence of a light-coloured Al horizon
Nodular	
Ochric	Presence of pedogenic salts more soluble than gypsum
	Salic
Silicic	Presence of decimeter-scale desiccation cracks, wedge-shaped peds, hummock and swale structures, slickensides or clastic dikes
Vertic	Presence of relict or actual glass shards or pumice
Vitric	

Figure 2.19- Most common subordinate modifiers for palaeosols, these can be used before the classification to describe one or more features that are not the most prominent within the palaeosol itself.

Gleysols

Gleysols are characterised by a horizon that displays prolonged low redox conditions. In contrast to other types of palaeosols, a gleysol cannot be characterised based on just one feature, such as a mottled horizon. Instead, the colour of the bed must be a blue-grey or pale green colour, and typically there will be nodules of iron or manganese oxide either below or within the unit as a result of displaced minerals. If all these conditions are met, then the palaeosol itself can be considered a gleysol and can be further described by a subordinate modifier such as 'Carbonaceous Gleysol' or 'Ferrallitic Gleysol'. If just one feature is identifiable, it can be used as a subordinate modifier in itself, such that a particular lamina within a palaeosol can be referred to as 'gleyed' if it displays the characteristic colour or mottling.

Oxisols

Oxisols are palaeosols in which the most prominent process is the alteration of chemically unstable minerals to clay and sesquioxides. Sesquioxides are oxic horizons that form when mineral oxides precipitate out of the soil, including iron oxides and aluminium oxides in the case of ferrallitic soils (Mack *et al.*, 1993). This combination of precipitated minerals and clays forms characteristic laminations of often intensely coloured beds. The formation of oxisols occurs typically in hot, humid regions where the heat can penetrate the surface. The colour of the soil horizons is indicative of the mineral and contains specific information regarding the climate at the time of deposition. In hot, dry climates, the freed iron oxide minerals can stay in situ and concentrate, unaffected by rainwater or acid hydrolysis that could occur in regions with a higher water level, leading to a stronger red or reddy-purple colour (Duchaufour, 2012).

Saline Soils

In humid climates, where free sodium ions are abundant, either in the form of sodium chloride or sodium sulphate, a unique class of palaeosol may form known as salsodic soils. This category is further broken down into 1) saline soils- soils in which the pH does not exceed 8.5 and 2) alkali soils- where the pH can exceed 8.5. Furthermore, saline soils are divided into subclasses to differentiate between the reduction powers of each class and their position on the spectrum of saline to alkali classification. The subclasses are as follows:

- 1) Saline soils with calcic complex- the ratio of sodium ions (Na^+) to the exchange capacity is always less than 15% (Duchafour, 2012)
- 2) Saline soils with sodic complex- the ratio of sodium ions (Na^+) to the exchange capacity is always greater than 15% (Duchafour, 2012)
- 3) Saline soils with sulphate reduction- this type of soil is exclusive to and indicative of marine muds deposited on coastal plains and estuaries. The composite saline muds and organic material have a strong reducing power, leading to the reduction of sulphides to sulphates and the free iron oxides into blue-grey gley horizons. These processes occur in the saline polders of coastal regions during a relatively high water level. When the water level falls again, the sulphides oxidise and hydrolyse to form sulphuric acid and ferric hydrate, which can leach into the below units, causing rusty patches and staining that has a strong yellow colour (Duchaufour, 2012).

2.5 Summary

This chapter documents the key processes, landforms and environments present along an aeolian marine margin, with specific detail given to the relevant areas of the Entrada/ Curtis/ Summerville transition. Understanding aeolian and coastal

processes is key to understanding the Moab Member and its contemporaneous deposits, and any terminology described will be used consistently throughout the remainder of this thesis. Aeolian environments include dunes, interdunes and sandsheets, whilst coastal environments comprise palaeosols, sabkha and tidal flats.

Chapter 3: Lithofacies of the Entrada/Curtis/Summerville Formations

Field observations of the Moab Member of the Curtis Formation and the Summerville Formation have identified seventeen facies (summarised in Table 3:1), each with unique lithological characteristics, textures, and sedimentary structures. Using these physical properties, ten facies associations have been created, based on the definition of an association as “More than one facies found together that define a possible depositional environment or environments” (Potter, 1959). The facies associations are further combined into four assemblages: a wet aeolian system, a dry aeolian system, a coastal plain and a tide dominated marine margin. The analysis has been conducted based on logs taken at five localities between Moab and the San Rafael Swell (Figure 3.1). A summary of the facies can be found in Table 3:1.

A total of ten sedimentary logs were completed at five localities, nine of these logs were carried out ~5 km apart, documenting the spatial interaction between the aeolian dune deposits and the contemporaneous coastal plain sediments. One further log was completed some 35km west, near the San Rafael Swell, providing a more distal analogue for the basin and providing key correlatable time surfaces. The total recorded sediment comprises 4km, covering 60km between the towns of Green River and Moab. The logs can be correlated via the top of the Entrada slick rock and the base of the Morrison Formation. In areas where the Morrison was inaccessible or not present, correlation was carried out via significant and traceable units that are laterally extensive.

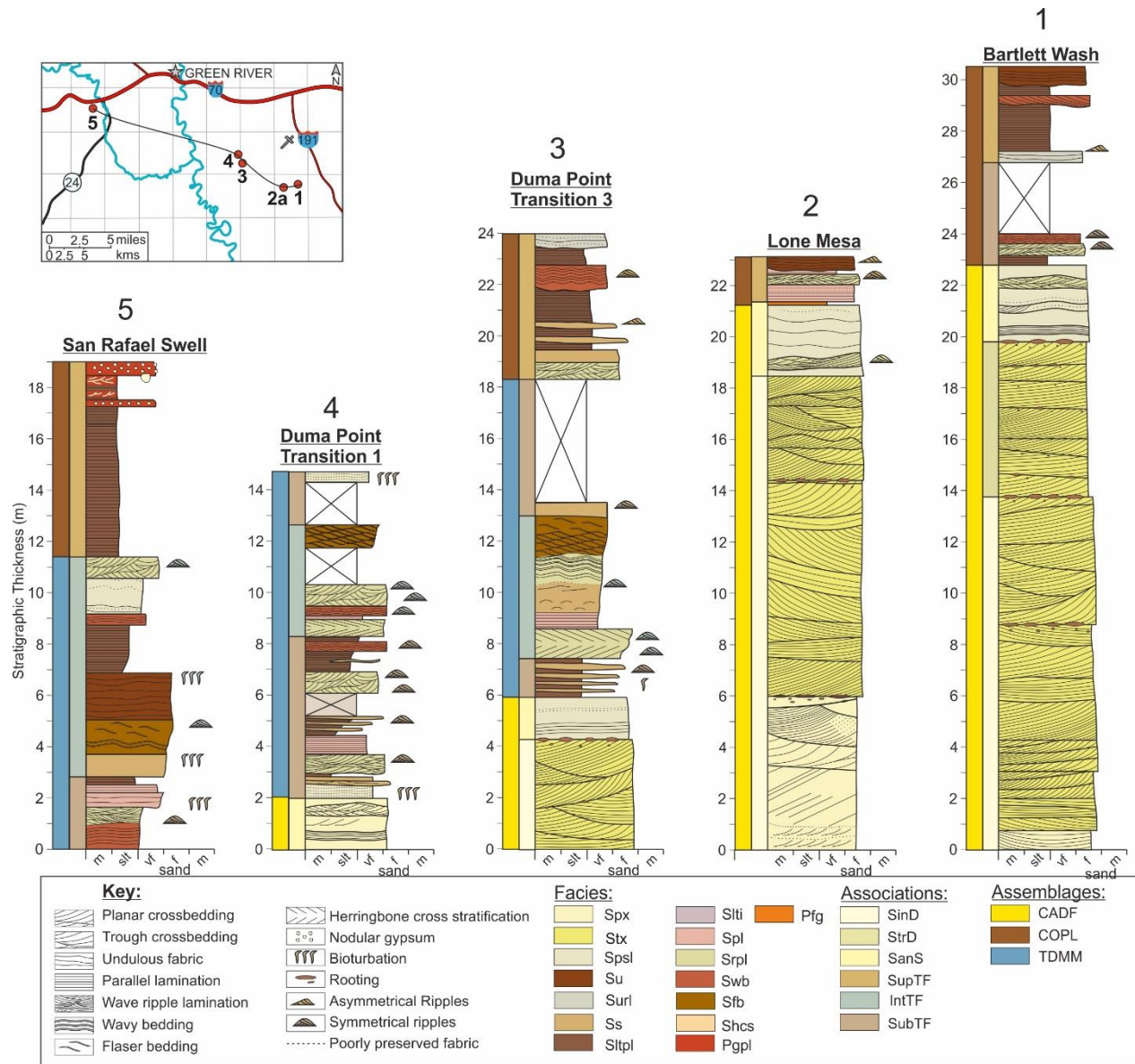


Figure 3.1.1- Locality map of the study area within South-eastern Utah, showing the positions of each of the localities at which sedimentary logs were taken. Figure 3.1.2-The relative position of the study area within the four corners region of the United States of America.

Facies	Code	Lithology & Texture	Sedimentary Structures	Interpretation	Photo Example	Reference
Planar Cross-Stratified Sandstone	Sxs	Yellow fine to medium-grained well-sorted and well-rounded sandstone	Planar cross-bedding with mm/cm scale alternations in grain size occurring in single or multiple sets <10cm, with localised rhizolith development/.	Alternating laminations of grainfall and grainflow and the migration of wind-blown straight-crested dune-scale bedforms. Rhizolith formation as the result of periodic stabilisation and elevated water table		Boggs (2006)
Trough Cross-Stratified Sandstone	Stxs	Light grey to reddish brown, fine to medium-grained, well-sorted and well-rounded sandstone.	Trough cross-bedding with mm/cm scale alternations in grain size occurring in single or multiple sets. Truncated foresets with asymptotic bases.	Alternating laminations of grain fall and flow and migration of wind-blown sinuous-crested dune-scale bedforms and dune trains.		Crabaugh & Kocurek (1993)
Planar Bedded Sandstone	Sfpd	Light grey to reddish brown, fine-grained, well-sorted and well-rounded sandstone.	Horizontal laminations with bimodal sorting (pinstripe) with sporadic shallowly climbing (<8°) rippleform laminae.	Saltation of fine-grained sand, which accumulates along the saltation wavelength. Reptation of coarser grains over accumulated grains, results in inverse grading.		Kocurek & Neilson (1986)
Undulose Sandstone	Sdun	Reddish-brown very fine to fine-grained, moderately-sorted, sandstone.	Structureless to undulose with localised desiccation cracks, clay lenses and root traces (rhizoliths).	Rapid suspension settling and accumulation of wind-blown sediment in areas affected by surface water, followed by drying.		Mountney (2012)
Undulose Sandstone with Ripple Laminations	Surpl	Reddish-brown to yellow, silt to fine grained, poorly-sorted and sub-rounded, siltstone and sandstone.	Parallel laminations with a sporadic undulose texture and symmetrical cross lamination.	Low energy, sub-aqueous setting, where the deposits have settled out of suspension. Undulose and oscillation-current ripples form in response to wind action on shallow waters.		Purvis (1991)
Parallel Laminated Siltstone	Sspl	Reddish-brown and grey, mud to very-fine-grained poorly-sorted mudstone and siltstone.	Structureless to faint parallel-laminations with normal grading and vertical burrows and sporadic rhizoliths and mottling.	Suspension fall out within low energy waters. Stabilization for vegetation to develop		Desjardins et al., (2012)
Ferrallitic Gleysol	Fegl	Yellow mottled reddish-brown very-fine-grained, poorly-sorted and moderately-rounded, sandstone.	Massive, dense concretions	The occurrence of mottles within a pale cream matrix is caused by Fe-Al enrichment during pedogenesis and the oxidation of Fe ²⁺ to Fe ³⁺ as the water table lowers. This high concentration of metals in conjunction with fluid flow leads to leaching and concentration within the nodules found at the base of the unit.		Leeder (2011)
Parallel Laminated Oxisol	Oxpl	Greenish-yellow and purple silt- to very-fine grained sandstone.	Fining upwards horizontal laminations, mottled. Sporadic symmetrical ripples.	Vegetation stabilisation and sediment binding; product of palaeosol development. Presence of primary sedimentary features indicates a relatively immature palaeosol most likely in proximity to fluvial channels or confined bodies of water		Mack et al., (1993)

Facies	Code	Lithology & Texture	Sedimentary Structures	Interpretation	Photo Example	Reference
Parallel laminated Sandstone	Spl	Pink very fine-grained, well sorted and moderately well-consolidated sandstone.	Parallel laminated, columnar weathering pattern	Suspension settlement of material transported by low energy currents, with episodic and uniform increases in energy within a calm sub-aqueous environment.		Flemming (2011)
Saline Soil with Sulphate Reduction	Sasr	Yellow silt to very-fine grained sandstone.	Clear horizons with fluid precipitations.	Vegetation stabilisation and sediment binding; product of palaeosol development. Presence of fluid horizons indicates secondary oxidization of sulphate minerals. Most likely due to reduction of water table in a restricted low lying sub-aqueous setting.		Duchafour (2012)
Structureless Sandstone	Scs	Yellow very fine- to fine-grained poorly-sorted, sub-angular to well-rounded sandstone.	Massive with basal load casts, and occasional mud rip ups.	Sub-aqueous non-Newtonian high energy mass sediment flow under high sediment load conditions into standing water.		Hughes (2011)
Parallel Laminated Silstones with Evaporites	Ssepl	Reddish-brown silt to very fine-grained, poorly sorted and moderately-rounded siltstone.	Parallel laminated to massive, often contorted by evaporite nodules.	Flow of saline fluid and subsequent precipitation of evaporites in the pore space as water evaporated at the ground surface.		Gustavson et al., (1994)
Parallel Laminated Inverse Graded Siltstone	Ssgpl	Light grey silt to medium grained, well-sorted and well-rounded siltstone and sandstone.	Undulose to parallel laminated columnar weathering pattern. Coarsens up to sand.	Sub aqueous suspension deposition within a sub tidal flat. Sub aqueous bedload deposition		Flemming (2011)
Ripple Laminated Sandstone	Srpl	Light grey, very-fine grained, moderately sorted and moderately-rounded, sandstone.	Crinkle cut ripple lamination peak crested ripples occasionally water escape structures.	Migration of ripple-scale bedforms in lower flow regime/waning flow conditions.		Kriesa & Moila (1986)
Herringbone Cross-Stratified Sandstone	Sxhc	Yellow to grey, very-fine to fine-grained, moderately sorted and sub-rounded sandstone.	Bi-directional cross-stratification with sporadic ripple cross-lamination and mud drapes.	Differences in direction of subaqueous flow and turbulence between periods of movement and quiescence.		Stride (1982)

Table 3:1- Summary table describing each of the facies, their lithologies, structures and the interpretations for depositional process. In addition, example photographs for each facies have been provided as well as a reference for the process and environment.

3.1 Wind-Blown Facies

Facies within this environment are interpreted to have been deposited by migrating sediments controlled dominantly by wind direction and level of the water table.

This includes dune and interdune facies, in addition to sandsheet facies.

3.1.1 Planar Cross-Stratified Sandstone- Sxs

Description- deposits of planar cross-stratified sandstone (Sxs) comprise yellow, pale cream planar cross-bedded sandstones that are medium-grained and well sorted. Strata contain millimetre to centimetre scale alternations in grain size occurring in single or multiple sets. At the base of the foresets, there is evidence of inverse grading separated by fine-grained laminae (Figure 3.2). Rhizolith horizons occur along set-bounding surfaces near the base of the unit (Figure 3.2). Foresets are truncated at the top, and asymptotic at the base, separated by parallel set bounding surfaces approximately 1m apart (Figure 3.2). These sets are stacked into cosets, the thicknesses of which vary across the study area. At Bartlett Wash (Log 1) and Lone Mesa (Log 2), cosets of planar cross-stratified sandstone (Sxs) are at their maximum thickness of 19m (Figure 3.2). However, at Duma Point Transition 3, the cosets are 5m, thinning further to just 1m at Duma Point Transition 1 (Figure 3.1).

Interpretation- Deposits of planar cross-stratified sandstone (Sxs) can be interpreted as straight-crested dune-scale bedforms. Inverse graded and fine-grained laminae represent grainflow and grainfall, while the planar bounding surfaces indicate straight-crested dune forms (Collinson, 2019). Rhizolith horizons demonstrate periods of stabilisation within which vegetation can prevail upon dune slopes (Mountney & Thompson, 2002).



Figure 3.2.1- Planar cross-stratification within units 1 & 2 of the facies Sxs, separated by an index surface. Figure 3.2.2- Planar cross stratification within dune package 3 of the facies Sxs. Figure 3.2.3- Outcrop view of units 1 & 2 within facies Sxs at the Lone Mesa Locality. Figure 3.2.4- Outcrop view of units 1 & 2 within facies Sxs at the Bartlett Wash locality. Figure 3.2.5- Rhizolith within Facies Sxs at the Lone Mesa Locality. Figure 3.2.6- Weathered Rhizolith within facies Sxs at the Bartlett Wash Locality. Figure 3.2.7- Planar cross-bedding and differential bleaching within unit 3 at Lone Mesa. Figure 3.2.8- Rhizoliths along foresets of facies Sxs at the Lone Mesa Locality.

3.1.2 Trough Cross-Stratified Sandstone- Stxs

Description- Trough cross-stratified sandstone (Stxs) is a light-grey to light pink quartz arenite, grains are well-sorted and well-rounded, with an average grain size of fine sand. Inverse grading is visible along the base of some foresets, interbedded with finer-grained material (Figure 3.3). Foreset thickness ranges from millimetre to centimetre-scale, whilst set thickness can reach up to 2m. Set-bounding surfaces truncate the tops of the foresets and meet at the base asymptotically; at outcrop scale, they have a convex or curved profile (Figure 3.3). Trough cross-stratified sandstone (Stxs) is most prominent in the east of the study area (Localities 3-5), with sets of 2m stacked into cosets that do not exceed 5m (Figure 3.3).

Interpretation- The trough cross-stratified sandstone facies (Stxs) represent deposits of sinuous-crested dune-scale bedforms created by wind-blown sands. This is evidenced by the couplets of inverse-graded and very fine-grained laminae exemplifying grainfall and grainflow strata, which serve as proof of an aeolian environment. The shape of the dunes can be obtained from the trough cross-bedding and curved set bounding surfaces. The trough cross-stratified sandstone (Stxs) was probably deposited in a regime whereby there was an overall positive sediment flux, demonstrated by the truncated tops and asymptotic bases of foresets, indicating subcritical climb (Collinson, 2019).

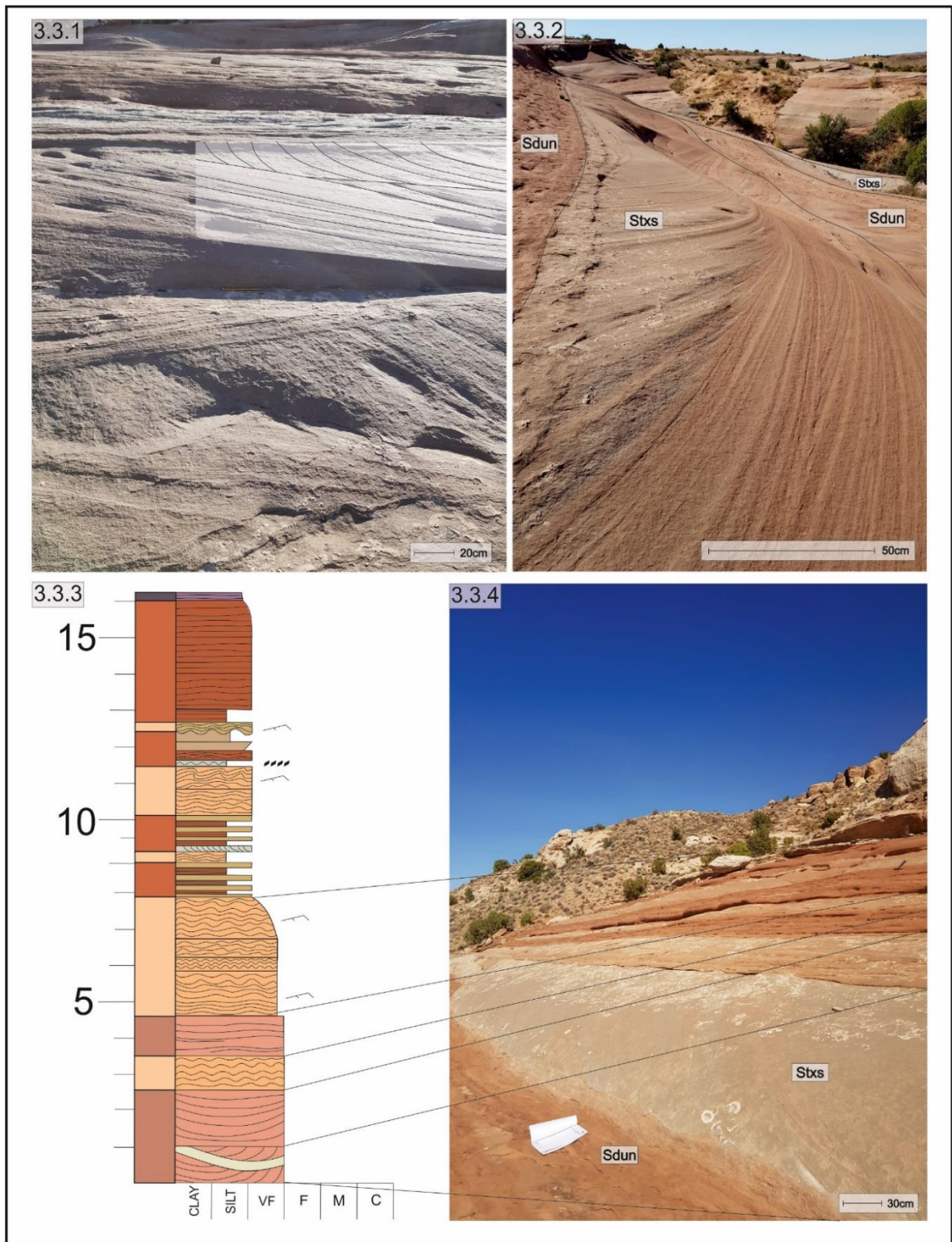


Figure 3.3.1- Prominent grainfall/ grainflow strata forming cross-bedding within the dune form of Stxs. The tops are truncated, whilst the base remains asymptotic. HB pencil for scale. Figure 3.3.2- Trough cross-stratification within a 2m thick unit of Stxs. Figure 3.3.3- Sample of the sedimentary log taken at Bartlett Wash showing occurrence of the Stxs facies. Figure 3.3.4- Relative thickness of the units within the Stxs facies interbedded with those of Sdun.

3.1.3 Planar Bedded Sandstone- Sfpd

Description- Beds of planar bedded sandstone (Sfpd) comprise horizontal laminations, no more than 20-30cm thick, with bimodal sorting and sporadic rippleform laminae. Detailed sedimentary structures within deposits of planar bedded sandstone (Sfpd) are often obscured by extensive weathering, also causing light-pink staining upon the surface of the unit (Figure 3.4).

Interpretation- Low-angle bedding combined with lithological characteristics indicate an aeolian environment in which sediment supply was insufficient to form dune-scale bedforms. Hence, ripple-scale bedforms were formed from the entrainment of sand grains into the wind and the saltation of fine-grained sand along the saltation wavelength (Kocurek & Neilson, 1986, Mountney & Jagger 2004). Thick deposits of planar bedded sandstone (Sfpd) that contain little to no defined cross-bedding despite a grainsize suitable for the formation of bedforms is linked to the development of a sand sea or sandsheet (Kocurek & Neilson, 1986).

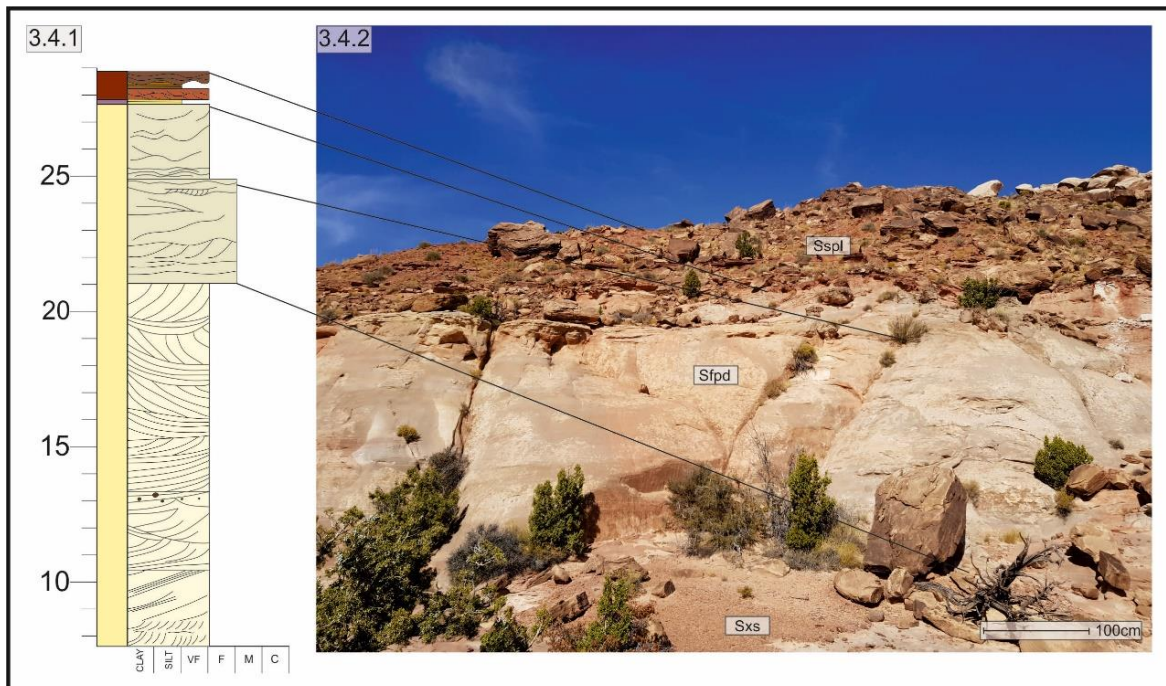


Figure 3.4.1- Sample of the sedimentary log taken at the Lone Mesa Locality, showing the facies Sfpd and the overlying units. Figure 3.4.2- Outcrop view of the Sfpd facies at the Lone Mesa Locality.

3.2 Ponded Water Facies

This section describes facies deposited within shallow-ponded water in any depositional environment. These facies are typically characterised by undulose bedding and ripple forms.

3.2.1 Undulose Sandstone-Sdun

Description- Undulose sandstone (Sdun) describes units of red-brown, moderately sorted, very fine to fine-grained sandstone, with sporadic lenses of argillaceous material. Metre-scale undulations define contacts between beds. The internal structure is mostly structureless with some small-scale undulations, localised desiccation cracks, clay lenses and sporadic rhizoliths. Towards the top of the unit, mottling and water escape structures are prominent. (Figure 3.5).

Interpretation- Occurrences of undulose sandstone (Sdun) are linked to the accumulation of wind-blown sediment between dune-forms within very shallow water via suspension settlement (Mountney & Thompson, 2002). The argillaceous material and water escape structures are a clear indicator of fluid flow and a high water table during deposition. Mottling is an indicator of vegetation, and its prevalence towards the top of the units highlights a flat and stable surface subject to periodic localised wetting and drying.



Figure 3.5.1-Outcrop scale view of a unit of Sdun as it is most commonly found, between units of Stxs at the Lone Mesa locality Figure 3.5.2- Units of Sdun interbedded with units of Stxs at Bartlett Wash (Locality 1) Figure 3.5.3- Outcrop scale view of figure 3.5.2, note that the interbedded units of Sdun become thinner and more frequent upwards.

3.2.2 Undulose Sandstone with Ripple Laminations-Surpl

Description- Undulose sandstone with ripple laminations (Surpl) is a dark reddy-brown lithic arenite of fine to medium grain size. The grains are sub-rounded and poorly sorted and contain a small percentage of clay particles. Key internal features include mud lenses and mud drapes that occur sporadically throughout the unit (Figure 3.6). Beds are typically 10-30cm thick, largely undulose, with some small foresets at the base, often overlaying some larger crude foresets at the base of the unit. In addition to the mud drapes, rippled beds occur sporadically throughout the unit presenting as symmetrical round crested ripples. The thickness of the undulose sandstone (Surpl) varies across the transect with no recognisable pattern. At Lone Mesa (Locality 2) and Bartlett Wash (Locality 1), the unit is no more than 10cm thick, whereas the thickest deposit, found at Duma Point Transition 3 (Locality 3), is 1m thick (Figure 3.1).

Interpretation- Undulose sandstone with ripple laminations (Surpl) represents sub-aerial facies indicative of the deposition of silty material. Thin laminations and ripples indicate subaqueous deposition and bedform development due to oscillating flow within shallow water. The undulose bedding occurs as a result of the lack of structure within fine-grained material and deposition upon small mounds (Desjardins *et al.*, 2012). Sporadic mud drapes can be explained by the deposition of muds by ponded water during small-scale flooding events (Purvis, 1991). Fine-grained sands and silts indicate deposition within a low-energy environment with limited sediment supply (Desjardins *et al.*, 2012).

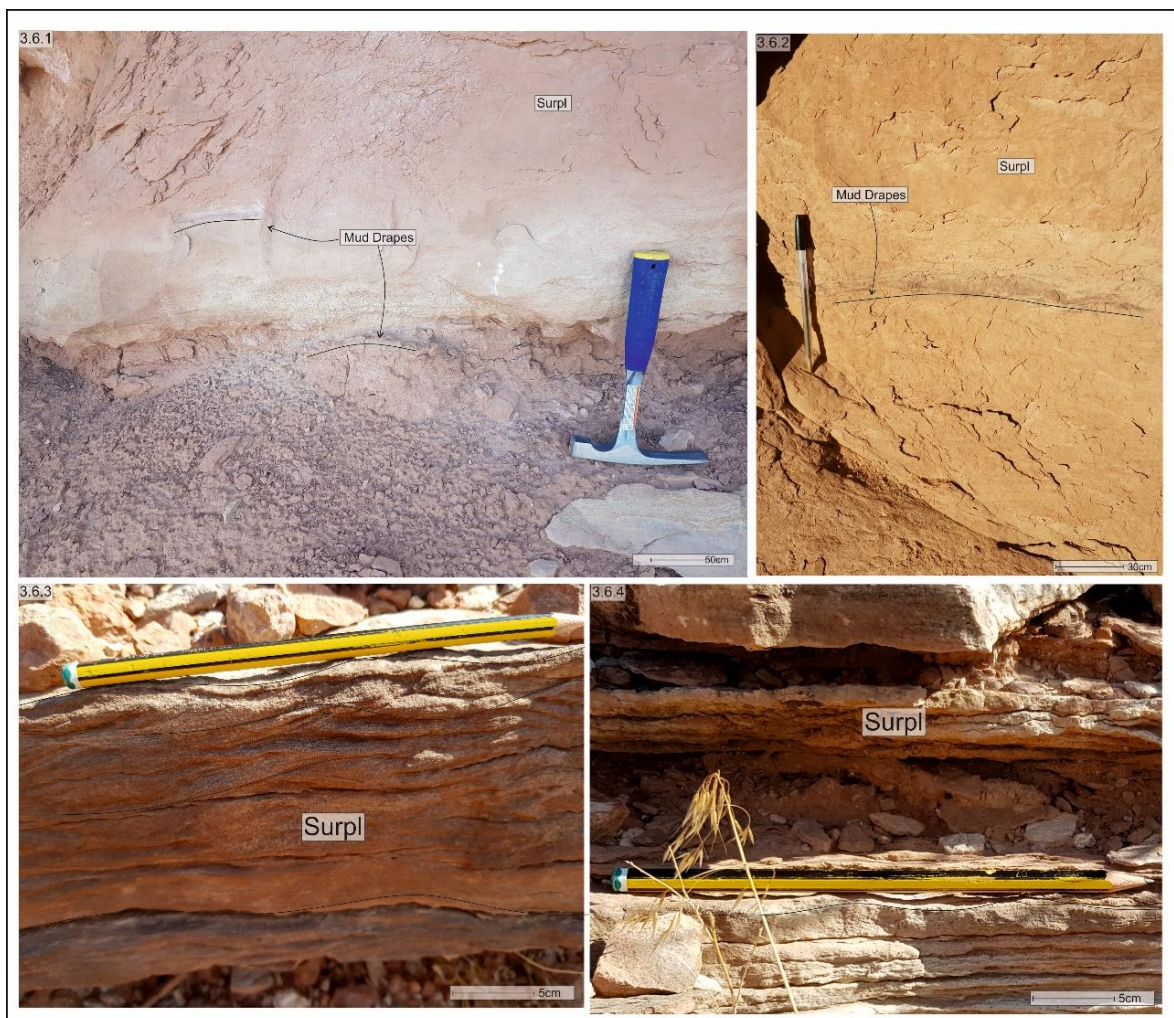


Figure 3.6.1- Mud drapes within facies Surpl at the San Rafael Swell (Locality 5), they occur sporadically and are usually isolated Figure 3.6.2-An additional example of the mud drapes within Sumd at Duma Point Transition 3 (Locality 3). Figure 3.6.3- Symmetrical round-crested ripples within facies Surpl at the Duma Point Transition 1 locality. Figure 3.6.4- Undulose bedding and symmetrical ripples within Surpl at Duma Point Transition1.

3.2.3 Structureless Sandstone- Scs

Description- Structureless sandstone (Scs) is best exposed at Duma Point Transition 1 (Locality 4); it consists of a red-cream argillaceous lithic arenite that forms lenticular beds that are mostly structureless. Units are well cemented and bleached in some areas. The lower bounding surface is erosive and contains load casts and very sporadic rip-up clasts (Figure 3.7).

Interpretation- This facies represents episodic channelised high sediment load non-newtonian flows. Load casts at the base demonstrate rapid deposition onto an unstable substrate. Discontinuous ripples towards the top of units of structureless sandstone (Scs) are indicative of reducing flow energy, and sediment load as the material is deposited, producing episodic lower flow regime conditions.

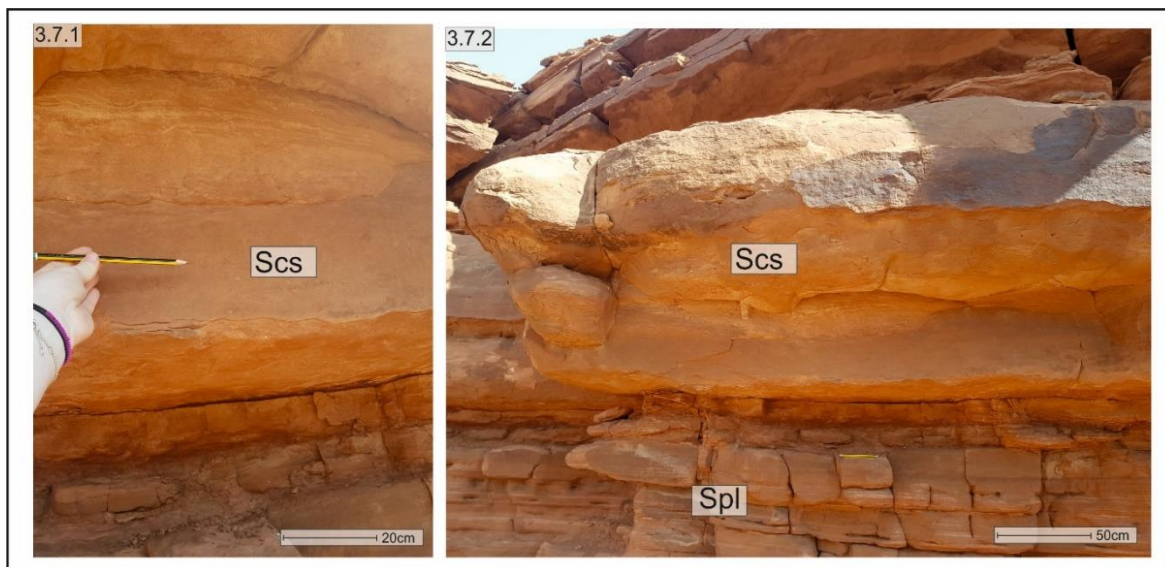


Figure 3.7.1- Unit of facies Scs approximately 60cm in height, with the first 40cm appearing structureless. Figure 3.7.2- 'zoomed out' view of the Scs unit, the base may also contain some load casts at Duma Point Transition 1 (Locality 4).

3.2.4 Parallel Laminated Siltstone- Sspl

Description- Parallel laminated siltstone (Sspl) is a red-brown, poorly sorted, moderately rounded siltstone interbedded with parallel laminated mudstone with an almost indiscernible difference in grain size between beds of each. The unit is poorly consolidated, which leads to slope-forming mounds of loose material (Figure 3.8). When the excess surface material is moved, the bedding can be picked out as parallel laminated. Along the top of the unit, there is some mottling and occasional vertical burrows.

Interpretation- Deposits of parallel laminated siltstone (Sspl) are probably caused by suspension fallout upon a flat surface within low energy shallow waters. The mottling and burrowing are clear indicators of vegetation and habitation; however, they occur sporadically due to varying and often harsh salinity levels within this environment (Desjardins *et al.*, 2012).



Figure 3.8.1- Parallel laminations within the Sspl facies as found at all localities overlying the planar cross-bedded sandstones (Sxs). Figure 3.8.2- Representation of the poorly consolidated nature of Sspl leading to large mound-like structures.

3.2.5 Parallel Laminated Siltstone with evaporites- Ssepl

Description- Parallel laminated gypsisol (Ssepl) is characteristically brown/red in colour, with a silt grainsize, deposits are poorly sorted, and the grains are moderately rounded. Beds of siltstone are punctuated by various gypsum structures, primarily nodules and satin spar gypsum (Figure 3.9). Internal structure varies slightly from parallel laminated to more undulose laminated.

Interpretation- Siltstone is indicative of suspension settlement within calm shallow water; the restricted environment is inferred from the presence of the gypsum, linked with saline rich waters. The morphology of the gypsum is the most reliable supporting evidence for this, with nodular gypsum forming via the displacement of host sediment by softer, damper sediment that is then subaerially exposed due to a very shallow and fluctuating water table (Dean *et al.*, 1975). This displacement is the most probable cause of the slightly undulating structure towards the top of the unit.

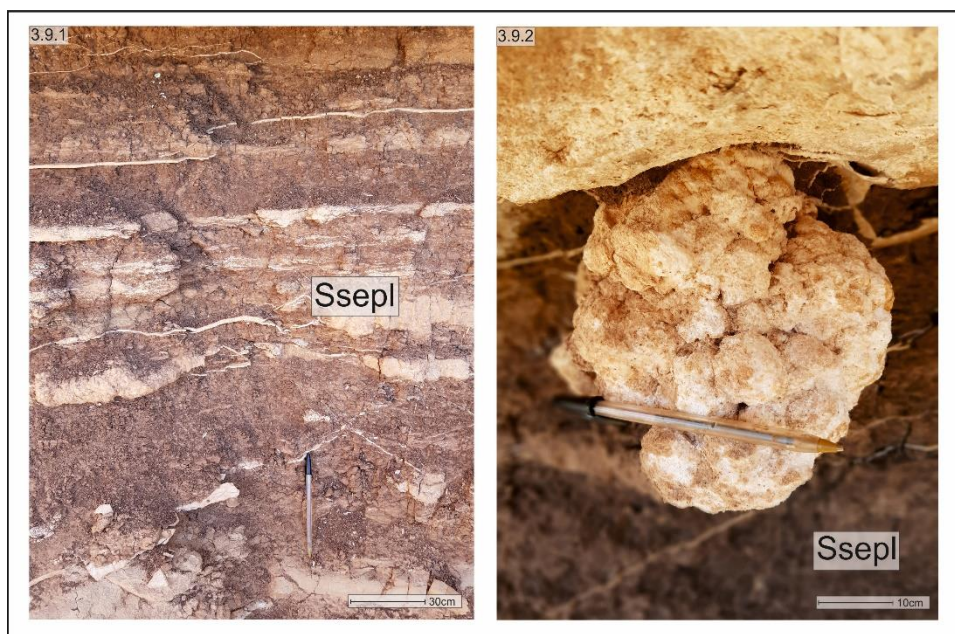


Figure 3.9.1-Parallel Laminated siltstone beds interlaced with satin spar gypsum at the San Rafael Swell Figure 3.9.2- Isolated nodule of gypsum occurring within beds of Sspl at the San Rafael Swell (Locality 5).

3.3 Palaeosol Facies

Palaeosols are soil horizons developed within sedimentary sequences that represent a significant time gap. The classification of palaeosol contains essential information about the climate at the time of deposition and some details of the minerals available within the environment.

3.3.1 Ferrallitic Gleysol- Fegl

Description- Ferrallitic gleysol (Fegl) is a pale cream, poorly sorted, poorly consolidated sandstone with red/brown mottles throughout (Figure 3.10). The internal structure appears structureless, with no evidence of bioturbation and vegetation. Concretions can be found along the base of the facies that are metallic grey and much denser and more consolidated than the surrounding material. This facies is exclusively found at Lone Mesa (Log 2) and is 1.5m thick. Due to its mottled appearance and nodular surface texture, this facies has been colloquially termed the 'popcorn facies' within the literature (Zuchuat *et al.*, 2019).

Interpretation- Deposits of ferrallitic gleysol (Fegl) represent a soil deposited within a fluctuating water table (Leeder, 2011). The occurrence of mottles within a pale cream matrix is caused by Fe-Al enrichment during pedogenesis, and the oxidation of Fe^{2+} to Fe^{3+} as the water table lowers (Table 3:2). This high concentration of metals in conjunction with fluid flow leads to leaching and concentration within the nodules found at the base of the unit (Buol & Eswaran, 1999).

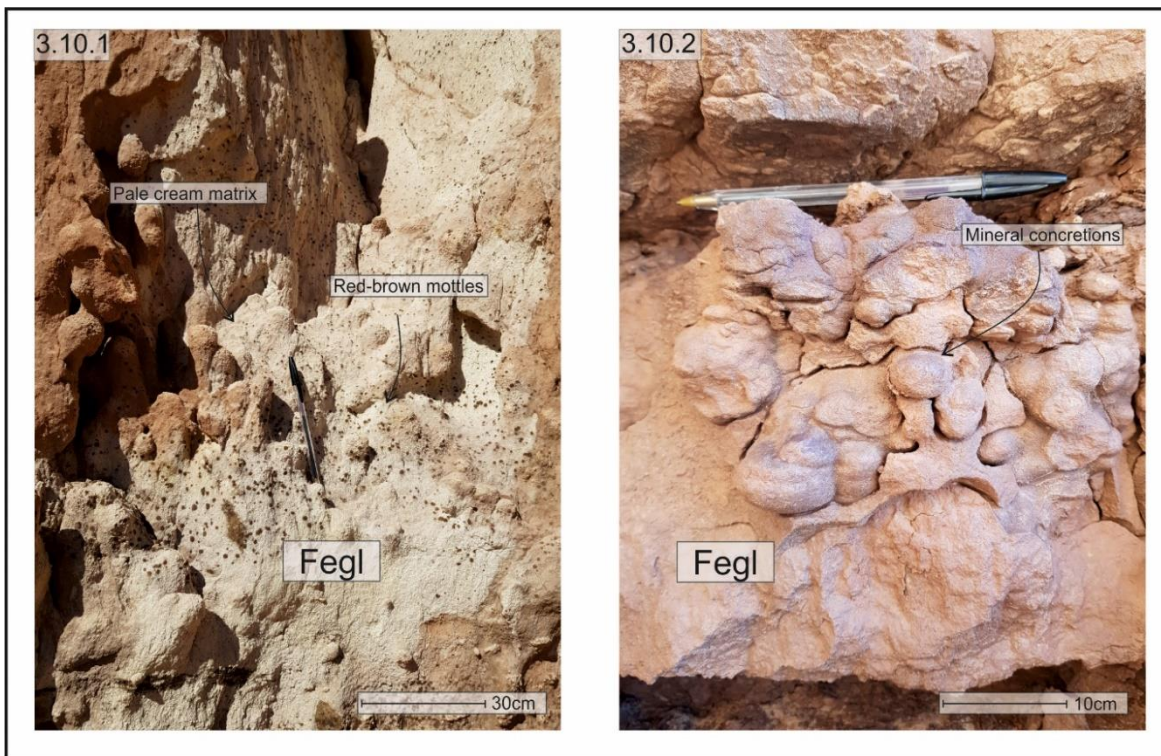


Figure 3.10.1- The informally named ‘popcorn facies’ characterised by red-brown mottles within a pale cream matrix, typical of a ferrallitic gleysol. Figure 3.10.2-oxidation of iron minerals during palaeosol formation leads to concretions of the minerals gathering in lower units.

Element	Content within sample (ppm)	Error (ppm)	Significance
Si	271365.13	1455.51	Normal
Fe	74780.65	580	Very High
Al	42010.68	1244.69	Very High
K	13491.01	353.74	Normal
Ba	11438.99	171.18	Very High
Mg	9844.55	4714.95	High
Ca	5584.75	370.17	Normal
Mn	4890.77	147.69	High
Ti	1267.12	137.37	Normal
Sr	140.94	4.71	High

Table 3:2- XRF element analysis of sample taken from facies P1. The main elements and their proportions are shown in addition to the error in parts per million. The significance here is a qualitative term used to provide context for the statistics and the errors. The highest proportions of expected elements are silicon and potassium, whereas the levels of iron and barium are significant as the proportions are higher than expected, with low margins of error.

3.3.2 Parallel Laminated Oxisol- OxpI

Description- Deposits of parallel laminated oxisol (OxpI) comprise a green, cream, and purple parallel bedded very fine-grained sandstone, with occasionally thin silty beds. Each bed is approximately 30cm in thickness (Figure 3.11). Grain size varies slightly between the different beds, with a general fining upwards trend. Sparse round-topped symmetrical ripples can be found within this unit.

Interpretation- Deposits of parallel laminated oxisol (OxpI) represent a palaeosol horizon under arid to temperate climatic conditions. The defined horizons are caused by differential oxidation of minerals forming oxic horizons termed sesquioxides. The purple colour and green colours are demonstrative of iron oxidation (Mack *et al.*, 1993).

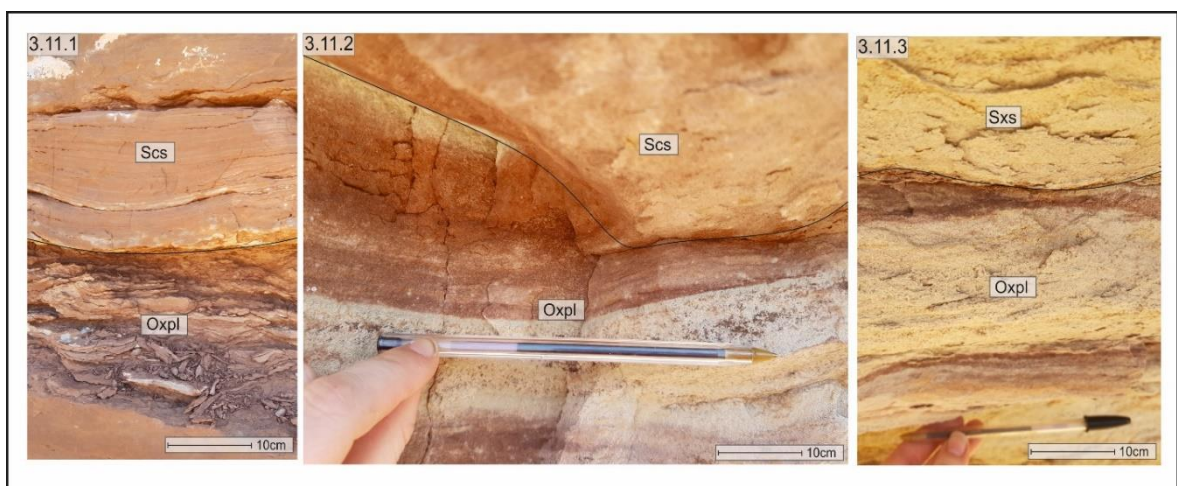


Figure 3.11.1-The most distal expression of the facies OxpI at Duma Point Transition 1 (Locality 4), the purple colour is characteristic of the oxidized iron minerals Figure 3.11.2- Characteristic yellow, green, and purple striping that defines a parallel laminated oxisol at Lone Mesa (Locality 2) Figure 3.11.3- The most proximal expression of OxpI, featuring the purple, green and yellow banding at Bartlett Wash (Locality 1).

3.3.3 Saline Soil with Sulphate Reduction- Sasr

Description- A strong yellow colour characterises this facies; the grain size is very fine-grained and unusually well-consolidated. Isolated staining patches occur in the lower units, which have the same colour as the unit itself (Figure 3.12). The bedding is parallel, with the strong yellow bands interbedded with thinner, blue/grey ribbons (Figure 3.12). This unit is no more than 20cm thick and occurs exclusively at Lone Mesa (Locality 2), making it somewhat anomalous.

Interpretation- The yellow colour, consolidation and staining are all secondary processes brought about by when the water table is lowered, oxidising sulphate minerals, producing sulphuric acid and ferric hydrate (Duchaufour., 2012). These processes occur in tracts of low-lying land that stand free of nearby water bodies, which may go some way to explaining the limited occurrence of the saline soil (Sasr).

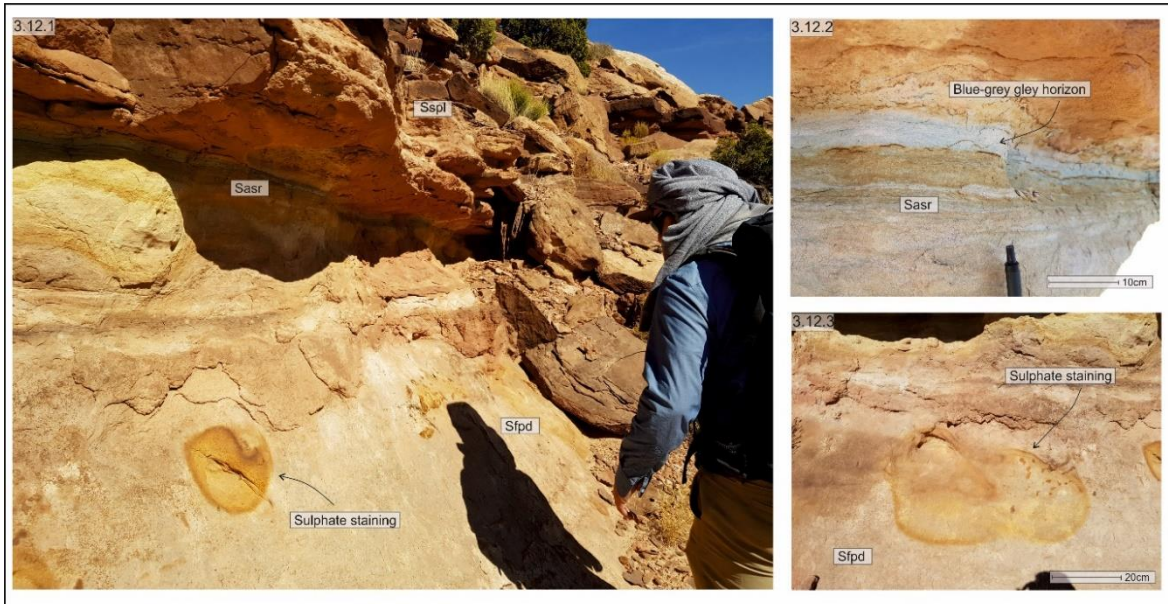


Figure 3.12.1-Yellow staining within unit's underneath Sasr, including the thin yellow bed and gley horizon that I visible above. Figure 3.12.2- Strong yellow bed rich in sulphate minerals, overlain by a blue grey gley horizon at Lone Mesa (Locality 2) Figure 3.12.3- Close-up of the yellow staining caused by sulphate leaching, unique to Lone Mesa.

3.4 Shallow Water Facies

Shallow water facies typically describes those deposited within the shallow marine tidal environment, defined as 0-200m below sea level. Facies found within this environment are dominated by thick fine-grained deposits with characteristic features such as ripples and herringbone cross-stratification.

3.4.1 Parallel Laminated Inverse Graded Siltstone- Ssgpl

Description- The grain size of the parallel laminated inverse graded siltstone facies (Ssgpl) is predominantly silt, inverse grading into sand towards the top of the unit. Grains are well-sorted and well-rounded and form beds of uniform thickness. Contacts between beds are slightly undulose, poorly consolidated, and have a distinct columnar weathering pattern (Figure 3.13).

Interpretation- The grain size and contacts between the beds are strong indicators of suspension settlement within shallow-moderate depth water (Flemming, 2011). Sub-aqueous deposition of silty sediments requires low energy water. However, the coarsening upwards trend also implies an increase in energy upwards. The columnar appearance on the surface of the siltstone (Ssgpl) is a secondary feature caused by the weathering of fine-grained material (Figure 3.13).

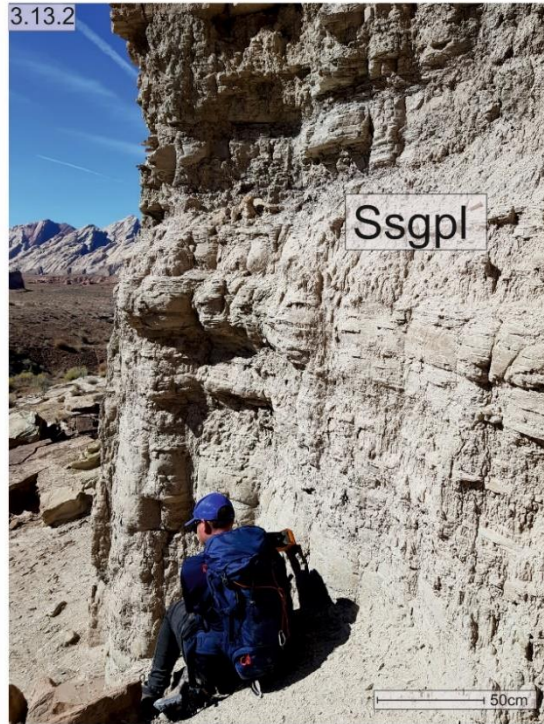


Figure 3.13.1-Cliff face formed of facies Ssgpl that has been weathered to appear columnar, note the characteristic grey colour of the unit when compared with the overlying coarser grained pink unit Spl. Figure 3.13.2-Closer view of the Ssgpl facies, beds can appear discontinuous, but this is likely to be a weathering feature than a depositional one. Figure 3.13.3- Outcrop scale view of Ssgpl and its overlying facies at the San Rafael Swell (Locality 5).

3.4.2 Parallel Laminated Sandstone- Spl

Description- Parallel laminated sandstone (Spl) is a characteristically pink, very fine-grained sandstone that is well-sorted and moderately well-consolidated. The grain size coarsens upwards from very fine at the base to fine-medium sand at the top. Units comprise 1m thick parallel laminated sandstones with slightly undulose contacts between the beds (Figure 3.14). The surface of the deposits features prominent weathering that appears columnar (Figure 3.14).

Interpretation- Parallel laminated siltstone (Spl) represents suspension settlement of very fine to fine-grained material transported by low energy currents. The coarsening grain size and thickness of the beds upwards implies episodic and uniform increases in energy within a calm sub-aqueous environment (Flemming, 2011).

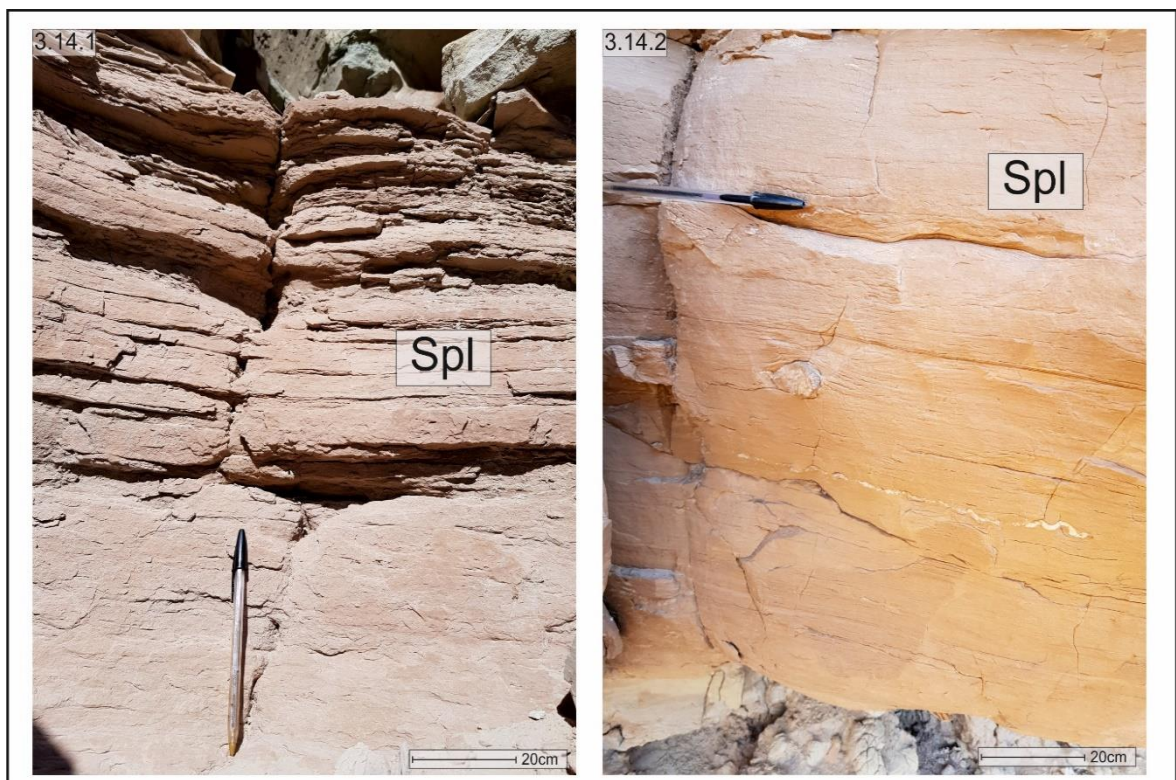


Figure 3.14.1- Characteristically pink unit of Spl that directly overlies the Ssgpl facies at the San Rafael Swell locality. Figure 3.14.2- Closer view of the Spl facies, parallel laminated sandstones are an unusual facies and appear only at this locality.

3.4.3 Ripple Laminated Sandstone- Srpl

Description- This facies comprises a light grey, moderately sorted, moderately rounded lithic arenite of very fine sand grain size. There is uniform lamination within the unit featuring incredibly well preserved 'crinkle-cut', round-topped ripples that proliferate upwards. Some flame structures can be seen sporadically, although often relatively small (millimetres) in scale. There are also clear foresets that can be seen intersecting within the ripples themselves (Figure 3.15).

Interpretation- Ripple laminated sandstone (Srpl) is formed by sub-aqueous migration of bedforms in lower flow regime conditions. The crest morphology is the most reliable indicator of environment. Round-topped ripples show a relatively deep water depth compared with those found in facies Surpl (Kreisa & Moila, 1986).



Figure 3.15.1-Bed of facies Srpl, featuring cross-laminated peak-crested ripples. Although this bed is only ~30cm thick, it can occur frequently in a succession, often interbedded with Mpl. Figure 3.15.2- Edited image of figure 3.15.1 highlighting the ripple crests and internal structure of the ripples.

3.4.4 Wavy Bedded Sandstone- Swb

Description- Light grey, moderately sorted, moderately- to well-rounded very fine- to fine-grained sandstone. Irregular undulous lamination with poorly preserved asymmetrical ripple forms. Siltstone laminations are present over ripple top bounding surfaces and basal set surfaces, preserving as siltstone in an undulous and wavy fabric.

Interpretation- Diurnal tidal variations may be the cause of mud and silt draping on foresets, set surface drapes may also be coincident with diurnal fluctuations, but may also be associated with large-scale annual variations. Drapes are commonly associated with a variation in the amount of suspended load sediment available during bedform deposition (Kvale, 2012; Philips et al., 2020).

3.4.5 Flaser Bedded Sandstone- Sfb

Description- Grey, moderately to well sorted, moderately- to well-rounded fine-grained sandstone. Irregular undulous laminations of siltstone can be found throughout. Ripple forms can be seen throughout, draped with siltstone. Base of the facies is indicative of more bifurcated type drapes, whereas simple drapes become more common upwards.

Interpretation- Alternation between oscillatory and unidirectional currents with periods of slack water (Howell, et al., 2022)

3.4.6 Herringbone Cross-stratified Sandstone- Sxhc

Description- The composition of this unit is a yellow-grey, moderately sorted, sub-rounded, argillaceous lithic arenite of very fine sand grain size. The internal structure varies somewhat; occasional ripple cross-lamination can be found at the top and base of the unit. However, a large percentage of the bedding can be

identified as cross-laminated with sets in opposing directions. Foresets within the beds display a periodic change in direction, with the foresets often being topped by mud drapes (Figure 3.16).

Interpretation- This type of structure is referred to as herringbone cross-stratification and strongly indicates tidal wave action (Stride, 1982). Differences in the direction of water flow and turbulence between periods of movement and quiescence create foresets that migrate in different directions (active periods, flow, and ebb tides), and mud drapes over them (periods of settlement, slack water).

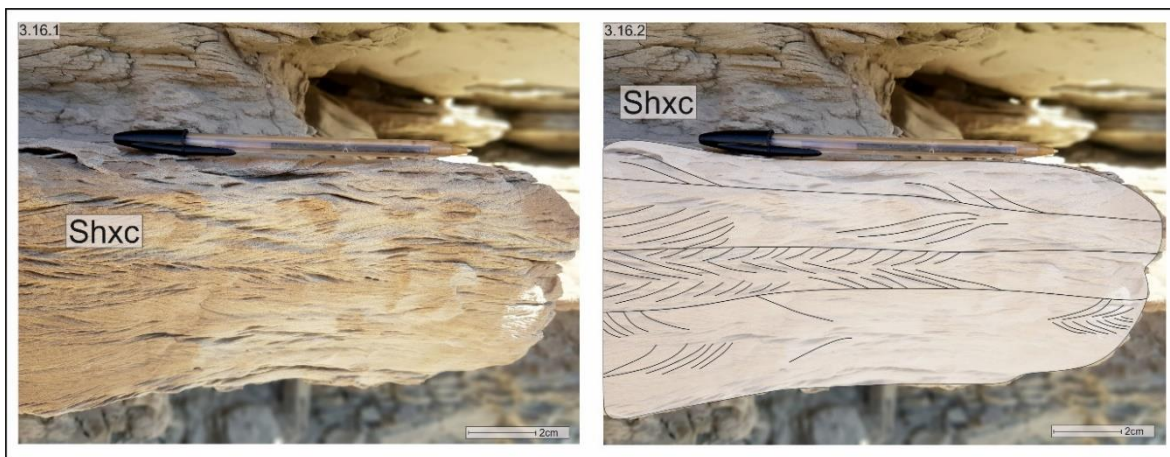


Figure 3.16.1-Bed ~30cm thick demonstrating textbook herringbone cross-stratification features bi-directional foresets with mud drapes separating them. The mud drapes have since been eroded away leaving the oval shaped depressions. Figure 3.16.2- Edited image of figure 3.16.1 highlighting the internal structure of the unit and the clear herringbone features.

3.5 Facies Associations of the Entrada/Curtis/Summerville Formations

Each of the facies identified at the localities across the study area can be grouped into associations based on several shared characteristics. When combined and contrasted, these characteristics highlight ten sub-environments into which the above lithofacies can be classified. Some of the previously described lithofacies fit into multiple associations. These associations can be placed alongside

sedimentary logs to provide a generalised idea of changing depositional environments with movement up a succession (Figure 3.17).

3.5.1 Sinuous-crested Aeolian Dune Association- SinD

Description- This association predominantly features units of trough-cross bedded sandstones (Stxs), stacked into sets that interfinger with small deposits of planar bedded sandstones (Sfpd). Units of trough cross-bedded sandstone (Stxs) comprise foreset grainflows between 3 and 10cm thick, topped by millimetre scale very-fine grained grainfall laminae. These sets are bounded by planar surfaces that truncate the tops of the foresets. The sets are then further arranged into cosets that thin upwards, also bounded by planar surfaces that are laterally extensive and slightly convex at outcrop-scale. The contact between trough cross-bedded sandstones (Stxs) and planar bedded sandstones (Sfpd) is conformable and distinct laminae can be found within the bed. Beds of planar bedded sandstone (Sfpd) are no more than 30cm thick and are found along the toesets of dune packages separated by set bounding surfaces. At the top of the succession a parallel laminated oxisol (Oxpl) is seen, represented by a 50cm thick bed containing three distinct bands of colour: a strong purple at the base, topped by a yellow-beige bed, capped by a greenish band within which sparse round-topped ripples can be found. At Lone Mesa, parallel laminated oxisol (Oxpl) is overlain by a ferrallitic gleysol (Fegl), identifiable from its red-brown mottles within a paler, sandy matrix. This unit is colloquially termed the 'popcorn facies' (Zuchuat *et al.*, 2018, 2019) after its bobbly surface texture. Along with the contact between parallel laminated oxisol (Oxpl) and ferrallitic gleysol (Fegl), mineral concretions can be found that are grey, have a metallic shine to them and are heavier than the surrounding sediment.

Interpretation- The grainfall and grainflow strata combined with the geometry of the bounding surfaces establishes the sinuous-crested aeolian dune association (SinD) as a migrating dune field, comprised predominantly of sinuous crested dune-scale bedforms. Wind ripples along dune toesets is an indicator of strong winds, or at the very least, winds with sufficient energy for traction to dominate (Kocurek, 1991). Parallel laminated oxisol and ferrallitic gleysol (Oxpl, Fegl) represent a marine incursion, creating calm shallow water conditions within which silty material could be deposited via suspension settlement. The strong colour banding and mottles are secondary features that occur when the water table lowers again, oxidising the iron minerals within the soil and creating the red/brown and purple colours. When found together parallel laminated oxisol (Oxpl) and ferrallitic gleysol (Fegl) tell a story of water level rise, creating a hot, humid soil, followed by a rapid sea-level fall, oxidising the minerals, creating concretions, and marking a transition from a damp, ustic regime to an arid one.

3.5.2 Straight-crested Aeolian Dune Association- StrD

Description- This association can be characterised by stacked cosets of planar-cross bedded sandstones (Sxs), overlain by finer-grained planar-bedded sandstones (Sfpd). Basal units of Sxs contain foresets up to 1m thick overlain by reverse-graded finer-grained laminae. These foresets are grouped into sets that can be up to 5m thick, with planar set bounding surfaces reaching beyond outcrop scale. Rhizoliths can sporadically be found along foresets, towards the top of sets within the planar cross-bedded sandstones (Sxs). With movement up a succession of the straight-crested dune association (StrD), sets of planar cross-bedded sandstone (Sxs) get thinner, and the bedding becomes lower angle. In addition, the toesets of cross-bedded units increasingly display small-scale wind-ripple lamination and bleaching (Sfpd). These stacked packages of planar cross-bedded

sandstone (Sxs) are then overlain by beds of planar-bedded sandstone (Sfpd) with a maximum thickness of 7m. Beds of planar-bedded sandstone (Sfpd) are characterised by low-angle foresets that are very fine-grained and separated by millimetre thick deposits of inverse-graded material. Thickness variations within the straight-crested aeolian dune association (StrD) are prevalent across the transect. At the Bartlett Wash (Log 1) and Lone Mesa (Log 2) localities, it is at its maximum thickness of up to 19m. At Duma Point Transition 3, the thickness is just 5m, which then pinch out almost entirely into a package just 1m thick at Duma Point Transition 1 (Figure 3.1). Very sporadically, occurring only at Lone Mesa, the saline soil (Sasr) outcrops. The bed is typically thin, no more than 50cm thick, comprising bands of silty sediment with distinct colour bands, similar to the parallel laminated oxisol facies (Oxpl), however, in this case, the colours are a strong yellow, interbedded with layers of blue-grey material. Whilst the unit of saline soil (Sasr) itself is only 50cm thick, patches of yellow staining can be found in lower units associated with the leaching of minerals from the yellow band above.

Interpretation- Straight-crested aeolian dune association (StrD) can be interpreted as deposits of migrating straight-crested aeolian dunes. Planar cross-bedded (Sfpd) set of fine-grained sand interbedded with reverse-graded finer material represents grainfall and grainflow structures that show well-developed dunes with slip-faces at or near the angle of repose (Hunter 1977, Mountney and Thompson 2002). The planar set-bounding surfaces are an indicator of dune morphology, which is straight-crested in this case. The laterally extensive surfaces that separate the stacked dune packages represent supersurfaces caused by periods of deflation, stabilisation, or flooding, supporting the separation of the straight-crested aeolian dune association (StrD) into five distinct packages, each representing a different state of the dune field at a given time (Mountney, 2006).

Decreasing bedding angle with movement up the succession also supports an increasing water influence within the system. This is further emphasised by the development of wind-ripple lamination and bleaching within the toesets of planar cross-bedded sandstone (Sxs), implying a rising water table (Mountney & Thompson, 2002). As sediment supply was restricted, possibly in response to the rising water table, bedform development was inhibited, and a sandsheet/ sand sea environment prevailed, preserved in the deposits of planar-bedded sandstone (Sfpd) (Fryberger & Schenk 1988, Mountney & Jagger 2004, Priddy & Clarke, 2020). The characteristic yellow facies of the saline soil (Sasr) are formed from sulphate rich very shallow waters upon a coastal plain in a warm tropical climate whilst settlement deposition of clay muds creates the blue-grey gley horizons. The limited occurrence could indicate a limited local-scale rise in the water table, or, more likely, the water level rise was on a larger scale, but the saline soil (Sasr) was only deposited at Lone Mesa as it was a saline polder which is itself a restricted environment.

3.5.3 Sand sheet Association- SanS

Description- This succession is typically dominated by undulose sandstones (Sdun) and intermittently interbedded by trough cross bedded sandstone (Stxs) and planar bedded sandstones (Sfpd). Towards the top of the succession, a ferrallitic gleysol is seen (Fegl).

Interpretation- The sand sheet association is formed by a dramatic reduction in sediment supply starving the system, due to the water table being at or near or above the sediment surface (Mountney and Jagger, 2004). High water table conditions can be seen in the development of undulous bedded sandstones and in the illuviation of a ferrallitic gleysol. Trough cross bedded sandstones indicate

some minor singular sinuous crested dune forms will have been present at the sediment surface, no evidence of bedform trains is further evidence that the association is sediment starved.

3.5.4 Damp Interdune Association-DInD

Description- This association is characterised by trough-cross stratified sandstone units (Stxs) interbedded with undulose sandstone units (Sdun). The contacts between the units are slightly undulose and defined by a strong colour change, from the light grey/pink of trough cross-bedded sandstone (Stxs) to the strong reddy-brown of the undulose sandstone (Sdun). Basal units of trough cross-bedded sandstone (Stxs) can be up to 2m in thickness, stacked into packages between 3m and 10m in thickness. The interbedded undulose sandstone facies (Sdun) also decrease in thickness with movement up the succession however, it occurs more frequently. Basal occurrences of Sdun are thin and infrequent, featuring some mottling, however, the units gradually become more frequent and stronger in colour, displaying some small scale-ripples.

Interpretation- Damp interdune association (DInD) is interpreted as migrating sinuous-crested bedforms interacting with damp interdunes within an environment where the water table is at or near the capillary surface of the dune plinths (Mountney & Thompson, 2002). Periodic flooding of the interdune environment creates small pools of water, enabling the growth of plant life hence preserving mottling and ripples. The occurrence of the damp interdunes becomes more frequent upwards, implying the water table is rising as time progresses (Kocurek 1981, Crabaugh & Kocurek 1993, Mountney & Thompson 2002, Mountney 2012). Furthermore, the preservation of defined bands of alternating dune/ interdune facies is caused by higher levels of cohesion within damp interdune sands that

make them less susceptible to erosion by migrating dunes (Crabaugh & Kocurek, 1993), hence producing parallel beds of alternating facies with slightly undulose contacts.

3.5.5 Wet Interdune Association-WInD

Description- Occurrences of the wet interdune association (WInD) are infrequent and often pinch out laterally at outcrop scale. It comprises structureless sandstones (Scs), interbedded with silty beds (Sspl) that have a strong red colour, sporadically interjected with discontinuously rippled beds (Surpl). Sediments are well-sorted, and in some, the contacts between overlying and underlying sediments are often planar but can be undulose on a small scale.

Interpretation- Wet interdune association (WInD) is interpreted as sediments found within a wet interdune, present in the topographical lows between migrating sinuous crested dune forms. This conclusion has been determined mostly from the 'pinching-out' morphology combined with the small-scale ripples that support shallow-standing pools of water. Ripples are formed sub-aqueously as a result of periodic flooding, linked to a rising water table (Mountney & Thompson, 2002). The undulose contacts result from higher cohesion levels within damp interdune sands that make them less susceptible to erosion by migrating dunes (Crabaugh & Kocurek, 1993).

3.5.6 Supratidal Flat- SupTF

Description- Associations of this type comprise tabular bodies with planar bounding surfaces containing 1-1.5m thick parallel laminated muds and silts (Sspl), which accounts for 80-90% of the association. Undulose bedded sandstones (Sdun) interbedded with 20-50cm thick discontinuous rippled siltstone (Surpl) facies comprise the rest. The undulose bedded sandstones of this

formation are typically very well consolidated with soft-sediment deformation at the base. The lateral extent of this association is 61km, and the vertical extent is between 10 and 15m. Evidence of vegetation is sparse and is limited to beds of parallel laminated siltstone (Sspl) approximately 1m thick, slightly more consolidated than surrounding material that is mottled. There may also be some poorly preserved burrows along the surface of exposed units. Deposits of discontinuous rippled siltstone (Surpl) are rare but can occur in beds no more than 10cm thick at each of the localities. In addition, very sporadic bleaching occurs within the sandstone units. In distal localities the muds, silts, and sands (Sspl & Spl) form laminae whilst gypsum presents in three main morphologies, laminated, nodular and satin spar. This association is overlain by the erosive basal deposits of the Morrison Formation.

Interpretation- Thick deposits of red-brown horizontally laminated muds and silts result from fallout deposition upon a supratidal flat. Supratidal flats are often sparsely vegetated and even more sparsely bioturbated due to high salinity levels, unsuitable for sustainable habitats (Desjardins *et al.*, 2012). The intermittent coarser-grained sands with mud drapes and discontinuous ripples represent storm deposits, highly charged influxes of sediment that can preserve a centimetre thick bed in just a few hours (Scholle *et al.*, 1983). The presence of gypsum in distal localities suggests a subaerially exposed sabkha in an environment very sporadically exposed to conditions suitable for the precipitation of salts. This implies a setting where there is some tidal influence leading to the deposition of muds and silts but is restricted enough to 'trap' the seawater and evaporate it in such concentrations to produce nodules of gypsum 3.8x the brine concentration of seawater (Handford, 1991). The satin spar gypsum was formed through diagenetic

processes whereby horizontal and inclined fractures are infilled via the recharging of low-salinity surface waters (Gustavson *et al.*, 1994).

3.5.7 Intertidal Mud Flat- IMF

Description- Associations of this type comprise tabular bodies with planar to undulose bounding surfaces containing parallel laminated siltstones and mudstones (Sspl) in addition to rippled sandstone facies (Surpl). The thickness of the parallel laminated siltstones is between 1 and 5m comprising 70% of the association, a further 10% of the association is formed of the mudstones whilst thin beds (20-30cm) of symmetrical round-crested ripples make up the rest (Surpl). The lateral extent of this unit is 44m, yet its vertical extent is just 1-6m. Bedding may vary slightly upwards from parallel to wavy, although some bedding features may have been weathered away as the unit is so poorly consolidated. Units of parallel laminated siltstone (Sspl) are between 1m and 5m thick, with the interbedded sandstones no more than 50cm thick.

Interpretation- Relatively homogeneous successions of parallel laminated mudstones are characteristic of upper intertidal flat environments, marking a sedimentological transition between a tidally influenced mudflat and the supratidal flat, impacted only by storm deposits. In areas where no storm deposits have been preserved, the mudflat environment may be indistinguishable from the supratidal flat environment.

3.5.8 Intertidal Mixed Flat- IMSF

Description- Associations of this type comprise tabular bodies with planar and undulose bounding surfaces containing interbedded muds and silts (Sspl) and parallel laminated and rippled sandstones (Spl, Surpl, Sxhc). Parallel laminated muds, silts and sands comprise 50% of the association, whilst the remainder is

40% rippled sandstones and 8% massive sandstones. The remaining 2% is comprised of sporadic herringbone cross-stratified sandstones (Sxhc), however, this only occurs in the west of the study area. The lateral extent is 44m, with deposits that are thickest at the San Rafael Swell and Duma Point Transition¹ comprising 3-5m of preserved sediment overlying intertidal sand flats (ISF). This association occurs either with a gradational contact between intertidal sand flats at the base and intertidal mudflats at the top, or where intertidal mudflats are not present, a sharp contact into the supratidal flat association.

Interpretation- Alternating silt and sand deposits are characteristic of changes in energy from periods of quiescence within which finer grain sizes can be deposited to higher energy periods in which sand deposition is more prominent. This implies a systemic and rhythmic interchanging of environments associated with a tidal influence. This is further supported by herringbone cross-stratified sandstones, a facies that is unique to tidal environments as it is the expression of bidirectional flow patterns. Intertidal mixed flats make up the bulk of preserved deposits within a tidally influenced environment.

3.5.9 Intertidal Sand Flat- ISF

Description- Associations of this type comprise channel forms with convex bounding surfaces containing ripple laminated sandstones (Surpl), structureless sandstones (Scs) and parallel laminated silts (Sspl). Lateral extents range from 2-10m with vertical extents of 1.5-2m. This association is only present at the San Rafael Swell and Duma Point Transition 1. ISF is split into two primary successions, the first features structureless sandstones that contain small poorly preserved ripple foresets (Surpl) at the base that erode into underlying parallel laminated silts. The base of the sandstones contains load casts, and the silts are

lenticular, pinching out rapidly on a scale that is visible in the field. At the San Rafael Swell, the second succession features structureless and parallel laminated sands of a much coarser grain size than both the underlying and overlying sediments. Here the lenticular siltstones are absent and instead form thin parallel beds that occasionally interrupt the coarser-grained sandstones.

Interpretation- Towards the distal end of the transect (at the San Rafael Swell), deposits of ISF form the intermediary between underlying mudflats (SBF) and overlying upper intertidal deposits. Evidence of coarser-grained sandstones belonging to this association can be found across the transition, with an erosive contact at all localities, implying a large-scale transgressive shallow marine flat that evolved into a tidal-channel beach complex as sea level fell again. The structureless sandstones and channel infill deposits represent a poorly developed sandy channel system prevalent upon open-coast tidal flats. By contrast, the more distal deposits of ISF are more conducive to a gently sloping, tidally influenced beach environment. The change in grain size from silts above and below these deposits creates a convex-upwards profile, a common morphodynamic feature within the sand flats of mud-dominated tidal flat complexes (Kirby, 2000, Fan, 2012).

3.5.10 Subtidal Flat- SBF

Description- Associations of this type comprise of tabular bodies with planar bounding surfaces comprising parallel laminated silts (Ssgpl) and parallel laminated sands (Spl). Lateral extents range from 6.2km with vertical extents up to 30m overlying wet interdune association at the San Rafael Swell. Two-thirds of the succession comprises silt that has a general coarsening upwards trend and

characteristic grey colour, whilst the grain size in the top third remains consistent and has a light pink colour—both units' weather in a distinct columnar pattern.

Interpretation- The parallel fine-grained sands and silts light grey to light pink in colour indicate sub-aqueous deposition upon a mud-dominated sub-tidal flat. The columnar pattern is caused by secondary weathering processes and is not a factor in the environment of deposition. Sub-tidal flats generally show a fining seaward trend (Fan, 2012), showing a decreasing water level with movement up the succession into coarser-grained material.

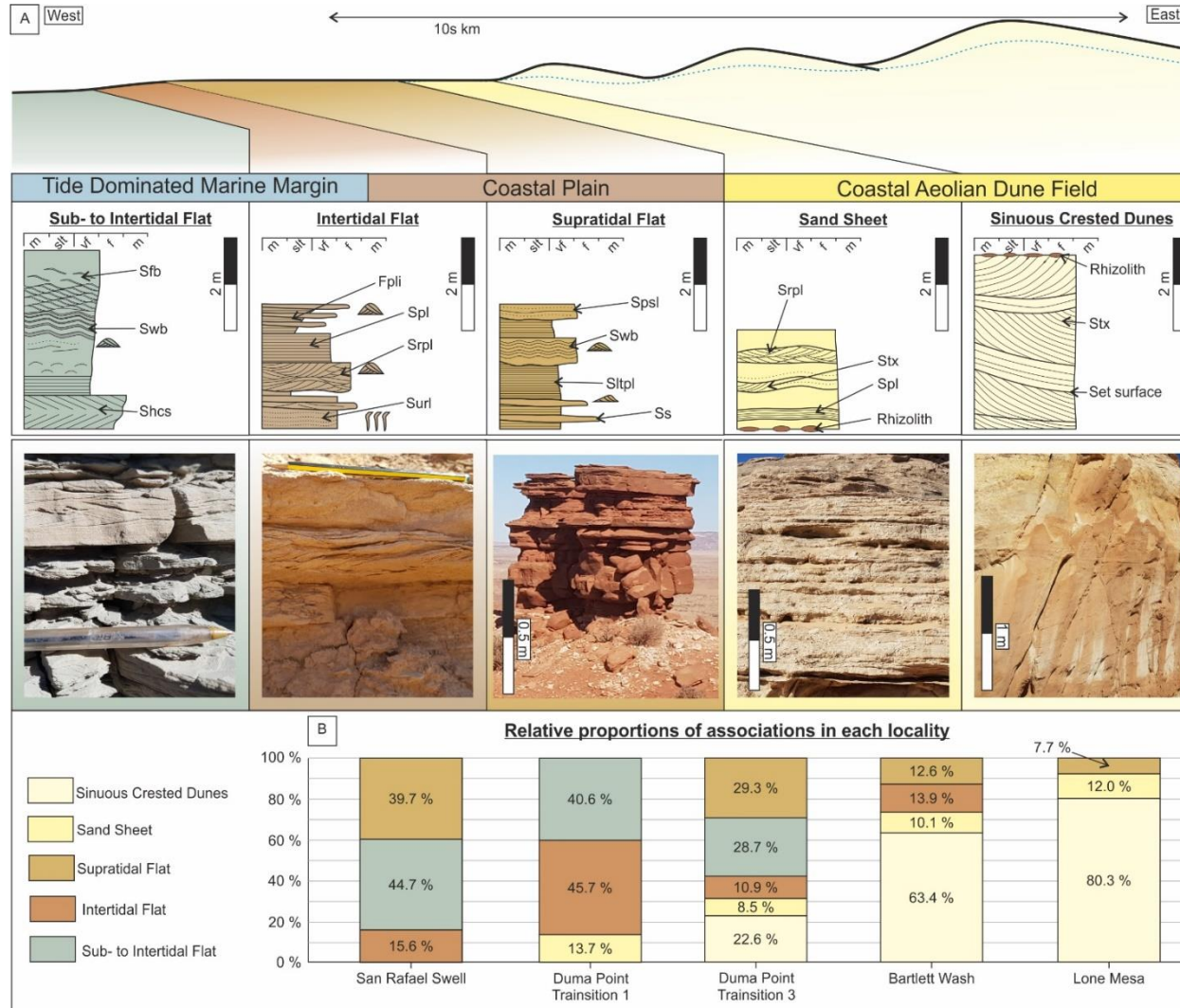


Figure 3.17- Schematic diagram showing the spatial transition between associations east to west across the study area. Sinuous crested dunes transition into smaller sinuous crested and straight crested dunes before deflating into a sandsheet. The supratidal flat expands both landward and seaward grading into an intertidal flat, and once the water depth becomes significant enough, a sub- inter-tidal flat. (B) Relative proportions of each association at each locality.

3.6 Assemblages of the Entrada/ Curtis/ Summerville Formations

The term 'assemblage' is used to mean the broad-scale depositional environment, combining the facies and associations described above.

3.6.1 Wet Aeolian Dune Field- CWDF

This assemblage is characterised by the interbedding of compound dune associations (CDA) and damp and wet interdunes (DInD, WInD). In this assemblage, dune facies are predominantly trough-cross bedded sandstone (Stxs) that are laterally extensive, stacking into cosets up to 10m thick with concave upper and lower bounding surfaces. These facies are typically overlain by undulose sandstones (Sdun) that are initially thin (0.3-0.5m) but increase in thickness and frequency vertically up to a maximum of 8m. Within the upper section of the environment, bands of rippled and silty sediment (Surpl, Sspl) are common, typically overlying the beds of Sdun, with the top of the assemblage marked by a laterally extensive palaeosol (Fegl, Oxpl) surface (Figure 3.18). These deposits represent an aeolian environment where sinuous crested dunes with damp and wet interdunes proliferate in the dune corridors (Kocurek 1991, Mountney & Thompson 2002). The increase in thickness and frequency of wet sediments (Sdun) up-section represents the environment becoming more humid with a decrease in the size and connectivity of dunes, resulting in more isolated sinuous dune forms surround by laterally extensive and interconnected interdune corridors, which are eventually stabilised as evident by the laterally extensive palaeosol that marks a final stabilisation of the dune field. These deposits form the stratigraphic units of the Entrada Slick Rock and the Entrada earthy facies and represent a damp and wet aeolian dune field. An idealised log through the wet aeolian dune field assemblage begins with deposits of trough-cross bedded

sandstone (Stxs) stacked into cosets with concave bounding surfaces that are up to 10m thick. Thin deposits of undulose sandstone (Sdun) begin to outcrop approximately two-thirds of the way up the succession. These deposits wet upwards become thicker and more frequent. In addition to the occurrence of damp interdunes, in the upper third thin bands of rippled and silty sediment (Surpl, Sspl) are evident, typically overlying the beds of Sdun. The top of the assemblage is marked by a palaeosol (Fegl, Oxpl), denoting the transition from a wet aeolian dune field into another environment (Figure 3.18).

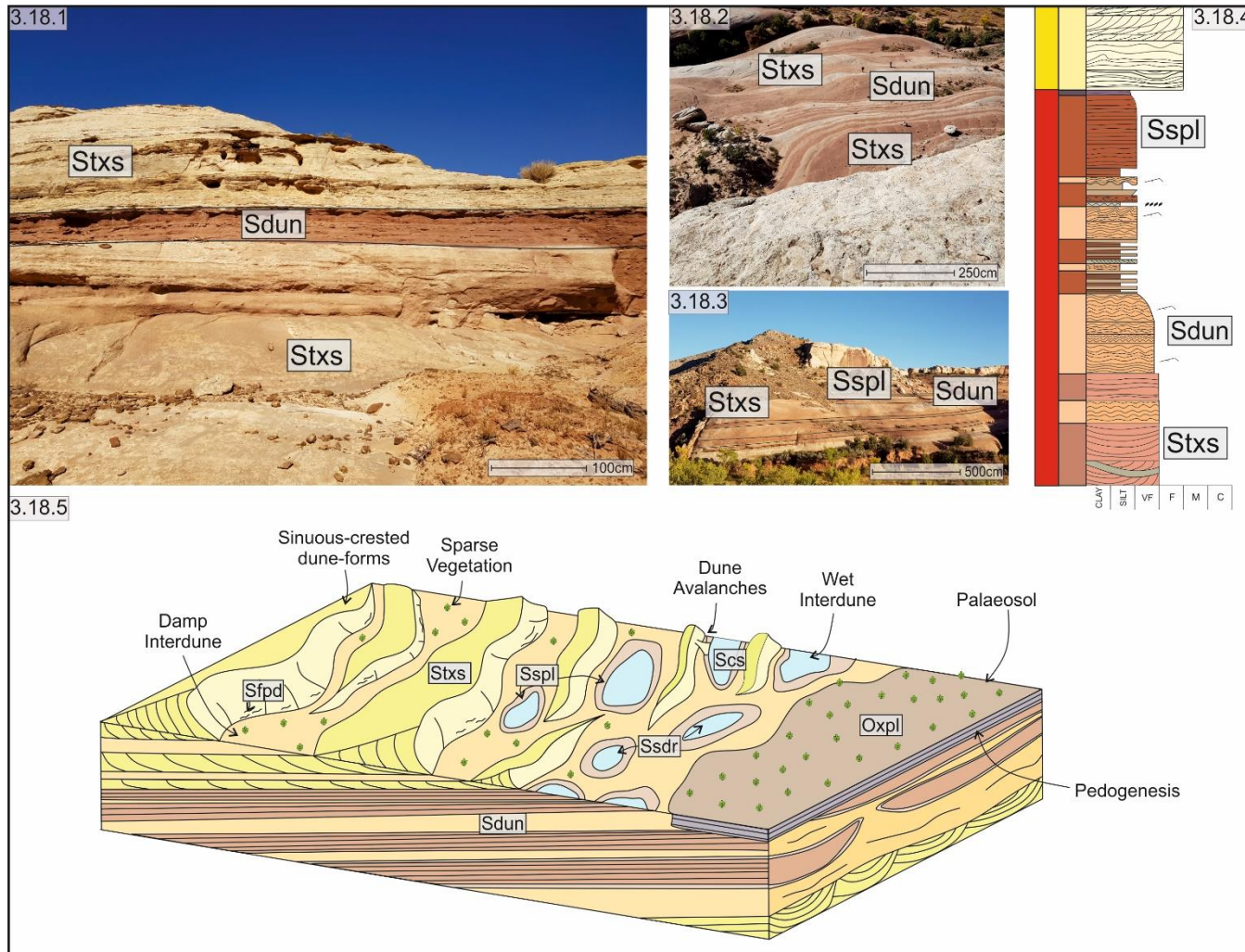


Figure 3.18.1- Field photo of the WDA, showing facies Stxs and Sdun. Figure 3.18.2- Aerial field photo showing the interbedding of Stxs and Sdun. Figure 3.18.3- Field photo taken at Bartlett Fault of the Bartlett Wash (Jedi-3D) outcrop. Figure 3.18.4- Numbered environments on the sedimentary log as identified within Figures 3.18.1, 3.18.2 & 3.18.3 1) Compound Aeolian Dune Association, 2) Damp Interdune Association, 3) Wet Interdune Association. The sedimentary log has been colour coded by facies, facies association and assemblage, with the red vertical bar representing the whole wet interdune assemblage. Figure 3.18.5- 3D depositional model showing the interaction between facies and associations within a wet aeolian dune system.

3.6.2 Coastal Dry Aeolian Dune Field- CDDF

This assemblage is characterised by the interbedding of compound dune associations (CLA) and wet interdune associations (WIA). An erosive boundary characterises the base of this assemblage and 1m thick deposits of structureless sandstone (Scs) with frequent loading and soft-sediment deformation features, these are in turn overlain by rippled and mud draped facies (Srpl). Dune facies overlie, predominantly planar-cross bedded sandstones (Sxs), and planar bedded sandstones (Sfpd) that are laterally extensive with planar upper and lower bounding surface. The thickest deposits occur in the east of the study area, stacking into five units up to 50m thick (Figure 3.19). Units 1-3 are comprised of planar-cross bedded sandstone (Sxs) with foresets truncated by local planar bounding surfaces, which are themselves truncated by super-surfaces that extend beyond outcrop scale with distinct rhizolith horizons along upper bounding surfaces. Units 4–5 consist of locally extensive thick deposits (7.5m) of planar bedded sandstones (Sfpd), which pinch out rapidly eastwards into coastal plain and shoreface environments, capped by a thin, isolated palaeosol with sulphate reduction surfaces (PS). Subsequent cosets of planar-cross bedded sandstones with truncated foresets indicate straight crested dunes which have formed into stacked prograding dune complexes. Rhizolith horizons on tops of coset/supersurface foresets indicate a hiatus between dune deposition, most likely in the form of ephemeral lagoons and saline lakes in periods of lower sediment supply/humidity/tidal flooding. The lateral extent of these combined with dune shape indicates straight interconnected interdune corridors (Pettigrew *et al.*, 2020). A change into planar bedded sandstones in upper units indicates a reduction in sediment supply and lack of dune development, resulting in a sediment bypass, forming a sandsheet that grades laterally into a tidally influenced marine setting.

The overlying palaeosol indicates restricted pooled water with a high saline content, within which sulphides can oxidise and hydrolyse into sulphuric acid, causing the yellow staining in the below units. Together these deposits form the Moab Member of the Curtis Formation and indicate a coastal dune field near a marine environment (Figure 3.19).

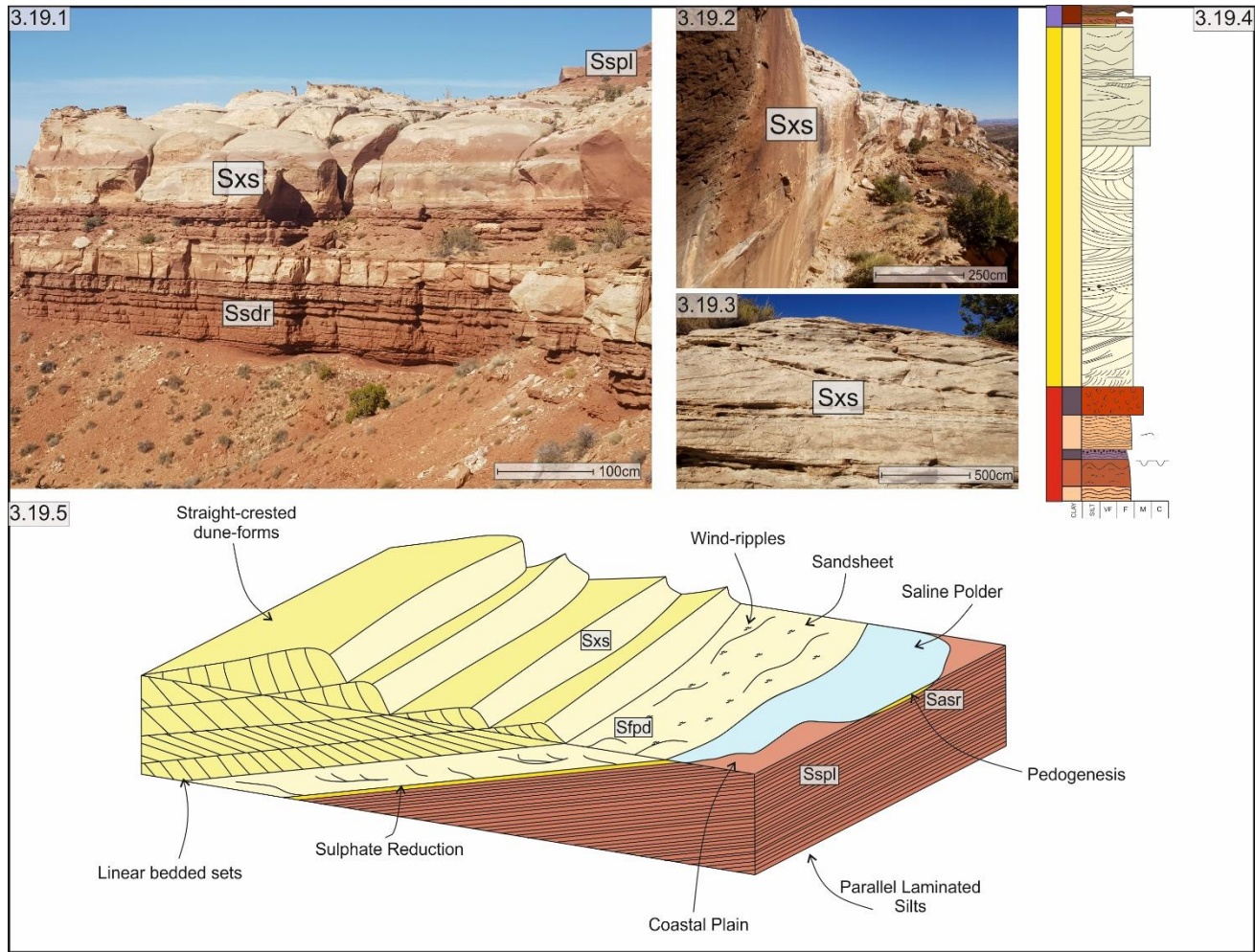


Figure 3.19.1- Field photo of the CDA at Dubinky Well showing the dry aeolian system overlying the wet aeolian system. Figure 3.19.2 Field photo of the CDA taken at Bartlett Fault. Figure 3.19.3- Field photo of the low-angle bedding within Sxs at Bartlett Fault. Figure 3.19.4 Sedimentary log with numbered environments showing the relationships between different cosets and associations within the assemblage. 1) Coset 1, 2) Coset 2, 3) Coset 3, 4) Cosets 4 & 5) Palaeosol & Coastal Plain. The sedimentary log has been colour coded by facies, facies association and assemblage, with the red vertical bar representing the wet interdune assemblage and the yellow bar representing the coastal dry aeolian assemblage. Figure 3.19.5- Depositional environment of CDA showing the interactions between the facies and associations described above, supported by field photos of the preserved succession.

3.6.3 Coastal Plain- COPL

This assemblage is characterised by the interbedding of intertidal mudflat, supratidal flat, and marginal marine sabkha associations, comprising thick successions up to 16m, of poorly consolidated, parallel laminated muds and silts. The contact between the saline soil (Sasr) and the overlying supratidal flat (SPF) is conformable and non-erosive. Successions of COPL are formed of basal units of silts and very-fine grained sands (Surpl, Sspl) interbedded with thin laminations of coarser-grained structureless sands (Scs). These units are laterally extensive with planar upper and lower bounding surfaces and stratigraphic thicknesses of 1.5-2m (Figure 3.20). In the east of the study area, basal deposits contain some evidence of mottling and vegetation, whilst the west of the study area contains deposits interbedded with laminae, nodules, and veins of gypsum. Top-most units contain a greater percentage of mud grained sediments displaying a fining upwards in grain size than lower units and are barren of vegetation. The proliferation of fine-grained laminated deposits represent a calm depositional environment in which the fallout of suspended sediment dominated the depositional process. The lack of vegetation and the presence of evaporites indicate an arid and saline environment. The succession is known as the Summerville Formation and represents the transition from an intertidal mudflat into a supratidal flat, reflecting a decrease in tidal energy in the landward direction (Figure 3.20).

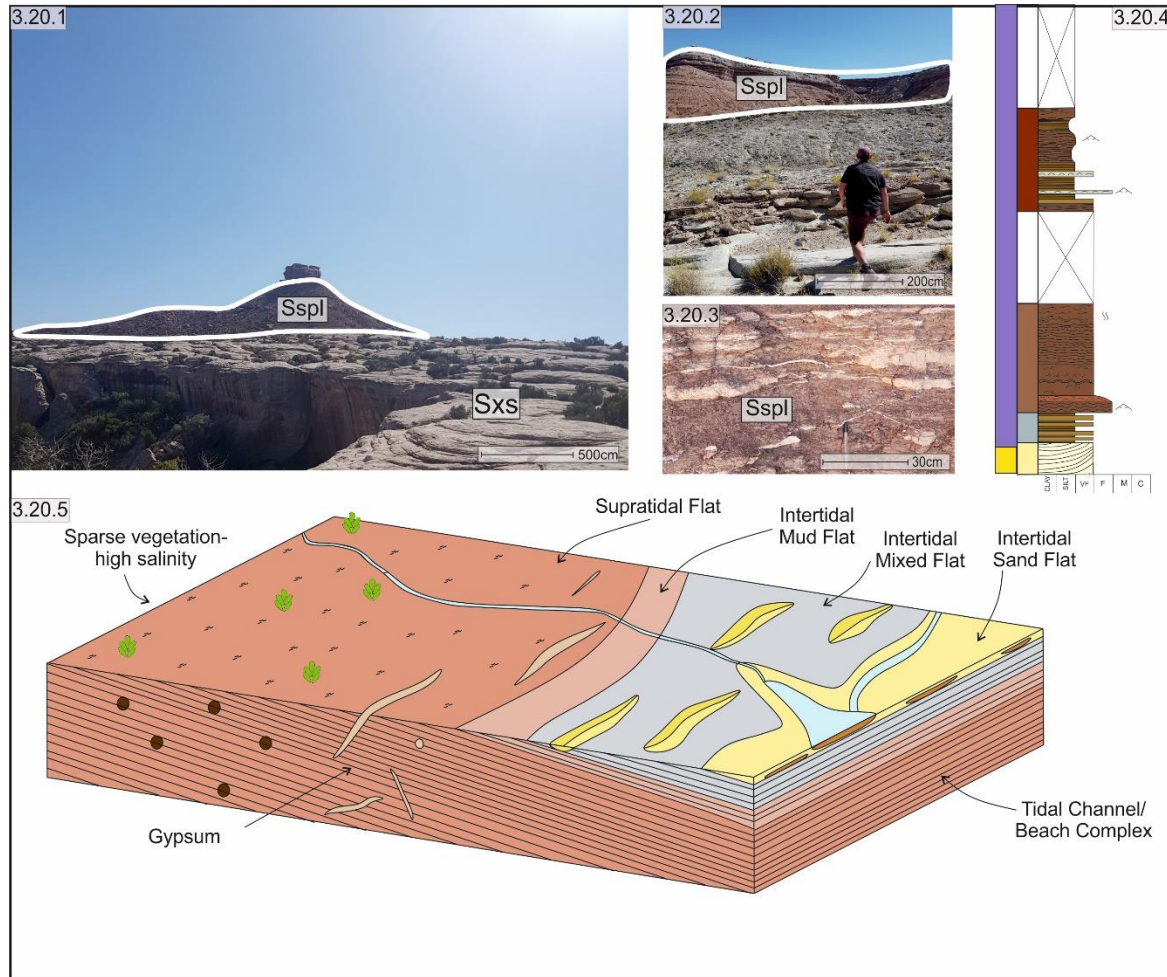


Figure 3.20.1- Field photo of the COPL assemblage overlying the coastal dry aeolian dune system at Bartlett Wash (Jedi 3D). Figure 3.20.2- Field photo of the COPL overlying the TISF assemblage at the San Rafael Swell. Figure 3.20.3- Field photo showing the gypsum morphologies visible within Ssepl/COPL at the San Rafael Swell. Figure 3.20.4- Sedimentary log with numbered environments showing the relationships between different associations within the assemblage. 1) Underlying aeolian dunes 2) parallel laminated silts of the coastal plain, 3) marginal marine sabkha. The sedimentary log has been colour coded by facies, facies association and assemblage, with the purple vertical bar representing the coastal plain assemblage. Figure 3.20.5- Depositional environment for the coastal plain assemblage showing the interaction between facies and environments described above, supported by field photos and sedimentary logs of the preserved succession.

3.6.4 Tide Dominated Marine Margin (TDMM)

This assemblage is characterised by sub-tidal flat and transitioning upwards through the inter-tidal sand flat and inter-tidal mixed flat environments before grading into the lowermost intertidal mudflat associations. Basal units comprise thick laterally extensive deposits (6.2km) of parallel laminated silts (Sspl) with planar upper and lower bounding surfaces. Up succession, the deposits become increasingly heterogeneous, interbedded with beds of very fine-grained parallel laminated sandstone (Ssgpl), which become progressively thicker and more prevalent (Up to 28.5 m). Above, an undulating erosive bounding surface separates the parallel laminated sands from coarser-grained, ladder rippled sandstones. Silt laminae (Sspl) overlie these sediments, interbedded with well preserved, peak-crested symmetrical ripples. The upper boundary between TDMM and COPL occurs without much significant change in sedimentology, and it is recognisable by a lack of vegetation and a slight decrease in average grain size (Figure 3.21). Deposits of TDMM are found best preserved at the San Rafael Swell (Locality 5), representing a full transition from sub-aqueous through to sub-aerial deposits of a shoreface environment. Subtidal flat deposits are characterised by heterolithic succession of parallel laminated muds and sands that coarsen upwards, occasionally interjected by coarser-grained sand deposits indicative of a low energy-restricted coastal environment subject to inundation by sporadic higher energy, possibly storm events. As the environment transitions into an intertidal sandflat, extensive coarser sandstones with prominent ladder ripples on the surface can be found at the San Rafael Swell and are correlative with channelised sandstones found at Duma Point (Transition 1). Heterolithic deposits of muds and sands found between the intertidal sand flat and the basal deposits of the coastal plain are indicative of a higher energy system subject to increased tidal

influence demonstrated by peak-crested symmetrical ripples, herringbone cross-stratification, and occasional mud-draping (Figure 3.21).

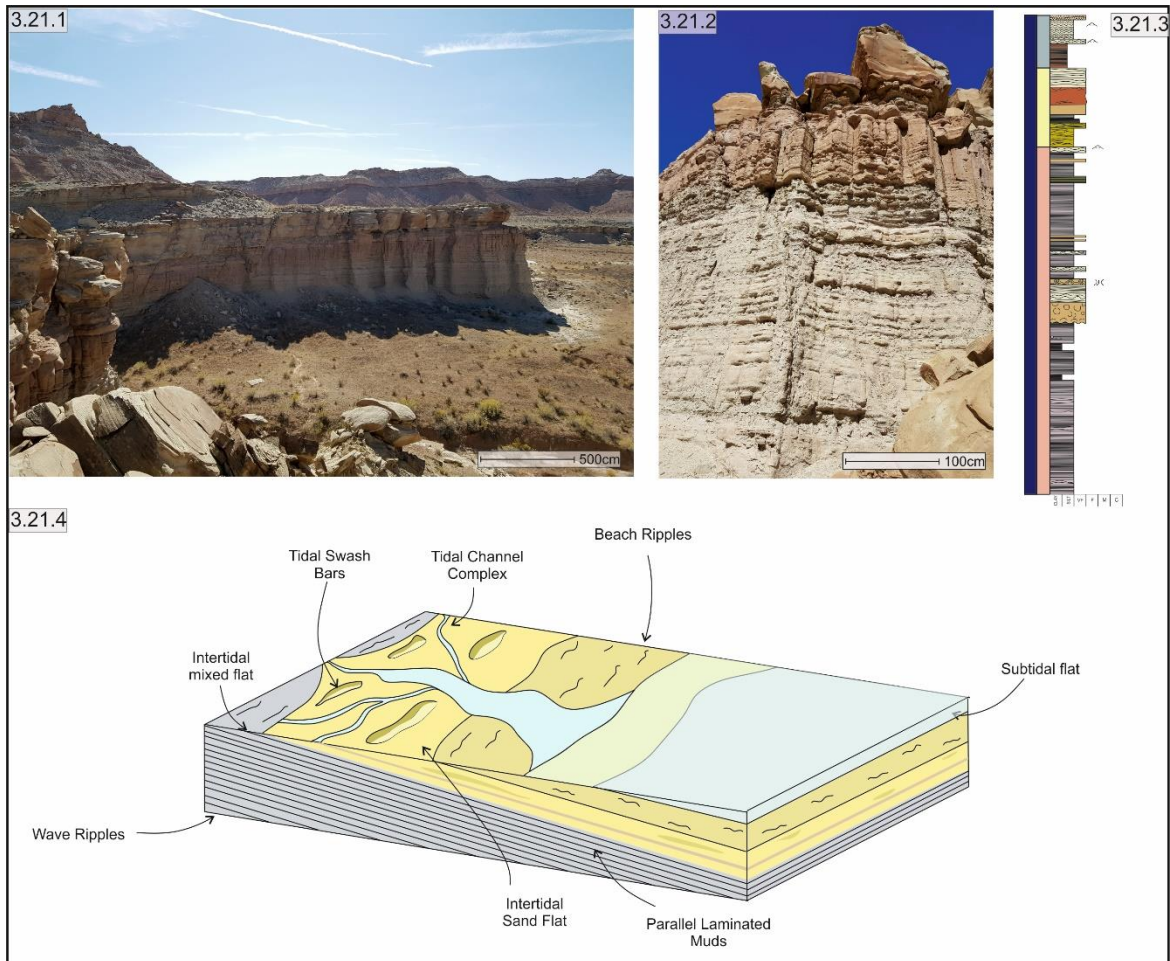


Figure 3.21.1- Field photo of the whole tidally influenced shoreface succession at the San Rafael Swell from the sub-tidal mud flat through to the intertidal mud flat. Figure 3.21.2- Field photo of the intertidal sand flat deposits overlying the subtidal mud flat deposits within the TISF, note the unique columnar weathering pattern. Figure 3.21.3- Sedimentary log with numbered environments showing the relationships between different associations within the assemblage. 1) Subtidal Mud Flat 1, 2) Subtidal Mud Flat transition 3) Intertidal Sand Flat, 4) Intertidal Mixed Flat. Sedimentary log has been colour coded by facies, facies association and assemblage, with the dark blue vertical bar representing the tidally influenced shoreface assemblage. Figure 3.21.4- Depositional environment model for the tidally influenced shoreface assemblage showing the interactions between facies and associations described above, supported by field photos and sedimentary logs of the preserved succession.

3.7 Summary

This chapter has summarised the facies, associations and assemblages identified at the five localities investigated by this study. The east to west transect crossing south-eastern Utah between the town of Moab and the San Rafael Swell document the occurrence of fifteen unique facies. These facies can be considered as indicators of small-scale environments, termed associations, that can establish local changes in controlling factors such as sediment supply, wind capacity or water level. When combined, large-scale assemblages can be established to determine influences on deposition and preservation, such as climate and relative sea level.

Chapter 4: Quantifying Dune Geometry on an Aeolian-Marine Margin

Recent advances in technology have seen the rise in studies that use photogrammetry to quantify dune form evolution, dune field migration and palaeo-dune morphology (Hugenholtz *et al.*, 2012, Solazzo *et al.*, 2018). Spatial analysis of preserved aeolian successions offers in-depth documentation of boundary conditions, dune activity, dune patterns, hierarchies, and inter-dune relations (Hugenholtz *et al.*, 2012). This chapter documents the spatial analysis carried out on the aeolian system neighbouring the palaeo Curtis Sea in southeast Utah via high-resolution photogrammetry. In the field, measurements of grainflow thicknesses were obtained from sedimentary logging where the outcrop was accessible. In areas where the outcrop was inaccessible, grainflow and set thicknesses were obtained from 3D photogrammetric models. In addition, the aeolian successions and the major surfaces that bound them were identified at each locality to provide an in-depth analysis of the individual outcrops studied.

Quantifying the palaeo dune height and sediment supply would enable the spatial interaction of the aeolian/marine margin to be established. Data obtained are interpreted in the context of changes in dune field complexity through time.

Increases or decreases in palaeo dune height are interpreted in terms of sediment supply and complexity changes towards the margin. Interpretations of large and small-scale bounding surfaces identify changes in deposition and preservation conditions, interpreted to result from local changes in sea level relative to the margin of the dune field through the evolution of the system.

4.1 Background

Unmanned Aerial Vehicles or UAVs are defined as any generic aircraft designed to operate with no human pilot onboard and can be colloquially referred to as drones (Remendino *et al.*, 2011). The use of drone photogrammetry to produce 3D models that can be analysed to supplement field observations is well practised (Seibert & Teizer 2014, Harvey *et al.* 2014, Jordan 2015), and modern use of photogrammetry comprises plan-view landform studies, digital elevation models, and vertical cliff-face sections (Priddy *et al.*, 2019). In aeolian systems, drone photogrammetry is often used to map the movements of active sand seas and the modern-day relationship between sand area and sand volume (Solazzo *et al.* 2018, Casella *et al.*, 2020). The parameters obtained from photogrammetry of ancient aeolian systems are different from that of modern systems but still provide a distinct advantage in terms of examining and quantifying spatial interactions and lateral outcrop visibility (Cousins, 2020). The nature of preserved aeolian successions is such that any significant deposit can represent any amount of time. The information critical to the observer, such as bounding surfaces and units, are often best interpreted at outcrop scale. Hence, drone photogrammetry provides a unique opportunity to view outcrops as a whole from a parallel viewpoint that is superior to the viewpoints accessible with the human eye (Cousins, 2020).

4.1.1 Principles of UAV Photogrammetry

Recent advances in unmanned aerial vehicle (UAV) technology have allowed for flexible generation of high-quality aerial photography at a relatively low cost. Consequently, drone-based photogrammetry lends itself to field use for geological research and produces low-cost, high-efficiency models for analysis. There is a range of viable UAVs that are of a suitable dimension for air transport between countries and by hand in the field, and they offer a wide range of potential uses in

a range of settings. The only limitations of such drones are the climatic conditions in which they can operate, such as temperature and wind speed. The appropriate temperature range for most commercially viable vehicles is 0-40°C, and they cannot operate at wind speeds higher than 10m/s. Whilst that makes flying in the UK somewhat of a challenge, climatic conditions in Utah are usually optimal for this kind of study during October.

UAVs are fitted with a gimbal allowing for three modes of stabilisation: pitch, roll, and yaw (Figure 4.1). Flight planning is important to consider before introducing the UAV into the field as an improper collection of data can lead to flawed models that are then hard to rectify (Uysal *et al.*, 2015). For the production of 3D models, the recommended flight path is horizontally along outcrops in uniform motion, flying incrementally higher along the yaw axis with each complete horizontal survey (Figure 4.3). To produce comprehensive and efficient models, the optimum overlap for photos is between 50-60%. This allows the processing software to establish enough common tie points to create a sparse point cloud that can later be textured (Bemis *et al.*, 2014). The resolvable surface captured by a UAV can be further improved by capturing a few images at a greater angle relative to parallel along the roll axis (Figure 4.2). However, this is limited to a change in angle of between 20-30°, after which point differences in lighting and perspective can interfere with the texture building. Therefore, to achieve optimal results for in-office analysis, photos should be taken along the horizontal axis, parallel to the outcrop, moving up succession in increments and with a change in the angle of the gimbal greater than 30° (Figure 4.2).

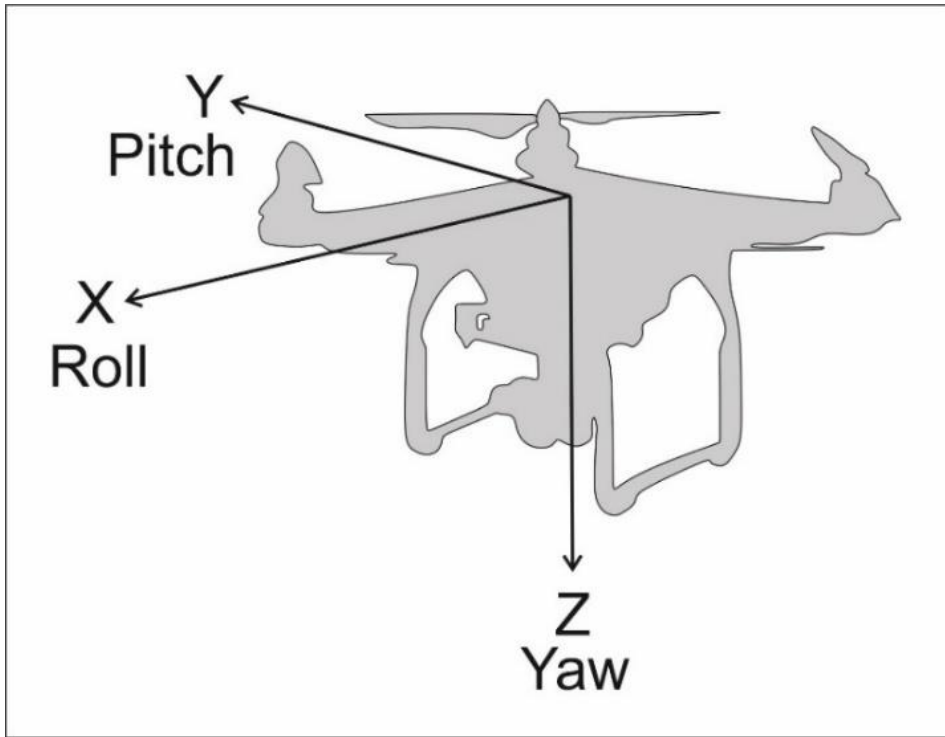


Figure 4.1- Graphic demonstrating the three stabilisation directions of UAV's that must be considered when flying and capturing footage.

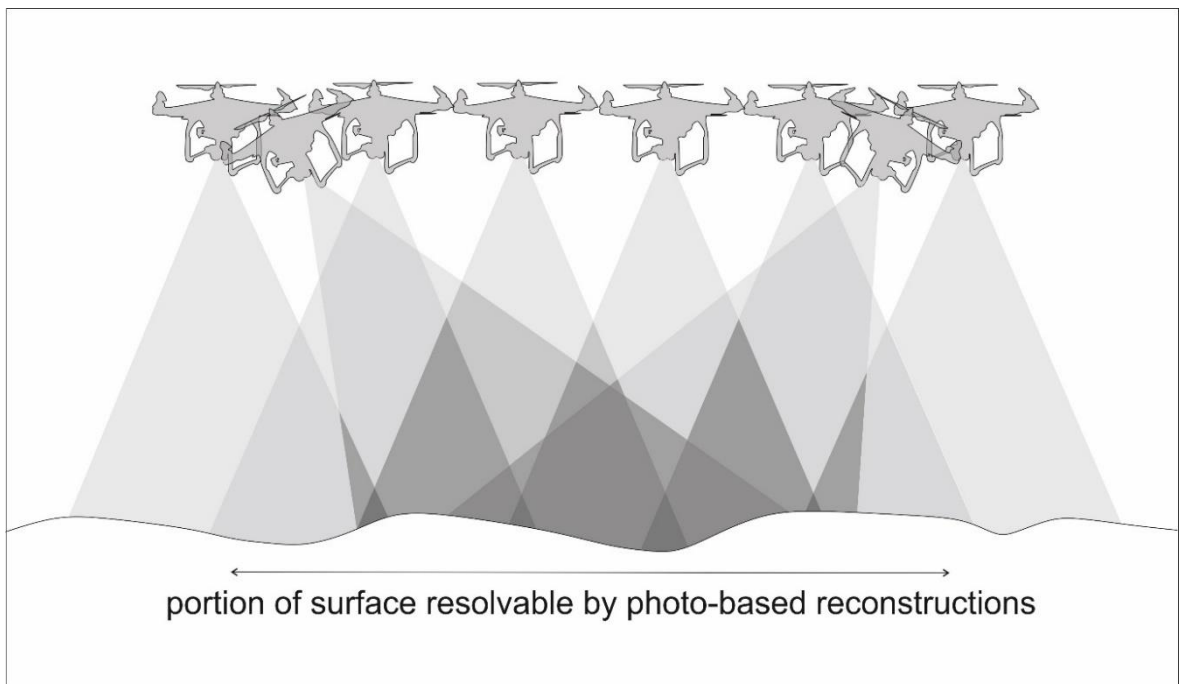


Figure 4.2- Overlapping field of view for a camera attached to a UAV, increasing darkness representing an increase in the number of cameras viewing that point.

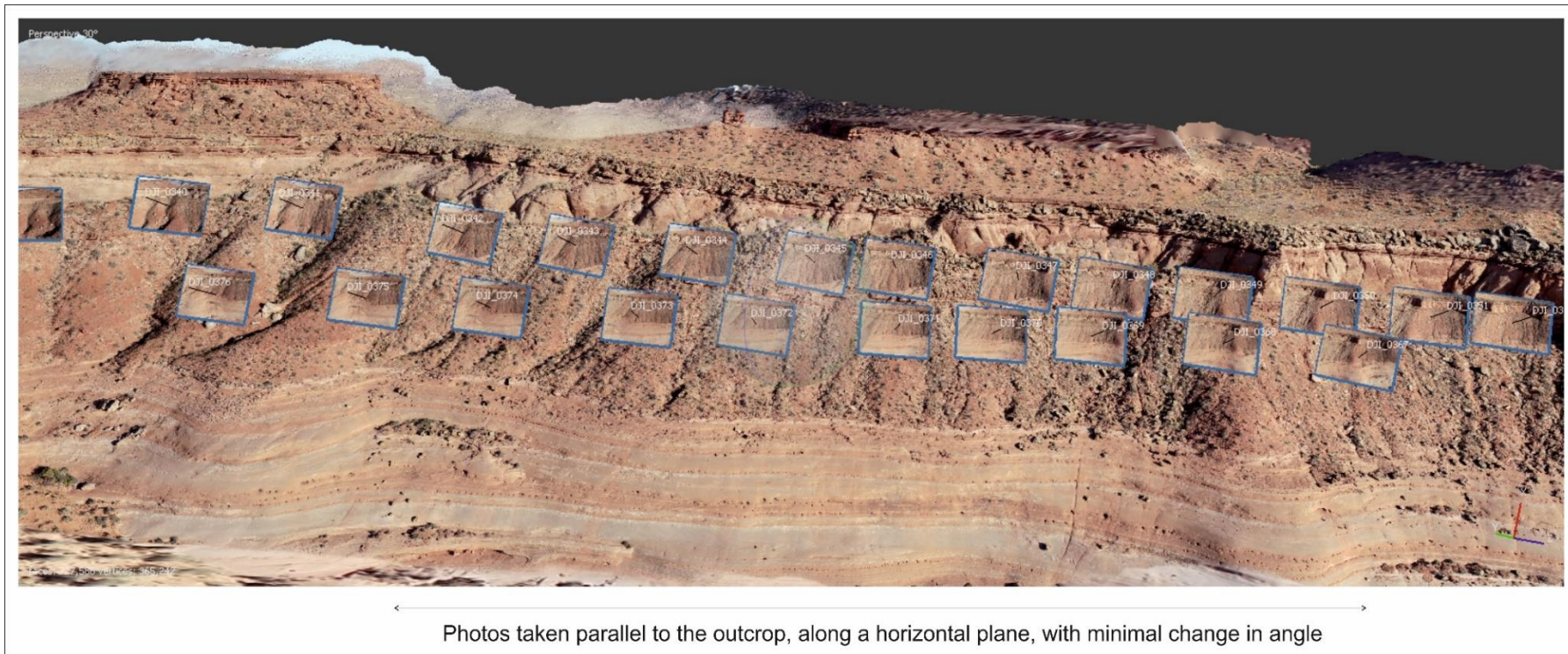


Figure 4.3-Panel showing the positions of photos taken by the UAV at the Duma Point locality, compared to the outcrop, note the distinct horizontal lines parallel to the outcrop at almost identical angles, to minimise the potential for error when composing the photogrammetric models.

Once the suitably georeferenced aerial photographs have been collected, they must be collated and stitched together using common tie-points to form a three-dimensional, interactive model (Figure 4.4). Image processing software has been developed that use algorithms to combine and interpret photos and construct 3D models. Structure-from-Motion (SfM) algorithms are the standard, and they enable the automatic orientation of large image sets without the need for additional data (Eltner *et al.*, 2016). Manual optimisation may be necessary to eliminate those with too little or too much overlap, differences in lighting or extreme contrasts in photo quality. A sparse point cloud can then be generated using common tie points identified by software algorithms as having at least an 85% overlap. Using these pre-defined tie-points, further data points are calculated to infill the gaps and form a dense point cloud. In the final step, dense point clouds are joined together to form a triangular mesh upon which a texture is overlaid, creating the final model. The triangulated mesh should then be imported into a 3D modelling application in which architectural elements can be identified and combined with palaeocurrent data to calculate volumes and geometries. Interpretation can be achieved up to cm-scale, providing the resolution is high enough, allowing for accurate measurement of set and coset bounding surfaces.

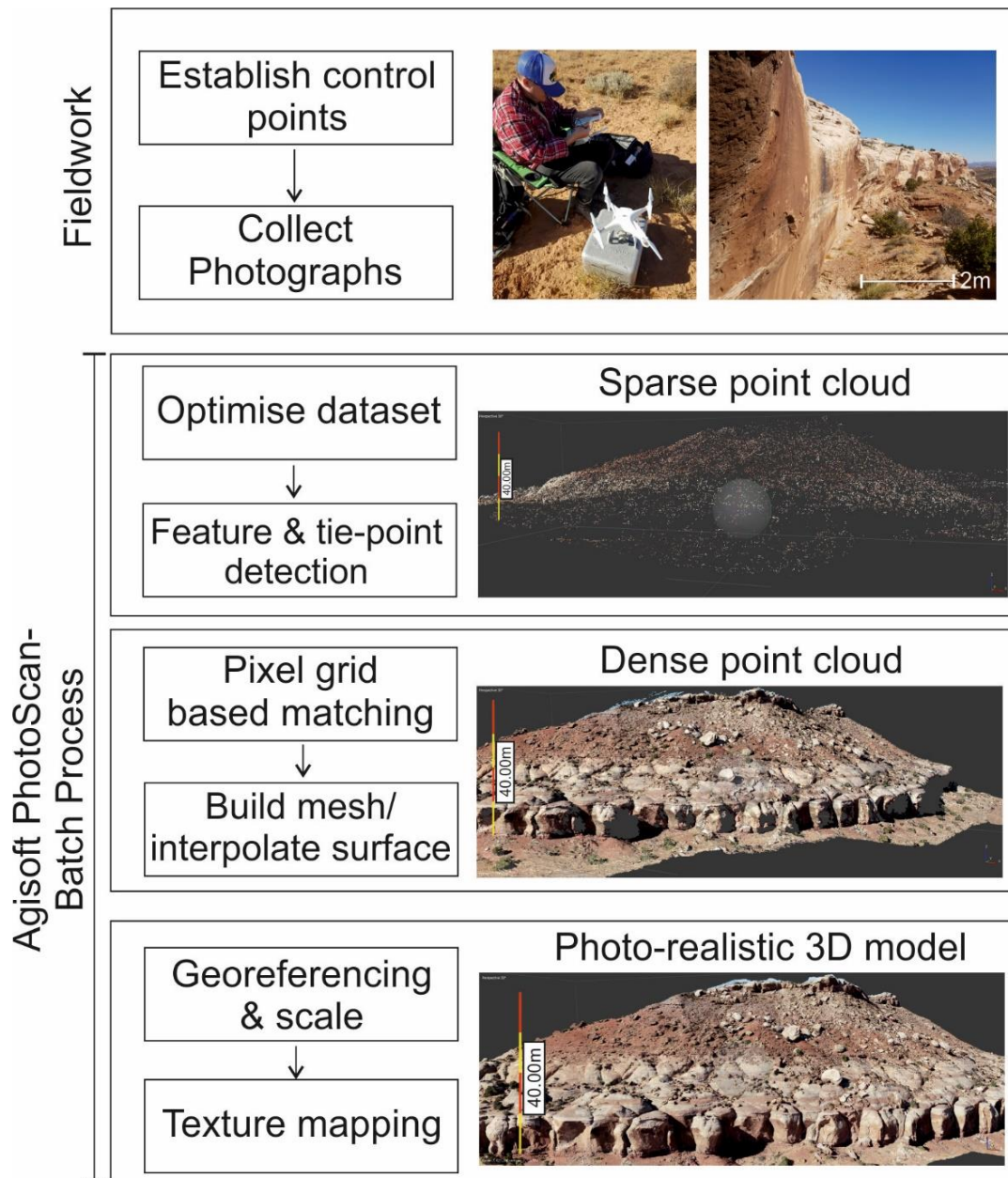


Figure 4.4-Workflow for producing a photo-realistic 3D model from UAV aerial photographs, using Agisoft Photoscan software

4.1.2 Use of UAV Photogrammetry within Preserved Aeolian Successions

In aeolian sediments, further analysis of field observations, measurements and 3D models obtained from UAV surveys can provide estimates of the controls upon the system at the time of deposition, i.e., the sediment supply and the sediment availability.

The interpretation of dune height from set thickness predates the use of commercially available drone flights to obtain such information. The relationship between the minimum grainflow thickness and slip face height is valuable in calculating the original minimum dune height (Kocurek & Dott, 1983). Contributing factors such as the rate of migration, the rate of sand supply, and the rate of subsidence may result in migrating dunes, leaving a variable thickness of preserved sets (Kocurek & Dott 1981). However, there is a more evident relationship between grainflow thickness and dune height (Howell & Mountney 1997, 2001, Romain & Mountney 2014, Romain 2014, Besly et al., 2018). There is a minimum height that a lee slope can reach before slip face failure occurs, and grainflow deposits can accumulate on the upper part of the lee slope (Wilson, 1971). Although there is no specific grainflow thickness attributable to 'large' or 'small' dunes, the thicknesses of grainflows within a single set of cross-strata are constant and can therefore be used to identify single dune heights within the system (Kocurek & Dott, 1981). By measuring a series of dune heights and grainflow thicknesses within the active Little Sahara Dune Field, Utah, Kocurek & Dott established a relationship between grainflow thickness in the toset region of the foreset and dune height. The graph for this relationship has been used as a template for predicted dune heights.

Comparing set thickness east to west across the transect is advantageous for mapping changes in the complexity of the dune field and the rate at which the dune field graduates into the neighbouring environments. The analysis of relative set and coset thicknesses can also be used in the context of establishing genetic packages, an aeolian accumulation capped by a super surface (Kocurek 1988, Kocurek & Havholm 1993, Crabaugh & Kocurek, 1993).

4.2 Methods

High-resolution photogrammetry was carried out to provide a 3D visualisation of the preserved aeolian successions. Initial field aerial photographs were obtained with a DJI Phantom 4 drone, used because of its extended flight time per battery (25-30 minutes), potential for high-resolution image capture, automatic georeferencing and ease of transport. Drone flight was carried out manually using the DJI remote application for mobile, allowing for real-time projection of the outcrop, ease of controls and instant photo back-ups, ensuring complete outcrop coverage. A further advantage of this UAV is that the application that allows flight and camera control contains automatic georeferencing information, reducing the need for additional data manipulation at the analysis stage.

Care was taken during the flight to ensure that aerial photographs covered the extent of the outcrop and overlapped to the degree that ensured complete and high-resolution models during later analysis. Changes in the camera angle along the 'roll' axis during horizontal surveys were limited, and where they did occur in excess, were removed in the image processing stage to maximise the potential for high-quality model creation (Figure 4.4). Photos were captured at three-second intervals, along a horizontal axis allowing for 50-60% overlap between images, at a near-parallel viewing angle (Bernis *et al.*, 2014).

UAV aerial study was completed at four individual localities at three field sites (Table 4:1). Due to the proximity of Bartlett Wash to Moab Airport, drone photogrammetry was not permitted, as small UAVs pose a risk to aircraft in flight (Cracknell, 2017) (Table 4:1). Therefore, the only method of visual analysis is field photographs of the outcrop; however, scaling, and exact measurements may have inaccuracies due to parallax error.

Agisoft Metashape version 1.6.5 (formerly Agisoft Photoscan) was used for image processing. For each stage of the model building (Figure 4.4), different levels of resolution enable the model to be stitched with a high enough level of detail whilst also allowing for smooth interpretation. The photographic dataset was sufficient to produce accurate and high-resolution models (Table 4:1). For the greatest efficiency, both Duma Point models were constructed with a low-resolution point cloud but a high-resolution dense point cloud and texture overlay, allowing for high-resolution detail with minimal processing lag (Table 4:1).

Interpretation of these processed models was carried out in Virtual Reality Geological Studio (VRGS) 2020 version 2.52.1. This software uses inputs from various sources, in this case, Structure from Motion (SfM), to visualise three-dimensional data and allow in-office interpretation of outcrops. This software was used to trace bounding surfaces and measure set and foreset thicknesses within the aeolian successions.

Locality		Nearby Landmarks	Area	Photo Coverage (Horizontal)	Log Coverage (Vertical)	No. of Photos	No. of Data Points (Dense Cloud)	Resolution
Bartlett Wash	Jedi 3D	6.25km east of Moab Airport	5km ²	250m	46.5m	N/A	N/A	N/A
	Bartlett Fault	6.25km east of Moab Airport			14m			
Lone Mesa		6km north of State Route 313 and 5.5km southwest of locality 1	1.5km ²	1km	28.5m	86	51,782,262	High-High-High
Dubinky Well		5.4km north from the intersection of State Route 313 and the Secret Safari Sprire Route	0.4km ²	250m	N/A	63	30,252,756	High-High-High
Duma Point	Transition 1	12km northeast of Lone Mesa, accessible via the Cystal Geysir Safari Route	10km ²	2.5km		29	60,742,080	Low-High-High
	Transition 3					16m	102	90,683,842

Table 4:1: Localities from which 4 three-dimensional models were constructed. The number of photos is shown at well as the data points generated in the dense point cloud stage (see Figure 4.4). The three-stage resolution relates to each stage of the process, both models taken at Duma Point have a low sparse cloud resolution to reduce the file size and build time as they cover a larger distance.

4.3 Results

Aeolian successions comprise complex interactions between foresets, sets, cosets, and their relative bounding surfaces. The correlation of these deposits is key to determining changing complexity in the dunes east to west across the study area and the consequences for aeolian-marine margin interactions. Clear surfaces are visible at every locality, dividing the successions into 'units' hereafter referred to as genetic packages (Kocurek 1988, Kocurek & Havholm 1993, Crabaugh & Kocurek, 1993), defined as an aeolian accumulation capped by a regional surface. These bounding surfaces will be referred to as index surfaces, referencing surfaces upon which smaller-scale surfaces terminate and are identifiable at outcrop scale.

The sedimentology of the aeolian successions examined in this study shows a decrease in the number of cosets present within the succession towards the west (section 3.1.1). Sedimentary logs clearly show aeolian sandstones, separated by correlatable index surfaces, comprising five genetic packages at Bartlett Wash and Lone Mesa. This decreases to three packages at Dubinky Well, rapidly decreasing over a short distance to one coset at Duma Point Transition 3 and Duma Point Transition 1.

4.3.1 Locality 1- Bartlett Wash

Three index surfaces have been picked out, labelled TS1, TS2 and TS4, which bound genetic packages labelled GP1, GP2, GP3 and GP4, that are traceable along the extent of the outcrop and at both the Jedi-3D and Bartlett Fault localities.

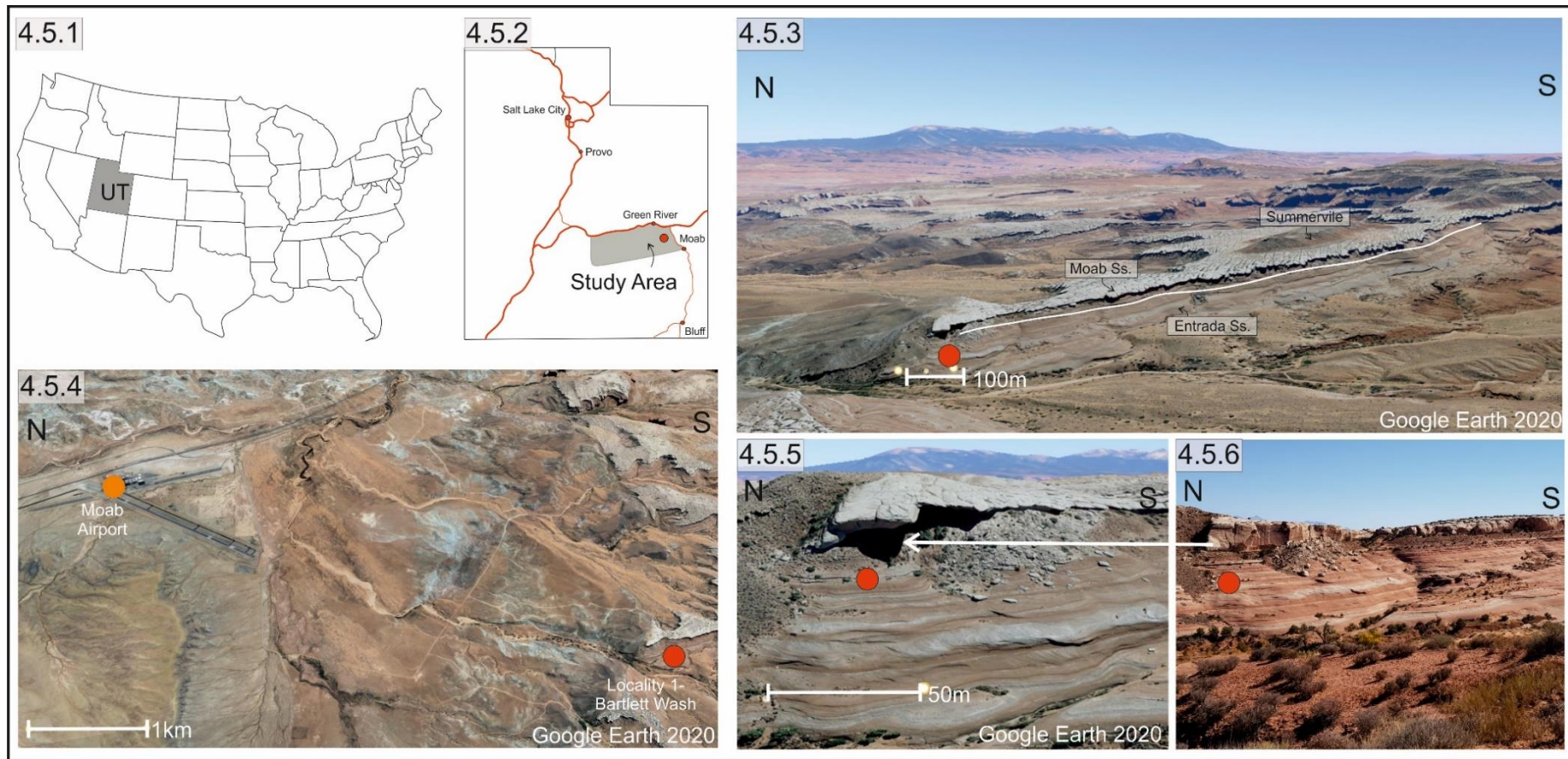


Figure 4.5.1- Location map showing the relative position of Utah within the United States of America. Figure 4.5.2- Position of the study area within the state of Utah. Figure 4.5.3- Lateral extent of Bartlett Wash (Jedi 3D) with lithostratigraphic labels. Figure 4.5.4- Position of the Bartlett Wash locality relative to neighboring landmarks such as Moab Airport. Figure 4.5.5- Google earth screenshot demonstrating the parallax errors from satellite surveys. Figure 4.5.6- True appearance of the Bartlett Wash (Jedi 3D) outcrop taken at Bartlett Fault in the field.

Index Surfaces

At the Bartlett Wash locality, four genetic packages (labelled GP1, GP2, GP3 & GP4) can be identified, each separated by parallel regional surfaces (labelled TS1, TS2 & TS4) that extend beyond outcrop scale (Figure 4.7). TS1 marks the boundary between a ferrallitic gleysol and the overlying planar cross-bedded sandstone via an erosive and undulose surface.

Index surface 2 occurs within the cliff-forming units of aeolian cross-strata. The surface extends throughout the outcrop and occurs at roughly the same vertical distance from surface 1 at both Bartlett Wash (Jedi-3D) and Bartlett Fault. Sporadic rhizoliths can be found along the surface and in the 10-20cm below within GP1.

Index surface 4 is the top-most outcrop scale surface at this locality and clearly defines the boundary between the cliff-forming sandstones and the thinner, low angle cross-strata that extend back to the Moab fault at this location. The deposits above TS4 comprise approximately 3m of sediment up to the boundary of the laminated mud and silts of the overlying coastal plain.

Genetic Packages

Genetic Package 1 is bound by the erosive surface TS1 at the base and TS2 at the top, forming a package 2.2m thick at Bartlett Fault and 2m thick at Bartlett Wash (Jedi-3D). The basal aeolian deposits overly the sharp surface resting upon green and purple parallel laminated silts (Fegl). Measurements of set thickness in the field show an average of 0.1m. Sets within this unit are somewhat convoluted and poorly defined at the point of contact with the basal surface, grading into more uniform planar cross-bedded sets towards the top of the unit. The maximum grainflow thickness is 0.7cm.

Genetic Package 2 is distinguishable from GP1 by TS2, a regional surface extending across both outcrops at Bartlett Wash and is bounded by a coset bounding surface, forming a unit approximately 3m in thickness. In the absence of exact field measurements for GP2 at this locality, estimations have been made from field photographs and sedimentary logs, which approximate a maximum grainflow thickness of 2.8cm. Cross-bedding is more defined, with predominantly planar cross-bedded sets of 1-2m thickness dominating the unit. A few asymptotic boundaries can be found sporadically towards the top of the unit. At the top-most boundary of this unit, isolated rhizoliths were found at one unique point at the Bartlett Fault location (they are absent at Jedi-3D).

Genetic Package 3 describes a 3m thick, cliff-forming unit of planar cross-bedded sandstones attributed to the Moab Member separated by a coset bounding surface at the base and TS4 at the top. The internal architecture of GP3 is similar to that of GP2, with mostly planar cross-bedded sets, occasional truncation, and asymptotic set bounding surfaces and a maximum grainflow thickness of 2.3cm.

Genetic Package 4 is the top-most unit found at this locality and is much thinner at only 2m thick; however, it is laterally extensive, extending back to the Moab Fault (Figure 4.7). A significant decrease in set and grainflow thickness occurs between GP3 and GP4, marking the transition between the cliff-forming succession to the laterally extensive 'bobbly' dune-forms most visible aerially (Figure 4.7). The maximum grainflow thickness for GP4 is 0.5cm (Figure 4.6).

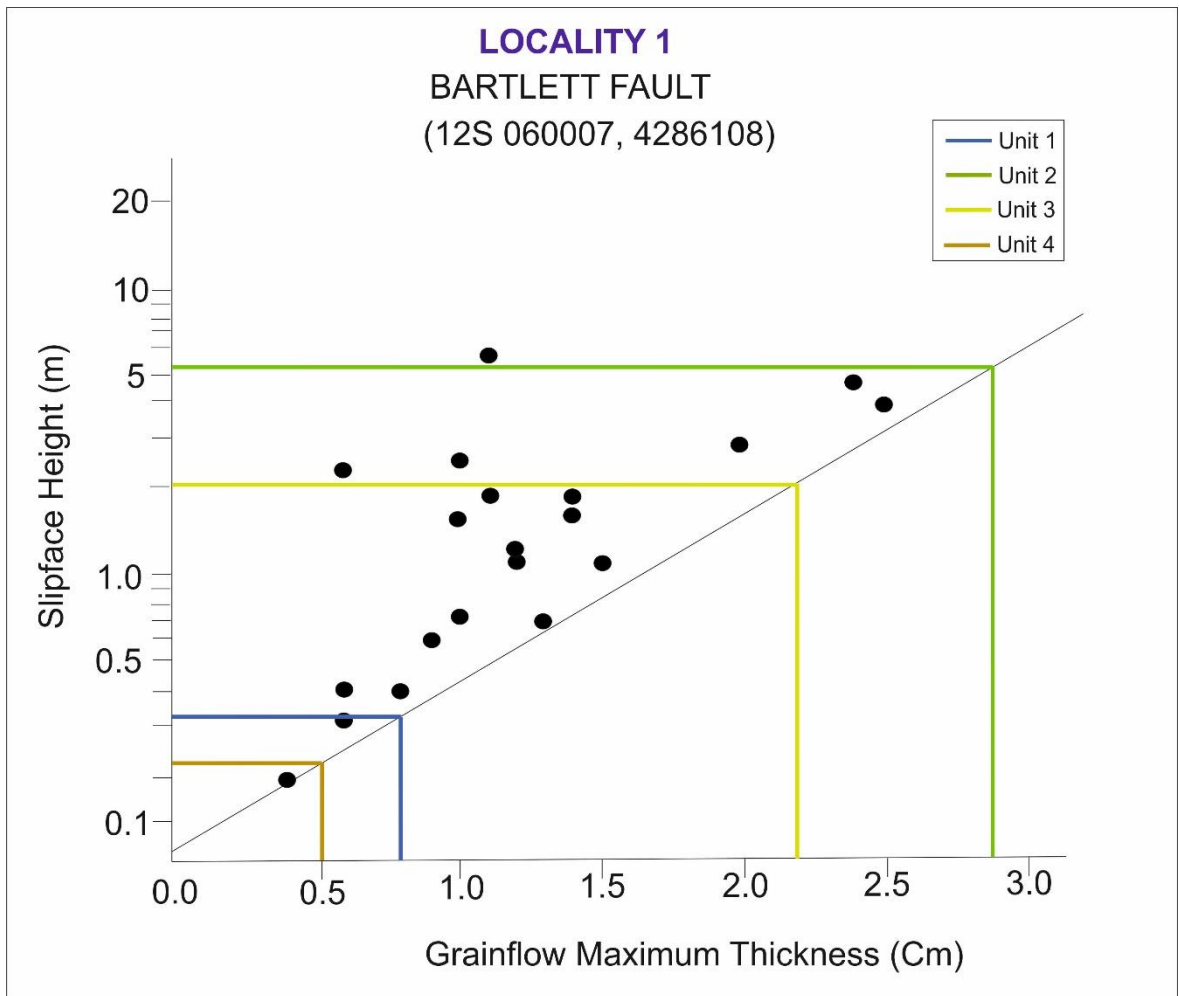


Figure 4.6- Relationship between maximum grainflow thickness and potential slip-face height of preserved dunes. Black dots are those obtained from field studies by Kocurek & Dott (1983), the lines represent average measurements taken from dunes in the field work for this study.

4.7.1

W

E



4.7.2

S

N



4.7.3

W

E



Figure 4.7.1- Field photo of the Bartlett Fault locality taken from Bartlett Wash (Jedi 3D) including the 4 index surfaces terminating upon the Moab Fault. Figure 4.7.2- Field photo of Bartlett Fault with a section highlighted to emphasise bounding surface relationships. Figure 4.7.3- Outcrop photo of Bartlett Wash (Jedi 3D) with the genetic packages highlighted by colour moving up the succession.

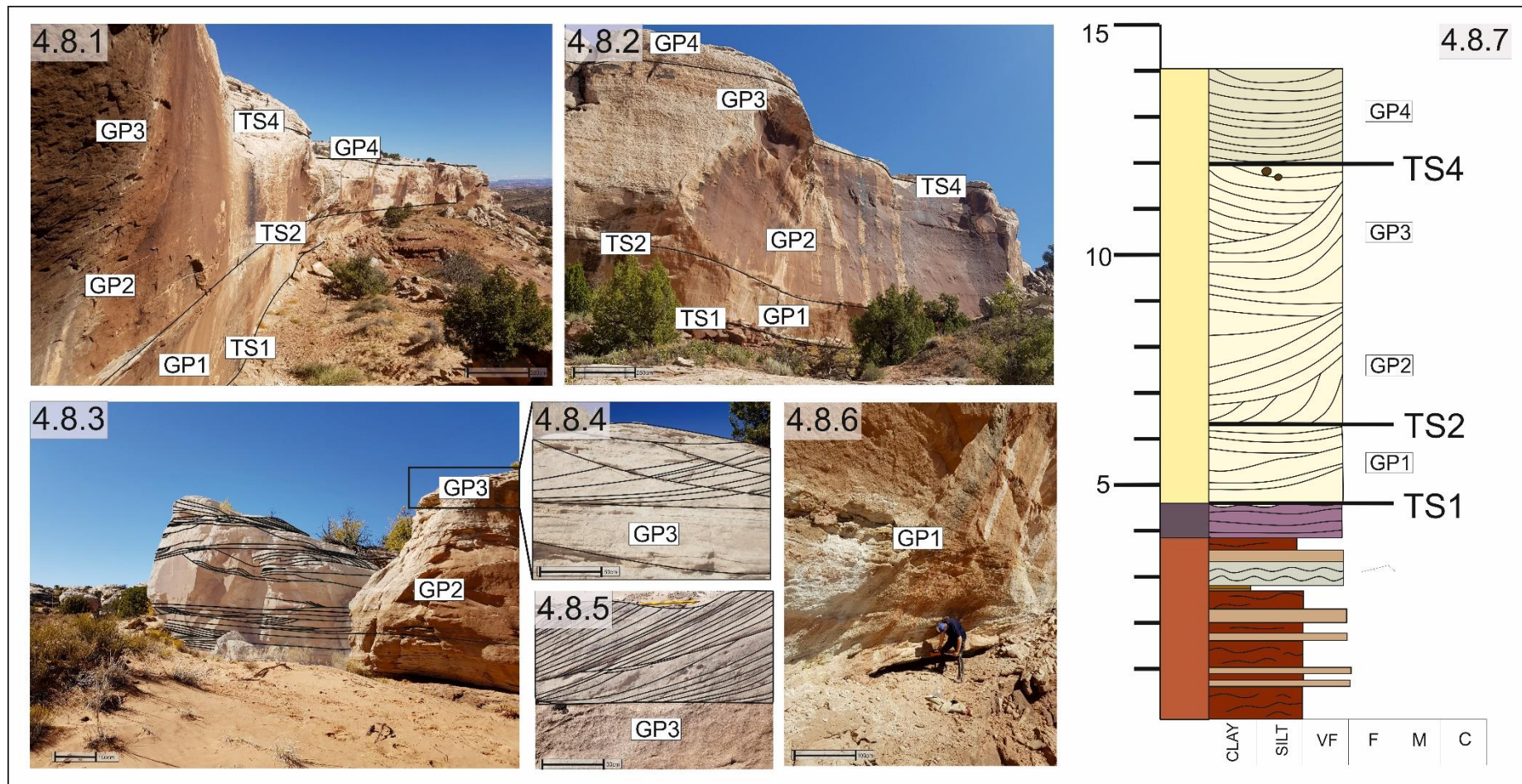


Figure 4.8.1- Field photograph of the aeolian succession at Bartlett Fault with the key index surfaces and genetic packages highlighted. Figure 4.8.2- Field photograph of the aeolian succession at Bartlett Wash (Jedi 3D) with the same correlatable index surfaces and genetic packages highlighted. Figure 4.8.3- Photograph of an outcrop at the Bartlett Fault locality, a section has been highlighted and the bounding surface relationships shown. Figure 4.8.4- Snapshot of genetic package 3 with bounding surfaces shown. Figure 4.8.5- Snapshot of a set genetic package 3 with foreset relationships shown. Figure 4.8.6- Field photograph of genetic package 1 at Bartlett Fault Figure 4.8.7- Sedimentary log taken at Bartlett Fault showing the identified index surfaces and genetic packages.

Interpretation

The link between bedform height and grainflow thickness is not a strongly defined one, and therefore the calculation is not definitive. Instead, it can provide a minimum slip-face height necessary to create grain flows of that thickness (Kocurek & Dott, 1981). The low angle bedding and poorly developed dune forms (no taller than 0.35m) indicates that Genetic package 1 represents aeolian dunes overlying a regional flooding surface marking the first deposition of the Moab Member dune field upon a damp and unstable substrate. This underlying sediment was likely to be sub-aerial for a significant period of time, leading to the formation of a palaeosol at this locality. This palaeosol was then susceptible to compaction and erosion hence the erosive surface that forms the basal boundary of this unit. As the sediment supply increased, dune accumulation also increased. This is indicative of the initiation of a dune field, resulting from an increasing sediment supply perhaps brought on by the regressing sea level. The top-most index surface that extends regionally, TS2, is interpreted as a period of non-deposition on the Moab Member dune field. Following this hiatus, straight-crested aeolian dune deposition continued to migrate with grainflow thicknesses implying a minimum dune height of 5.0m. The dominant planar cross-bedding of genetic package 2 demonstrates the dunes were mostly straight crested (see section 3.1.1); however, sporadic asymptotic bounding surfaces may imply an increase in complexity into the early formation of sinuous-crested dune forms.

Towards the top of the unit, a bounding surface extends throughout the outcrop against which all underlying surfaces terminate, implying a hiatus at this point. This surface probably represents a period of stabilisation of the dune field, as evidenced by the rhizoliths, as the dune field entered a period of quiescence the stable slip faces presented a habitable environment for vegetation. Genetic

package 3 represents the migration of aeolian dunes over a flat, stable surface. Maximum grainflow thickness implies palaeo-dune heights of 2m, a decrease when compared with GP2. This implies the onset of a reduction in sediment supply, where dune height is beginning to decrease, but there is still a sufficient environment for dune migration and preservation. The final deposits at this locality, genetic package 4, are indicative of a dramatic decrease in sediment supply leading to thinner foresets and lower angle cross-bedding, preserving dunes no more than 0.2m tall.

Initial set thickness within GP1 is no more than 0.1m, increasing to between 0.5m and 1.0m thickness up to the boundary between GP2 and GP3. Set thickness within GP3 then begins to decrease again, down to 0.3m for GP3 and 0.05m for GP4 (Figure 4.6). Combined with the results from measured and estimated grainflow thicknesses, it is shown that with movement up the succession from TS1, the dune field was expanding from initially minimal and closely spaced dune forms. A period of non-deposition separates these deposits from overlying well-developed, straight crested dunes that extend up to TS4. At this point, there is a notable change in the grainflow thickness such that it begins to decrease; this implies the initiation of a shut down in sediment supply which probably led to more restricted dune forms.

4.3.2 Locality 2a- Lone Mesa

Lone Mesa provides the best access for the full extent of the Moab Member dune field, showing the transition from wet aeolian erg centre through dry aeolian erg centre to coastal plain in the proximal section of the transect.

The planar cross-bedded sandstones unconformably overlie silty deposits at this locality and can be found as cliff-forming sandstones. As at the Bartlett Wash localities, these deposits can be separated into genetic packages (GP1, GP2, GP3, GP4 and GP5) divided by index surfaces that extend across the outcrop (TS1, TS2, TS3, TS4, TS5).

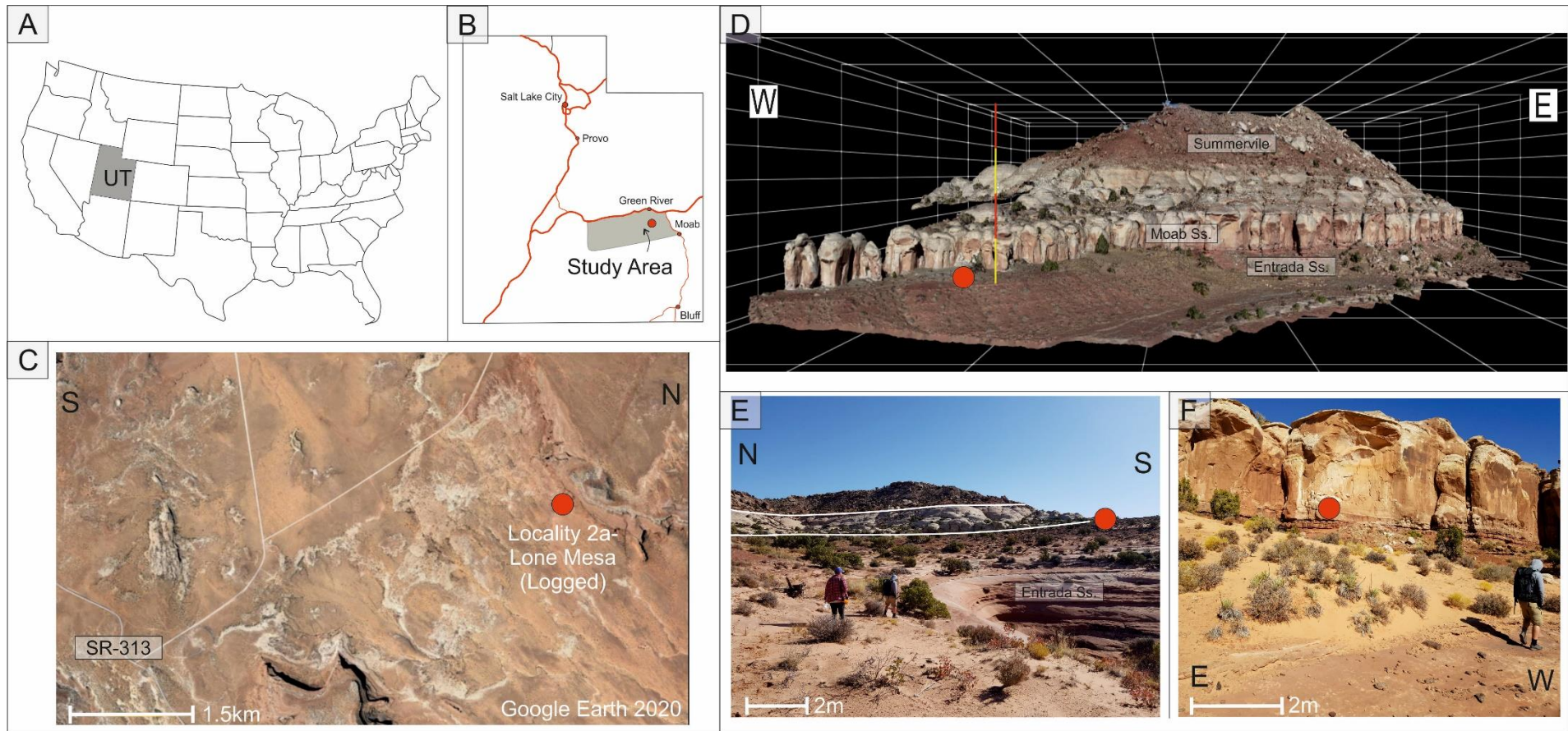


Figure 4.9.1- The position of Utah within the United States of America. Figure 4.9.2- Location of the study area within the state of Utah. Figure 4.9.3- Google Earth photo of the outcrop showing lithostratigraphic unit names, scale references foreground measurement. Figure 4.9.4- Position of the outcrop relative to the nearest landmark, State Route 313. Figure 4.9.5- Field photograph of the outcrop, red dot marks the reference point common to all photographs as above. Figure 4.9.6- Field photograph of the planar cross-bedded aeolian succession at the Lone Mesa locality.

Index Surfaces

TS1 represents the same erosive boundary that occurs at Bartlett Wash, separating the underlying coastal silts from the overlying aeolian sands. In contrast to Bartlett Wash, however, the composition of the sediments immediately underlying the boundary has a greater percentage of metallic components, forming nodular concretions. This occurs only sporadically throughout this locality and has been attributed to a ferrallitic gleysol. The surface itself extends throughout the outcrop and beyond; however, vegetation, loose sand and scree somewhat obscured the surface from the view of the UAV.

TS2 marks a period of non-deposition and stabilisation within the dune field, as evidenced by the rhizoliths that occur due to the preservation of roots from vegetation. Widespread vegetation within a dry aeolian system generally arises from a period of quiescence suitable for vegetative root systems to grow without being removed by an advancing slip face grain flows.

TS3 marks the most prominent outcrop surface at this locality, marking the separation between the cliff-face sandstones and the somewhat preserved dune forms that extend northwards. Upon this horizon, there is evidence of foreset bleaching, indicating a fluid flow component at or just after the time of deposition.

TS4 represents the uppermost surface separating the planar cross-bedded sandstones from an anomalous yellow sandstone unit found immediately above. This unit only occurs in this locality, is only 20cm thick and is overlain by the Summerville formation silts.

Finally, TS5 separates the preserved aeolian deposits from the overlying coastal plain by a mostly planar surface. The exact transition is hard to identify due to intense staining and a large amount of scree. However, the surface does not appear erosive, implying a conformable transition.

Genetic Packages

Basal Genetic Package 1 comprises a unit of planar bedded sandstones (Sxs) at the base of the cliff face bound by TS1 and TS2. At the basal boundary, TS1, there is evidence of high water level and subaqueous influence, i.e., bedforms are small, poorly developed, and there are some soft-sediment deformation structures. Within the unit, both set thickness and grainflow thickness increase towards TS2. Set thickness is 0.2m on average, with grainflow thickness not exceeding 1cm.

TS2 and TS3 bound genetic package 2, which comprises approximately half of the cliff face section extending up to 8m. The set thickness reaches the greatest extent within this unit, with maximum thicknesses of 2.2m. Grainflow thicknesses follow a similar pattern, reaching their greatest thickness within GP2 at 2.5cm on average. As at Bartlett Wash, GP2 is dominated by planar cross-bedded sets, however, towards the top of the unit, the basal contacts with set bounding surfaces become slightly asymptotic.

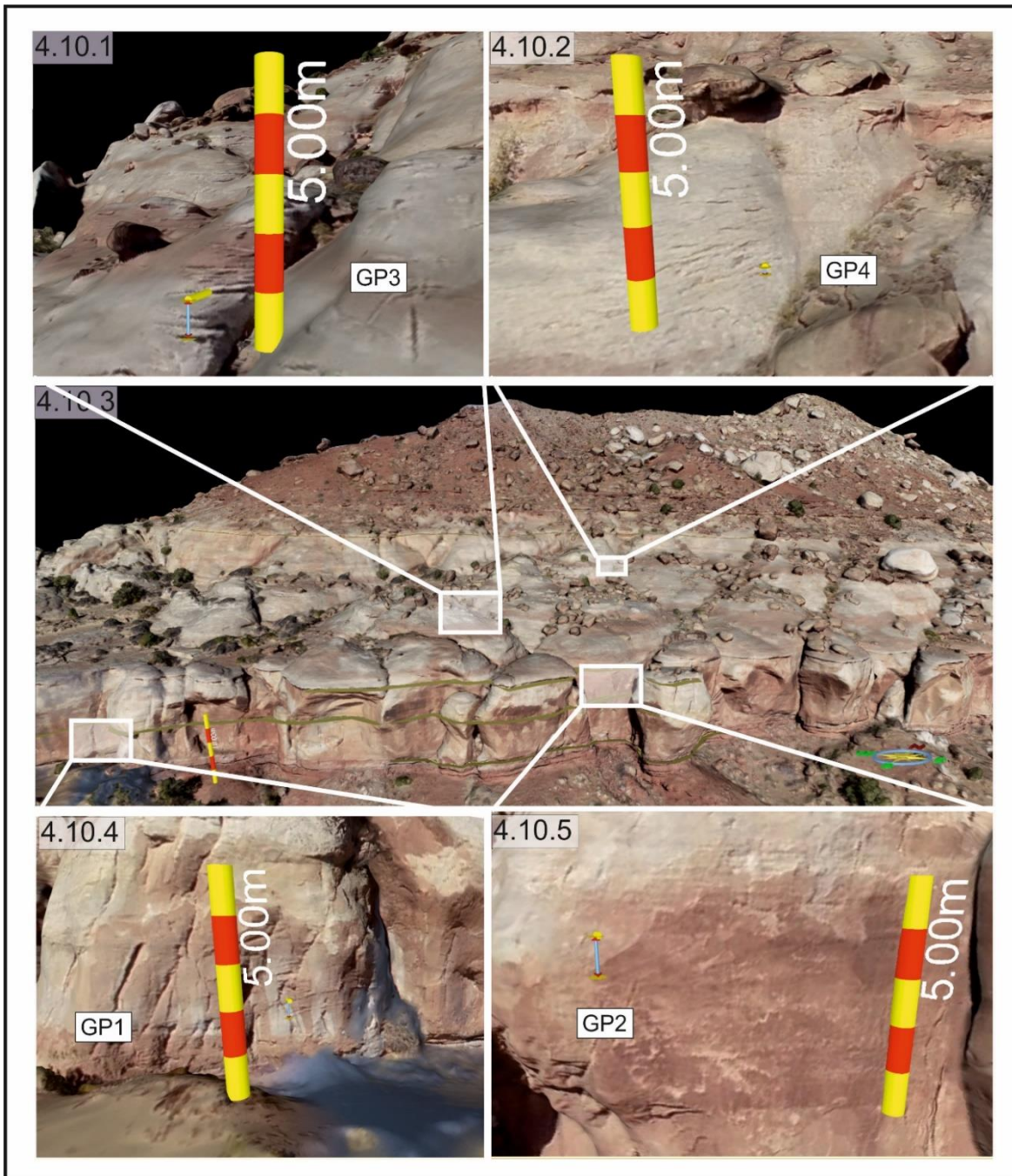


Figure 4.10.1- Snapshot from VRGS showing GP3 to scale with a representative foreset thickness measurement. Figure 4.10.2- Snapshot from VRGS showing GP4 to scale with a representative foreset thickness measurement. Figure 4.10.3- Panel diagram showing the dune measurements for each unit from the drone photogrammetric model. Each arrow shows one representative grainflow thickness from each unit, which can then be compared with the virtual scale to give an estimation for grainflow thicknesses. Figure 4.10.4-Snapshot from VRGS showing GP1 to scale with a representative foreset thickness measurement. Figure 4.10.5-Snapshot from VRGS showing GP2 to scale with a representative foreset thickness measurement.

Genetic Package 3 represents the thickest preserved sediment at this outcrop, extending up to TS4 (Figure 4.11). This unit contains significant evidence of bleaching within toesets, forming an interdune like pattern when viewed aerially (Figure 4.11). There is no change in lithology, hence these patches of darker and lighter coloured sandstones have not been classified as separate facies. Between GP2 and GP3, there is a notable reduction in set thickness, with sets becoming thinner upwards of TS3, minimum set thicknesses here are approximately 0.6m. Grainflow thickness also decreases to no more than 1.5cm.

The boundary between Genetic Package 4 and the underlying low angle planar cross-bedded strata of GP3 is less prominent than the other index surfaces. The sediments deposited above this boundary may have some poorly defined and discontinuous cross-bedding; however, the unit is mostly planar bedded and comparatively thick as a unit, up to 7m. Where cross-bedding occurs, the maximum grainflow thickness is approximately 0.3cm (Figure 4.12). As with genetic package 3, the unit is very pale grey with only isolated lenses of pinky-red coloured sediment.

Genetic Package 5 comprises an anomalous thin 20cm bed of sandstone that is incredibly well consolidated. The thickness of this unit is such that it cannot be viewed using UAV photography (Figure 4.11), however yellow patches that have leached from the horizon can be identified within GP4 (Figure 4.11). The unit itself can be split into two main components. The base of the unit is marked by a blue-grey finer-grained deposit that conformably overlies the GP4 sandstones with a planar contact.

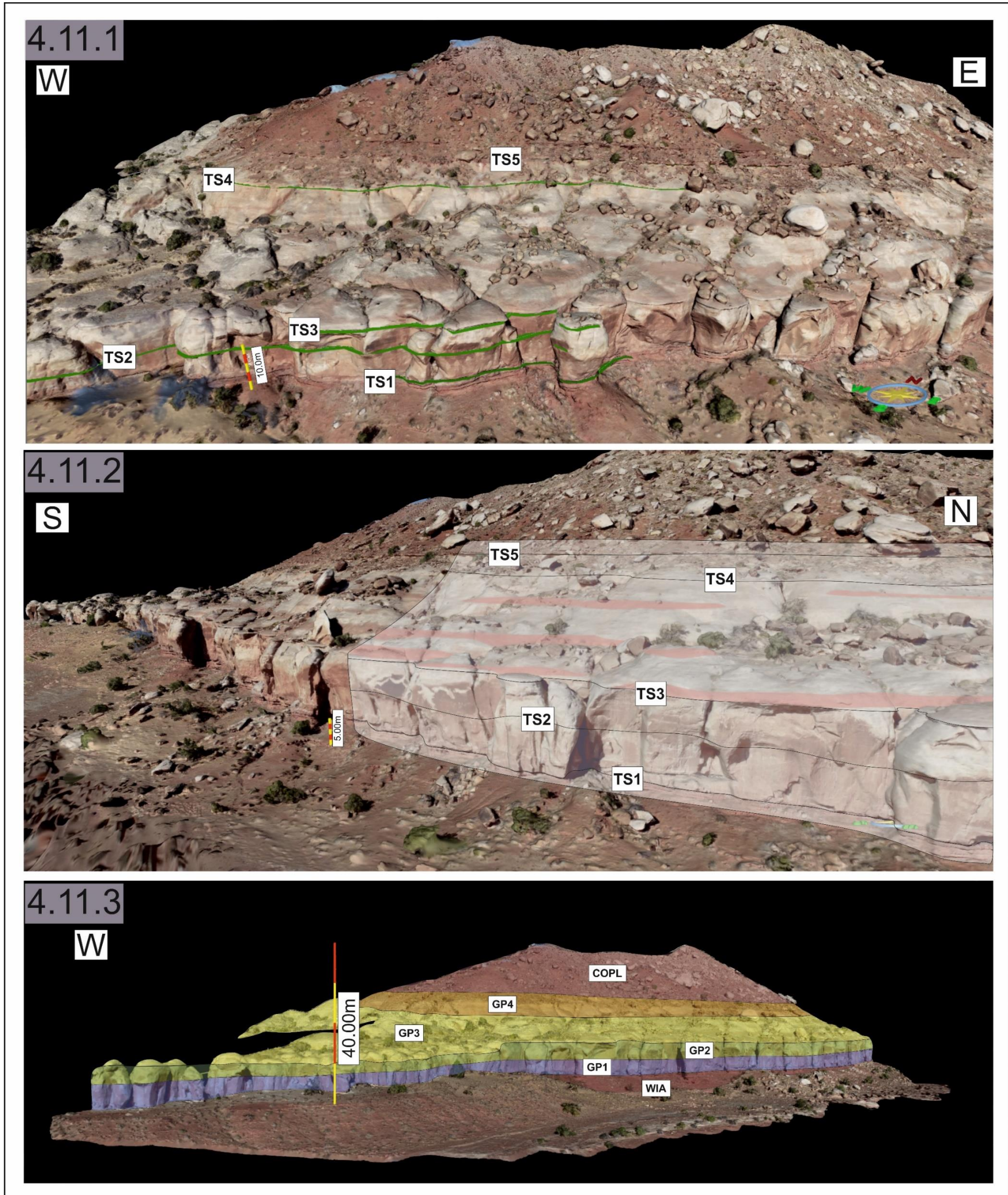


Figure 4.11.1- Interpretation of the Lone Mesa outcrop, processed within VRGS, showing the key index surfaces that divide the outcrop into genetic packages. Figure 4.11.2- Virtual outcrop model of the Lone Mesa outcrop with a section highlighted to further demonstrate the relationships between index surfaces. In addition, areas of differential bleaching have been highlighted. Figure 4.11.3- Complete outcrop view of Lone Mesa, taken from VRGS with the genetic packages shown, WIA refers to the underlying wet interdune deposits, whilst COPL refers to the overlying coastal plain.

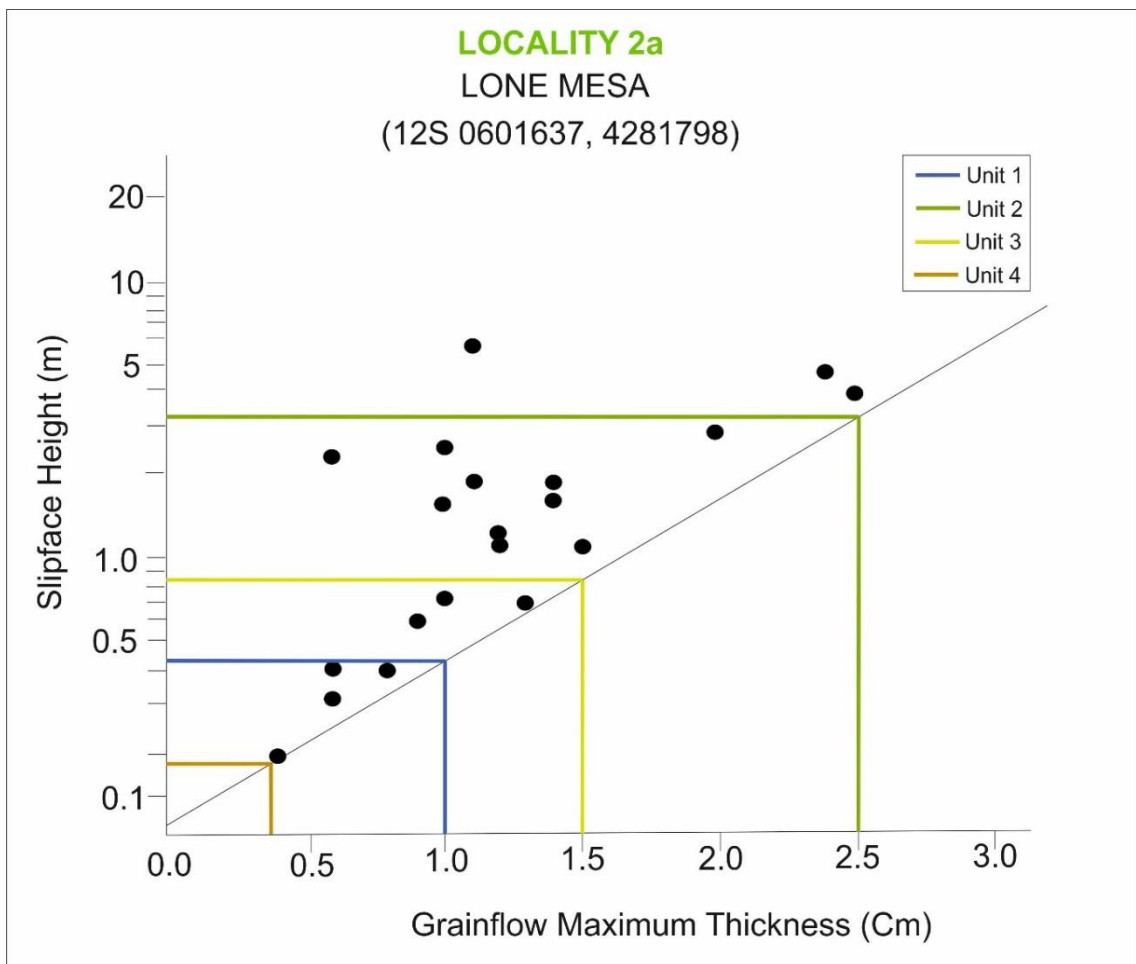


Figure 4.12- Graph representing the linear relationship between maximum grainflow thickness and potential slip-face height of preserved dunes. Black dots are those obtained from field studies by Kocurek & Dott (1983), the lines represent average measurements taken from dunes in the field work for this study.

Interpretation

Sedimentologically, the units found at Lone Mesa are largely correlative with those found at Bartlett Wash (Jedi-3D) Bartlett Fault. Preserved sediments from genetic package 1 indicate a palaeo-dune height of 0.4m, obtained from estimates of maximum grainflow thickness, which have a generally linear relationship with minimum slip-face height (Kocurek & Dott, 1983). These deposits represent aeolian dunes overlying a regional flooding surface marking the first deposition of the Moab Member dune field. Construction of the dunes began on a damp and unstable substrate leading to small and poorly developed dune forms. The palaeosol at this locality is likely to have formed under different conditions to that

found at Bartlett Wash. At Lone Mesa, the palaeosol immediately underlying TS1 is characterised by metallic nodules formed by precipitation as sea-level falls. This is further evidence of fluid flow within the base of the planar cross-bedded sandstones at this locality in the form of the colloquially named 'popcorn facies', which is further precipitation of iron minerals in response to fluctuating water levels. Genetic package 2 comprises the preserved deposits of continued dune field growth, preserved foresets steepen, and the grain flows increase in thickness, equivalent to a palaeo-dune height of 2.2m. The most prominent index surface, TS3, separates deposits of GP2 and GP3, indicating a significant period of non-deposition upon the dune field. The paler sandstones here demonstrate bleaching via fluid flow in the toesets of the dune forms post-depositionally. This indicates there were periodic inundations of water and localised rises in water level throughout dune deposition. After this point, the average dune height decrease, and the cross-bedding becomes much more low-angle, and grain flows become thinner. Within this unit, the dune height is estimated to be 0.85m. Genetic package 4 represents the thickest deposits at this outcrop, comprising very fine-grained sands with poorly developed and discontinuous cross-bedding. Where found, the grainflow thicknesses indicate a dune height of just 0.2m. This indicates a sandsheet evidenced by the thick deposits of planar bedded sands with occasional wind ripple facies and poorly developed bedforms. The extensive bleaching with only isolated lenses of unaffected sediment implies a marginal setting with increased influence from the local water table. The final unit comprises a 20cm thick palaeosol bed. Whilst no dune height analysis can be conducted, the presence of this unit supports a marginal environment as sulphate soils such as this typically form within saline polders, i.e., restricted, and isolated pools of water within a coastal environment.

As the dune forms begin to coalesce and sediment supply increases, dune height also increases up towards TS2, which marks a hiatus in the preservation of dunes within this locality. The minimum slip-face height within this unit is 0.4m high.

4.3.3 Locality 2b- Dubinky Well

This locality comprises a more westerly equivalent of the Lone Mesa outcrop comprises a complete vertical succession of Entrada Sandstones, Moab Member sandstones and Summerville Formation coastal plain deposits.

As this locality was inaccessible to sedimentary logging, interpretations have been estimated from drone photogrammetric models alone. They show that the Moab Member Sandstones unconformably overlie extensive deposits of Entrada earthy facies, even containing some coastal dune forms itself. At this locality, the deposits of planar cross-bedded sandstones are thinner and are separated into three genetic packages, GP1, GP2 & GP3, divided by four index surfaces labelled TS1, TS2, TS3 and TS4.

Index Surfaces

As at Lone Mesa and Bartlett Wash, TS1 marks an erosive contact between the cross-bedded sandstones and underlying parallel laminated silts. There are no palaeosols visible via UAV photogrammetry. However, the base of the succession immediately overlying TS1 appears to be more stained, with a deeper pink colour, than at previous localities.

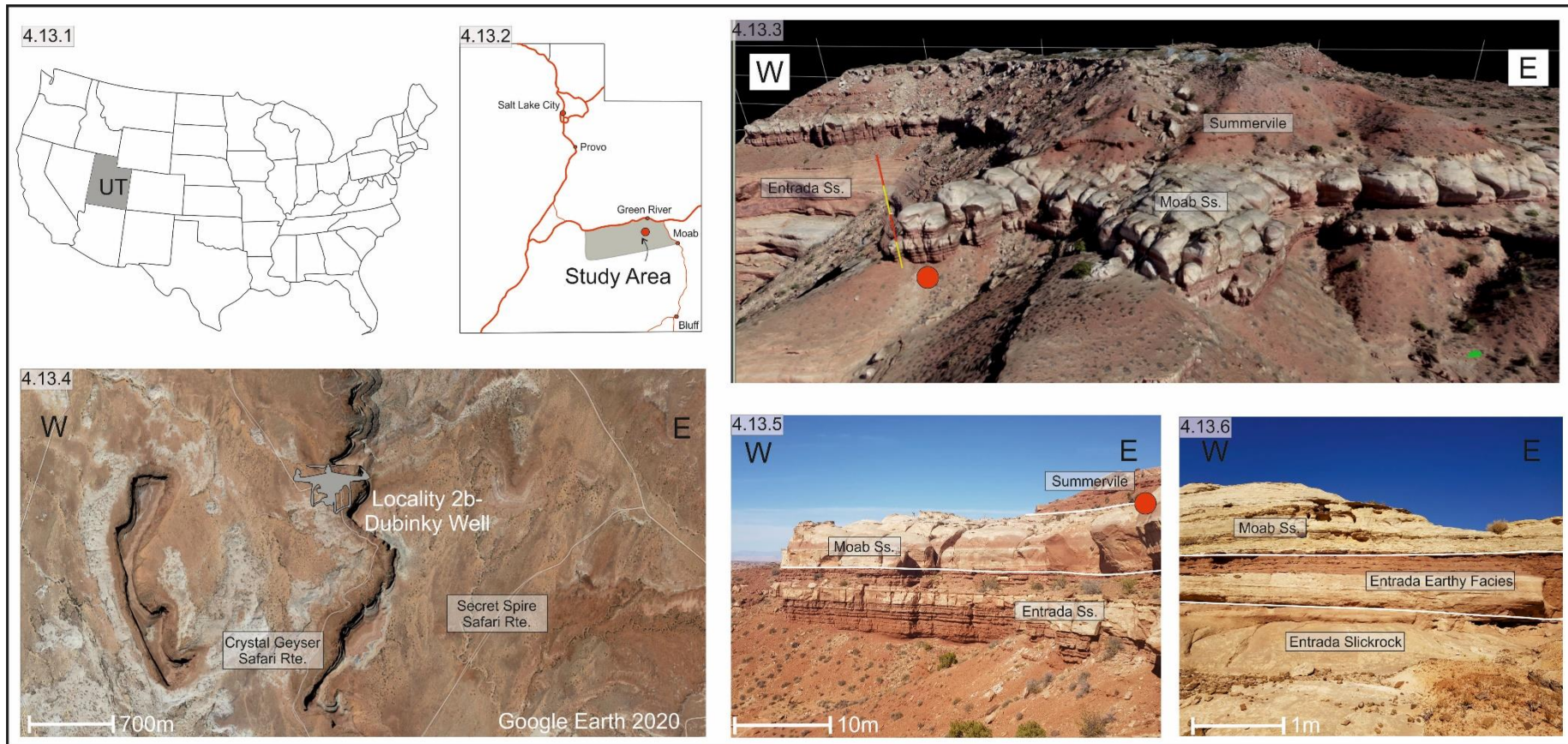


Figure 4.13.1-The position of Utah within the United States of America. Figure 4.13.2- Location of the study area within the state of Utah. Figure 4.13.3- Google Earth photo of the outcrop showing lithostratigraphic unit names, scale references foreground measurement. Figure 4.13.4- Position of the outcrop relative to the nearest landmark, the Secret Spire Safari Rte. Figure 4.13.5- Field photograph of the outcrop with lithostratigraphic units, red dot marks the reference point common to all photographs as above. Figure 4.13.6- Field photograph of the planar cross-bedded aeolian succession at Dubinky Well.

TS2 occurs approximately one-third of the way up the cliff-face at Dubinky Well, 4m above the boundary of TS1. This surface is planar and is marked primarily by a horizon of intensive bleaching, appearing as a definitive white horizontal line across the cliff at outcrop scale. In some areas, this surface forms a slight overhang to the cliff face.

TS3 is less prominent at this locality, however, it still marks a transition from thick sets of planar cross-bedded sands into much thinner, low angle deposits that in some places are even preserved as form-sets. The contact between the two units is very planar, and there is no evidence of rhizoliths.

TS5 is the next evident index surface at this locality, separating GP3 from overlying coastal plain deposits in the absence of GP4 or GP5 deposits.

Genetic Packages

Basal genetic package 1 is comprised of planar cross-bedded sandstones within which foreset angle and grainflow thickness appear to increase upwards. The beds at the base of this unit are more planar and occasionally have undulose contacts. As the dune field migrates and develops, the cross-bedding becomes more defined, and grain flows thicker. Exact grainflow thicknesses are challenging to obtain due to the resolution of the texture within the model; therefore, they have been estimated by taking the average of identifiable set thicknesses and dividing by the estimated number of grainflows within. For GP1, this is calculated to be about 1cm. A strong white horizontal boundary separates this unit from the overlying GP2.

Genetic package 2 comprises lower angle planar cross-bedded sandstones punctuated by horizontal areas of lighter sandstone that are laterally extensive in some areas but do not extend the full width of the outcrop. The set thickness

within this unit is somewhat difficult to determine due to extensive weathering and exposure of the cliff face. Where visible, the same method as in genetic package one has been used to estimate foreset thickness. For genetic package 2, this is estimated to be 1.5cm.

Genetic Package 3 is the uppermost unit at this locality, comprising 5m of planar cross-bedded sandstone from TS3 to TS4, the boundary separating these deposits from overlying silts. As with GP2, the grainflow thicknesses are hard to determine due to extensive weathering upon the outcrop; however, the likely grainflow thickness is 0.5cm from estimates of set thickness. The upper contact between the sandstones and overlying silts is planar and conformable right across the outcrop. This unit is stained pink throughout with a few distinct horizontal patches of white sandstones.

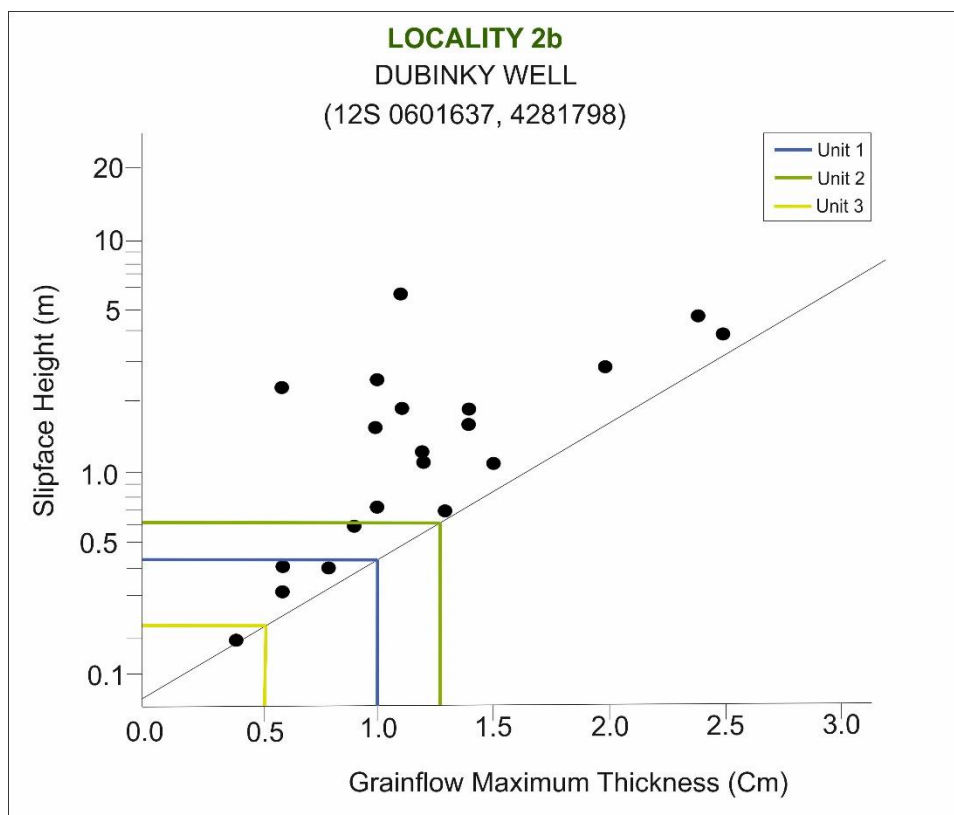


Figure 4.14- Graph representing the linear relationship between maximum grainflow thickness and potential slip-face height of preserved dunes. Black dots are those obtained from field studies by Kocurek & Dott (1983), the lines represent average measurements taken from dunes in the field work for this study.

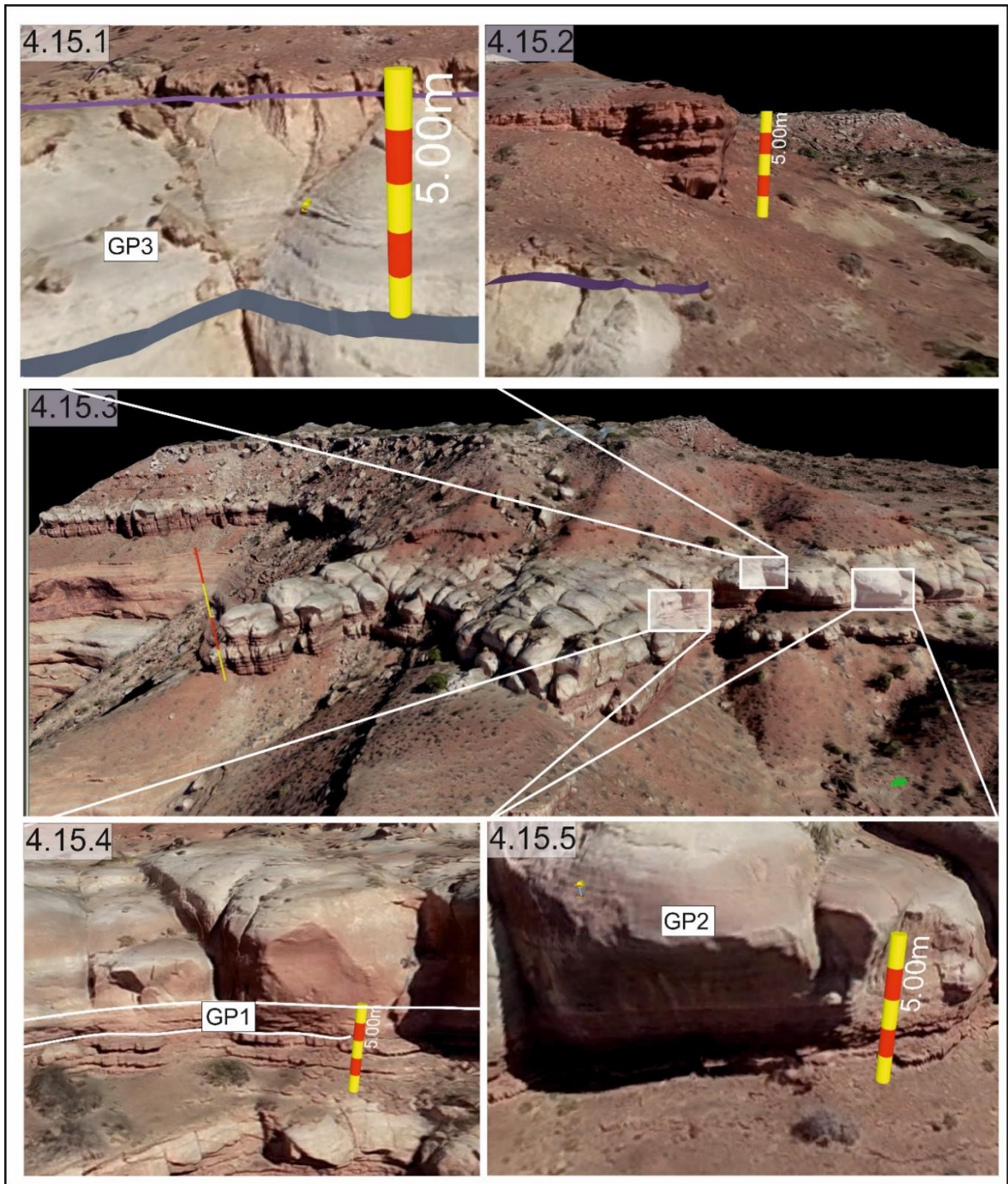


Figure 4.15.1- Snapshot from VRGS showing GP3 to scale with a representative foreset thickness measurement. Figure 4.15.2- Snapshot from VRGS showing the overlying coastal plain with a representative foreset thickness measurement. Figure 4.15.3- Panel diagram showing the dune measurements for each unit from the drone photogrammetric model. Each arrow shows one representative grainflow thickness from each unit, which can then be compared with the virtual scale to give an estimation for grainflow thicknesses. Figure 4.15.4-Snapshot from VRGS showing GP1 to scale with a representative foreset thickness measurement. Figure 4.15.5-Snapshot from VRGS showing GP2 to scale with a representative foreset thickness measurement.

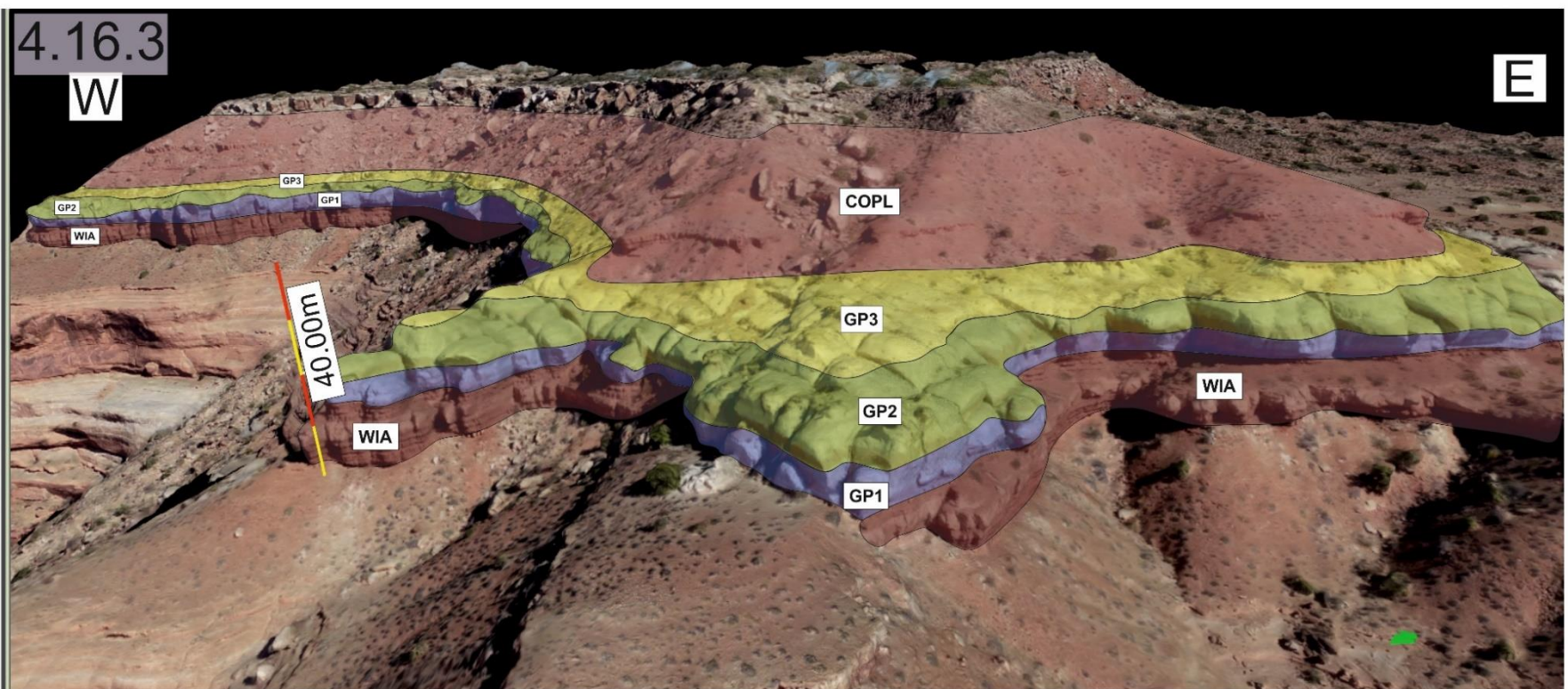
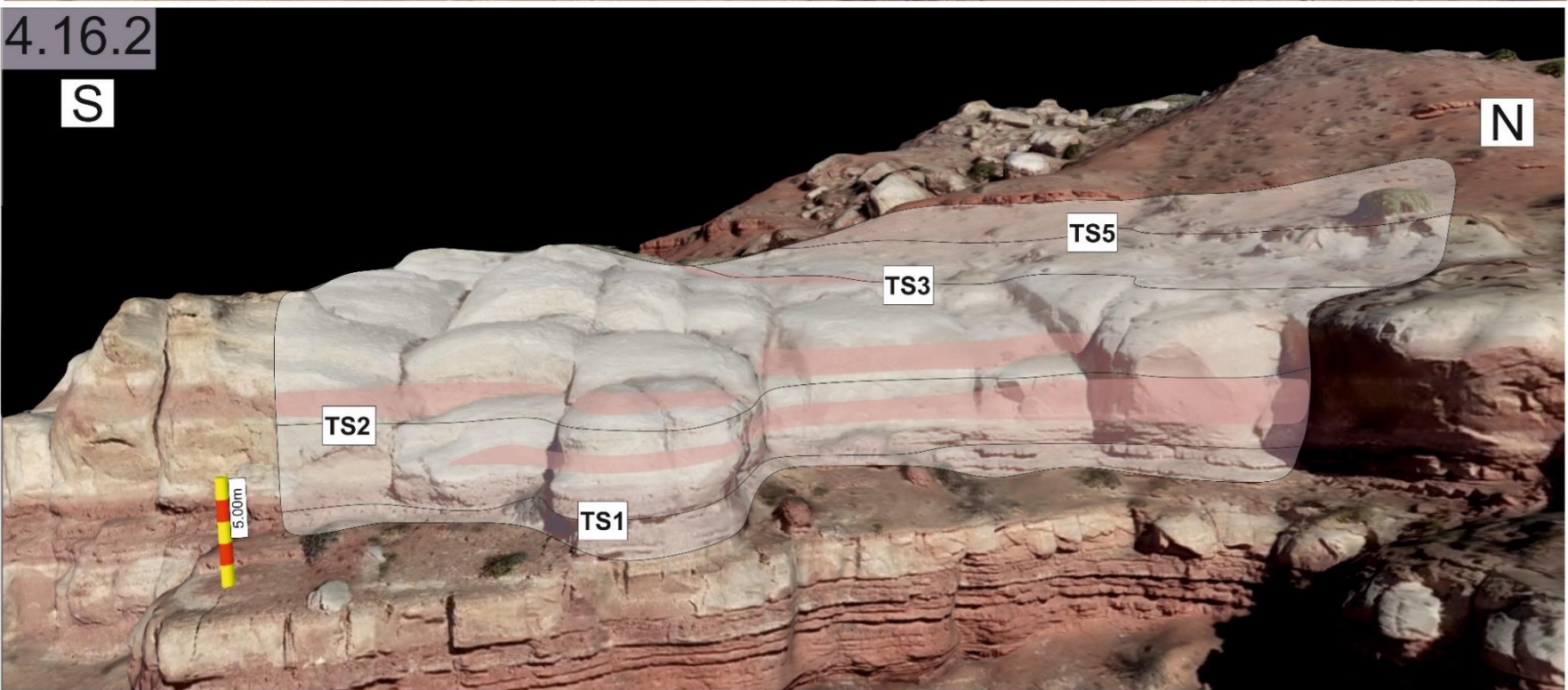
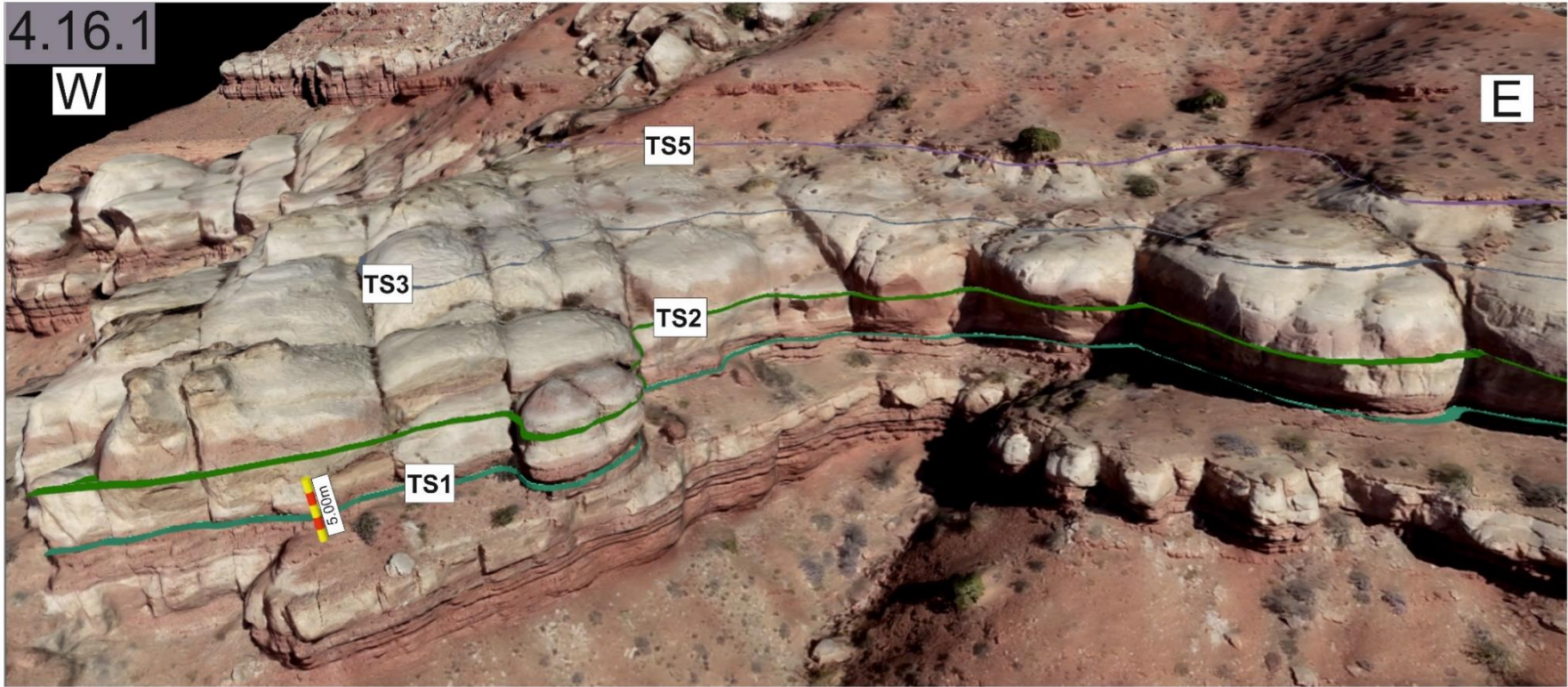


Figure 4.16.1- Interpretation of the Dubinky Well outcrop, processed within VRGS, showing the key index surfaces that divide the outcrop into genetic packages. Figure 4.16.2- Virtual outcrop model of the Dubinky Well outcrop with a section highlighted to further demonstrate the relationships between index surfaces. In addition, areas of differential bleaching have been highlighted. Figure 4.16.3- Complete outcrop view of Dubinky Well, taken from VRGS with the genetic packages shown, WIA refers to the underlying wet interdune deposits, whilst COPL refers to the overlying coastal plain.

Interpretation

This locality represents the fluctuations in the deposition of an aeolian dune field in an environment strongly influenced by changes in the water table. Here the dunes show the same pattern up-succession as at other localities, i.e., an increase in foreset thickness, grainflow thickness and consequently dune-height. Genetic package one features poorly developed dunes with undulose beds graduating to fully formed dunes of approximately 0.45m, showing the initial growth of the dune field. The deposits represent straight-crested aeolian dune forms migrating across a damp substrate leading to a slightly erosive and undulose contact between the sandstones and the underlying silts. No palaeosol is present at this locality that is visible using UAV photogrammetry, however as palaeosol horizons are typically thin beds, the resolution of the models may struggle to pick it up. The upper planar boundary results from a period of non-preservation of sediments either through deflation or insufficient sediment supply for sub-critical climb to occur. After a small hiatus marked by a heavily bleached horizon, the dune field continues, with estimated dune heights of up to 0.6m. The decrease in dune height and increase in toe set bleaching throughout this package implies an environment where dune growth can occur but is somewhat restricted by periodic and localised fluctuations in the water table. Finally, the uppermost package features dunes just 0.25m high, indicating a lack of available sediment supply and the decline of the dune field.

When comparing the evolution of the dune field at this locality with that of Lone Mesa and Bartlett Wash, the pattern of increasing dune complexity, followed by a hiatus and then a decline, is similar. However, one difference is the scale at which this occurs, i.e., dunes at this locality do not reach the same grainflow thicknesses and, hence, slip face height. In addition, the bleaching at this locality is the strongest and produces the most distinct patterns of horizontal white sandstones

and more patchy pink sandstones. The frequency and uniform pattern of these bleaching horizons implies that the deposition and preservation of sediments at this locality were influenced by a uniformly fluctuating yet consistently high water table, akin to a coastal tidal environment.

4.3.4 Locality 3- Duma Point Transition

Duma Point is a key locality in which the last occurrence of the Moab Member sandstones can be found, marking the point of lateral transition from the dune field to a coastal plain environment.

At this locality, the planar cross-bedded sandstones of the Moab Member unconformably overlie the silty deposits of the Entrada Earthy Facies and can be found as cliff-forming sandstones. At Duma Point, the thickness of the sandstone decreases rapidly within the locality, forming a cliff face 10m thick in the east of the locality, referred to as Duma Point Transition 3, and a 1m outcrop towards the west referred to as Duma Point Transition 1. In this locality, the thickness and occurrence of genetic packages rapidly drop off between Transition 3 and Transition 1. Duma Point Transition 3 represents three genetic packages (GP1, GP2 & GP3), as at Dubinky Well, whereas Duma Point Transition 1 represents just one package (GP1), bound by an erosive undulose surface at the base (TS1) and a planar surface on the top (TS4).

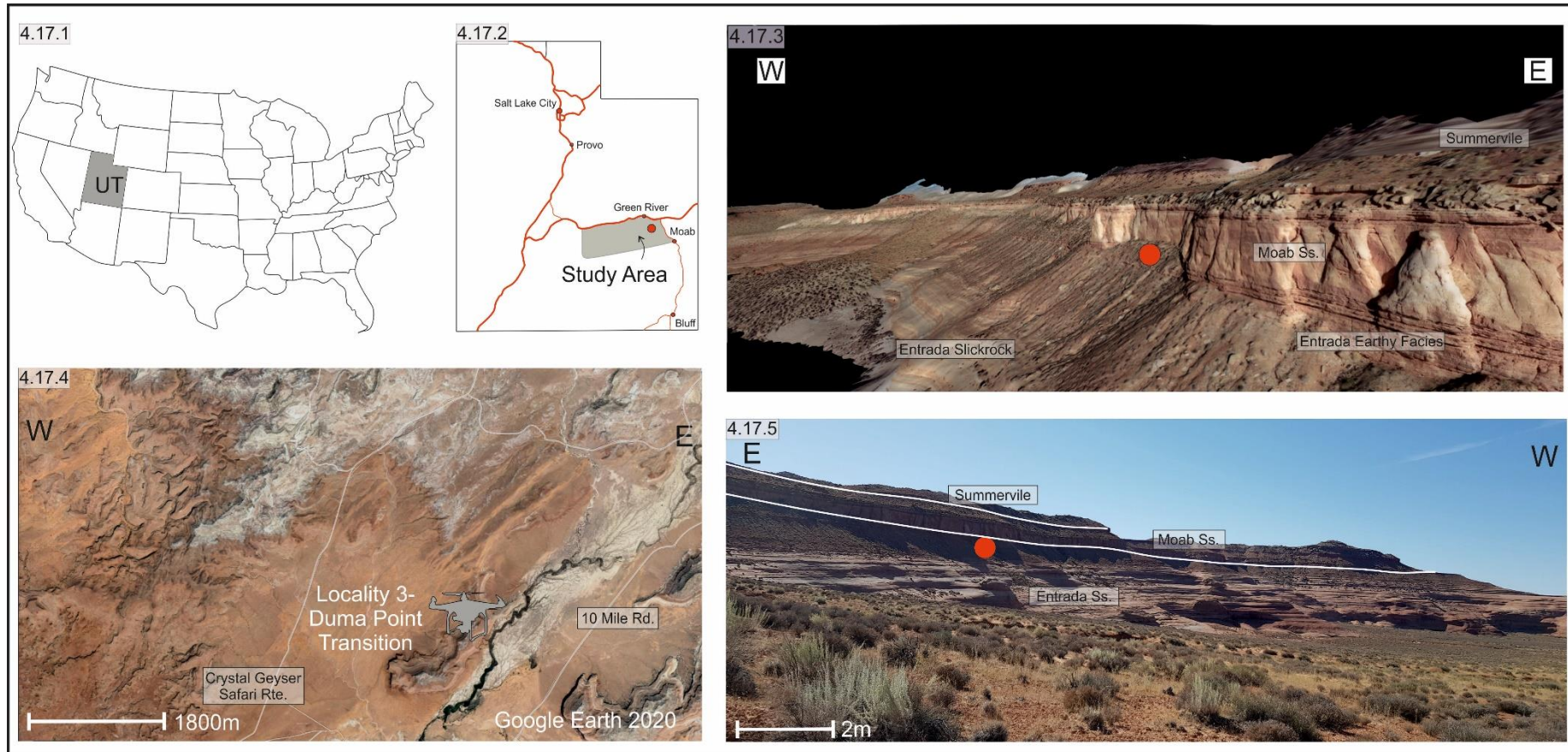


Figure 4.17.1-The position of Utah within the United States of America. Figure 4.17.2- Location of the study area within the state of Utah. Figure 4.17.3- Google Earth photo of the outcrop showing lithostratigraphic unit names, scale references foreground measurement. Figure 4.17.4- Position of the outcrop relative to the nearest landmark, the Crystal Geyser Safari Route. Figure 4.17.5- Field photograph of the outcrop including lithostratigraphic units, red dot marks the reference point common to all photographs as above.

Index Surfaces

As at all other localities, TS1 at Duma Point Transition 3 is a characteristic very undulose erosive surface separating wet interdune deposits (WIA) and the overlying Straight-Crested Dune Association (CLA). At this locality, TS1 is distinctly more undulose than at Bartlett Wash, Lone Mesa and Dubinky Well, with significant load casts eroding into the substrate with some small-scale ripple forms proliferating up from the boundary. At Duma Point Transition 1 the surface TS1 is poorly accessible and has therefore been inferred from the change from red silty deposits into pale, fine-grained sandstones.

TS2 occurs at Duma Point Transition 3 and separates the units characterised by soft-sediment deformation and load casts from the overlying cross-stratified sandstone units. The surface itself is planar, with some small-scale ripple-forms immediately above the surface that graduate into larger and more developed dunes up-succession.

TS4 marks the boundary between dune packages at Duma Point Transition 3. It is a planar surface separating planar cross-stratified sandstones from a relatively thick deposit of sandstone with very poorly developed cross-bedding and sporadic wind ripples. At Duma Point Transition 1, TS4 marks the boundary between the small 1m thick dune package and the overlying coastal plain channel sandstones.

TS5 marks the top-most boundary separating the sandstones from overlying silts and sands of the COPL association at Duma Point Transition 3. It is important to note that the boundary is very planar and marked by a ledge forming siltstone that contains some root traces and sporadic burrowing.

Genetic Packages

Genetic Package 1 comprises the basal part of the succession at Duma Point Transition 3 and the entire succession at Duma Point Transition 1. At Duma Point Transition 3, the base of GP1 is incredibly undulose and erosive, with large load casts and soft-sediment deformation. There are also some ripple forms with a wavelength of 30cm and a height of 4cm at the base of the unit just above the load casts. At Duma Point Transition 1, Genetic Package 1 is just 1m in thickness with a very poorly defined internal structure. It is located at 12S 0590497E 4293490N, the point which this study believes to be the most westerly occurrence of the Moab Member sandstones. Some thin cross-bedded sets contain foresets approximately 5cm with grainflows no more than 0.4cm thickness.

At Duma Point Transition 3, up-succession, the ripple-forms fade out and are replaced by the planar, low-angle beds with significant bimodal grain sizes of Genetic Package 2. This structure continues throughout the rest of the unit, with some sporadic cross-bedding towards the top but still a majority component of parallel bedded sands between 0.5 and 5cm thickness. The grain flow thicknesses within the cross-bedding where it does occur are 0.7cm.

Genetic Package 3 is the final unit found at Duma Point Transition 3, comprising much lower angle and poorly developed cross-bedding. The cross-bedding is sporadic, occurring inconsistently throughout the unit, with occasional wind ripples along foreset bounding surfaces. Due to the poorly preserved cross-bedding, grainflow thickness within this unit is hard to determine and may be inaccurate.

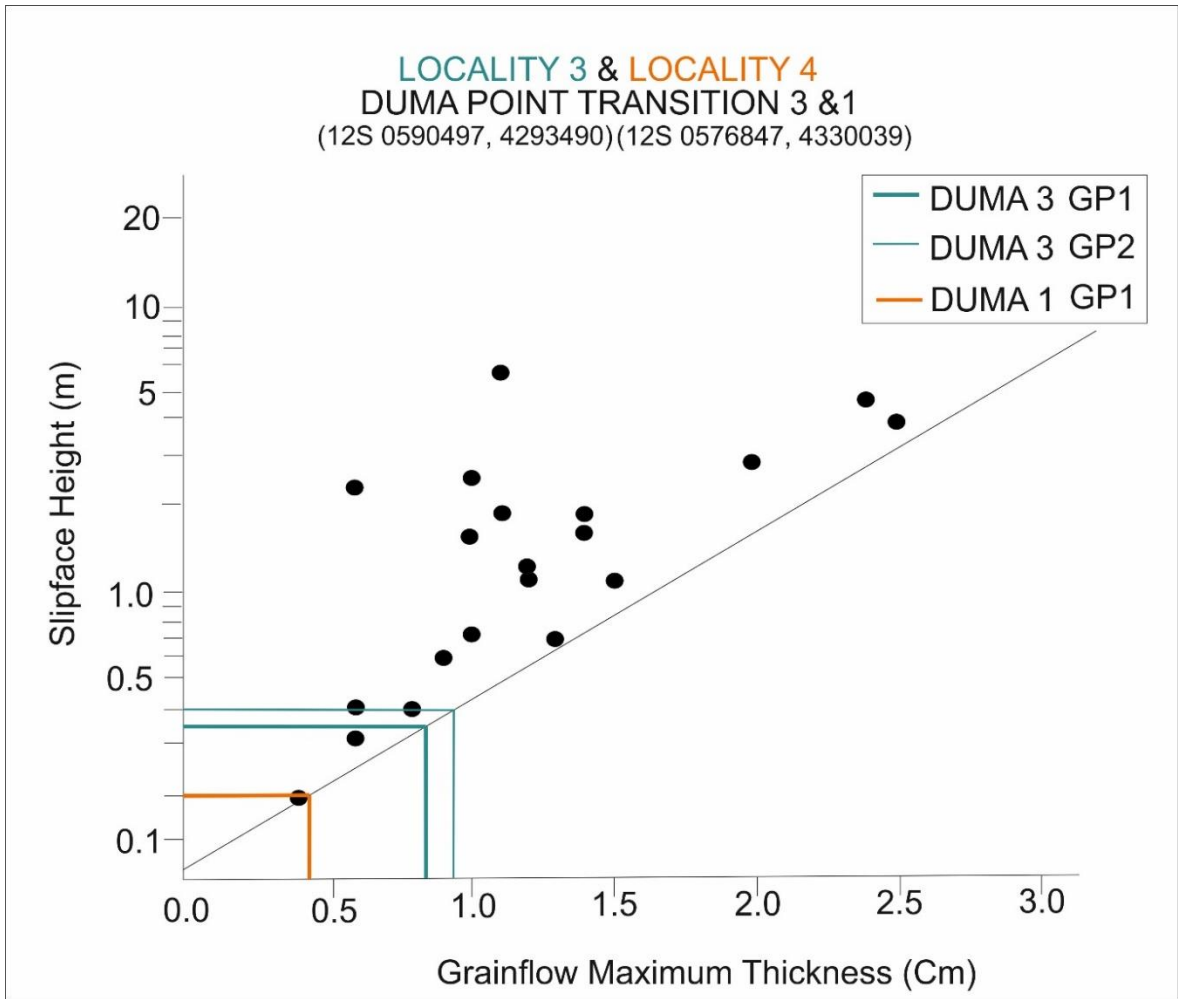


Figure 4.18- Graph representing the linear relationship between maximum grainflow thickness and potential slip-face height of preserved dunes. Black dots are those obtained from field studies by Kocurek & Dott (1983), the lines represent average measurements taken from dunes in the field work for this study.

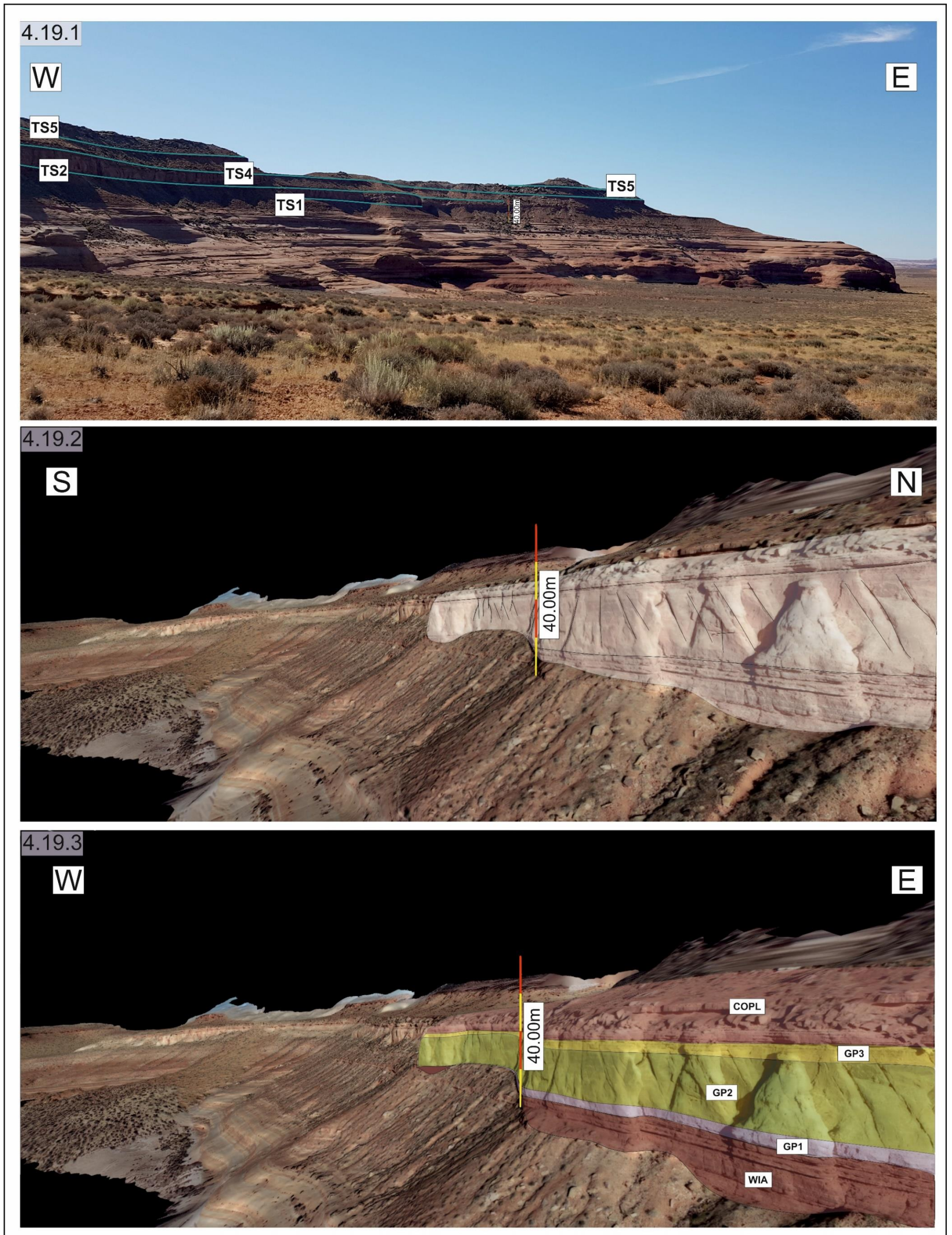


Figure 4.19.1- Interpretation of the Duma Point Transition 3 outcrop, processed within VRGS, showing the key index surfaces that divide the outcrop into genetic packages. Figure 4.19.2- Virtual outcrop model of the Duma Point outcrop with a section highlighted to demonstrate the relationships between index surfaces further. The diagonal features shown are likely to be post-depositional fracturing of the sandstone. Figure 4.19.3- Complete outcrop view of Duma Point, taken from VRGS with the genetic packages shown. WIA refers to the underlying wet interdune deposits, whilst COPL refers to the overlying coastal plain.

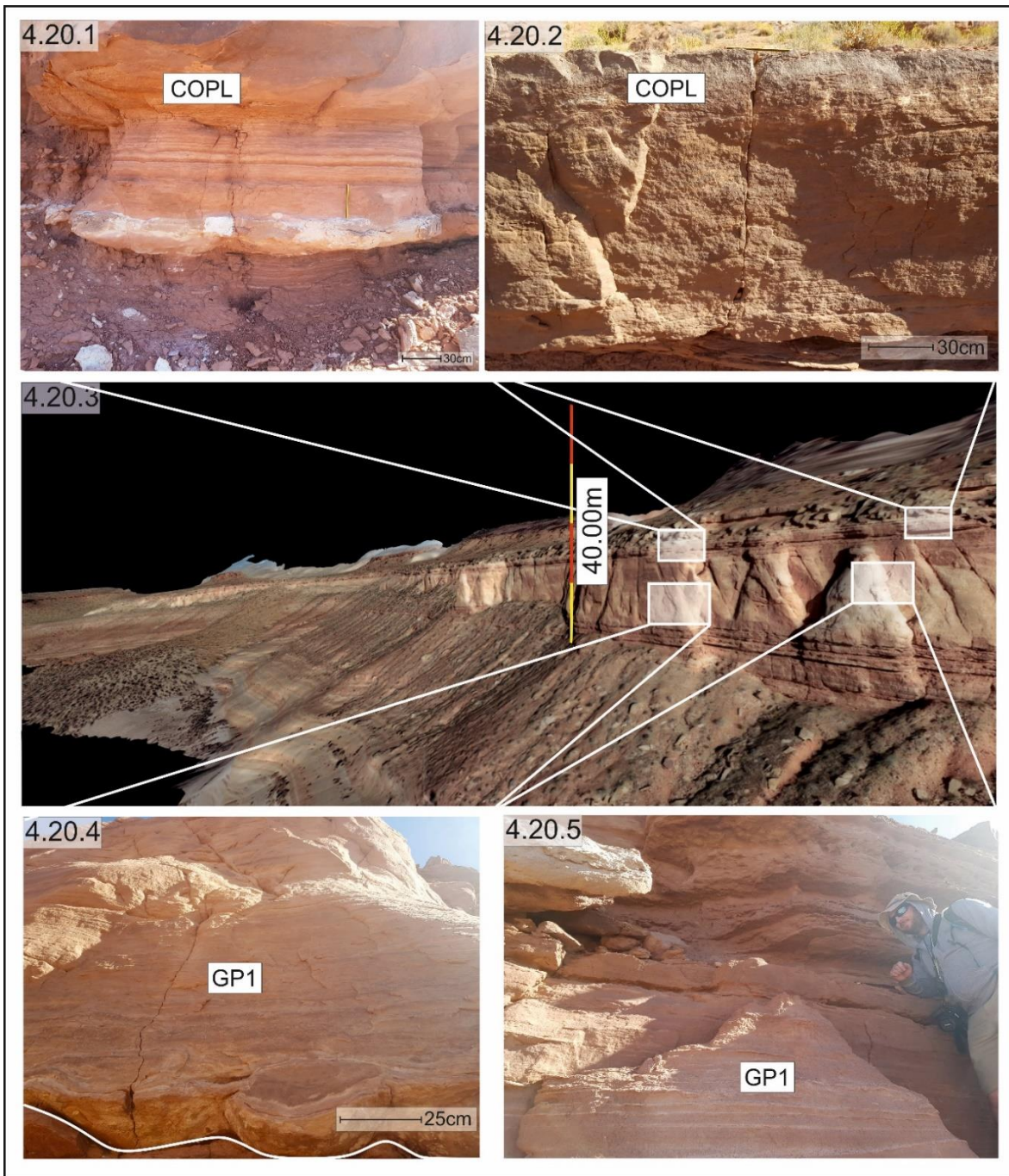


Figure 4.20.1-Field photo of the coastal plain deposits at Duma Point Transition 3. Figure 4.20.2-Field photo of burrowing within the coastal plain deposits at Duma Point Transition 3. Figure 4.20.3- Panel diagram showing the dune measurements for each unit from the drone photogrammetric model. Each arrow shows one representative grainflow thickness from each unit, which can then be compared with the virtual scale to give an estimation for grainflow thicknesses. Figure 4.20.4- Snapshot from VRGS showing TS1 and GP1 to scale with a representative foreset thickness measurement. Figure 4.20.5-Snapshot from VRGS showing GP1 to scale with a representative foreset thickness measurement.

Interpretation

This locality represents the greatest extent of the Moab Member sandstones. After a period of significant flooding forming an erosive base, a large amount of sediment was introduced to the environment forming a massive base unit with load casts and soft-sediment deformation. With movement up the succession, sediment supply stabilised but is still too restricted to preserve dune-scale bedforms. Instead, ripple-scale bedforms and pinstripe laminations are preserved, highlighting a sandsheet environment. The grainflow thicknesses imply a minimum dune height of 0.4 at Duma Point Transition 3 and just 0.2m at Duma Point Transition 1. This locality shows an apparent decrease in sediment supply upwards through the cliff succession and westwards between Duma Point Transition 3 and Duma Point Transition 1. In addition to the presence of just one sandstone package, there is also more significant evidence of water influence in this succession, implying a more coastal environment influenced by a highly fluctuating local water table. The overlying coastal plain sediments further support this with root traces and some burrowing indicating a habitable environment.

The Duma Point Transition 3 sandstones likely represent a marginal sandsheet, subject to strong aqueous influence, forming the erosive base, water escape, soft-sediment deformation, and small-scale ripple forms. The environment is likely to have then supported a number of small, sub-critically climbing dunes as a marginal dune field. The lack of well-defined cross-bedding in the unit above indicates a transition to a sandsheet environment with an insufficient sediment supply to develop and preserve dune-scale bedforms. It is important to note here that the photogrammetric models and field photographs show several linear cross-cutting structures within this unit, however, these are most likely to be syn-depositional as they cross index surface boundaries.

The preserved sediment at Duma Point Transition 1 is the most westerly deposit of the Moab member sandstones, also presenting as a sandsheet environment at this locality. The sporadic and thin cross-bedded sets and the thin deposit overall imply an environment with a restricted sediment supply.

4.4 Summary

Each of the genetic packages and their respective index surfaces is correlatable east to west across the transect. At the easternmost locality, Bartlett Wash, the preserved aeolian succession comprises four packages separated by five index surfaces. Northwestward to Lone Mesa, the same four genetic packages and five index surfaces can be identified, with the same geometries and features such as rhizoliths. Westward at Dubinky Well, the succession comprises of three genetic packages with the correlatable index surfaces occurring at the same vertical position up the succession as at Bartlett Wash and Lone Mesa. At the most westerly locality, Duma Point, there is just one genetic package separated by a basal and a top index surface. This is the last occurrence of the aeolian deposits, further west of this locality, the deposits are coastal or shallow marine. Analysis of set and foreset thickness shows a rapid thinning of units towards the west of the study area corresponding with the decrease in packages and surfaces. The distinct pattern of genetic package separated by a surface that is correlatable across the whole study area implies a 'pulse-like' behaviour of the dune field. Such that the dune field reaches an extent, then there is a change in conditions resulting in a lack of preservation, after which the dune field reactivates and is preserved to a greater extent and this process repeats. Palaeo dune height measurements from each of the genetic packages further support the pulsing of the dune field in response to changes within the aeolian system. Showing that not only did the dune field thin westward but dune height also decreased up-succession with the

dunes becoming larger up until a significant event at TS2, after which the dunes begin again to decrease in height until the boundary with the coastal plain sediments.

This chapter takes a closer look at the units within the planar cross-stratified sandstone facies (Sxs) at each locality within an east-west transect from Bartlett Wash to Duma Point. Analysis of varying grainflow thickness within each of the identified units at each locality provides an estimate of palaeo-dune height, which can establish changes in the complexity of the dune field spatially and temporally. At Bartlett Wash (Jedi 3D) and Bartlett Fault, Lone Mesa, and Dubinky Well, analysis of dune-heights up-succession showed an increase in dune complexity and sediment supply up to an index surface, after which the sediment supply appeared to decrease again. Despite following the same general trends upwards, there was a change in thickness of the respective units and the number of units decreased westward between the localities.

Results, therefore, show an overall decrease in complexity of the dune field with increasing proximity to the palaeo marine margin. At the most proximal part of the study area in the east, at Bartlett Wash, each genetic package comprised relatively well-developed dune forms and additional features such as rhizoliths that indicate periods of dune accumulation and preservation consistent with an extensive dune field. However, westward, preserved set thickness within the genetic packages begins to decrease, with bedding becoming lower angle. This pattern is consistent with the gradation away from the erg centre in response to wetting conditions with proximity to the marine margin.

Chapter 5: Spectral Gamma-Ray Characterisation of an Aeolian-Marine Margin

Geophysical analysis encompasses a wide array of methods and techniques such as nuclear, electrical, magnetic, and gravitational analysis. It is used to provide qualitative and quantitative data that enables the characterisation of both surface and subsurface successions. This method is advantageous as it offers a more comprehensive understanding of an outcrop than traditional techniques, such as sedimentary logging, in isolation (Hooshyari-Far *et al.*, 2015).

This chapter uses the modern theories behind spectral gamma-ray to correlate sedimentary logs taken across an aeolian/marine margin. To complement this, and lithofacies analysis (Chapter 3), the gamma-ray logs have been further analysed to provide facies cross-plots and log motif trends. Significant peaks have been identified and analysed at each locality using suitable ratios of the detected isotopes, namely potassium (K), thorium (Th), and uranium (U). Trends in the grouping of data within the cross-plots will enable a description of shifts in the environment spatially whilst the correlation of significant values in the gamma-ray logs will provide a correlatable point in time with which to tie together the depositional story across the margin (Davies *et al.*, 1999).

5.1 Background

Spectral Gamma Ray (SGR) logging, a nuclear geophysical technique, is particularly effective as a tool for characterising outcrops. Although typically applied to boreholes, SGR analysis at the surface can include the determination of mineralogy (Hesselbo & Parkinson 1996, Schnyder & Ruffell 2006), palaeoclimate (Ruffell & Worden 2000, Ruffell *et al.* 1999) and cyclicity (Sierro *et al.*, 2000).

Contemporary uses of SGR logging have focused on the identification and

correlation of sequence boundaries and sequence stratigraphical surfaces within preserved deposits and borehole data (Aranda *et al.* 2019, Pettigrew 2019, Nobre *et al.*, 2020).

SGR uses the naturally occurring background radiation of three key elements - Potassium (K), Thorium (Th) and Uranium (U) - to produce a detectable signature that can be documented and compounded to provide a quantifiable record of an outcrop. The data can then be further analysed to determine the ratios between these elements (Serra & Abbot 1980, Kumar & Kishore 2006).

5.1.1 Principles of Spectral Gamma Ray

Gamma rays are defined as bursts of high-energy electromagnetic waves emitted during the decay of radioisotopes. This phenomenon is naturally occurring and relies on three radioisotopes: potassium-40 and the daughter products of the uranium and thorium decay series (Cripps & McCann, 2000). Detection of each of these elements relies on the energy level of photons produced by radioactive decay, the levels of which are distinct and element-specific. Potassium-40 results in gamma photons of 2.62 MeV (million electron volts), whilst Uranium-238 and Thorium-232 have several attributable peaks but are most commonly detectable at 1.76 MeV and 1.46 MeV respectively (Cripps & McCann, 2000) (Figure 5.1). In sedimentary rocks, radioactive elements tend to be concentrated in clays and siltstones, or in other facies in which there is high organic content. The best example is potassium-40, which readily gathers in mica and clay minerals that are more abundant within argillaceous and marine strata. By contrast, more quartz-rich strata (such as those deposited in an aeolian system) have relatively little potassium-40. The contrast between signals produced within a more dominantly clay environment and a more dominantly quartz one will produce a series of

positive or negative peaks that, whilst they are not facies unique, can add weight to interpretations of the environment (Cripps & McCann, 2000).

Modern technological developments have enabled the use of handheld spectral gamma-ray tools within the field. As the device is sensitive to the surface morphology of the outcrop and the position of the tool relative to the bedding, the position of the sensor relative to the surface of the rock is important (Svendsen & Hartley, 2001). Both convex and concave surfaces can negatively affect the accuracy of the instrument, it is therefore important to measure the flattest available surface (Figure 5.2). Furthermore, it is important to calibrate for background radiation as the device can be sensitive to all emissions.

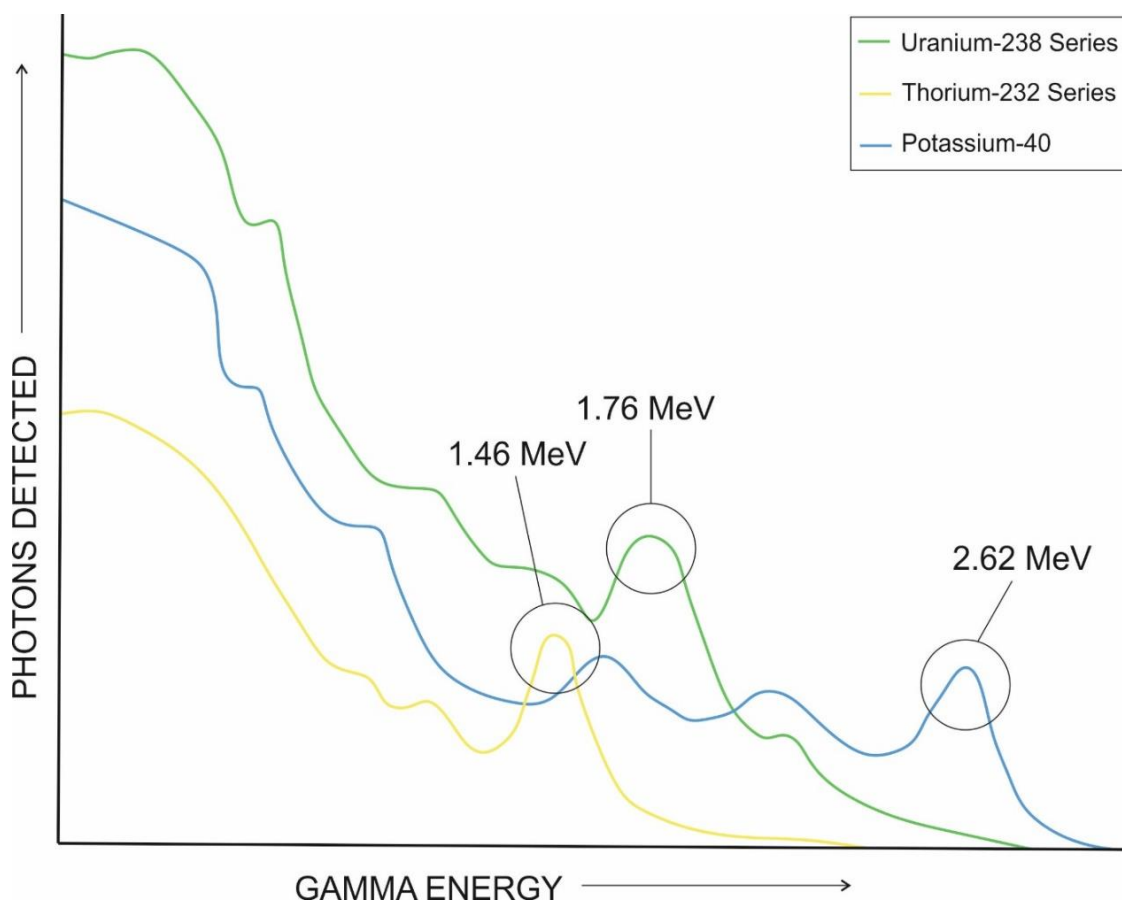


Figure 5.1- Gamma Ray spectra of the most prominent naturally occurring radioisotopes, potassium-40, thorium-232 and Uranium-238. Spectral Gamma Ray detectors use these peaks as their controls values with which to distinguish and present levels of the elements within the rock (After Cripps & McCann, 2000).

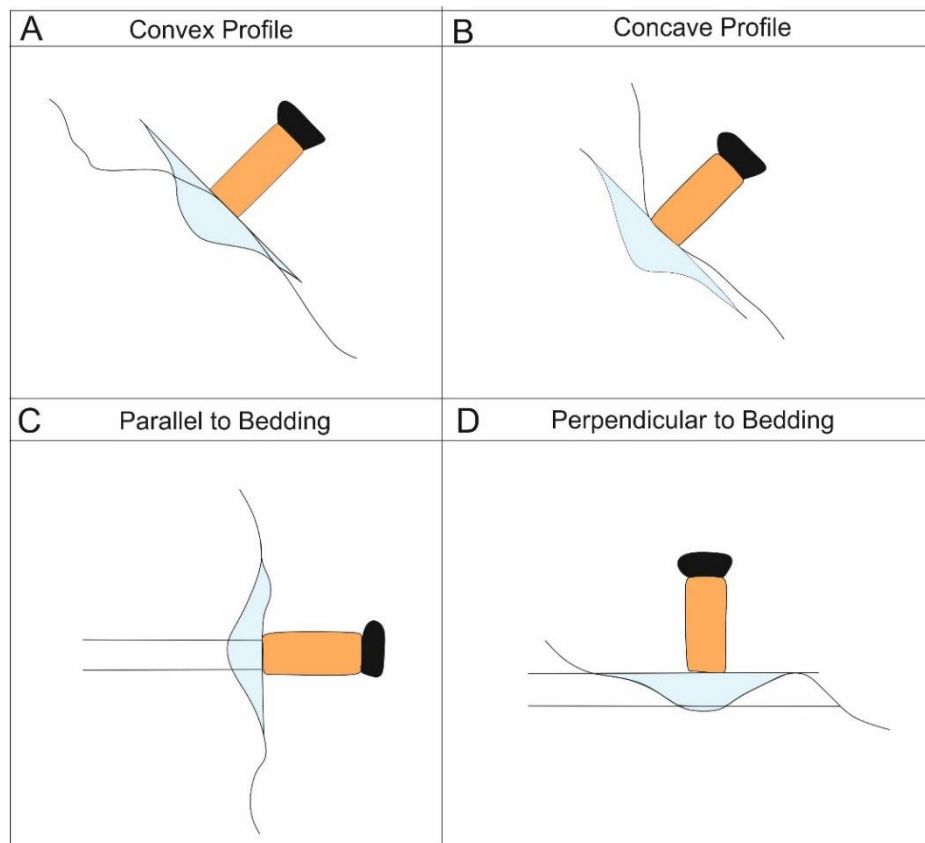


Figure 5.2-The effects of spectrometer positioning on outcrop SGR measurements. Blue represents the expected measuring volume of the tool which is reduced for a convex profile (A), increased for concave (B), diluted for thin bed readings (C) or concentrated when placed on the bedding plane (D) (After, Svendsen & Hartley, 2001).



Figure 5.3- Positions of the spectrometer were chosen based on the most effective angle for measurement as outlined by Svendsen & Hartley, 2001.

As the concentration of uranium within preserved successions can be three to four times smaller than thorium ratios, some studies state that a longer count time of 120-180 seconds is required (Løvborg & Mose 1987, North & Boering 1999, Svendsen & Hartley 2001). Whilst this may have been true for previous uses of spectral gamma-ray (Adams & Weaver 1958, Kull & Ginaven, 1970), modern handheld devices possess calibration and standardisation instruments that produce a negligible difference in values, regardless of total count time (Sêco *et al.* 2021, Pettigrew, 2019).

5.1.2 Facies Cross-plot Analysis

To augment the qualitative nature of lithofacies analysis, analysis of trends within grouped data points in potassium thorium (K:Th) cross-plots can infer depositional environment. Relative amounts of thorium, potassium and uranium in isolation do not provide robust facies discrimination as their deposition and preservation is dominated by grain size (Gould *et al.*, 2014).

Each facies and depositional environment display a plot trend which once constructed will isolate any outliers to this trend, limiting problems arising from misidentification of facies. As a generalisation, cross-stratified sandstones, and limestones cluster in the lower left-hand corner of K:Th cross-plots, containing a relatively small amount of both potassium and thorium. By contrast, sediments with a higher percentage of clay minerals cluster towards the right of the graph. They are harder to distinguish from each other but consistently contain high levels of K and Th (Bristow & Williamson, 1998). Due to vastly different and unique depositional environments, K:Th cross-plots representing palaeosol facies can have various spatial morphologies and often occupy the whole range of the graph in a linear trend. The uniformity of silt fallout deposits within a coastal plain is

reflected strongly in the K:Th cross-plots, displaying a linear trend from the bottom left to the top right of the plot with a strong positive correlation (Bristow & Williamson, 1998, Šimíček & Bábek, 2015). Finally, tidal sub-aqueous facies are neither pure silt nor pure sandstone, and hence occupy an intermediary trend displaying low left-hand clusters of sandstones but also high values representing the influence of marine muds and clays (Šimíček *et al.*, 2012).

Statistical Analysis

Whilst visual trends can establish clustering and linearity associated with different lithofacies and environments, statistical analysis provides a quantitative value for this relationship. There are two main statistical tests used to establish the relationship between data points, the coefficient of correlation and the coefficient of determination.

Pearson's coefficient of correlation can be a useful tool in establishing the relationship between K and Th values for each facies (Asfahani, 2014):

$$r = \frac{\sum(x_i - \bar{x})(y_i - \bar{y})}{\sqrt{\sum(x_i - \bar{x})^2} \sqrt{\sum(y_i - \bar{y})^2}}$$

Where x_i = variable X \bar{x} = mean of x_i \sum = sum of
 y_i = variable Y \bar{y} = mean of y_i

[1]

It measures the strength and direction of linear trends between two variables producing a value between -1.0 and 1.0, represented by the r number [1]. Positive values indicate high potassium levels that correspond with high thorium levels, whilst near-0 values indicate no relationship.

Whilst the coefficient of correlation is used to determine whether the facies exhibit a linear trend or a cluster, the coefficient of determination is used to establish the error in a set of data:

$$r^2 = \frac{(\frac{1}{N}) \sum (x_i - \bar{x}) (y_i - \bar{y})}{(\sigma_x \sigma_y)^2}$$

Where x_i = variable X \bar{x} = mean of x_i σ_x = standard deviation of x_i Σ = sum of
 y_i = variable Y \bar{y} = mean of y_i σ_y = standard deviation of x_y N = number of
variables

[2]

The r^2 value [2] defines how much the variability of one factor is dependent on another. In this case, the amount of thorium for any given facies is directly controlled by the amount of potassium. The coefficient of determination is the square of the correlation between predicted values and actual values [2]. For graphs with linear regression, the coefficient of determination is equal to the square of the correlation between x and y values.

Facies with a positive correlation are defined as those with a coefficient of correlation $0.5 < r < 1$. This relationship implies a trend such that for high values of Th, there will be similarly high values of K and vice versa. Facies with a near-zero correlation have a coefficient of $0 < r < 0.5$. Whilst not strictly a negative correlation (which would still imply a relationship, just a negative one), the closer the number is to 0, the weaker the relationship between the data points. Facies with an insufficient dataset will not return a statistically significant r [1] or r^2 [2] value and should therefore be discounted.

5.1.3 Log Motifs & Trends

The primary way patterns can be established from total counts logs is log motifs (Rider 1990). These are identifiable trends that lend themselves to a specific broad-scale depositional environment. The motifs themselves cannot provide a definitive analysis of facies, and the use of log motifs and spectral gamma-ray logs as rigid interpretations is documented to have its pitfalls (Hurst 1990, Hurst & Milodowski 1996). However, even a broad description of the shifts in depositional environment along the margin through time can be useful when used in conjunction with facies cross-plots and isotope ratios.

The shapes of the motifs themselves are an indicator of grain size in most instances and are based on three fundamental shapes (Serra & Sulpice 1975): bell, funnel, and cylinder. A 'bell-shape' or convex profile represents an increase in gamma radiation upwards and hence a fining-up grain size trend (Figure 5.4). A 'funnel-shape' or concave profile shows coarsening upwards or upwards 'cleaning' trend (Serra & Sulpice 1975, Martinius *et al.*, 2002, Keeton 2012). Cylinder log motifs have a consistent total count value. A cylinder motif with consistently low total counts values may be due to no significant change in grain size within the succession or exceptionally 'clean' deposits. Whilst this is a valuable trend, it is important to note that grain size is not a determining factor in radioisotopes within the sediment. The pattern is most likely to be caused by other depositional factors such as the depositional process and provenance of the material, which are typified by different grain sizes within different environments (Martinius *et al.*, 2002).

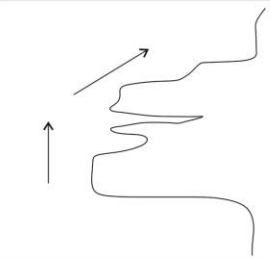
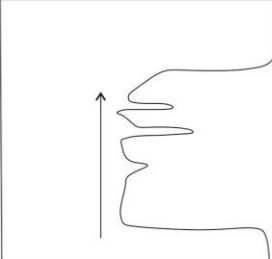
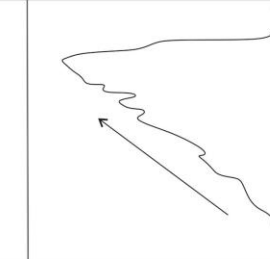
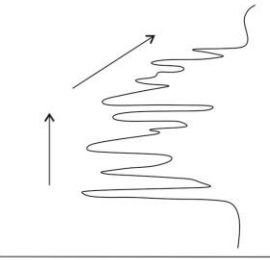
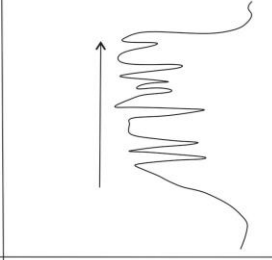
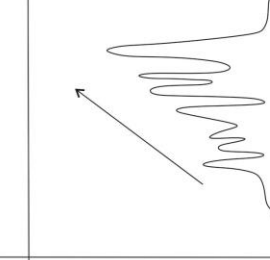
BELL-SHAPED	CYLINDER-SHAPED	FUNNEL-SHAPED	DESCRIPTION
			SMOOTH
			SERRATE
Retrograde/Waning deposition (channel)	Aggrading deposition (sequence stacking)	Prograding deposition (delta front/splay)	

Figure 5.4-Log motifs identifiable within spectral gamma-ray logs of preserved successions. Bell-shaped motifs imply retrograding sets and therefore transgression, cylinder motifs, aggradation, and funnel-shaped motifs progradation and hence regression (After Martinus *et al.*, 2002).

5.1.4 Application of SGR in Geological Interpretations

Relative quantities of K and Th can distinguish between continental and more marine influences within the depositional environment, whilst the presence of varying levels of uranium can support the occurrence of a hiatus or time-gap at this point (Fertl *et al.* 1982, Ehrenberg & Svana, 2001). When used in conjunction with sedimentary analysis, K:Th cross-plots and log motifs, total count and Th/U logs are a powerful tool in determining facies, environments, time-gaps, and relative trends to provide a quantitative analysis of otherwise qualitative datasets (Rider 1996, Hampson *et al.*, 2005). Spectral-gamma ray logs are most commonly used to identify the clay concentration of deposits to describe potential depositional environments. In addition to clay content, however, SGR logs provide useful information about different environmental characteristics. Each of the radioisotopes detectable by a handheld SGR tool has a distinct set of characteristics that can help define changes in the environment at the time of

deposition (Table 5:1). As individual radioisotopes contain unique information about environmental conditions, the ratio between these isotopes also holds crucial information such as sedimentary conditions, distance to palaeo shorelines, and the detection of basic discontinuities (Klaja & Dudek, 2016). Three main isotope ratios are used in the geological interpretation of spectral-gamma ray data, thorium/uranium (Th/U), uranium/potassium (U/K) and thorium/potassium (Th/K) (Table 5:1).

Ratio	Significance
Th/U	1) Analysis of sedimentary conditions -Th/U >7 continental environment, oxidising conditions, weathered soils etc. -Th/U <7 marine sediments, grey and green shales, greywackes -Th/U <2 marine black shales, phosphorites, reducing conditions. 2) Estimation of organic matter content in claystones 3) Detection of basic discontinuities 4) Used in stratigraphic correlations by determining transgressive-regressive conditions
U/K	1) Evaluation of the organic matter content in clay sediments 2) Used in stratigraphic correlations 3) Detection of diagenetic changes in clay and carbonate sediments, etc. 4) Used in correlation of natural fissure systems in deeper formations
Th/K	1) Recognition of types of sediments representing various facies 2) Determination of sedimentary condition types, distance to palaeo shorelines 3) Determination of diagenetic changes in clay sediments 4) Determination of the type of clay minerals

Table 5:1-The uses and significance of different ratios of the common isotopes detected by spectral gamma-ray analysis of preserved successions (After Fertl *et al.*, 1982).

Th/U Ratio

Firstly, the thorium/uranium (Th/U) ratio is primarily used to determine the depositional environment and identify a hiatus within a succession (Klaja & Dudek, 2016). Naturally occurring thorium isotopes are insoluble in water. This means they are largely unaffected by local movements in the water table or by regional sea-level change. By contrast, uranium isotopes, associated with organic matter, accumulate on exposed surfaces but are readily dissolvable into solution. Therefore, it can be inferred that a significant peak in a Th/U log implies the accretion of uranium isotopes on a surface that has been exposed for a significant

period of time, i.e., a greater level of uranium vs thorium. A significant peak is produced from the accumulation of uranium upon exposed surfaces, creating a higher Th/U ratio. Th/U ratios can also describe the environment by value alone, such that a ratio of Th to U greater than seven implies strictly continental deposition or oxidising conditions; less than seven but greater than two implies shallow marine sediments. Finally, less than two implies marine shales or reducing conditions. However, it is important to note that these are not absolute values; whilst they can be used as an indicator of the dominant environment, intermediate environments can produce results not within the boundaries described above. For example, the increased aqueous influence of a fluvial system that borders aeolian dunes or an aeolian-marine margin may affect these definitive ratio classes. To use these criteria exclusively risks an oversimplification of often complex, interfingering environments (North & Boering, 1999).

U/K Ratio

The ratio between uranium and potassium, are less frequently used as they mainly relate to the diagenetic behaviour of clay materials and the correlations of fissures within deep formations; however, they can also be used for stratigraphic correlations. Due to the relatively high potential of potassium to be leached versus the relative stability of uranium along exposed surfaces any major peaks are correlatable to large scale events affecting all marginal environments (Hampson & Davies, 2005).

Th/K Ratio

Finally, as established, the ratio between Th/K within a cross-plot is a suitable analytic tool for determining lithofacies and inferring depositional environments. Th/K logging also provides valuable information about the sedimentary conditions and, critically, the position of these depositional environments to a palaeoshoreline

(Klaja & Dudek, 2016). The principles of this method are that thorium is an incredibly stable isotope under oxidising conditions and does not readily dissipate into solution (Serra & Baldwin, 1980, Rider 1996). By contrast, potassium dissolves into interstitial fluids with relative ease, and hence flooding surfaces will be identifiable in the rock record by peaks of Th that correspond with K depletion. In addition, surfaces defined by palaeosols have a distinct potassium-leached character that is indicative of the removal of potassium relative to the stability of thorium. The mean Th/K ratio of associations is largely constant, attributed to the depositional environment. Therefore, it can be assumed that a sudden change or peak in Th/K is an indicator of a dramatic environmental change or potentially an unconformity (Ehrenberg & Svana, 2001).

5.2 Methods

This section describes the methods carried out in the field using a handheld gamma-ray tool in order to obtain a detailed description of the facies in a transect across an aeolian/marine margin.

5.2.1 Spectral Gamma Ray Field Techniques

In conjunction with sedimentary logs, spectral gamma-ray logs were taken at five localities. An RS-230 BGO Super-SPEC Handheld Gamma-ray Spectrometer was used for logging the accessible sediment at each outcrop. This tool uses a 103 cm³ Bismuth Germanate Oxide (BGO) scintillator crystal as a detector and automatically calculates the concentrations of radioisotopes in assay mode (Sêco *et al.*, 2021, Radiation Solutions, Inc., Canada).

At each outcrop, measurements were taken at 20cm intervals, vertically upwards with as little deviation as accessibility would allow. The spectrometer was held directly against the flattest surface of the rock for 90 seconds and the data was

recorded subsequently. Although the device itself does not contain a radioactive source, calibration of the background emissions of the study area is still required and was automatically carried out and stored by the spectrometer before direct measurements were taken.

5.2.2 Cross-plots and Statistical Analysis

Once the data had been collated, they were input directly from the spectrometer into a spreadsheet. The data included levels of thorium in parts per million (ppm), uranium in parts per million (ppm) and potassium in weight percent (%). In addition, the total counts in both parts per million (ppm) and counts per minute (cpm) were recorded. These data were manually separated into different sets for each facies and associations based on their relative position within the sedimentary logs (Chapter 3).

Within a spreadsheet, ratios of the various isotopes, Th/U, U/K and Th/K, were calculated, and line graphs and scatter plots produced, that have been used throughout this study. Processed data has been split between each locality and colour-coded by both locality and type of radioisotope to visualise otherwise large and convoluted data sets.

5.2.3 Spectral Gamma-ray Logs

Five spectral gamma-ray logs were taken at five localities in conjunction with sedimentary logs (Chapter 3, Figure 3.1), representing the transition between a tidal flat/coastal plain environment into a dominantly aeolian environment.

Readings were taken at 20cm intervals for 90 seconds per reading. Data collected from the handheld spectrometer was collated and inputted into a spreadsheet, within which the line graph function was used to create logs of Th/U, U/K and Th/K and total counts against height.

5.3 Identification of Facies from K:Th Cross-Plots

This section displays cross-plots of potassium (K) against thorium (Th) for each of the facies and associations as identified in the sedimentary logs and facies (Chapter 3). A summary of all the gamma-ray data collected at each locality against their respective sedimentary logs can be found in Figure 5.5. In addition to the cross-plots, total counts and radioisotope logs are shown correlated to their respective sedimentary logs for each locality.

Figure 5.7-Figure 5.10 shows the K:Th cross-plots for associations at each locality. Plotting the associations on one graph per locality leads to a large cluster of convoluted and hard-to-read data. Hence, for clarity, the K:Th cross-plots have been separated into facies and colour-coded by the locality in which they occur (Figure 5.11-Figure 5.14).

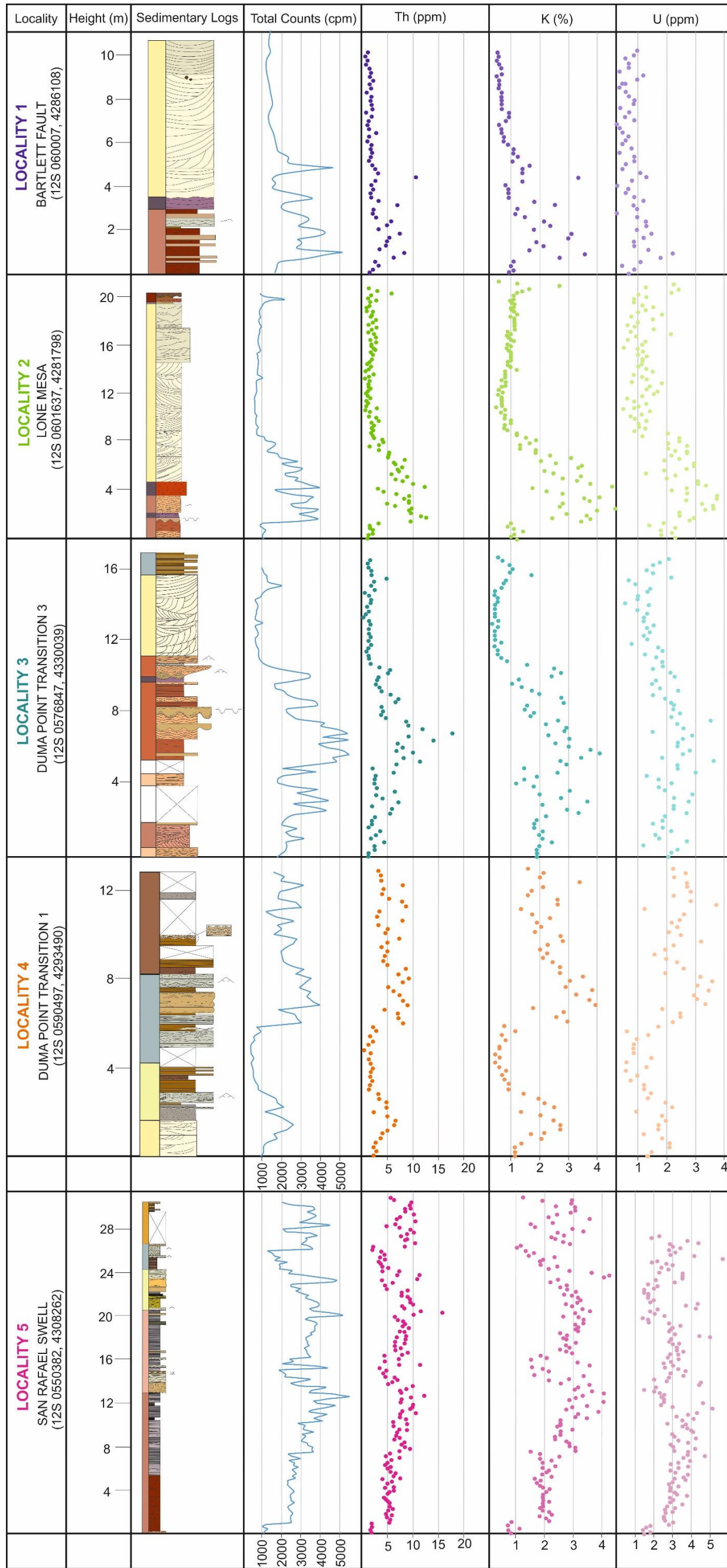


Figure 5.5-Summary of spectral gamma ray data obtained from localities 1-5, visualised as the total amount of each element (total counts), and the amount of each element (U,Th & K) against height.

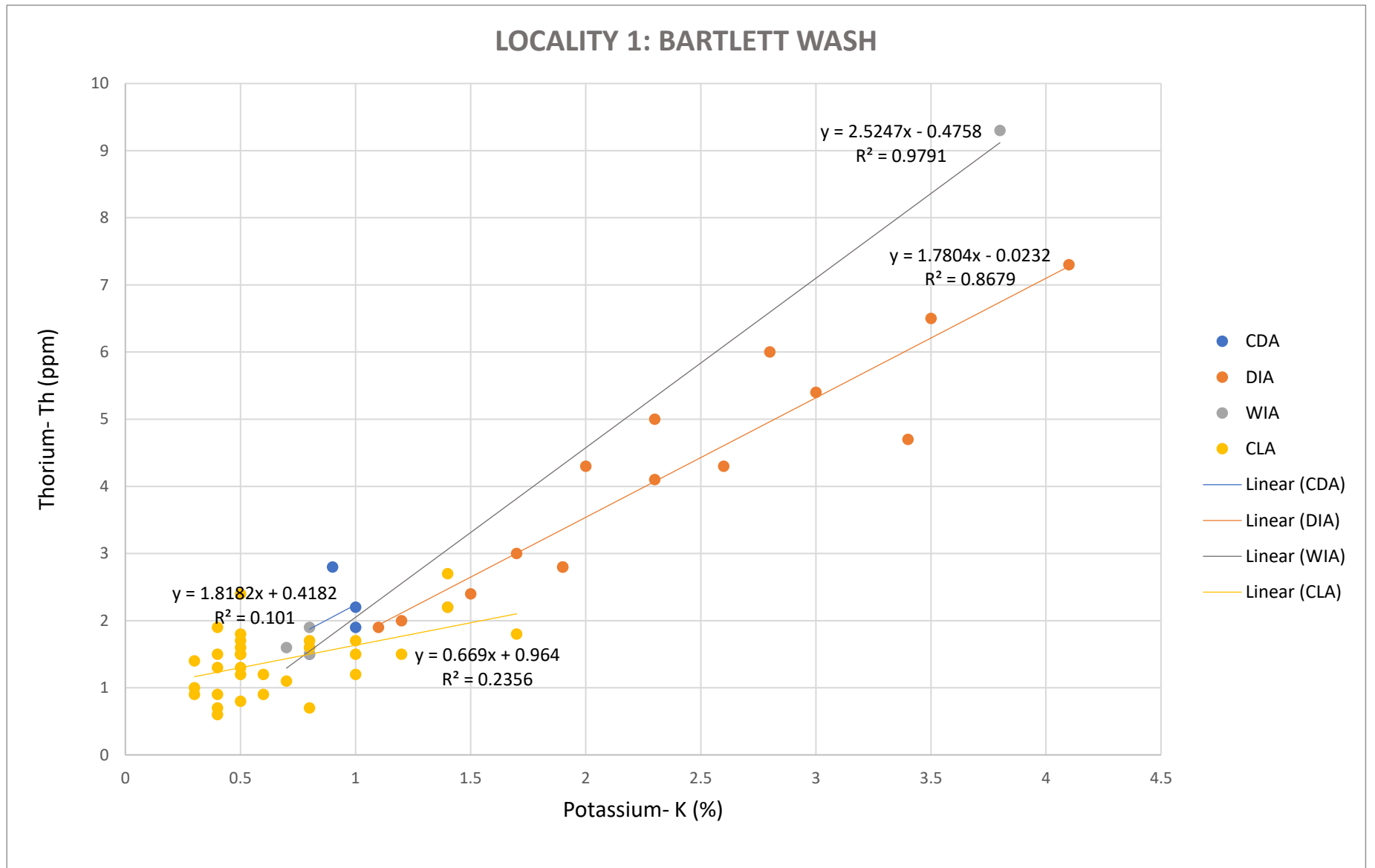


Figure 5.7- Ratio between potassium and thorium isotopes found at Locality 1. Bartlett Fault logged by a handheld spectral gamma ray tool. The trendlines for each association have been added showing the equation of the line and the coefficient of determination (r^2).

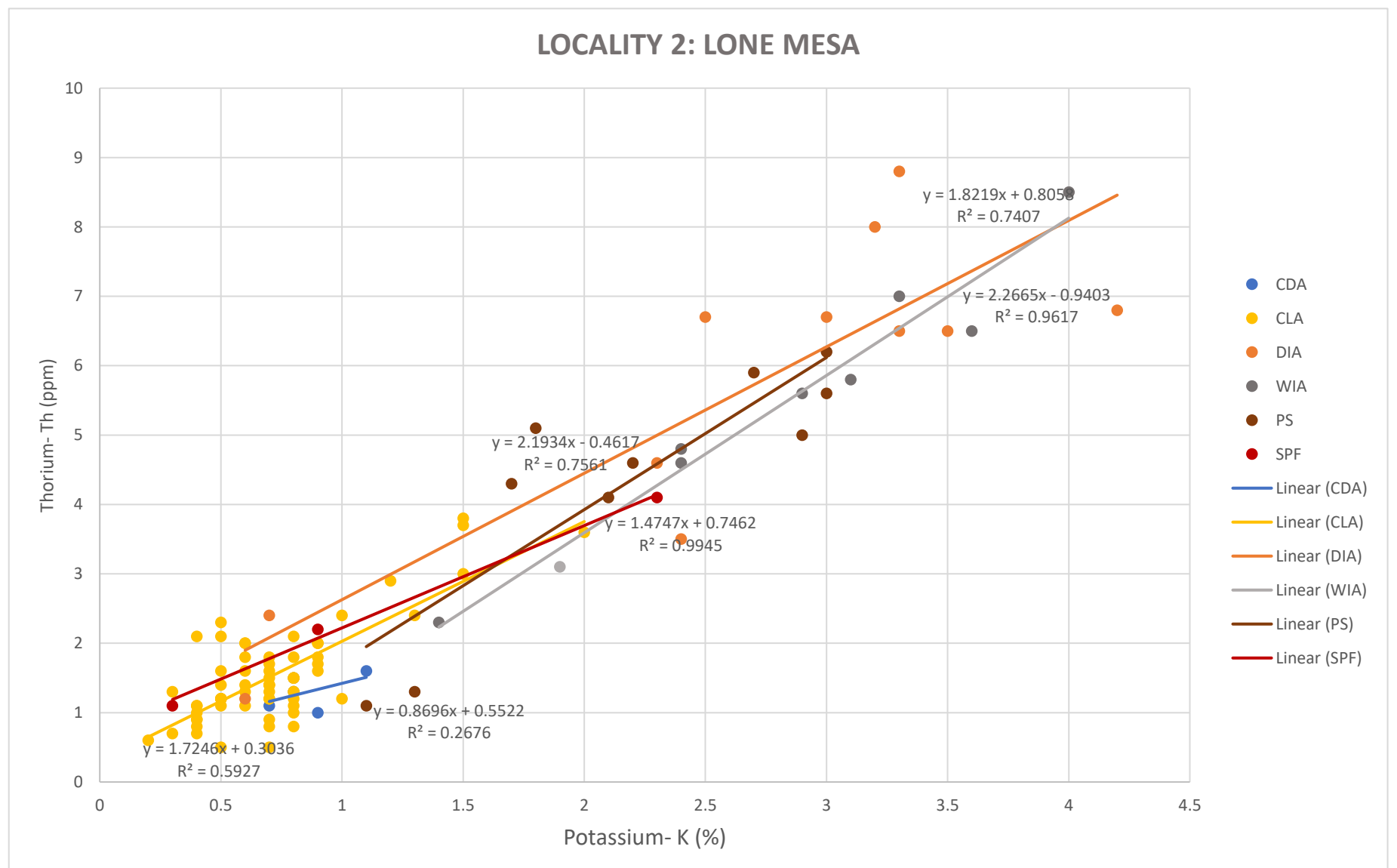


Figure 5.6- Ratio between potassium and thorium isotopes found at Locality 2a Lone Mesa by a handheld spectral gamma ray tool. The trendlines for each association have been added showing the equation of the line and the coefficient of determination (r^2).

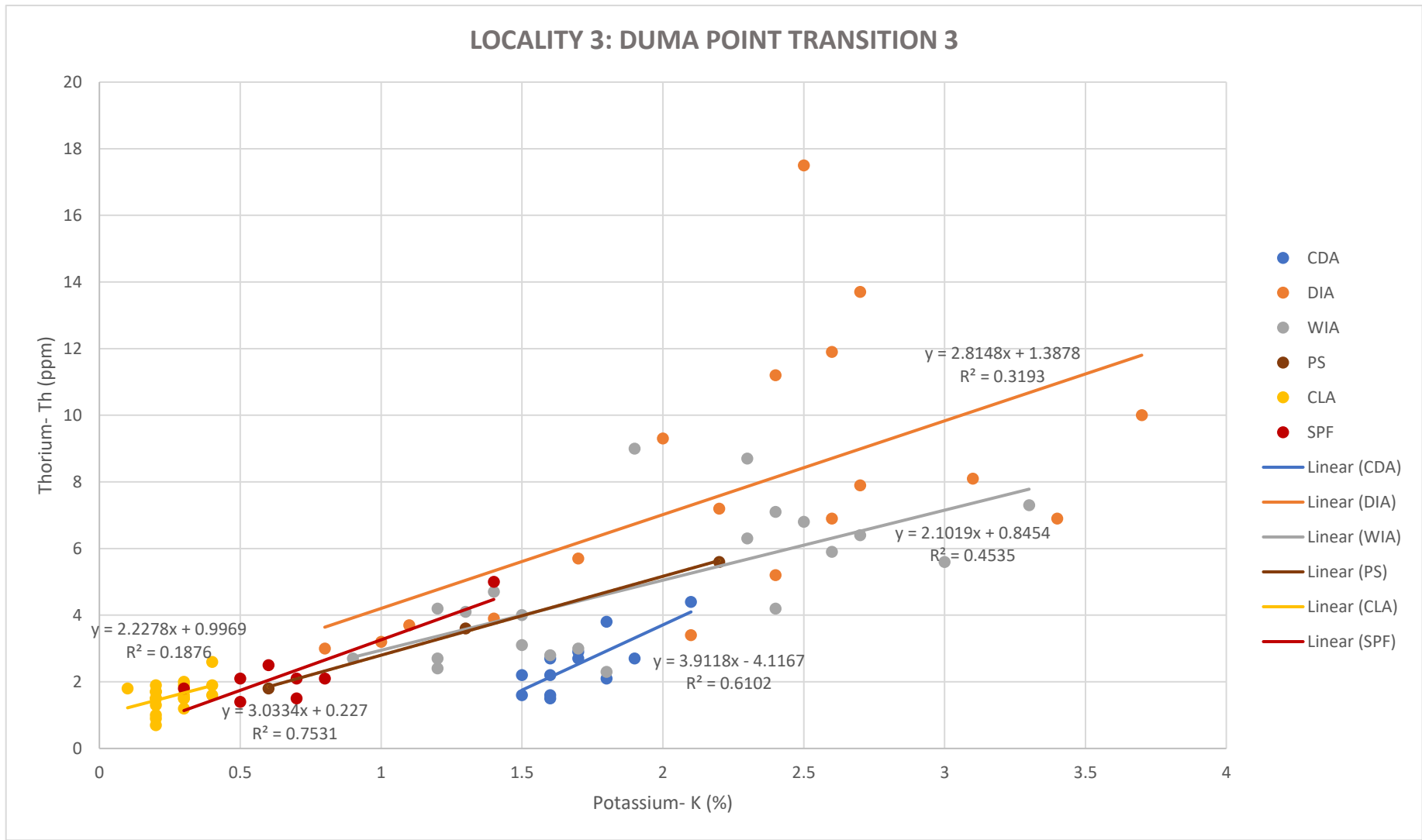


Figure 5.9- Ratio between potassium and thorium isotopes found at Locality 3 Duma Point Transition 3 logged by a handheld spectral gamma ray tool. The trendlines for each association have been added showing the equation of the line and the coefficient of determination (r^2).

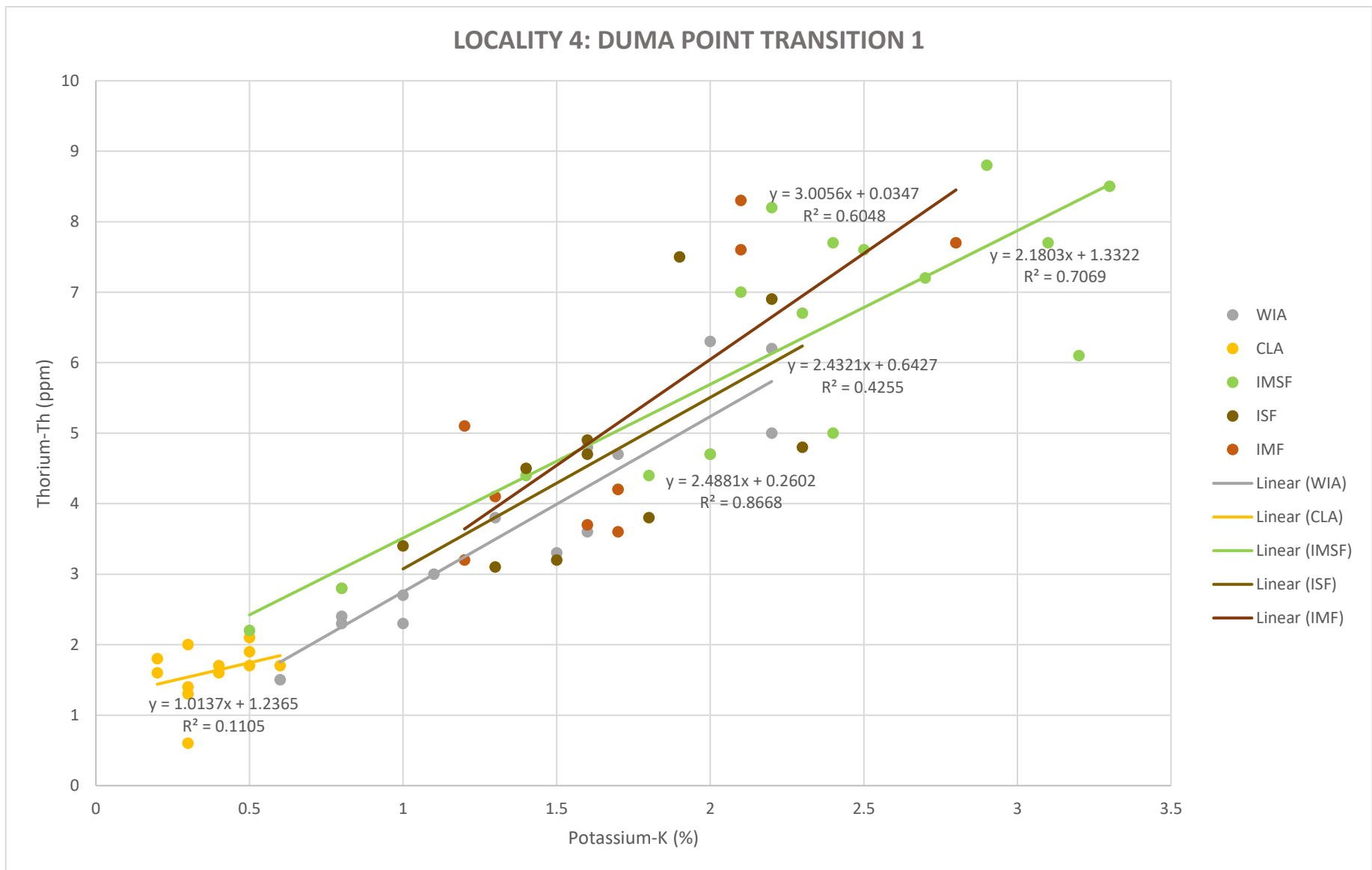


Figure 5.8- Ratio between potassium and thorium isotopes found at Locality 4 Duma Point Transition 1 logged by a handheld spectral gamma ray tool. The trendlines for each association have been added showing the equation of the line and the coefficient of determination (r^2).

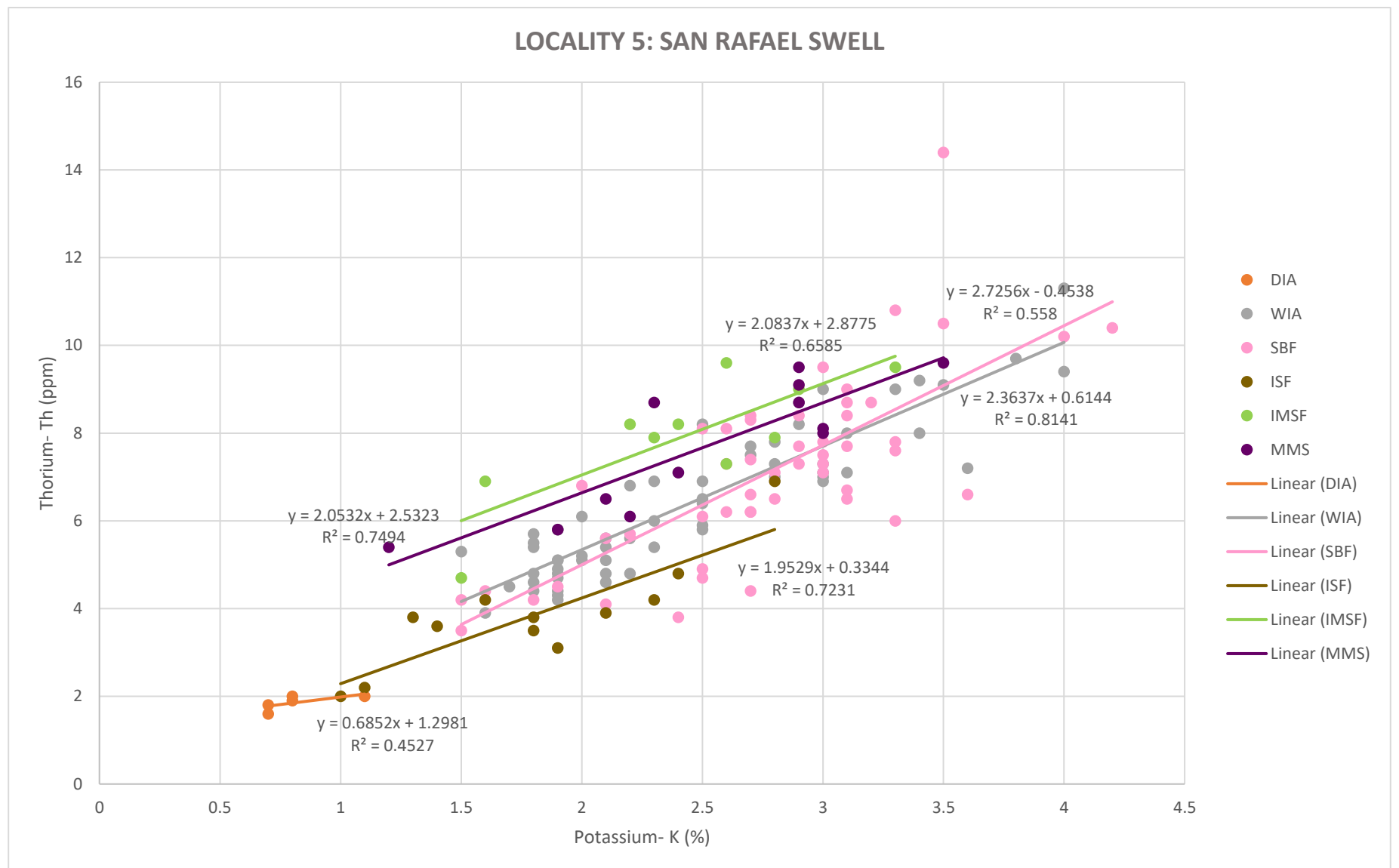


Figure 5.10-Ratio between potassium and thorium isotopes found at Locality 5-San Rafael Swell logged by a handheld spectral gamma ray tool. The trendlines for each association have been added showing the equation of the line and the coefficient of determination (r^2).

In order to clarify the above diagrams, the data have been separated and regrouped independently of the locality at which they were found. This allows for comparison across the margin and can also be used to identify outliers, or anomalies, which could point to the misidentification of facies.

The facies have been grouped into depositional settings or associations that distinguish the facies whilst allowing for a distinct comparison. These are described in more detail below.

5.3.1 Results

Wet Aeolian Dune Field

Within this association, trough cross-bedded sandstones (Stxs) represent dune-forms (Figure 5.11), and wind-rippled sandstone (Sfpd) represent wind-ripples along the stable dune slip-faces. The trough cross-bedded sandstones (Stxs) show distinct clustering of data in the lower left-hand corner of the graphs, with further distinguishable groups forming from each individual locality. Localities 1, 2 and 5 (see Chapter 3, Figure 3.1) show similar clusters around the 1% K, 2ppm Th mark. The same trend can be seen at locality 3 with higher K values of 1.5-2% and 2-5ppm Th.

Interpretation- The higher values at Locality 3 could indicate a higher level of detrital clay or at the very least an increased proportion of potassium feldspar, glauconite or mica. Locality 3 is within a short distance of Locality 4, the point of transition between the aeolian and marine environments and hence the additional detrital clay could be due to increased sub-aqueous influence nearby.

Interdune facies cross-plots are discernible from aeolian facies by much higher counts and data points that show a wider spread spatially. In contrast to the clustered aeolian deposits (Stxs, Sfpd), interdune plots have a significantly more

linear trend. Data for undulose sandstones (Sdun) is dispersed between 1-4.5% K and 2-14ppm Th. There is an outlier value at 2.5% K and 18ppm Th. The trend at Localities 1 and 2 is very linear, whereas locality 3 is widely dispersed and has the lowest r^2 value. The undulose sandstone facies that contains mud drapes (Sdun) displays the most linear intra-locality trend of any facies, however, it has a strong inter-locality variability. At Locality 2, the data points are very low, as expected within an aeolian environment, whereas at Locality 5, the values are much higher, more reminiscent of mud-rich facies. This trend of positive correlation but high dispersal continues within the parallel laminated mudstone/siltstone facies found within this interdune association (Sspl). This facies demonstrates the strongest trend between localities as it is one of the only ones to be found at every locality. The data fell within a wide range, 0-4.5% K and 0-10ppm Th, and shows an overall decrease in average values from east to west across the transect.

Interpretation- A strong dispersal and overall linear trend can be attributed to higher levels of clay minerals within the depositional environment. Within damp and wet interdune environments, this is likely attributed to a rise in the water table, promoting more silt and mud rich sediments to proliferate in the interdune corridors, hence increasing the clay levels and the SGR signature (Cannon, 2015).

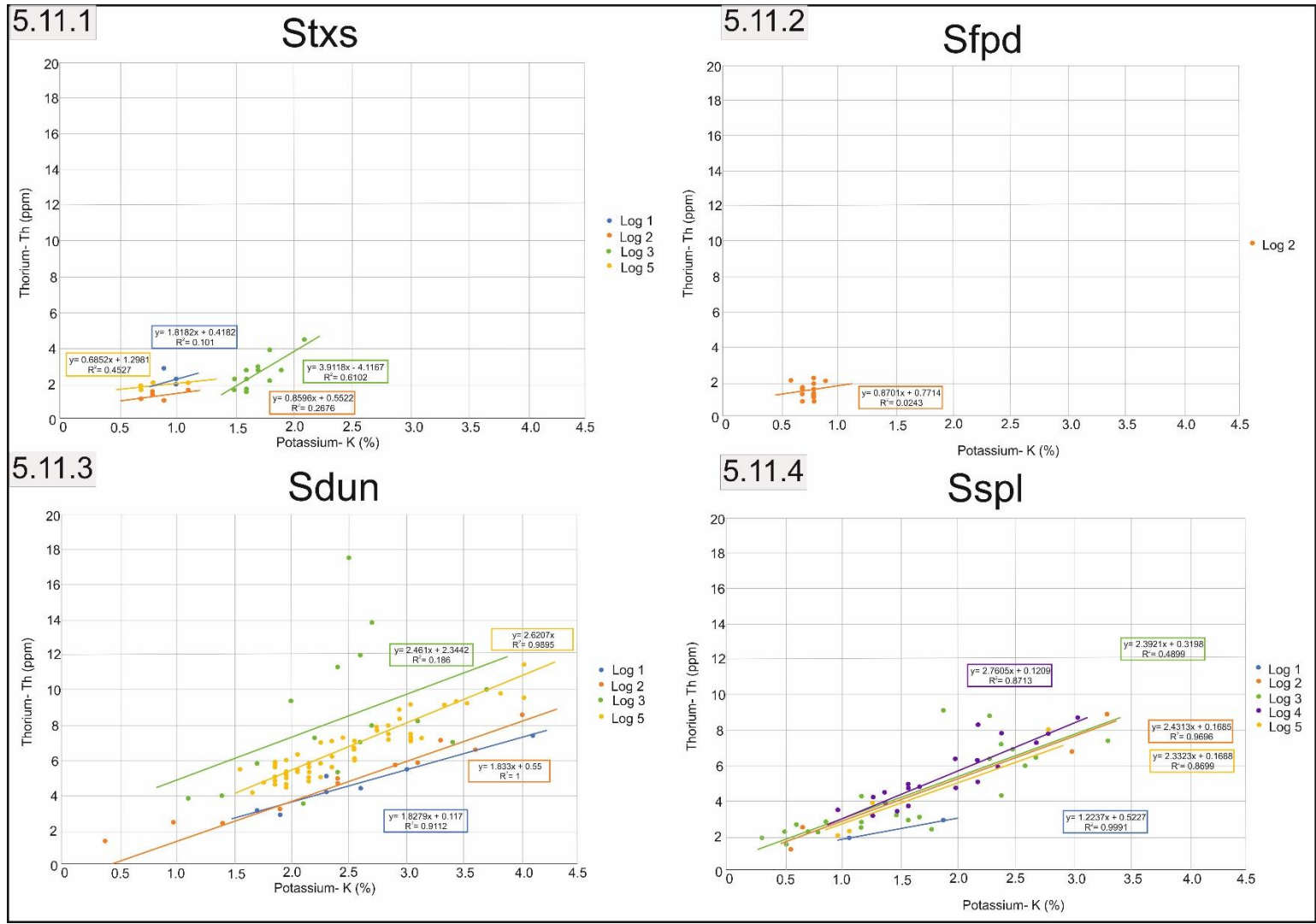


Figure 5.11.1- K:Th cross-plot for trough cross-bedded aeolian dunes, note the clustering in the lower left-hand corner. Figure 5.11.2- K:Th cross-plot for planar bedded aeolian dune facies. Figure 5.11.3- K:Th cross-plot for the undulose bedded sandstone facies, which has a more linear trend compared with the facies in 5.11.1. Figure 5.11.4- K:Th cross-plot for parallel laminated siltstones.

Coastal Dry Aeolian Dune Field

The K:Th cross-plots for this association show a distinct pattern of clusters, with relatively little variation in values across each locality, attributable to planar cross-bedded sandstones (Sxs) (Figure 5.12.1) and planar bedded sandstones (Sfpd) (Figure 5.11.2). Planar cross-stratified sandstone (Sxs) is the best example of this, data points for each locality cluster with the same pattern and within the same range (0-2%K and 0-4ppm Th). The clusters show a general narrowing and grouping of the data westward, such that localities 1 and 2 have the most dispersed data, whilst logs 3 and 4 have very tightly clustered values in the lowest left corner of the plot. The planar-bedded sandstone facies (Sfpd) exclusively occur at Locality 2, and therefore a trend similar to that shown within the cross-plot for cross-stratified sandstone (Sxs) could not be established. However, a clear cluster can be seen in the lower left of the plot between 0.5 and 1% K and between 0 and 2.5ppm Th.

Interpretation- The distinct grouping that becomes tighter westward and displays lower values is likely to be attributed to an extensive reworking of the sediment on the coast. The more the sediment was reworked, the lower the clay levels will be as it is likely to have been 'washed' away (Cannon, 2015). This could explain why the data are more dispersed for the cross-stratified sandstone (Sxs) at localities 1 and 2 (the most easterly) than the dataset from localities 3 and 4, contrary to what may be expected. Whilst the data from the planar bedded sandstones (Sfpd) cannot support this theory, due to it only being found at one locality, the low values that fall within the same range support deposition within the same environment as the cross-stratified sandstone (Sxs).

Palaeosols

Palaeosols such as ferrallitic gleysols (Fegl) and parallel laminated oxisols (Oxpl) can be found underlying the aeolian dunes within this association, whilst the restricted saline soil (Sasr) palaeosol can be found only at locality 2, Lone Mesa, overlying the preserved dune succession. Ferrallitic gleysols (Fegl) have widespread data points, comprising mid-range K values (1.5-3.0%) and mid-range Th values (4-6ppm). This trend is reflected in the saline soil facies (Sasr), however, there are not enough data points to conclusively establish a pattern. The data within the parallel laminated oxisol (Oxpl) has a similar linear trend, however, the data is much wider spread and covers a wider range, 0.8-4.3% k and 2-10ppm Th.

Interpretation- Palaeosols have a notoriously widespread distribution, meaning detail can often be lost in comparison with other facies. The thickness of palaeosol beds can greatly reduce the potential for data collection, for example, Sasr only occurs at one locality, within which it is 30cm thick, and hence only 2 data points can be collected. Whilst ferrallitic gleysols (Fegl) and parallel laminated oxisols (Oxpl) are thicker and occur at more localities, the nature of palaeosols mean the trend cannot be attributed to one specific depositional environment. However, it can be inferred that values higher and more varied than in other environments could be attributed to mineral enrichment during periods of exposure (Fertl *et al.* 1982, Ehrenberg & Svana, 2001).

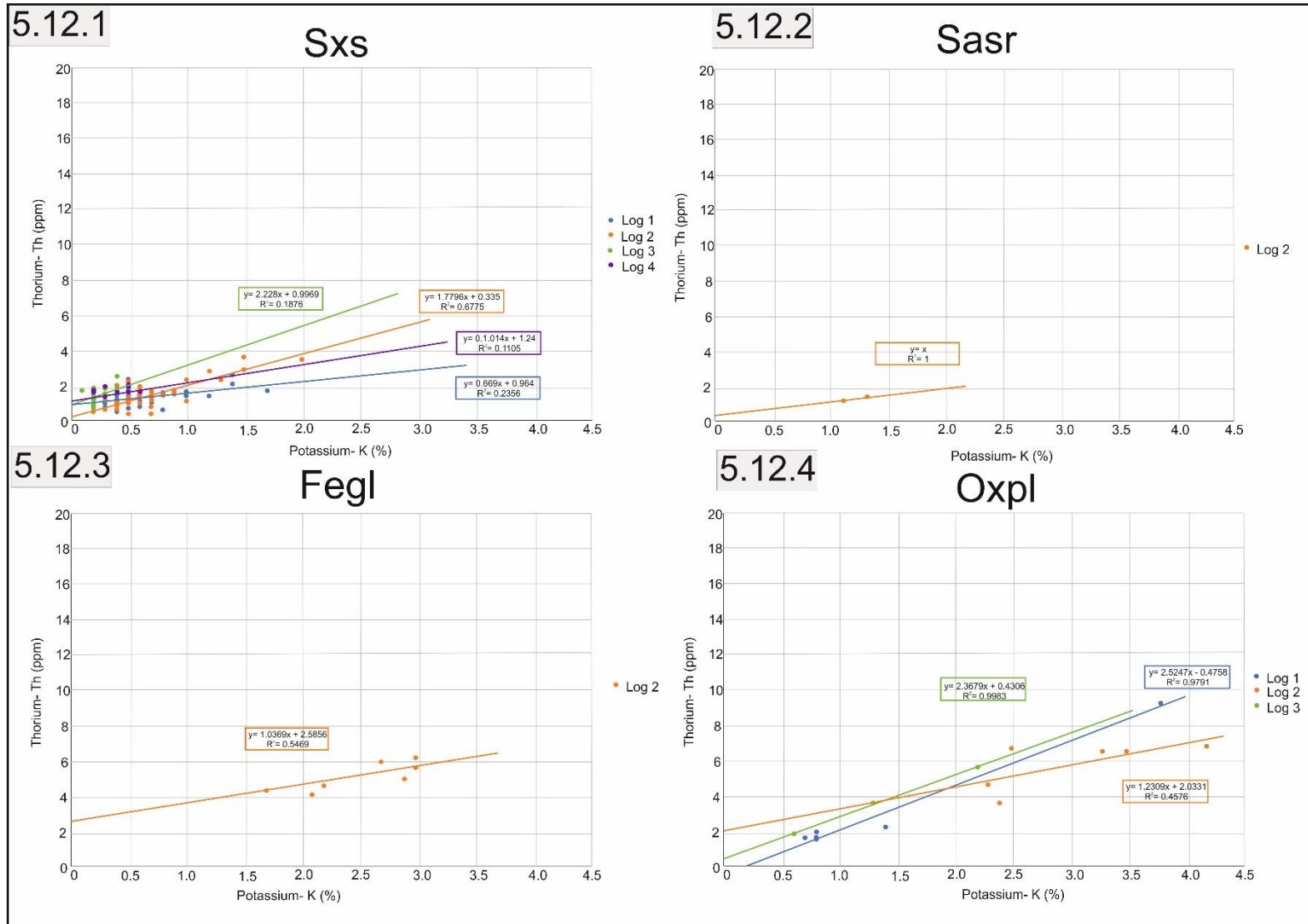


Figure 5.12- K:Th cross-plot for the planar cross-bedded sandstone facies with distinct clustering in the lower left-hand corner. Figure 5.12.2- K:Th cross-plot for the saline soil palaeosol facies. Any results gained from this graph is insignificant and should be discounted as there are only two data points. Figure 5.12.3- K:Th cross-plot for the ferrallitic gleysol palaeosol facies. Figure 5.12.4- Facies K:Th cross-plot for the parallel laminated oxisol facies.

Coastal Plain Facies Cross-plots

The main facies within this environment are parallel laminated silts and mudstones (Sspl), occasionally interbedded with discontinuous ripple facies, and even evaporites (Surpl & Ssepl). Mass sediment flows can be found in more westerly localities producing structureless sandstones with load casts (Scs). These facies have a characteristic strong linear trend with very high r^2 numbers (0.7 and above). The range of values varies but is generally spread across the lateral extent of the graph and occupying the lower half of the plot vertically. This is consistent across the transect, with little variation between the muds and silts in the east (Sspl) and their evaporite bearing counterpart (Ssepl), in the west. Non-newtonian flows produce structureless sandstones, occasionally with load clasts or rip-up clasts (Scs). The data points for these facies are spread over the majority of the plot, between 0.5-3.5% K and 1-8ppm Th, with strong linear trends and high r^2 values.

Interpretation- Each facies has a strong linear trend and fall within the same range, typical of silt/ clay-rich deposits. Sedimentologically the transition from the above supratidal flat into an intertidal mudflat is almost indistinguishable, and this is reflected within the spectral gamma-ray data. Supratidal flat deposits grade into intertidal mudflat deposits with proximity to the margin. Structureless sandstone units produce plots as expected from a sandstone deposit with a clay/mud influence, data points cluster in the middle of the plots, not displaying the low values demonstrated by pure sandstones, but also not the high values expected from pure mudstones.

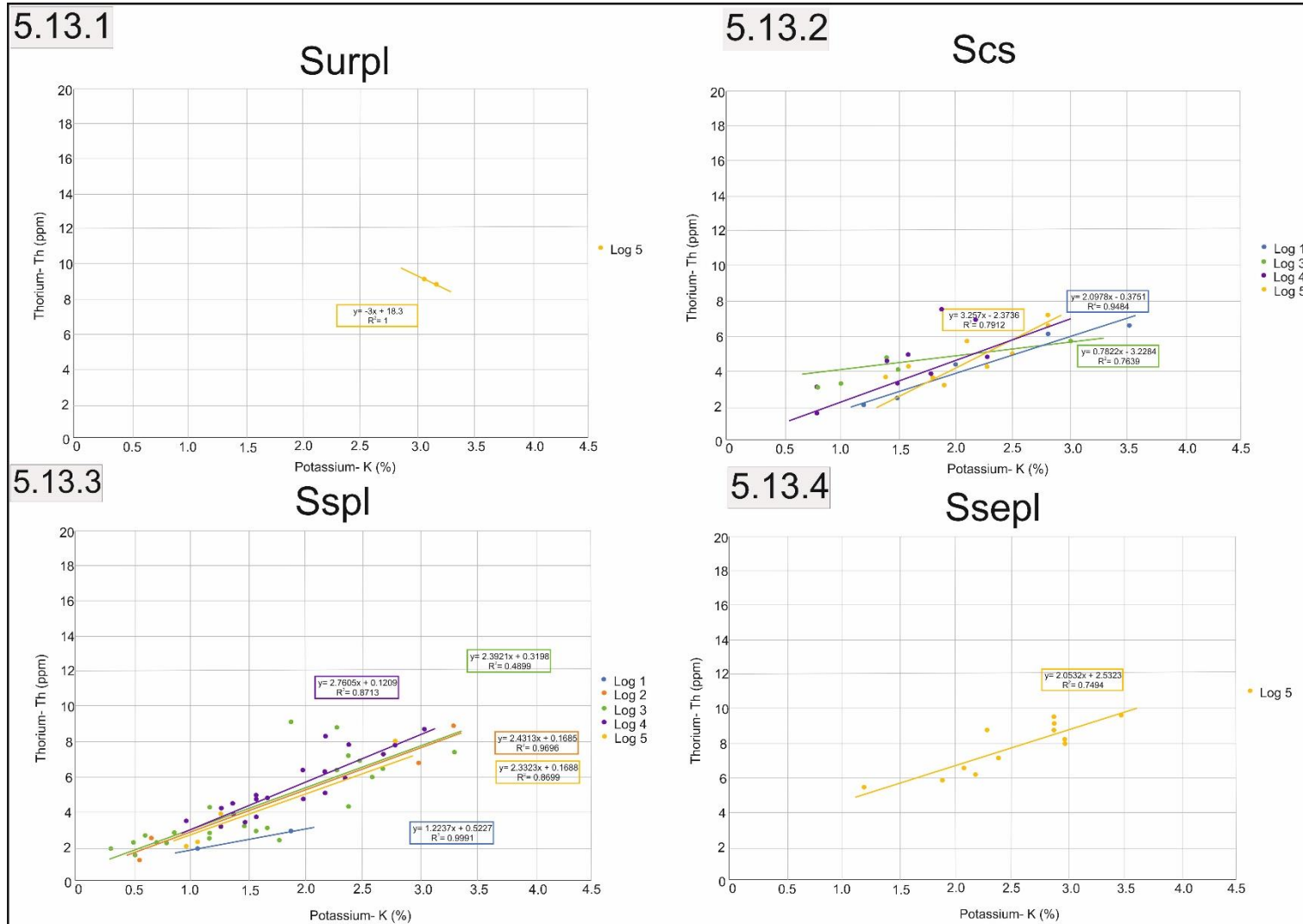


Figure 5.13.1- K:Th cross-plot for the undulose ripple laminated sandstone facies. Figure 5.13.2- K:Th cross-plot for the massive sandstone with load cast facies. Figure 5.13.3- K:Th cross-plot for parallel laminate siltstone (same diagram as 5.11.4, added here for comparison to similar coastal plain facies). Figure 5.13.4- K:Th cross-plot for the parallel laminated siltstone with evaporites facies.

Tidally Influenced Shoreface

Facies found within intertidal mixed flats, sand flats and sub-tidal mudflats represent those deposited sub-aqueously, or at the very least highly influenced by water levels. K:Th plots for facies within this environment are the most dispersed of any depositional environment previously discussed, they have an overall positive correlation, however, low r^2 values indicate high scatter. Data points are typically found within the mid and upper right-hand side of the graph, occupying ranges between 1.5-4.5% K and 4-16ppm Th.

Interpretation- The facies present within an intertidal sandflat are a mix of sub-aqueous and non-newtonian sandstones with occasional interbedding of very thin silt deposits. This is reflected by K:Th values clustered on the right-hand side of the plot (Figure 5.14), directly contrasting to the 'cleaner' aeolian sandstones. Sub-tidal flat facies (Ssgpl, Spl) have very similar, almost indistinguishable plots implying the same depositional environment. In contrast, the intertidal flat deposits (Srpl, Sxhc) have much higher dispersal and lower r^2 values (Figure 5.15).

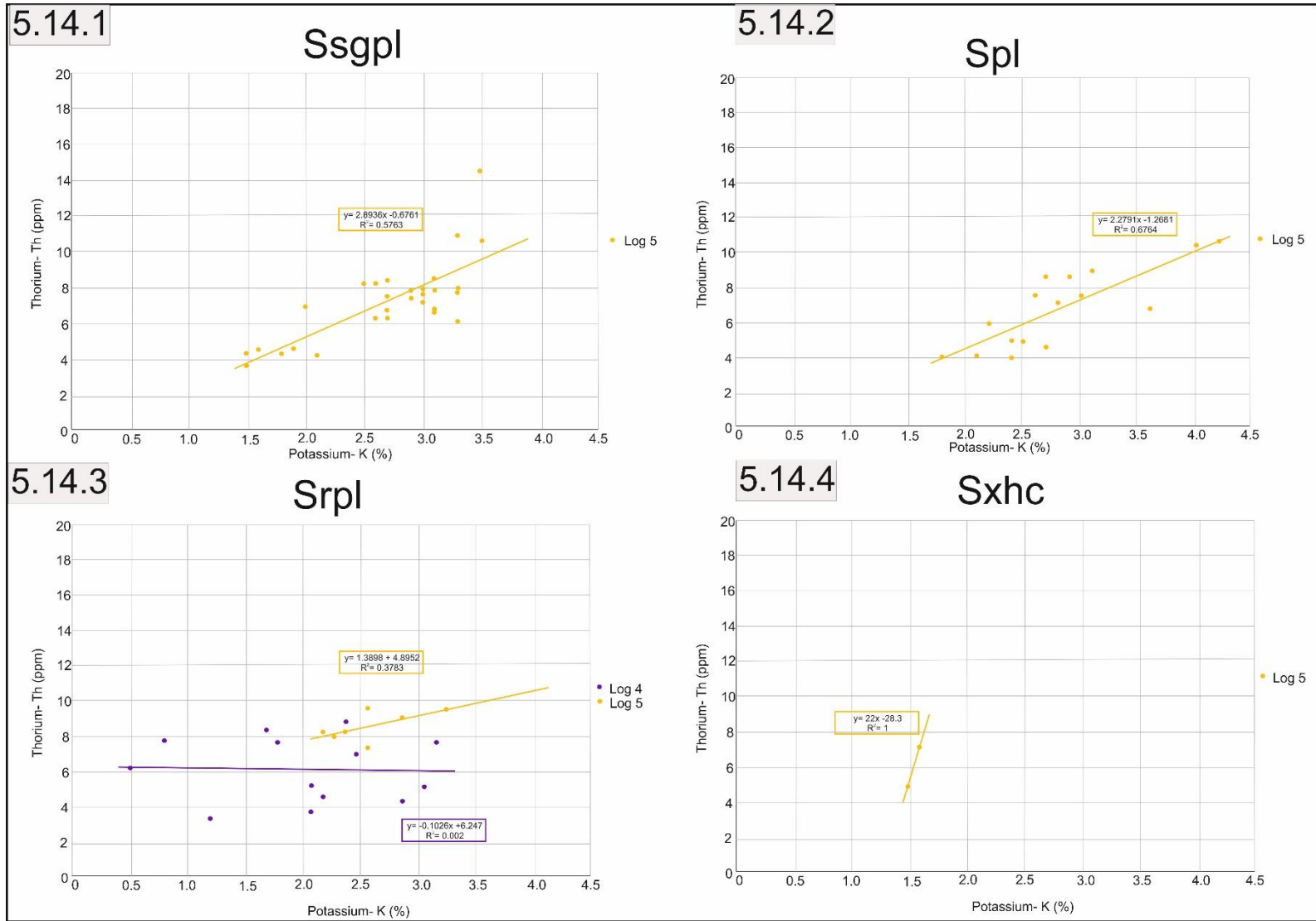


Figure 5.14.1- K:Th cross-plot for the inverse graded parallel laminated siltstone facies. Figure 5.14.2- K:Th cross-plot for the parallel laminated sandstone facies. Figure 5.14.3- K:Th cross-plot for the ripple laminated sandstone facies. Figure 5.14.4- K:Th cross-plot for the herringbone cross-stratified sandstone facies.

5.3.2 Interpretation

Facies cross-plot data shows a general trend both in terms of aqueous influence within the depositional environment and upon individual facies moving westward across the study area.

Environmental Trends Across the Margin

K:Th cross-plots for aeolian environments show a strong clustering in the lower left-hand corner associated with low potassium and thorium values. Within each of the facies typically associated with aeolian environments (Stxs, Sxs, Sfpd), the plot trends show a general increase in thorium combined with a relative decrease in potassium at each locality east to west across the study area. This tracks a trend moving to the left and upwards with the datasets from each locality. This shows a clear increase in the water level moving westwards and up succession as thorium is an insoluble isotope, whereas potassium is readily dissolved and transported sub-aqueously. Therefore, it can be inferred that the potassium isotopes within the aeolian facies were removed incrementally with proximity to the west of the study area in response to the proximity of the local water table. This trend can also be seen in mud and silt facies that display higher levels due to the clay component and follow the relatively high thorium trend compared with potassium moving east to west across the study area.

Those facies already deposited sub-aqueously do not follow this same trend but characteristically display high values and strongly linear trends. The variation east to west is predominantly represented by an increase in both potassium and thorium as expected from a marine setting in which there will be a greater percentage of detrital clay.

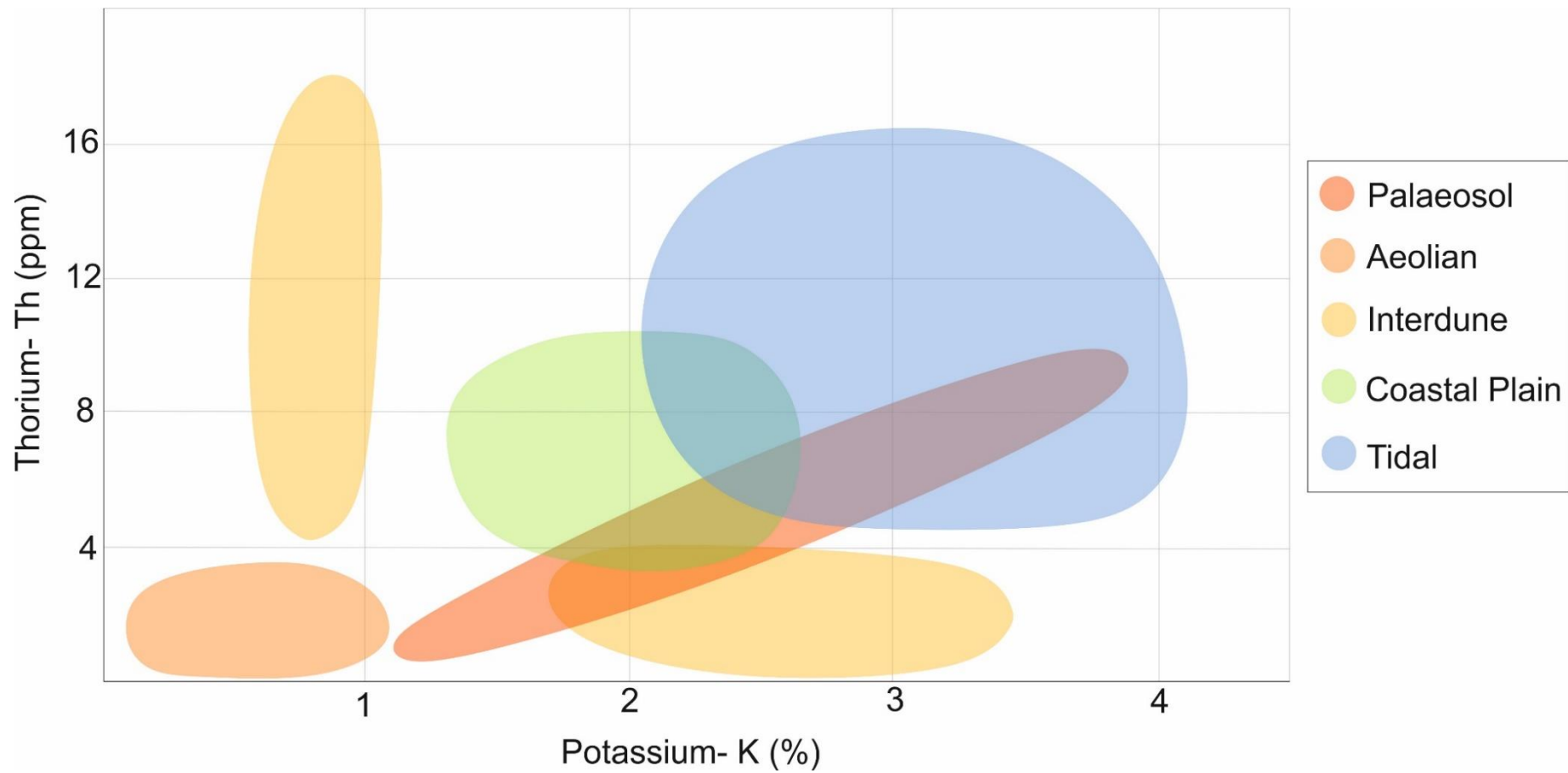


Figure 5.15- Clustering and trends of the broad scale depositional environments within a thorium-potassium cross-plot. Estimated areas have been obtained from the average values of potassium and thorium for each facies attributed to the depositional environment. Aeolian environments produce a distinct cluster in the lower left corner of the graph, interdune environments create two separate linear trends that could be explained by the difference in aqueous influence between damp and wet interdunes. The palaeosol facies occupies an incredibly linear are in the center of the graph. Coastal and tidal environments both create a cluster in the center of the graph spreading over a wide data range.

Box plots can be used as an additional statistical tool to compare the total gamma-ray counts for different depositional environments and show the variation east to west (Bristow & Williamson, 1998). As shown (Figure 5.16), a strong pattern emerges from the comparison of total gamma-ray values both across the transect and within each locality. Each plot shows the spread of data from the median, including the upper and lower quartiles and the minimum/maximum data points. To enhance the comparison, three different types of sandstones found within three different depositional environments were chosen, i.e., an aeolian dune sandstone (Sxs), a coastal plain sandstone (Scs) and a sub-aqueous sandstone (Srpl). The box plots demonstrate that aeolian sandstones have the lowest total count values across the localities, all with similar medians and spreads, albeit slightly decreasing towards the margin. This is in accordance with the hypothesis that towards the west, the aeolian sediments will be more influenced by water level, reworked to a greater degree, and, therefore, 'cleaner' with a lower total count value. Coastal plain sediments have the next highest average for total count values; however, the spread is much more varied, clearly demonstrating the higher level of irregularity within coastal plain successions. There is, however, a strong trend in decreasing total count number with proximity to the margin, this could be explained by a greater proportion of sand deposits compared with mud, leading again to 'cleaner' deposits with lower overall counts. Finally, the sub-aqueous sandstones have the highest total counts on average, with the median value consistently greater than the coastal plain and aeolian sandstones.

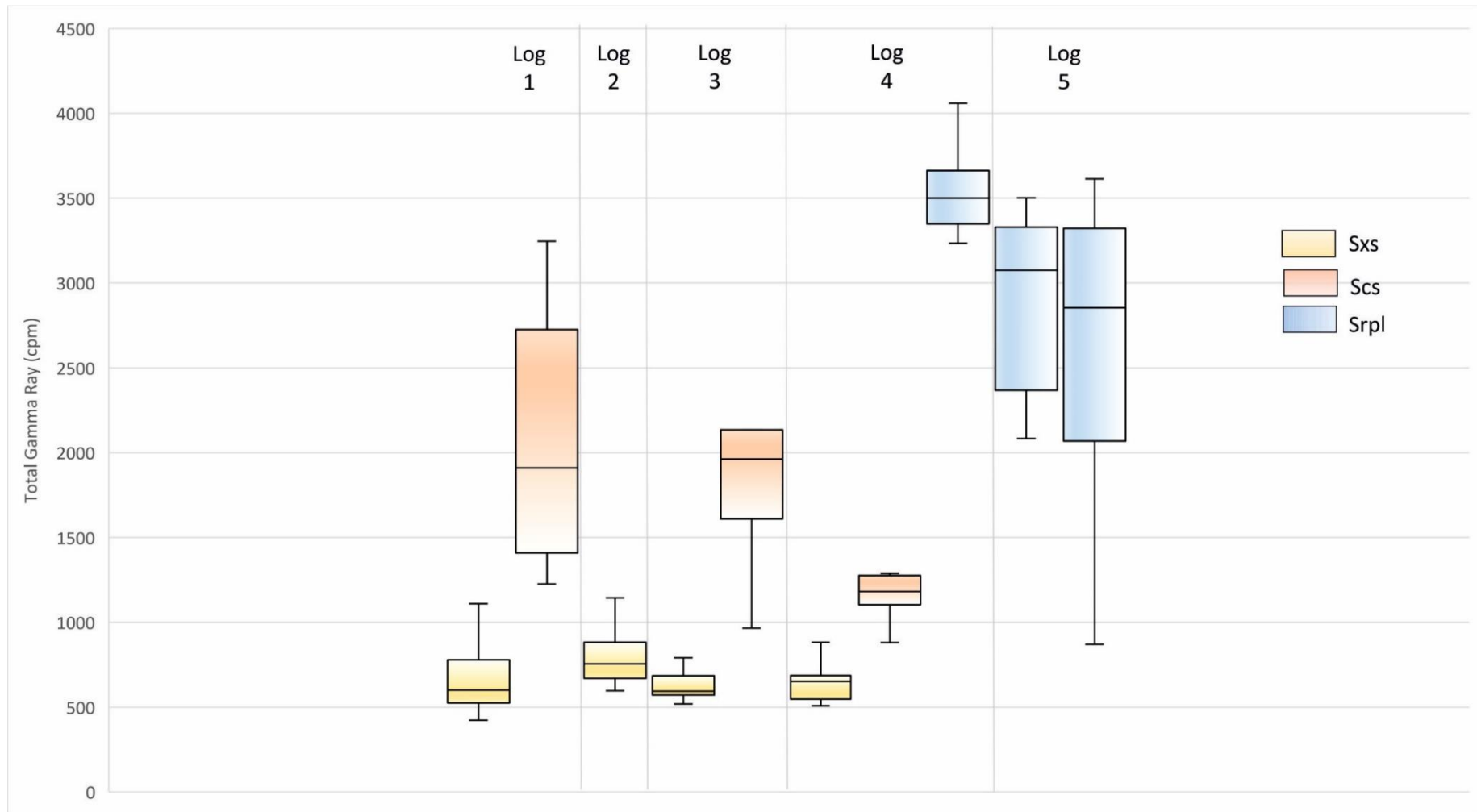


Figure 5.16- Comparative box plot showing the total gamma ray values at each locality for sandstones within different depositional environments i.e., cross-stratified aeolian sandstones (Sxs), coastal plain sandstones (Scs) and sub-aqueous/tidal sandstones (Srpl).

Statistical Trends

Due to the somewhat speculative aspect of facies analysis, attributing spectral gamma-ray data to predetermined facies can lead to some errors or misattributing data to the wrong facies. It is therefore important to consider the statistical significance of data for each facies. The facies have been grouped by depositional environment to determine whether a general trend can be applied to the K:Th plots for a specific kind of environment, and hence confirm that the data have been attributed to the correct facies and that the facies fits within their given depositional environment (Table 5:2).

	Facies	Mean X Values (average K(ppm))	Mean Y Values (average Th(ppm))	Coefficient of Correlation (r)	Coefficient of Determination (r ²)
Aeolian	Stxs	1.25	2.1	0.668	0.446
	Sxs	0.58	1.53	0.563	0.316
	Sfpd	0.78	1.45	0.156	0.024
Inter- dune	Sdun	2.55	6.64	0.387	0.150
	Sspl	0.98	3.21	0.978	0.957
Palaeosol	Fegl	2.43	5.10	0.730	0.547
	Oxpl	2.04	4.25	0.924	0.854
	Sasr	N/A	N/A	N/A	N/A
Coastal Plain	Scs	1.77	4.08	0.893	0.797
	Surpl	N/A	N/A	N/A	N/A
	Ssepl	2.53	7.72	0.866	0.749
Marine	Ssgpl	2.71	7.17	0.759	0.576
	Spl	2.81	6.58	0.822	0.676
	Srpl	2.17	6.51	0.814	0.662
	Sxhc	N/A	N/A	N/A	N/A

Table 5:2- Data for each facies, separated by depositional environment (note that one facies can apply to more than one environment). Mean x and y values represent the average of the datasets across all localities, these values were then applied to the formulas for the coefficients of correlation and determination to produce the r and r² values.

The coefficient of correlation shows the same trend in environment with respect to linearity vs clustering within the facies cross-plots. Aeolian gamma-facies have a relatively low r-value (0.1-0.6) associated with clustering trends. By contrast, marine gamma-facies have higher r values (0.7-0.8), indicating very linear regression. However, a somewhat unexpected outcome is that the highest r values result from coastal plain and palaeosol gamma-facies (0.7-0.9). This shows a very strong positive correlation and linear trend within the plot.

The observed trends are concurrent with low levels of potassium and thorium resulting from the lower level of the water table within aeolian environments. The lower r-value of marine sediments compared with coastal plain deposits, despite a greater aqueous influence and clay content, can be explained by muds often eroding first within tidal environments, hence the r value would reflect sand-dominant sediments instead.

It is important to note that facies displaying N/A in the table above do not indicate there is no correlation but instead reflect the poor distribution and accessibility of the facies themselves. Each facies only occur in one locality and are notably thin where they do occur. Due to the nature of spectral gamma-ray data collection, this means that only one or two data points can be obtained from each bed, leading to a restricted dataset that cannot provide reliable analysis. Furthermore, the count value of the bed and the surrounding material will inevitably impact the data obtained, i.e., if the bed itself has low counts but is surrounded by deposits with high counts, the results can skew.

The coefficient of determination shows how dependant the level of potassium is on the thorium level, i.e., how much can the level of thorium found in succession predict the amount of potassium there is. This analysis reveals an interesting trend

across the different depositional environments. The average r^2 values for aeolian gamma-facies are much lower (0.02-0.4) when compared with marine and coastal sediments (0.5-0.9). This implies that within an aeolian environment, the level of one isotope is not directly impacted by the other. Such that the isotopes accumulate and preserve independently. Whereas, in environments with a direct aqueous influence, either marine or subject to periodic flooding such as coastal plains, the level of thorium detected within the preserved sediment is linked to the level of preserved potassium detected.

5.3.3 Discussion

Facies cross-plots produced from gamma logs of each locality show a distinct trend attributable to a unique assemblage (Figure 5.16). Aeolian dune facies such as trough cross-stratified sandstone (Stxs), planar cross-stratified sandstone (Sxs) and planar bedded sandstone (Sfpd) cluster in the lower left-hand corner of the graph associated with low levels of potassium and thorium isotopes detectable by the handheld gamma-ray. It has been suggested previously that little useful information can be obtained within aeolian successions due to these exceptionally low values (North & Boering, 1999), however, this study has shown that within wet and coastal aeolian systems, the data is significant enough to provide key information about marginal interactions. Each of the facies (Stxs, Sxs and Sfpd) demonstrates a trend within the cluster whereby potassium level decreases with movement west across the study area, whereas the level of thorium increases. As thorium is a stable and insoluble isotope, it is likely that this trend is caused by the reworking of aeolian sediment by a nearby body of water, hence removing potassium in solution and leaving behind the more stable thorium isotopes.

Facies cross-plots are most used in coastal and marine sediments, these environments show a higher level of both thorium and potassium when compared with aeolian systems as there is a higher percentage of potassium bearing clays and muds. The east to west trend across the study area is less pronounced but still documents a decrease in potassium relative to an increase in thorium with distance westward.

Statistical significance has been used in this study to support the identification of facies and environments within the preserved succession at each locality. In subsurface studies, where lithofacies analysis is restricted, but gamma studies can be carried out via borehole, the trends displayed by the cross-plots can be a strong indicator of depositional environment. Such that clusters likely represent aeolian facies, dispersed with a moderate positive correlation may be marine and very strong linear positive correlation, coastal. However, this study only comments on those environments associated with an aeolian-marine coastal setting. Further study is needed to document the interactions and K: Th trends of other environments.

5.4 Peak Correlation

Collating data obtained from spectral-gamma ray analysis produces logs that show the total counts of the potassium [K], thorium [Th] and uranium [U] levels within the isotope and the ratios between them, namely Th/K, U/K and Th/U. When used in conjunction with sedimentary analysis, these logs are a powerful tool in determining facies, environments, time gaps, and relative trends to provide a quantitative analysis of otherwise qualitative datasets.

This study aims to understand the spatial and temporal variation across a transverse margin in an aeolian to coastal margin setting. One way this can be achieved is to correlate across the margin to establish the time equivalent deposits. When correlating sedimentary logs, a hinge line must be established that links deposition across the margin to one common time point. This provides a correlatable surface with which the spatial and temporal variation in facies can be identified. For the purposes of this study, the candidate datum lines will be determined using the Spectral Gamma Ray logs in conjunction with the sedimentary logs. Logs 1-4 represent a complete transect across the aeolian marine margin. For continuity and correlation, Log 5, taken 50km away at the San Rafael Swell, has been included, in addition to another intermediate log within Duma Point hereafter referred to as Log Z (from Zuchuat *et al.*, 2019).

5.4.1 Results

The most effective starting point in the correlation of logs across environments is the identification of significant stratigraphic surfaces (Miall, 1997). Once a reliable surface has been identified, shifts in environments in relative time up-succession can be established, allowing the studied deposits to ultimately be placed within a wider context. This study has correlated a time significant surface using Th/U

ratios that can be found at all localities attributed to the recognised surface, the J-3 (Zuchuat *et al.*, 2018, 2019). After this point, further peaks and surfaces have been established within the overlying aeolian and coastal plain successions using Th/K and U/K ratios in order to determine smaller-scale interactions in the marginal environment (Davies & Elliot 1994).

Sedimentary Log Correlation

Within the studied deposits, the most significant surface is represented by the erosive boundary between the planar-cross bedded sands and the underlying wet interdune deposits, previously identified as TS1 (Chapter 4). This surface is recognisable by an erosive surface, often with load casts, overlying a palaeosol. The hiatus represents a transition from a continental to a marine setting. Across the study area, the surface TS1 is related to aeolian deflation and erosion. However, in other regions not covered by this study, it is more readily affected by deformational processes (Zuchuat *et al.*, 2018). As is evident in sedimentological principles, these processes will not have occurred simultaneously and are affected by predominantly different allo-controls. Hence, correlating the logs across the basin based on the sedimentological expression of the J-3 is problematic, as it cannot provide a definite tie point with which to establish coeval depositional environments (Figure 5.17).

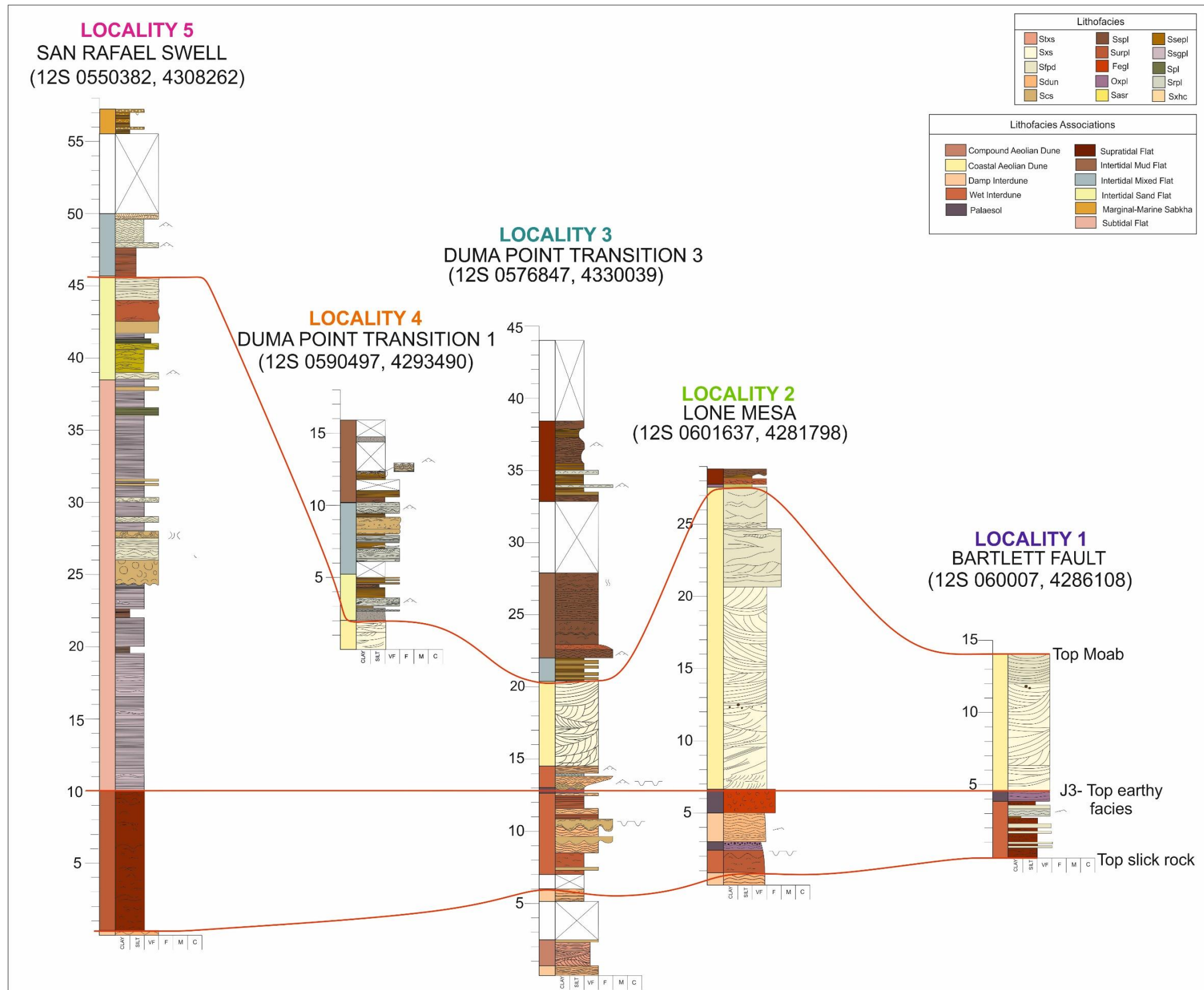


Figure 5.17- Log correlation across the West to East transect from the San Rafael Swell (Locality 5) to Bartlett Wash (Locality 1) based on the sedimentology alone.

Th/U Log Correlation

Initially, Th/U peaks were compared with the sedimentary logs to correlate across the margin and identify any other key surfaces within the succession. Five main peaks have been identified at each of the localities 1-5 corresponding with the five significant surfaces established within the photogrammetric analysis of each outcrop.

At locality 1, there are three significant peaks in the upper half of the succession, coinciding with the relative stratigraphic position of the index surfaces described in Chapter 4. These index surfaces by nature indicate outcrop scale bounding surfaces traceable between localities and often marked by rhizoliths or palaeosols. The initial peak corresponds with a peak in both thorium and uranium, implying a high level of isotopes within that region, attributed to an exposure surface, TS1, as described above. The second peak occurs further up the succession marked by TS2. In contrast to TS1, this surface can be identified by a depletion in uranium versus thorium, as uranium is a more soluble isotope than thorium this implies a 'wet' surface or the removal of uranium in response to a change in conditions. The third peak, TS3 corresponds with an aeolian bounding surface found only at Lone Mesa. The fourth identifiable Th/U peak represents TS4, the significant peak in uranium over thorium identifies it as an exposure surface, further documented by the presence of rhizoliths at this surface. The fifth and final peak represents TS5, the boundary between sandstone and silty coastal plain sediments. The occurrence of these five significant peaks in the Th/U log, concordant with the five index surfaces found at Bartlett Wash, implies two things; that these surfaces represent aeolian bounding surfaces representing changes in dune field conditions, and that bounding surfaces of this magnitude are detectable by spectral gamma-ray analysis.

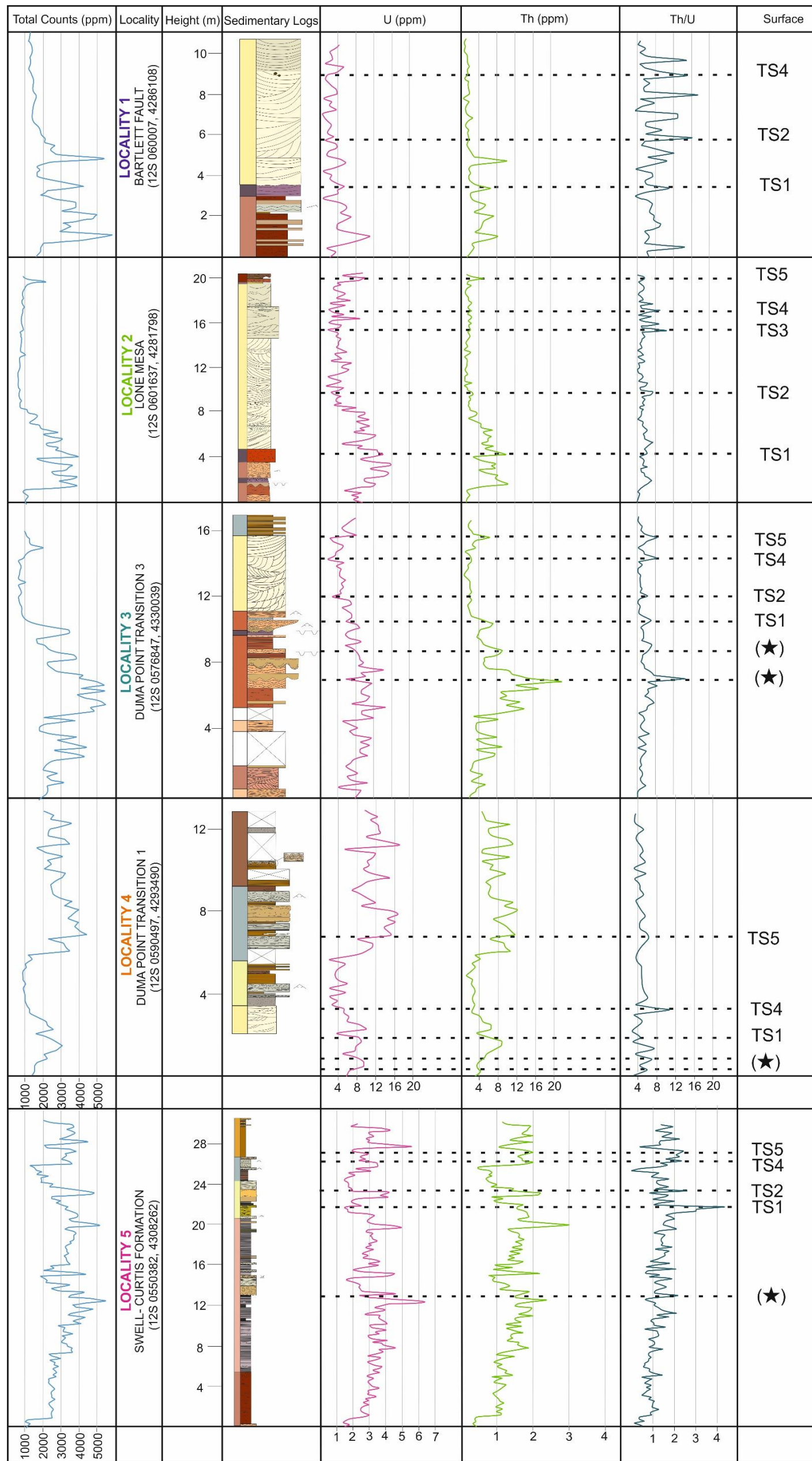


Figure 5.18-Thorium-Uranium logs separated by locality with individual bounding surfaces highlighted and annotated. Each surface has been identified by the relative proportions of thorium and uranium and compared with the relative position of bounding surfaces in the sedimentary logs, where a key surface is present but does not correlate with any surface previously identified by this study a (★) has been used.

Th/K Peak Correlation

Using the Th/K logs to augment the sedimentary logs, instead of using them in isolation, allows for the quantification of changes in environment. Th/K ratios are most used to identify types of sediments and sedimentary conditions and to determine the distance to palaeo shorelines (Fertl *et al.*, 1982). Within preserved successions, the relative leaching of potassium compared with the stable levels of thorium produces significant peaks indicative of sudden changes in climatic conditions or relative sea level. It is important to note that the actual levels of isotopes found within any aeolian units are very low, as is to be expected from sediments with relatively little detrital material, however when comparing the two values as a ratio, significant peaks arise.

At locality 1 (Bartlett Wash), the first significant peak occurs at the transition from wet interdune facies into aeolian dunes. Further significant peaks appear to correspond sedimentologically to bounding surfaces, highlighted by the annotated sedimentary logs. As in the thorium/uranium logs, the same significant peaks, corresponding with the aeolian bounding surfaces can be found in the preserved successions at localities 2, 3, and 4. In addition to the significant peaks observable at the bounding surfaces, there is an increase in smaller peaks within the succession. The 'noise' of the signal, i.e., how many peaks both small and large there are, increases westward to locality 4. The log with the most noise occurs at locality 5 (San Rafael Swell) however there are still notable peaks that can be picked out corresponding with changes in the environment as in the annotated simplified logs (Figure 5.20).

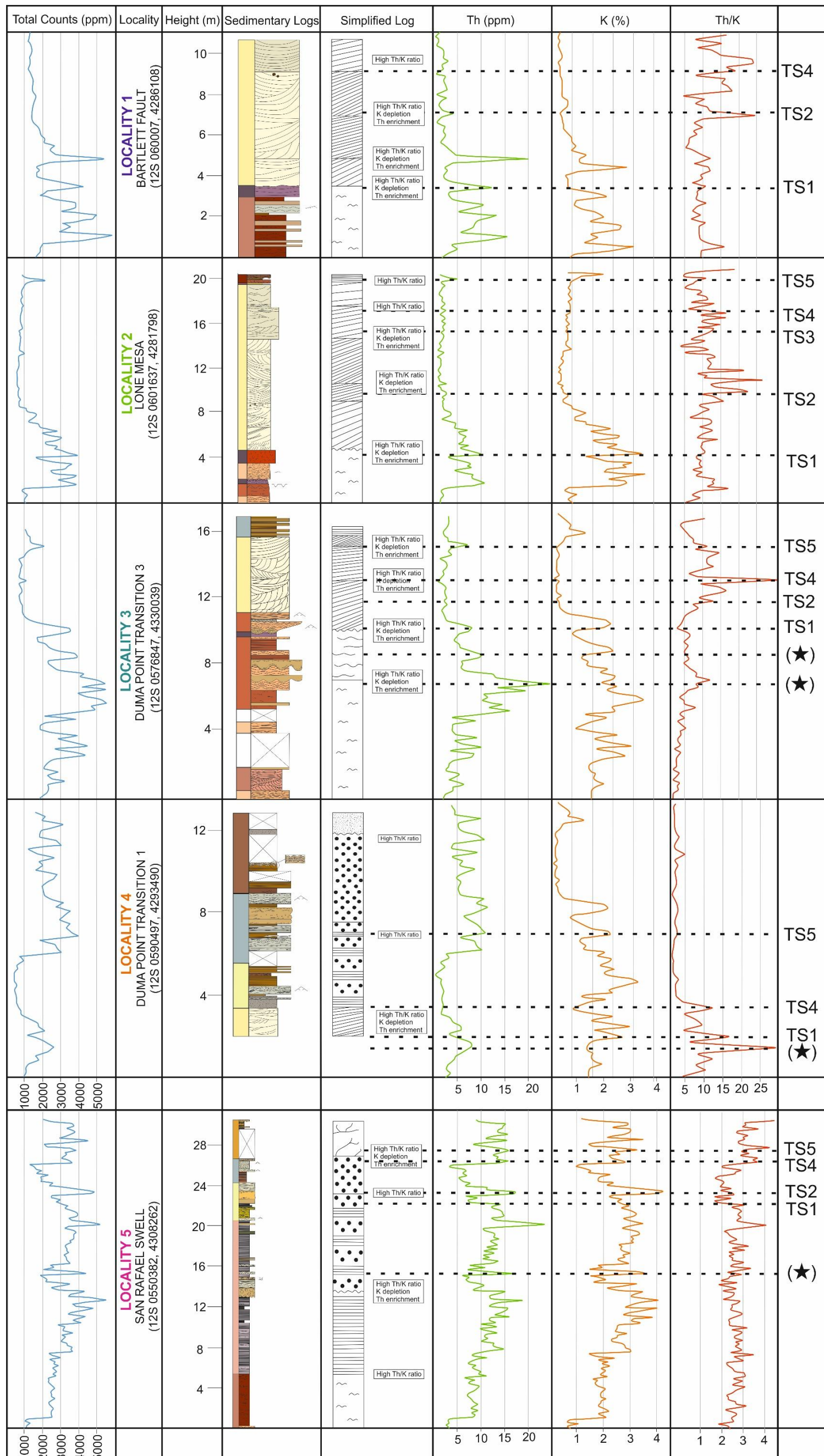


Figure 5.19- From left to right, the total counts logs, sedimentary logs, simplified and annotated sedimentary logs demonstrating the relative proportions of measured thorium levels in ppm and the measured potassium levels by % for each locality. Within the Th/K ratio surfaces have been identified corresponding to previously identified surfaces, where a peak has been identified that cannot be correlated but is of interest a (★) has been used.

U/K Peak Correlation

The ratio between uranium [U] and potassium [K] is most commonly used to identify discontinuities in the succession (Fertl *et al.*, 1982). As with Th/K ratios, the contrast between the build-up of uranium that occurs on exposed surfaces relative to the amount of potassium leached is a clear indicator of a time surface within a preserved succession. Similarly, to the Th/K ratios, the actual values of the isotopes are less significant as aeolian and coastal environments are less likely to have high levels of isotopes compared with marine environments (Martinius *et al.*, 2002). Instead, the ratio between the values is significant for understanding changes within the succession.

When comparing the U/K ratios east to west across the transect, a negative peak is the clearest indicator of a significant stratigraphic surface. This is due to the predisposition of both uranium and potassium to be removed or leached from surfaces, especially in areas where palaeosols develop (Hampson & Howell, 2005). At localities 1 to 5, TS1 is characterised by a significant drop in potassium, known to be associated with palaeosol development that can also be identified within the sedimentology. The presence of a positive peak towards the top of the succession is likely to be related to the 'wetting' surface identified in the Th/U peaks, associated with TS4. This peak could be caused by the movement of isotopes by interstitial fluids, or by the preferential removal of uranium in solution.

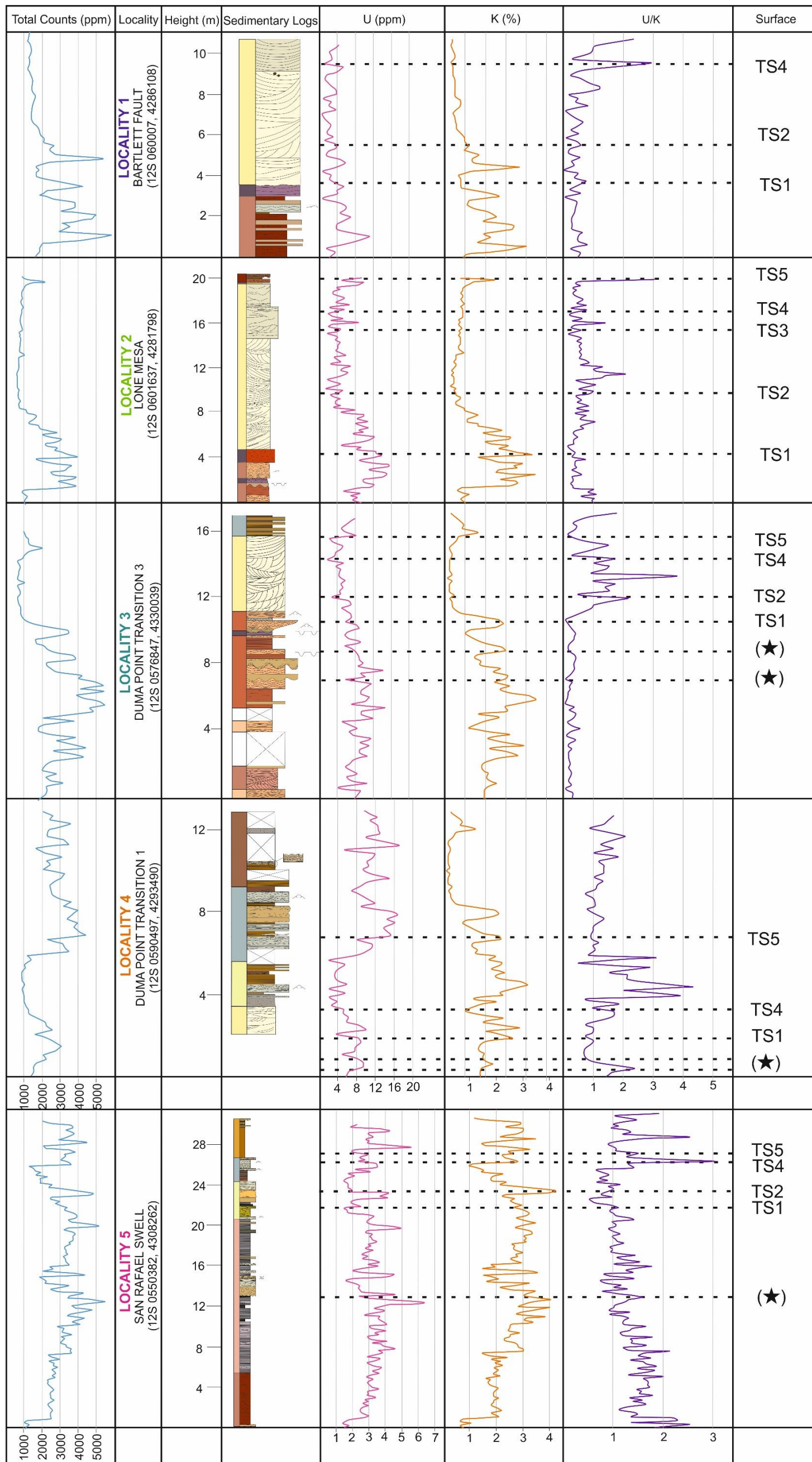


Figure 5.20- Uranium and Potassium logs separated by locality with individual bounding surfaces highlighted and annotated. Each surface has been identified by the relative proportions of uranium and potassium and compared with the relative position of bounding surfaces in the sedimentary logs, where a key surface is present but does not correlate with any surface previously identified by this study a (★) has been used.

5.4.2 Interpretation

Each of the isotope ratios, Th/U, Th/K and U/K support a transition from a wet aeolian environment to a dry aeolian environment, separated by a time significant surface. Sedimentologically, this is represented by a thin palaeosol implying a significant depositional hiatus where the surface was exposed for a considerable period of time. A peak in the Th/K log is conducive to this hypothesis, implying a flooding surface in which insoluble thorium accumulated whilst potassium was depleted by the transgression and subsequent regression of the water level. This peak is traceable, with increasing magnitude towards the west of the study area. This same peak is traceable within the U/K logs, increasing in magnitude and noise westward, implying greater proximity westward.

Smaller peaks in the Th/U log, occurring within the aeolian succession, most likely represent aeolian bounding surfaces linked to changes within the aeolian system. Combining these peaks with preserved sedimentological evidence such as rhizoliths indicates that these surfaces occurred as a result of localised dune stabilisation, exposing the surface for a substantial period of time within which uranium accumulated creating the peaks. These peaks are visible within both the aeolian and marine successions indicating that the controlling factors on fluctuations within the dune field also impacted the depositional environments of the marine setting causing relative peaks in thorium and uranium levels at these points.

5.4.3 Discussion

Initially, an attempt at correlation was made, based on sedimentology alone. For this method to be accurate, the assumption must be made that the surface is isochronous, and sedimentation occurred almost instantly at all points. This is

discordant with the field observations of a palaeosol in the proximal realm cut by an erosive boundary that extends across the transect, which is diachronous by nature. To eliminate any question of statistical significance and establish a hinge line that is reliable to a fair degree, this study has investigated using Th/U, Th/K and U/K ratios, in line with previously discussed methods of establishing discontinuities within preserved successions (Hampson *et al.*, 2005, Klaja & Dudek, 2016) (Figure 5.21).

Using the Th/K logs was most useful in establishing large-scale chronostratigraphic surfaces. At each of the significant sequence boundaries, a significant depletion in K corresponds with a relative peak in Th. Although the sizes of these peaks varied, the pattern of Th enrichment vs K depletion persisted and is highlighted in the annotated simplified sedimentary logs (Figure 5.19). The same trend was easily detectable in the U/K ratios, tracing a significant surface east to west across the study area. At this point, a significant peak, corresponding to the relative enrichment of uranium versus the depletion of potassium, is a clear indicator of a time surface, especially within a succession that has low total counts readings at this point.

In identifying smaller scale surfaces, the Th/U ratio proved the most useful, highlighting several significant peaks within the succession corresponding to the approximate stratigraphic position of the index surfaces TS1-TS5 identified previously (Chapter 4). At localities 3, 4 and 5, significant peaks have been identified and marked with (★) to represent events that are of note but appear to have no detectable sedimentological expression. The surface TS1 occurs at every locality and is traceable within aeolian, coastal and marine sediments.

Th/U peaks can be used to determine basic discontinuities; in this case, the Th/U peaks and the palaeosol/erosive surface present at this point in the preserved successions can be attributed to the J3, a regional surface attributed with the transgression of the Curtis Sea into the study area. The smaller scale peaks represent changes in the aeolian succession. Establishing whether these peaks can be found in other environments will identify whether the changes were brought about by autocyclic fluctuations in the dune field or allocyclic changes in sea level affecting the whole system. This study found 4 additional significant peaks within the marine succession preserved at the San Rafael Swell correlatable with the 4 aeolian bounding surfaces above the one attributable to the J-3 at localities 1-4. Although these peaks cannot give an idea of the exact time scale implied by the increase in uranium vs. thorium it does imply that the cause of the enrichment occurred at every locality across the transect. This, therefore, implies that the controlling factors on the fluctuations of the dune field, preserving the unique pattern of five genetic packages separated by five index surfaces was allocyclic and impacted the margin, although the sedimentological preservation of this within the marine setting has been overwritten by autocyclic tidal resonance.

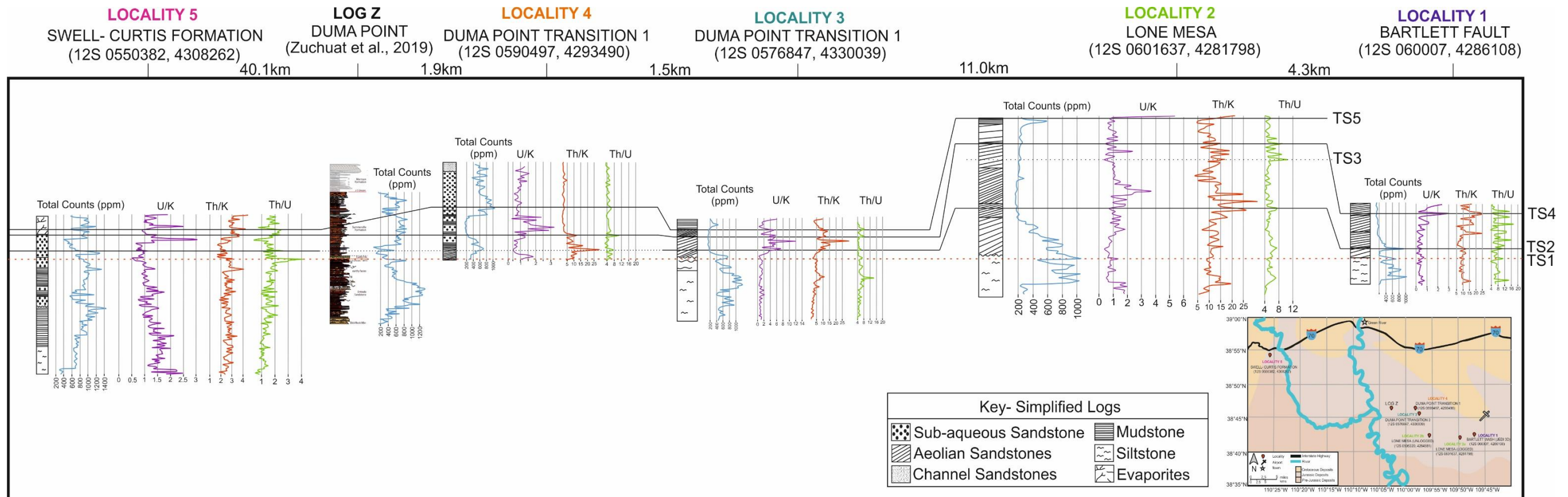


Figure 5.21- Correlation of the surfaces TS1, TS2, TS3, TS4 and TS5 east to west across the study area, starting with Locality 1- Bartlett Wash in the East and ending with Locality 5- San Rafael Swell in the west. The relative distances in km have been shown between each of the localities in addition to their position on a map of the study area (bottom right-hand corner). For ease of correlation simplified sedimentary logs have been used as opposed to the detailed logs found in figures 5.17, 5.18, 5.19 & 5.20.

5.5 Log Motifs

One additional characteristic obtained from the gamma-ray data is the shift in environments relative to transgressive and regressive systems. Patterns in the logs can be used to identify basic cyclicity within the succession. To identify motifs within the total count data, the values obtained in parts per million (ppm) have been chosen over the values for counts per minute (CPM), as it represents more accurately represents the radioisotopes produced (Figure 5.22).

5.5.1 Results

At each locality, the total counts log has been described by general trends in the shape of the curve, i.e., log motifs. Descriptions follow the three general shapes of log motifs that are present in datasets, bell, cylinder, and funnel. Each of these distinct shapes combined with the serration or 'noise' of the curve can provide an indicator of stacking pattern and hence the movement of the sea level relative to the deposition of the sediments.

At locality 1, the log motif can be split into two key patterns, a serrated funnel shape at the bottom with a sudden change to a smooth cylinder at the relative position of the change in sedimentology from damp deposits such as interdune and palaeosol to the drier aeolian deposits. This pattern continues at localities 2 and 3 with a serrated funnel followed by a smooth cylinder motif (Figure 5.18). At locality 3 the addition of an initial smooth cylindrical motif corresponds with the aeolian dune facies found at the base of the succession. At locality 4, where the succession begins from aeolian deposits and extends into coastal plain deposits the reverse pattern can be observed, an initial smooth cylinder with an abrupt change into a serrated funnel shape. Locality 5 involves a wider array of log motifs representing more frequent changes in environment. Initially, the motif displays a

smooth cylindrical trend, which rapidly moves into two cycles of serrated bell-shaped motifs and serrated funnel motifs. After another abrupt change, the shape of the logs returns to smooth cylindrical (Figure 5.18).

5.5.2 Interpretation

Log motif trends within the total counts logs can identify shifts in depositional environment and transgressive or regressive relationships. Localities 1,2, 3 and 4 all display similar log motifs, documenting an aggrading system characterised by a serrate cylinder motif, followed by progradation represented by a serrate funnel shape. A final stage of aggradation is marked by a smooth cylinder motif with a slightly concave morphology. This is indicative of aeolian environments (Martinius *et al.*, 2002). At locality 5, there are four separate stages within the succession, firstly an aggrading system that corresponds with the undulose mudstone. As the environment transitions into a sub-tidal flat, the motif documents retrogradation consistent with the flooding of loess dunes by a shallow marine environment. Following this, there is evidence of a subsequent regression. A further transgressive-regressive event demonstrated by the funnel and bell-shaped log motifs can be found within the intertidal sand flat deposits coeval with the aeolian dune T-R event at localities 1,2,3 and 4. The final motif at locality 5 is an aggrading sequence, starting at the transition between the intertidal mixed flat and the overlying deposits and continuing through the marginal marine sabkha.

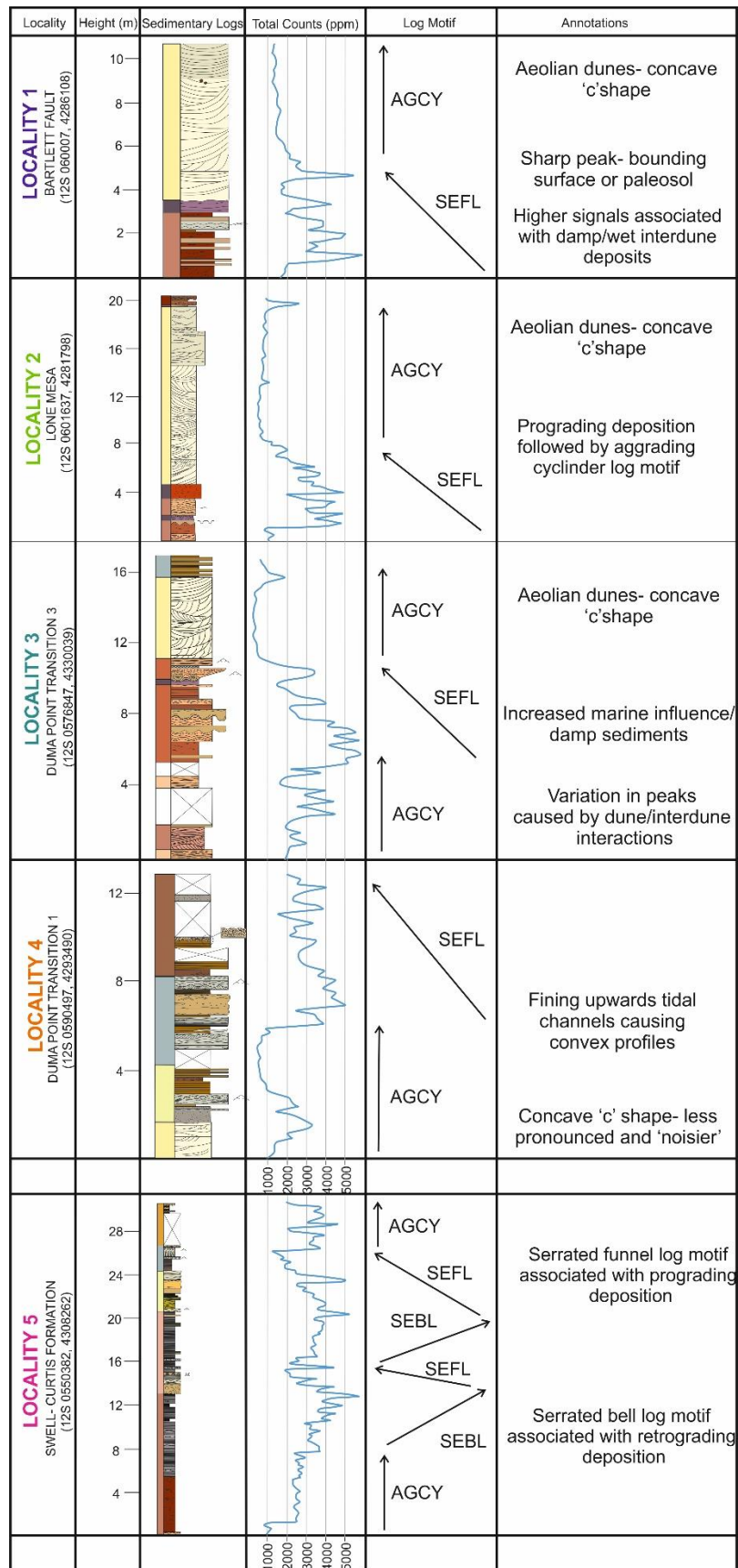


Figure 5.22- Log motifs and annotations for the total count logs, at each locality in parts per million. These logs are correlated with their respective sedimentary logs to emphasise any trends in depositional environment. AGCY- Aggrading cylinder motif, SEFL- serrated funnel motif, SEBL- serrated bell motif.

5.5.3 Discussion

The pattern of log motif trends at each locality upwards through aeolian, coastal and tidal deposits can document changes in relative sea level at the time of deposition. The correlation of these patterns across the margin can also provide the over-arching story of sea-level fluctuations upon the margin and the consequences this had for the depositional environments.

At the most easterly localities Bartlett Wash (locality 1) and Lone Mesa (locality 2), the succession is split up into two main trends, a serrated funnel indicative of prograding deposits and a cylinder motif implying aggrading sediments. From the base of the succession, it can therefore be established that there was an initial relative sea-level fall throughout the deposition of the Entrada earthy facies that reached a maximum at the boundary between the Entrada Formation and the overlying Moab Member sandstones. After this maximum, throughout the deposition of the aeolian sediments, there was little change in grain size and no significant change in sea level at those localities. This same pattern can be found at Duma Point Transition 3 (Locality 3), the same relative sea-level fall can be seen in the Entrada earthy facies until it reaches a maximum point after which the cylindrical motif prevails and the relative sea-level becomes stable for the duration of deposition of the aeolian sediments. At this locality, the same smooth cylindrical pattern can be identified in the deposits of the Entrada slick rock, again indicating little change in relative sea level throughout the deposition of these dunes.

The trends visible at Duma Point Transition 1 (Locality 4) begin from the base of the Moab member as the underlying sediments were inaccessible at this locality. The aeolian deposits show the same motif trend as at localities 1-3. Notably, the serrated funnel morphology of the overlying coastal plain sediments implies that

regression continued after the deactivation of the dune field, corresponding with the growth of the dune field at the marine margin.

There are a number of additional transgressive-regressive patterns that can be identified at the San Rafael Swell that are not visible within the successions preserved at the other localities. There may be several reasons for this, firstly the trends in log motifs are strongly influenced by changes in grainsize, which are more likely to occur in a tidal, shallow marine shoreface depositional environment than within an aeolian succession. Secondly, the basin at the time of deposition of the lower, middle, and upper Curtis units was of the right dimensions for tidal resonance, causing the overprinting of the sea-level variations identified in the log motifs at more proximal localities by smaller-scale sea-level fluctuations. In order to correlate the trends observed at Locality 5 with the other localities, further methods should be incorporated to identify a time-significant surface and determine the changes in sea level around that point.

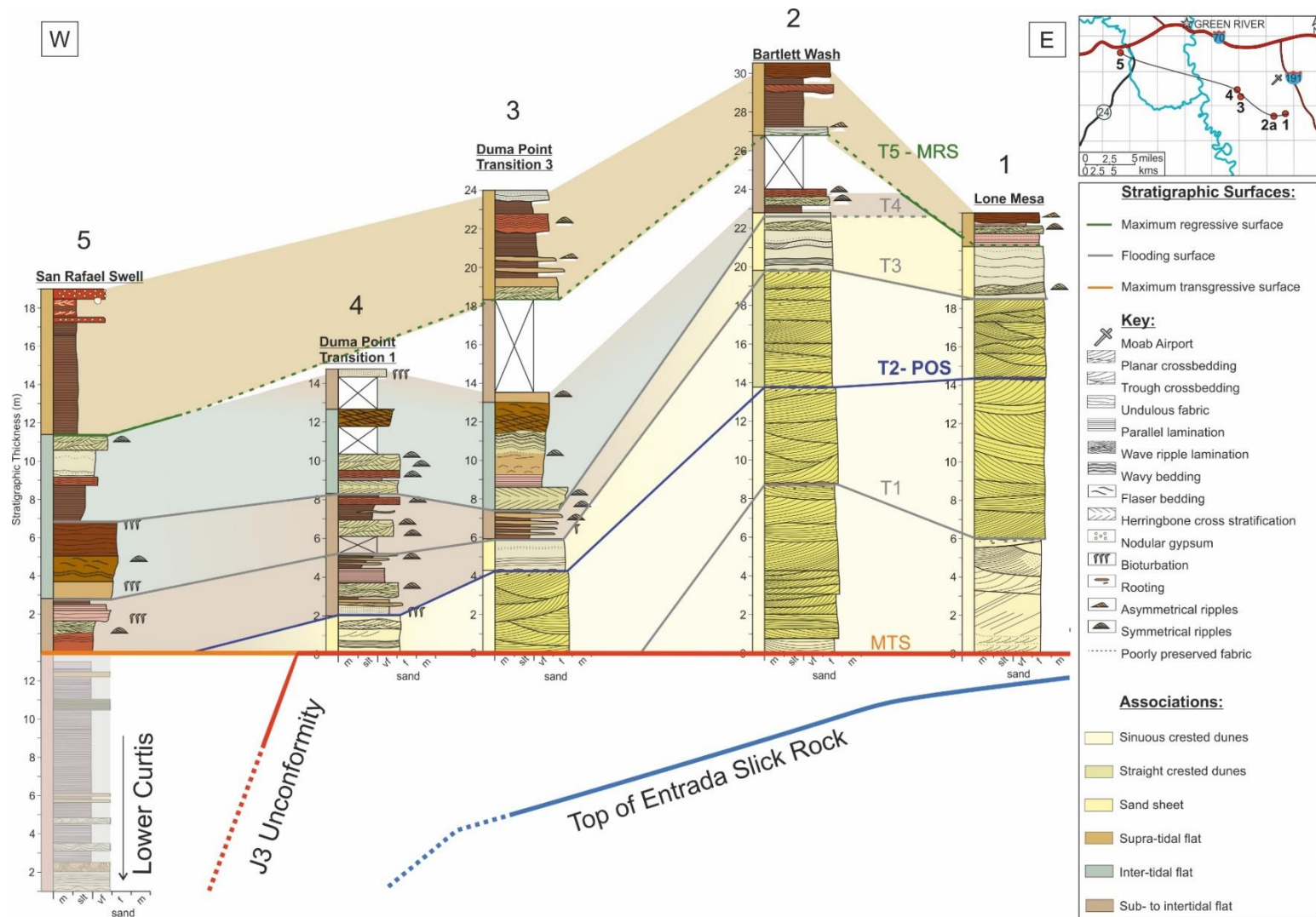


Figure 5.23- W-E correlated panel from the tide-dominated shallow-marine margin at 5: San Rafael Swell to the aeolian dune successions at 1: Bartlett Wash. The logs have been coloured by facies; correlation has been made by association. Sedimentary structures of note are shown on the right-hand side of each log. Where outcrops were inaccessible, the depth has been estimated and marked with a cross.

5.6 Summary

A total of five spectral gamma-ray logs were obtained from data collected at five localities spanning an east to west transect of the Curtis/Summerville transition, Southeast Utah. This work has used spectral gamma-ray data combined with statistical tests in a variety of ways to produce a significant description of the facies found within an aeolian/marine marginal setting.

Initial analysis of K:Th cross-plots identified that whilst it is difficult to isolate individual facies at each locality, due to a high level of overlap and widespread datasets, by looking at the facies individually, key trends can be picked out. It was shown that each facies had a unique trend that could also be linked to a specific depositional environment, i.e., aeolian sediments displayed low values with strong clustering, whereas sub-aqueous facies displayed a more linear trend with a wider dispersion.

To overcome this largely speculative gamma-ray facies identification, a number of statistical tests were carried out to confirm the presence of a relationship and ensure each facies has been attributed to the right dataset and depositional environment, respectively. These include: 1) Pearson's coefficient of correlation, used to establish linearity in the data, 2) the coefficient of determination, the square of the former, used to determine the error in the data and 3) box plots, to highlight the contrasts between the data from each distinct depositional environment.

In addition, correlation of the deposits across the transect was attempted using sedimentary logs alone, however, this was unsuccessful as the J-3 surface is characteristically diachronous and hence cannot be reliably correlated across the margin. Spectral gamma-ray logs were then used in conjunction with the

sedimentary logs to identify a correlatable tie point. The most suitable candidate for this was a significant peak in the Th/K ratio and Th/U ratio across the margin. A peak in these logs is significant as a flooding event was likely to have deposited a large number of isotopes such as potassium and uranium, leading to a spike in the total counts. However, as regression occurred, more water-soluble isotopes would have been removed, leading to a peak in the Th/K ratio. Using the same principle, bounding surfaces within aeolian successions can be identified. This uses significant peaks in the Th/U ratio log as aeolian supersurfaces arise from periods of non-deposition, flooding, or deflation, leaving behind increased uranium levels compared with thorium and hence a peak.

Chapter 6: Application of Spectral Gamma-Ray upon Aeolian-Marine Margins

This chapter will combine all the previous sedimentological and geophysical analysis to describe the interactions upon an aeolian/marine margin at small-scale i.e., the local fluctuations of the dune field and the neighbouring coastal plain, and at a bigger scale i.e., how changes in relative sea-level impacted deposition along the margin. Using a correlated time significant surface from the Th/U, Th/K and U/K log trends will provide a hinge-line from which the evolution of the dune field and coastal plain deposits respectively can be determined and represented as a series of 3D models.

Combining the facies analysis, quantification of changes in the dune field with proximity to the margin and the identified trends in logs obtained from the SGR data will provide an overall view of local changes in an aeolian dune field in response to sea-level fluctuations. As a final step, the small and large scale interactions upon the margin and the respective changes in sea-level fluctuations in the Jurassic can also be linked to cyclicity and the possible influence of Milankovitch cycles on the deposition and preservation of the aeolian/marine margin.

6.1 Interpretation

Combining all the information from facies analysis, gamma-facies, gamma log motifs and finally, the established changes in the dune field, 2D and 3D palaeogeographic reconstructions can be created that document the interaction between coastal environments and arid aeolian ones.

6.1.1 Reconstructing the Aeolian-Marine Margin

Using the established J-3 hinge line, time points were chosen that display the environment at the time of deposition (Figure 5.18). To document the complex interaction between aeolian and coastal environments, six key time slices have been chosen, including the time of the J-3, labelled T1, T2, T3, T4, T5 and T6 (Figure 6.2).

At T1, the transect is dominated by a coastal wet aeolian dune field that corresponds to the preserved deposits of the Entrada slick rock sandstone and earthy facies. At this time, the Curtis Sea is transgressing following an incursion of the Sundance Sea from the north. This gradual wetting of the environment can be picked up in the log trends of the spectral gamma-ray peaks, which curve with a convex pattern upwards from the base of the logs to the boundary of T1 (Figure 5.18). This overall pattern is also punctuated by smaller peaks dictating small sea-level changes indicating smaller 4th order sequences within the overall Transgressive-Regressive sequence of the Entrada/Curtis/Summerville succession. T2 marks the point of major transgression, at which point all localities within the transect show a dramatic change in environment, picked up within the spectral gamma-ray logs as a spike in all isotopes at this point and the correspondent Th/U peak representing a discontinuity (Figure 5.20). At Locality 5, the most westerly point of the study area, this flooding event marks the boundary

between the Lower Curtis and Middle Curtis deposits. Moving eastward, the rise in sea level is marked by increasingly damp sediments, damp palaeosols with increased mineral content and soft-sediment deformation. As the Curtis Sea began to regress, it enabled sediment re-working into the Moab Member dunes. Initial sediment was heavily re-worked by the Curtis Sea regression leading to 'clean' material, i.e., that with low clay content, as shown by the facies cross-plot for Sxs (Chapter 5 Figure 5.13). As the sea regressed to the point of T3, the dune field extended to its greatest reach, depositing small dunes at Locality 4, the westernmost extent of the Moab Member. The same dunes are not found at Duma Point and are instead replaced with the coastal plain deposits of the Summerville, which occur coevally to the tidal channels of the Upper Curtis and the shallow marine/littoral sands of the Middle Curtis. As the Curtis Sea continued to regress towards T4, several smaller-scale sea-level fluctuations can be picked up within the aeolian sediments corresponding to the supersurfaces between dune packages that feature higher levels of uranium and thorium vs potassium within the SGR logs. Continued sea-level fall to T5 and both the landward and seaward extension of the coastal plain environment shut off the sediment supply and initiated the shutdown of the Moab Member dune field. This led to the aeolian sediments at the localities where the dune field remained, i.e., localities 1 & 2, being less re-worked by the tidal marine waters and having higher levels of potassium and thorium, hence plotting higher within the facies cross-plots (Chapter 5). T6 marks the complete take-over of the Summerville Formation supra-tidal and intertidal mudflat deposits. In the areas previously dominated by shallow marine shoreface deposits, remaining moisture within the soil promoted small evaporite pools within which gypsum deposits of the marginal marine sabkha were deposited.

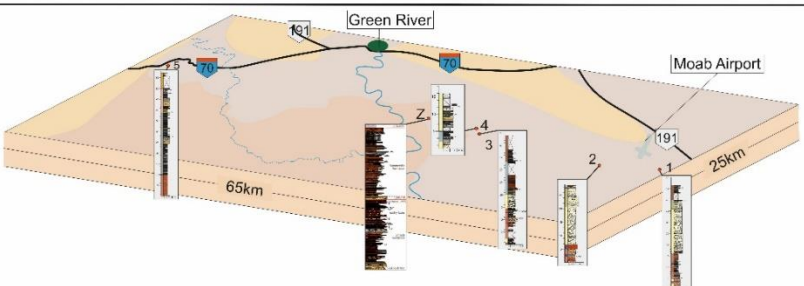
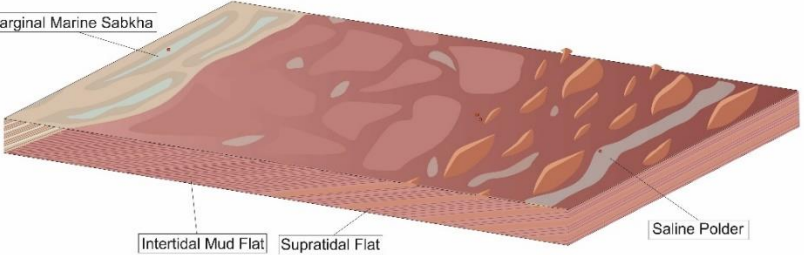
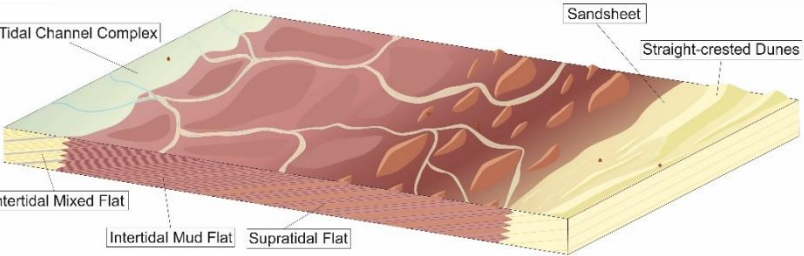
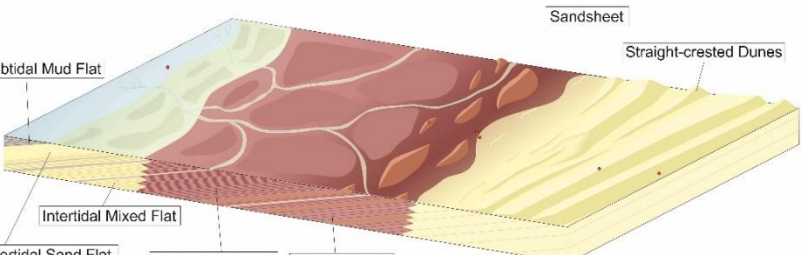
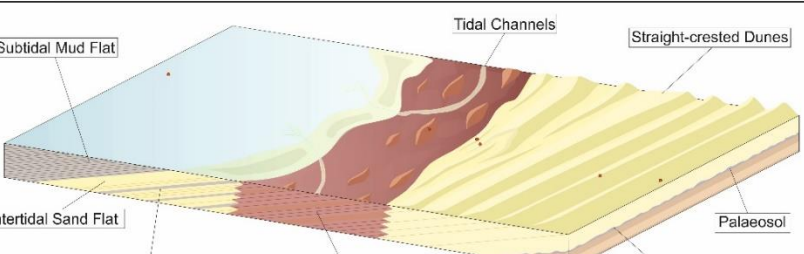
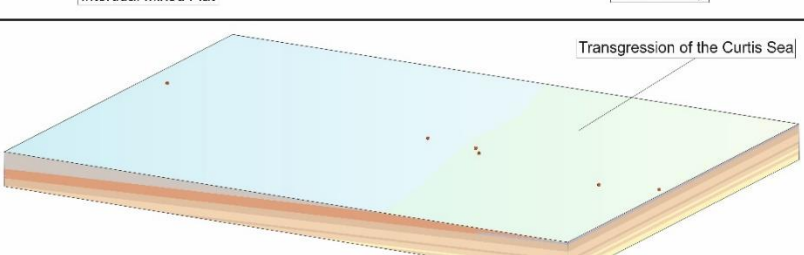
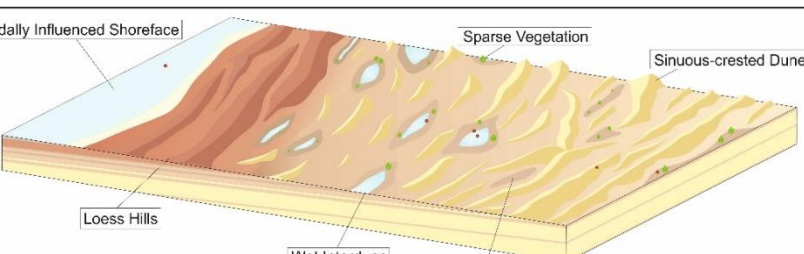
Period	Age	T	Depositional Environment	Formation	Depositional Environment Models Through Time	Description	
UPPER JURASSIC	KIMMERIDGIAN	152 Ma	Modern Day Environment			Map of the study area as in its modern day environment. Localities and the logs taken at each are marked including the main highways and landmarks. Yellow shading indicates Post-Jurassic deposits, light brown, Jurassic, and dark brown, pre-Jurassic deposits.	
		6	Marginal Marine Sabkha Intertidal Mud Flat Supratidal Flat	Summerville		Maximum regression within the study area leading to a complete takeover of the coastal plain depositional environment. Some tidal channel deposits expand into a saline polder preserved by a restricted palaeosol in the subsurface. The previous shallow marine deposits are overlain by a marginal marine sabkha, where deposits of nodular gypsum are preserved within small evaporite pools. This environment persists until the end of the Jurassic.	
	OXFORDIAN	157 Ma	5	Intertidal mixed flat Intertidal mud flat Supratidal flat Coastal dry aeolian dune field	Upper Curtis, Summerville, Moab Member		Expansion of the coastal plain further enabled the shut-down of the dune field (Moab Mbr.). As the sea regressed to the East, the tidal channel complex grew to its greatest extent (Upper Curtis). This environment coexisted with the intertidal mud flat, supratidal flat (Summerville) and aeolian dune field (Moab Mbr.), albeit it a rapidly deteriorating one. Dune forms are poorly formed and graduate into a sandsheet at the margin.
		4	Subtidal mud flat Intertidal sand flat Intertidal mixed flat Intertidal mud flat Supratidal flat Coastal dry aeolian dune field	Lower Curtis, Middle Curtis, Summerville, Moab Member		Further regression shut down the sediment supply necessary for the growth of the dry aeolian dune field. The aeolian margin was dominated by a sandsheet with continued sea level fall promoting the expansion of the coastal plain towards both the East and West of the study area. A tidal channel complex (Upper Curtis) begins to form in conjunction with the shallow marine tidal flats (Middle Curtis), the coastal plain (Summerville) and the dunes (Moab Mbr.).	
		3	Subtidal mud flat Intertidal sand flat Intertidal mixed flat Intertidal mud flat Supratidal flat Coastal dry aeolian dune field	Lower Curtis, Middle Curtis, Summerville, Moab Member		Regression of the Curtis Sea continued, allowing the birth and expansion of a coastal dry aeolian dune field (Moab Member). The dune field reached its maximum at this time, bordering a supratidal flat with some poorly developed silty dune forms and tidal channels (Summerville Fm.). This was the onset of the coastal plain and the regressive tidal flat environment (Middle Curtis) that would continue to expand outwards as the sea level continued to fall.	
		2	Major Transgression	Time of the J-3 Unconformity		A major transgression of the Curtis Sea caused a flooding event across the entire area. This caused shallow marine sands (Lower & Middle Curtis) and a paleosol to be deposited on top of the wet aeolian deposits after the onset of regression. This transgression and subsequent regression is likely to have occurred relatively quickly due to the flat topography and shallow slope of the Curtis Basin.	
1	Tidally influenced shore face Damp loess Coastal wet aeolian dune field	Lower Curtis, Earthy Facies, Entrada Slick Rock		As the Curtis Sea transgressed from the north the coastal wet aeolian system (Entrada Slick Rock) got gradually wetter upwards. Damp and wet interdunes became more frequent whilst dune deposits became thinner. The dune system graduates into a damp muddy coastal plain within which small loess hills develop preserving mottled mud deposits in the subsurface informally termed the 'earthy facies' of the Entrada Formation.			

Figure 6.1- 3D environment reconstructions showing the transition between depositional environments upon an aeolian-marine margin in the Jurassic Period. The diagrams go in chronological order from the bottom to the top, with the topmost diagram representing the modern-day environment, with the relative positions of the localities, the town of Green River and Moab Airport. T1-T6 refer to individual time-points and not necessarily to the surfaces described above (TS1-TS5). The approximate age for the deposits has been given between 160Ma and 152Ma placing the deposits of the Moab Member within the Oxfordian Age.

6.1.2 Spatial and Temporal Evolution of the Dune Field

Whilst using grainflow thicknesses as an estimate of dune height is a logical and proven method to describe changing complexity within a dune system (Hunter 1977, Kocurek & Dott 1983, Sweet *et al.*, 1988), there are additional extraneous factors that may not have been considered (Cornwall *et al.*, 2018). These factors include changes in wind velocity resulting in more or thicker grain flows, entrainment of sediment, and destabilisation of grains caught in the mid-dune area known as the 'lock-up' zone, increasing grain flow thicknesses and are parameters independent of dune height (Cornwall *et al.*, 2018). Reconstructing the interactions of the aeolian dune system and the neighbouring coastal environment, therefore, requires a combination of dune height estimates from grain flow thicknesses, a comparison of the unit thickness to determine the amount of sediment available and the interactions of the dune field with proximity to the margin, and finally a correlation of unit bounding surfaces to tie the deposits to a time point across the margin.

As established in Section 6.3.2, patterns within the total counts gamma-ray logs are limited to visible trends within each depositional environment. A concave trend is evident from the basal bounding surface up to the topmost boundary (Hampson & Howell, 2005). This concave log motif is indicative of a dry aeolian dune system and was believed to have been the limit of the analysis at this stage (North & Boering 1999). However, this study has identified significant peaks attributable to the supersurface boundaries discussed above that present themselves within Th/U peaks.

Combining the above correlation of small-scale stratigraphic surfaces with the established changes in dune height at each locality from Bartlett Wash to Duma

Point allows for a 3D transitional diagram to be created. Similar to Figure 6.2, which describes the transition in environments from dune field to coastal plain to shallow marine.

Figure 6.3 shows the initial encroachment of the dune field in response to a local increase in sediment supply, unconformably overlying the pre-deposited palaeosol. This creates the erosive and undulose surface identified by this study as TS1, corresponding to the J-3 within published literature (Zuchuat *et al.*, 2019). Following initial deposition, the rapid growth of the dune field creates another super-surface, TS2, above which foresets are much steeper, and sets become thicker, there is also an increase in dune height at localities 1 & 2 and deposition of smaller dune-forms closer to the margin at localities 3 & 4. This point marks the greatest extent of the Moab Member dune field; after this point, the sediment supply is dramatically reduced, the dune field retreats, and dune forms become smaller. The preserved deposits here are referred to as unit 3. Before the deposition of unit 3, however, a hiatus is visible as a prominent supersurface at all localities. At units 3 and 4, the retreating dune field promoted the growth of the coastal plain in a landward direction. Another period of non-deposition developed the system of inter-tidal channels in response to further sea-level fall. As the growth of the coastal plain continued, the sediment supply to the dune field was critically cut off, depositing sandsheet deposits at locality 1 that were also eventually overlain by the coastal plain deposits.

Therefore, this analysis concludes that by using the principles of spectral gamma-ray to identify correlatable bounding surfaces and statistical analysis to document the change in complexity with proximity to the margin, the full depositional environment of the Moab Member sandstones through time can be identified.

Unit/ Supersurface Deposition	Moab Member Transition Through Time	Description
Modern Day Environment		Map of the study area in its modern day environment. Localities and logs taken at each are marked, including the main landmarks and highways. Yellow shading indicates post-Jurassic deposits, light-brown, Jurassic deposits and dark brown, pre-Jurassic deposits.
TS5		The end of the deposition of the Moab Member is marked by the final super surface Ss5, separating the sand sheet deposits from the coastal plain sediments that migrate over the top.
Unit 4 deposition		The final period of deposition within the dune field is marked by a sand sheet, deposited as the remaining sediment supply was cut off. Preserved sediment can be found only at locality 1. <u>Dune Height:</u> 1-0.20m
TS4		As the coastal plain environment continued to expand landwards another period of non-deposition within the dune field promoted the growth of an intertidal channel system as regression continued. This is marked in the succession by TS4.
Unit 3 deposition		Following the hiatus that formed TS3 deposition on the dune field was dramatically reduced leading to the retreat of dunes from localities 3 & 4 and smaller dune forms at localities 1 & 2. <u>Dune Height:</u> 1-2.0m 2-0.85m
TS3		During another period of non-deposition upon the dune field vegetation was able to develop, leading to the preservation of rhizoliths in the subsurface, producing the surface TS3.
Unit 2 deposition		Following deposition of Unit 1 the dune-field grew to its greatest extent with straight-crested dune forms deposited at localities 1-4. The migration and preservation of these dunes also preserved the surface TS2. <u>Dune Height:</u> 1-5.0m 2-3.20m 3-0.25m
TS2		During a period of non-deposition and deflation upon the dune field vegetation was able to develop, leading to the preservation of rhizoliths in the subsurface. This gap produced the most prominent surface within the succession, TS2.
Unit 1 deposition		As sediment supply increased, dune forms began to migrate over the palaeosol and damp sediment creating the unconformable surface TS1. Initial deposition comprised of small, poorly developed dune forms at each locality. <u>Dune Height:</u> 1-0.35m 2-0.45m 3-0.30m 4-0.20m
Unconformity & palaeosol TS1		Following the onset of regression of the Curtis Sea, a palaeosol developed in the East of the study area. In the West, damp sediment was deposited with continued sea-level fall.

Figure 6.2- 3D diagrams representing the behaviour of the aeolian dune field at the time of deposition of genetic packages 1-5 and during periods of non-deposition represented by the surfaces TS1-TS5, working chronologically upwards from the bottom to the top. Significant features of each unit have been annotated and a description of changes in the dune field can be found in the right hand column.

6.1.3 Cyclicity of the Curtis Formation

The aeolian-marine margin studied and described above, lithostratigraphically relates to the Entrada slick rock (wet aeolian dune field), the earthy facies (damp/wet interdune), the Moab Member (coastal dry aeolian dune field), the Summerville Formation (intertidal mudflat, supratidal flat and marginal marine sabkha), and the Lower, Middle and Upper Curtis Formation (subtidal mudflat to intertidal mixed flat).

Interpretation of spectral gamma-ray logs identified two sets of chronostratigraphic surfaces, large-scale and small-scale, whilst facies analysis and log motifs documented facies shifts upon the margin. The large-scale chronostratigraphic surfaces represent possible sequence boundaries, namely the maximum flooding surface (MTS) and maximum regressive surface (MRS) (Figure 6.4). As shown (Figure 6.2 & 6.3), transgression began with the transition of the Entrada Sandstone from extensive sinuous-crested aeolian dunes into the damp and wet interdune complexes of the earthy facies. This steady transgression was an indication of imminent marine transgression from the approaching Sundance Sea in the north. This rapid, regional transgression flooded extensively over the study area with sub-aqueous deposition evident at localities 3 & 4 but only damp palaeosols at localities 1 & 2, implying very shallow water at this point. The infilling of sediments caused a drop in accommodation space resulting in rapid regression over the flat expanse of the Entrada/Curtis plains, forming an erosive surface termed the J-3, denoted by TS1 in this study. This significant surface can be picked up in both Th/K and Th/U ratios and represents the Maximum Flooding Surface of the T-R sequence. After this point, normal regression continues, with the Curtis Sea retreating backwards and with it bringing the aeolian Moab dunes. Isotope ratios identify an additional two significant surfaces TS2 and TS4

correlatable within both the aeolian and marine successions. Additional signals within the spectral gamma-ray at surfaces TS3 and TS5 appear to pick up distinct surfaces, correlatable only within the aeolian succession representing smaller-scale fluctuations in sea-level, the signal of which is lost in the marine and coastal successions perhaps as a result of allocyclic overprinting by tidal resonance (Zuchuat *et al.*, 2019). The maximum regressive surface marks the end of normal regression and the onset of forced regression, represented by the J-5 stratigraphic surface.

Total counts log motifs show the stacking patterns of the sequence through the interpretation of trends. Geometries such as funnel, bell and cylinder motifs represent progradational, retrogradational and aggradational patterns, respectively. Within the context of the Curtis Formation sequence stratigraphy, this reveals that the lower sinuous-crested aeolian dunes comprise a highstand systems tract that evolves into a transgressive systems tract with the onset of regression through deposition of the subtidal flat and damp/wet interdune deposits. The MTS separates this transgressive systems tract from the overlying highstand systems tract, which continues until the MRS, completing the transgressive-regressive sequence.

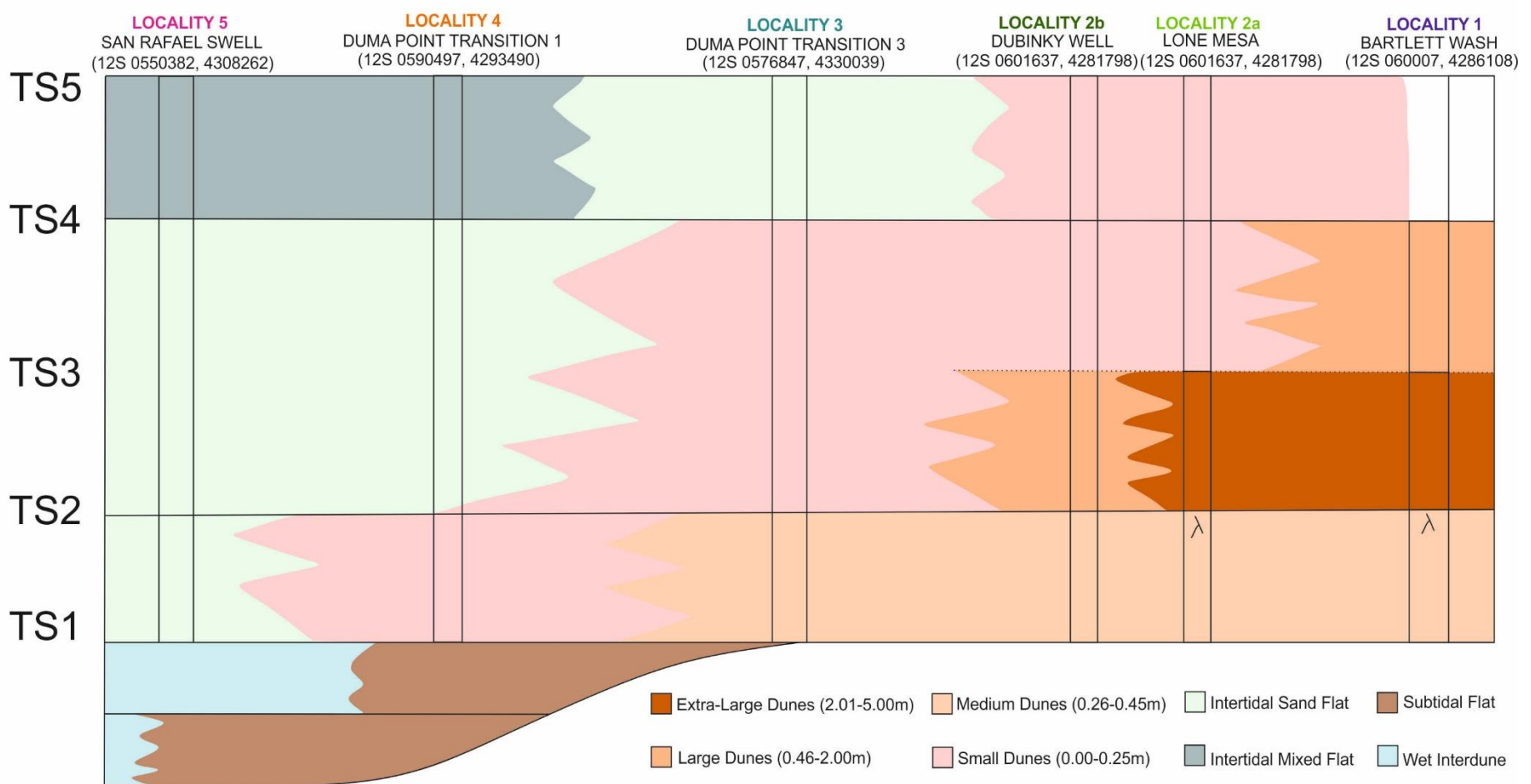
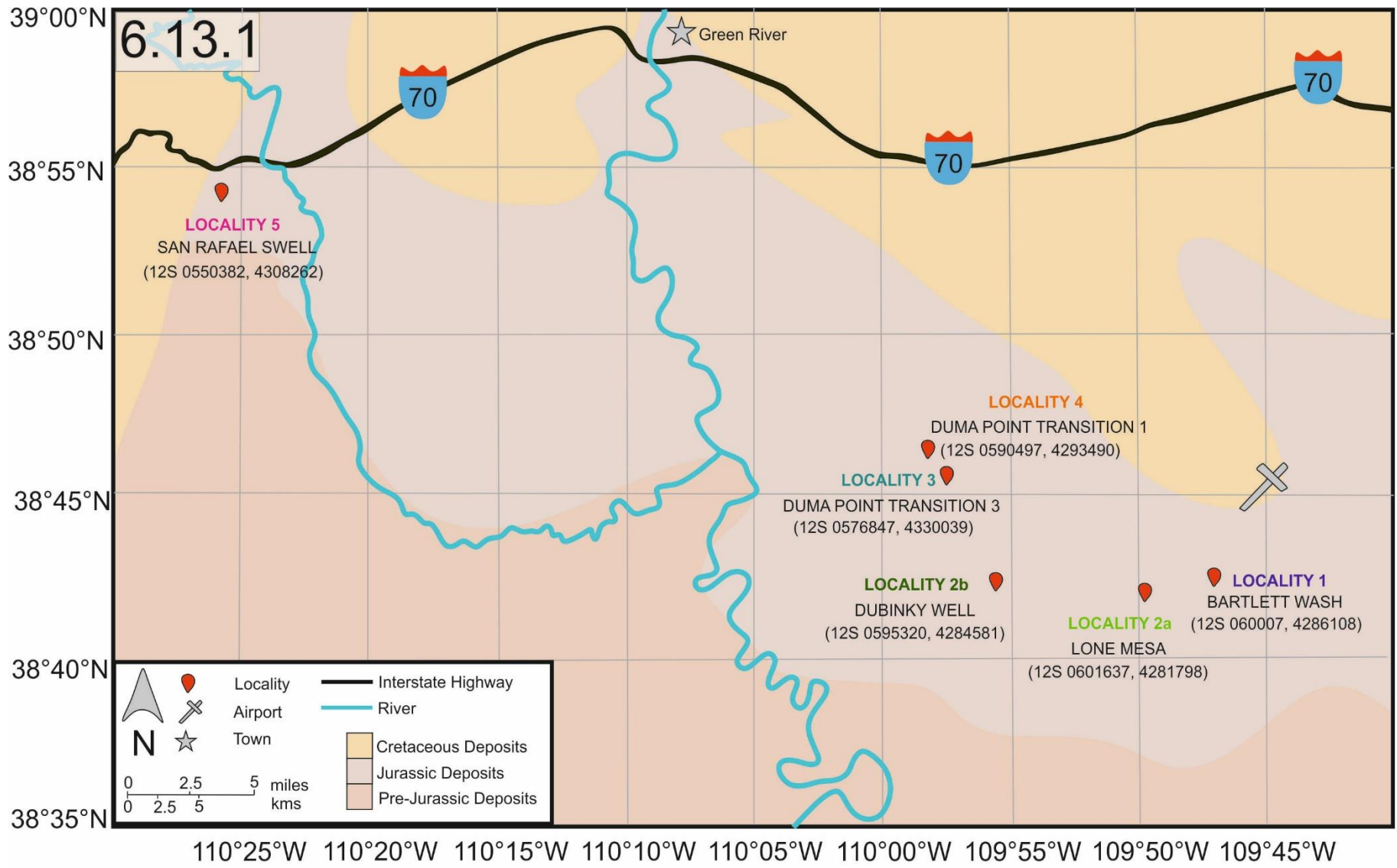


Figure 6.3- Locality map and sequence stratigraphy of the study area, from Bartlett Wash in the East to the San Rafael Swell in the west. The key environments have been colour coded with the aeolian dunes further broken down into classifications based on size, as identified in Chapter 4. The key surfaces traceable across each of the localities have been shown as well as their main identifiers such as rhizoliths.

6.2 Discussion

The correlation of significant chronostratigraphic surfaces across the study area, from an aeolian dune field in the east to a tidally-influenced shallow marine shoreface in the west, relies on a variety of analytical techniques. This chapter documents the various uses of spectral gamma-ray (SGR) logging to characterise environments and surfaces within preserved successions.

Thorium and potassium are statistically reliable isotopes at the 90-second measurement interval and were used in this study to determine the sedimentary conditions and distance to the palaeoshoreline. The logs found a peak occurring at the same point in the succession at localities 1-5, correlating into a significant chronostratigraphic surface. From this hinge line, the changes in sedimentary conditions can be seen. Beneath this peak, in the aeolian succession at localities 1-4, the signals are much higher compared with the data above this peak which has much lower values and instead shows a much smoother concave motif concurrent with an arid environment at this point (Martinius *et al.*, 2002).

Thorium/uranium ratios identify the same significant chronostratigraphic peak representing the surface TS1 in this area. In addition to this large-scale chronostratigraphic surface, many other significant peaks can be picked out within the aeolian deposits. Their relative position and high levels of isotopes compared with the typical values expected from aeolian sediment imply they represent points of non-preservation of the dune field during which uranium and thorium can accumulate on the exposed surface. The peaks show 5 'pulses' of the dune field, with initial deposits encroaching from the east as the water level dropped following the major flooding event in the area. At the termination of this first pulse of the dune field, dunes can be found exclusively at localities 1 and 2. A peak in both the

Th/K and Th/U at the approximate height of the first genetic package implies a minor flooding surface followed by the exposure and stabilisation of the dune field; small vegetation grew on the surface, preserving as rhizoliths and uranium isotopes accumulated on the exposed surface producing the characteristic Th/U peak.

Further peaks up the succession represent similar bounding surfaces traceable within the aeolian succession. If these peaks resulted from minor transgressions of the neighbouring sea driven by allocyclic processes, some evidence should exist within the coeval sediments of different depositional environments. This study has identified some candidate peaks, however, without a sedimentological expression, it is difficult to correlate these surfaces across the margin conclusively.

6.3 Summary

This chapter combines the analysis of gamma-ray logs with previously described facies analysis, sedimentary logs and statistical analysis of dune deposits using drone photogrammetry.

Finally, large-scale, and small-scale stratigraphic surfaces were combined to produce two figures representing the interactions within an aeolian/marine margin. Firstly, a large-scale depositional model accounts for changes in the environment from the proximal part of the study area (East) to the distal (West). Secondly, a smaller-scale model documenting the local interaction between dune and coastal deposits and its effect on dune complexity with proximity to the margin.

Chapter 7: Discussion of Allocyclic and Local-scale Sedimentary Processes upon an Aeolian-Marine Margin

The Jurassic deposits of south-eastern Utah provide a complete transition through an aeolian-marine margin, from an arid aeolian dune field in the east to a tidally-influenced shoreface in the west. The preserved succession documents both allocyclic (external) and autocyclic (internal) controls on the system determined through sedimentary and spectral-gamma ray analyses at localities across the transect. These analyses and the consequent results will be discussed below to contextualise the research completed in this thesis.

7.1 Allocyclic vs Autocyclic Processes

The work of Zuchuat *et al.* (2019) proposes that, as a result of tidal resonance, allo-cyclic processes within the Curtis Basin are over-printed by auto-cyclic, local, sea-level changes. The work presented here uses spectral gamma-ray data to establish key time surfaces within the Moab Member of the Curtis Formation and provide correlatable stratigraphic surfaces that add to the story of sea-level fluctuations within this basin.

The controlling factors of dune field migration and preservation fall into two main categories, allogenic, i.e., external factors such as climate change, tectonics and eustatic sea-level rise, and autogenic, i.e., local scale mechanisms such as sediment supply and wind capacity (Kocurek & Havholm 1993, Miall 2010, Catuneanu 2019). The marine sediments of the Lower Curtis document three parasequences that show both allocyclic and autocyclic controls (Zuchuat *et al.*, 2018). The gamma-ray log motifs for the preserved Lower Curtis at the San Rafael Swell separates the deposit into three distinct sections represented by a serrate bell motif followed by a serrate funnel motif and then another serrate bell motif

concurrent with retrogradational, progradational and retrogradational parasequences, respectively (Martinius *et al.*, 2002) (see section 6.3.2). Coeval deposits of Entrada Sandstone and the Earthy Facies similarly display wetting upwards trends within the log motifs of the spectral gamma-ray, documenting an overall increase in the level of the water table in this wet aeolian system, proliferating frequent damp and wet interdunes with a greater frequency supporting an imminent marine transgression.

The base of the Middle Curtis represents a regional transgression that flooded the basin and the surrounding environments (Zuchuat *et al.* 2018, Zuchuat *et al.*, 2019). This study has identified a signal related to this regional flooding surface correlatable to significant peaks in the Th/U ratio across the transect. The peak occurs within different environments at different points up-succession, reflecting the diachronicity of the surface (see section 6.3.2). Regression of the Curtis Sea then began in response to the rate of sediment supply outpacing the rate of accommodation creation. This study hypothesises that the marine margin at the time of deposition of the Moab Member was located within the modern-day Duma Point area (UTM WGS84 12S 0590497, 4293490). The creation of accommodation space and an influx of sediment supply from the rapidly eroded Uncompaghre Highlands led to the accretion of sediment later preserved as the Moab Member dune field and was coeval with the Middle Curtis deposits (Fillmore 2010, Zuchuat *et al.* 2018, 2019). Thorium/uranium (Th/U) ratios within the aeolian sediments detail five 'pulses' of the dune field, depositing genetic packages across the margin between locality 1 and locality 4 (Chapter 4). At each locality, the aeolian succession contains between one and five significant peaks potentially representing those allocyclic signals, overprinted by tidal resonance within the lower, middle, and upper Curtis deposits. Sedimentologically along these surfaces

are preserved rhizoliths, bleaching horizons and sporadic palaeosol development (Chapter 3). These surfaces are significant within the constraints of this study, however additional work on the Moab member sandstones extending north and south of the study area is necessary to fully define these significant surfaces as supersurfaces, hence placing them within a wider regional context. As climatic conditions upon the Colorado Plateau throughout the Jurassic Period fluctuated with global glacial-interglacial cycles changes, these surfaces likely represent the stabilisation of the dune field in response to changes in sediment supply associated with minor changes in the environment from very arid to more humid (Kocurek & Dott 1983, Peterson 1994),

As the Curtis Sea continued to regress from the area, the gamma-ray logs show another serrated funnel motif through the Upper Curtis and coeval deposits in the east of the study area (see section 6.3.2). This demonstrates progradational deposits concurrent with continued regression (Martinius *et al.*, 2002). The marginal marine sabkha and coastal plain sediments that overlie the Upper Curtis marine and Moab Member aeolian sediments have a cylindrical motif reflecting the aggradation of the Summerville Formation. These allocyclic signals preserved within the Curtis and the Summerville are likely also related to the climatic variations influencing the oscillating sediment supply to the dune field and hence the contemporaneous sediments.

7.2 Characterising the Aeolian-Marine Margin

By combining three-dimensional photogrammetric models, spectral gamma-ray, and sedimentary logs, a comprehensive story of sediment supply, sea-level fluctuations, and dune field migration upon an aeolian marine margin can be built. Drone photogrammetry provides high-resolution imaging, that when compiled in

software such as Agisoft Metashape, is an invaluable tool in recreating localities, enabling in-house data collection, and augmenting field observations.

The results obtained from these methods can quantify the morphologies and geometries of the dune field in response to the regional regression at the time of deposition (see section 6.4.2). Previous work on the Moab Member is limited to work done alongside the coeval Curtis Formation and hence does not describe the behaviour of the dune field in great detail (Caputo & Pryor 1991, Peterson 1994, Doelling 2001, Zuchuat *et al.*, 2018, 2019). This study used foreset thicknesses within the framework of Kocurek & Dott's work on the Entrada Formation to establish changes in dune height. Dune height increases between genetic packages 1 and 2 as the dune field expanded westward. The initial deposits of the Moab Member, i.e., genetic package 1, are preserved only at Bartlett Wash (Locality 1) and Lone Mesa (Locality 2) (Figure 3.1). With the expansion of the dune field westward in response to regression (Peterson, 1994), the dune field reached its maximum extent at locality 4, preserving genetic package 2 across the margin. After this point, the dune height and set thickness of preserved dune packages decrease rapidly, indicating the shut-down of the aeolian dune field at this point. As the climate at this time was stable and dry and spectral gamma-ray does not show a regional transgression causing the shutdown of the aeolian dune field, it is most likely related to a change in sediment supply (Kocurek & Dott 1983, Peterson 1994).

Sediment sources for Jurassic ergs originate from palaeorivers traversing the continental interior sourcing and transporting material from the Appalachian orogenic belt and the Ancestral Rocky Mountains (Blakey 1994, Dickinson & Gehrels 2003). Towards the end of the Jurassic Period, the Ancestral Rocky Mountains have been all but completely eroded, which may have led to the

restriction of available sediment within the Moab dune field and initiated its decline into sandsheet deposits and finally a coastal plain (Thomas, 2011, Lawton, 2014, Ejembi 2018).

There is evidence that the proximity of the dune field to the marine margin reworked the sediments of the Entrada dune field to supply some material for the Moab Member dunes. The thorium/ potassium cross-plots for each aeolian dune facies showed that the Moab Member had much lower values of both thorium and potassium than the Entrada despite greater marine influence, implying the reworking of sediment by the Curtis Sea. However, the present study contains insufficient data to corroborate this hypothesis and would require a provenance study comparing the Entrada dunes and the dunes of the Moab Member to confirm this hypothesis.

7.3 Sequence Stratigraphy and Global Context

The Curtis Formation deposits represent one complete transgressive-regressive sequence bound by regional surfaces comprising tidally influenced shallow marine sediments and coeval coastal plain and aeolian dunes (Zuchuat *et al.*, 2018, 2019). Deposits of Lower Curtis at San Rafael Swell and the Entrada Slick Rock and Earthy facies represent a transgressive systems tract as the sea level rose. This is supported by the gamma-ray trends established by this study, in particular the log motif trends associated with total counts logs. A major transgressive event marks the maximum flooding surface representing the bounding surface for a transgressive-regressive sequence (Zuchuat *et al.*, 2019), most likely associated with the surface TS1. The overlying Middle and Upper Curtis and Moab Member deposits within the study area suggest a highstand systems tract (HST) deposit. Comprising prograding shoreline deposits contemporaneous with prograding

coastal plain deposits that expand landward and seaward over the regressing dune field.

The lack of fossil material within the Curtis marine sediments and the varied preservation rate of aeolian sediments make an exact time constraint for this succession challenging. Global sea-level change is caused by two main processes, the melting and freezing of polar ice-caps and the changing volume of ocean basins with the creation and destruction of ocean ridges and swells (Hallam 1992, Hallam 2001). Climate fluctuations and relative sea-level curves for the Jurassic Period are still widely debated and therefore the exact cause of the major transgression that resulted in the flooding and consequently, the formation of the J-3 is similarly challenging to pinpoint. Ash deposits from the Entrada have conclusively dated the uppermost parts of the formation to 160.8 ± 0.2 Ma, when considered within a global context it is possible to fit the cycles of the Moab Member packages within established long and short eccentricity cycles after this point. Such that the five identified packages may have occurred as a result of pulses caused by 405kyr cycles, leading to an overall time of deposition for the Moab Member sandstones of 2.025 Myr.

Chapter 8: Conclusions and Further Work

This chapter summarises the initial aims of this project and how they have been met throughout this thesis. Work has been carried out to enhance our knowledge of aeolian-marine margins and the methods available to describe them. Furthermore, this chapter will highlight any opportunities for future research that have arisen.

8.1 Research Aims

This section will describe how each of the aims and objectives outlined in Chapter 1 has been met through the fieldwork, data analysis and composition of this thesis.

8.1.1 Establish local-scale interactions of contemporaneous aeolian and marine margins.

The use of sedimentary logging and drone photogrammetry proved successful in establishing the local-scale movements of the Moab Member dune field with respect to the neighbouring Curtis Sea. Sedimentary logging determined the thickness of dune packages, the position of bounding surfaces, index surfaces and unique sedimentary features that helped define the depositional environment. High-resolution photogrammetry then enabled in-office recreation and further analysis of outcrops at a scale not attainable in the field. Using these techniques in conjunction meant that foreset thicknesses could be established, which, when placed within the framework outlined by Kocurek & Dott (1989), gave an estimate for minimum palaeo-dune height. Doing so meant patterns of deposition and unique units could be identified from erg centre to marine margin. Results showed the accumulation of the dune field following a flooding event. As the sea regressed, the dune field extended westward to its maximum extent. A decrease in sediment supply led to the restriction of dune accumulation, regression of the dune field and the landward spread of a coastal plain environment. The coastal plain

continued to expand both seaward, in response to continued regression, and landward with the termination of the dune field, eventually eliminating all dune preservation. Therefore, this study has shown, via the use of logging and photogrammetry, the behaviour of a dune field upon an aeolian-marine margin experiencing regression.

8.1.2 Identify significant bounding surfaces traceable within proximal deposits and their distal counterparts.

The spectral gamma-ray analysis identified significant surfaces at a large scale observed within the aeolian deposits and the shallow marine succession. A number of peaks observable within Th/U, Th/K and U/K logs also identified time-gaps in the aeolian succession at a smaller scale representing periods of non-deposition between advances of the dune field. It was previously thought that the use of spectral gamma-ray within aeolian systems was unreliable due to the relatively low levels of potassium bearing minerals such as clays.

8.1.3 Reconstruct an aeolian-marine margin and identify sea-level fluctuations upon it.

The combination of facies analysis, gamma facies analysis, sedimentary logging, spectral gamma-ray logging, and high-resolution drone photogrammetry built a comprehensive picture of both large- and small-scale interactions the aeolian-marine margin. The composition of three-dimensional models at both scales demonstrates sea-level fluctuations. These models show that deposition of the Entrada dune interdune complex was shut down by a basin-wide flooding event that produced the regional surface titled the J-3. The expression of the J-3 within SGR logging provides a snapshot of the margin and a tie-point from which other surfaces and depositional environments can be correlated through time. These

models show the impact allocyclic influences upon sea-level had at the time of deposition of the Moab Member and allows for correlation of such events across the margin despite the complications of enhanced autocyclic influences from the tidal resonance of the basin (Zuchuat *et al.*, 2019).

8.2 Summary of Findings

Previous studies have sought to identify allocyclic and autocyclic influences upon sea-level within the Curtis basin but have been met with challenges as the allocyclic signals were likely overprinted by autocyclic tidal resonance (Zuchuat *et al.*, 2019). This study identifies peaks related to allocyclic sea-level rise forming the J-3 surface identifiable within the marine Curtis formation (Zuchuat *et al.* 2018, 2019), but also an additional four significant peaks within the coeval Moab Member related to allocyclic sea-level fluctuations lost in the tidal resonance of the Middle and Upper Curtis.

This study also established the behaviour of aeolian dunes with proximity to a marine margin such that dune height and set thickness decrease rapidly and sediments preserve much fewer isotopes picked up within spectral gamma-ray studies. In addition to the dune field decreasing in complexity with proximity to the marine margin, the dunes also respond to external factors, controlling dune height and dune geometry through time. Five 'pulses' of the dune field were established with dune height and set thickness gradually decreasing upwards through genetic packages 1-5, each separated by regional surfaces marked by rhizoliths and occasional palaeosol horizons. The research carried out has successfully characterised an aeolian-marine margin both spatially and temporally, defining the allocyclic and autocyclic controls on a basin in tidal resonance and identifying the sequence stratigraphical context of the preserved sediments.

In conclusion, using spectral gamma-ray analysis, sedimentary logging techniques and high-resolution drone photogrammetry this study has proven it is possible to accurately reconstruct an aeolian-marine margin, identifying both transgressive and regressive phases and the relative interactions of neighbouring contemporaneous environments.

8.3 Future Work

This study describes the large and small scale interactions upon an aeolian-marine margin, using gamma-ray and photogrammetric methodologies. In doing so, a number of areas for further research have been identified that would be of benefit to the wider scientific community.

8.3.1 Provenance of the Moab Member- Reworked Entrada dunes?

Preliminary studies completed in the field show that on a K:Th plot, deposits typically associated with Moab Member dune plot with very low values compared with the Entrada dune material, which plots more in the centre of the graph. This relationship implies that the sediment available to form the Moab Member dunes was 'cleaner,' i.e., contained less potassium bearing clay material than the Entrada dunes despite its marginal marine environment. This could perhaps imply that a large percentage of the material available for the formation of the Moab dunes is reworked Entrada material that was 'cleaned' as the sea level regressed following the flooding event that formed the J-3; however, more work on the provenance of material in the area would be needed to confirm this theory.

This study has proven that after a significant transgressive event there was a subsequent regression of the Curtis Sea that has the potential to have released a large amount of sediment available for the construction and migration of the Moab Member dune field. The presence of a number of highlands surrounding the Curtis

Basin at the time of deposition of the Moab Member was previously thought to be a potential source for the dunes themselves, most significantly the Ancestral Front Range and the Uncompaghre high. However, detrital zircon geochronology has shown that there was an abrupt change in provenance towards the end of deposition of the Entrada associated with stream capture and drainage reorganisation (Potter-McIntyre *et al.*, 2016). It is therefore unlikely that the sediment supply for the Moab Member originated from the same source. Further comprehensive spectral gamma-ray analysis of the Entrada dunes could provide clues as to the provenance of the material in both the Entrada Formation and the Curtis Formation and hence the provenance of the Moab Member itself.

8.3.2 Supersurfaces and Sequence Stratigraphy

This study has highlighted several key surfaces that appear within the preserved aeolian sediments of the Moab Member correlatable across the margin from east to west, referred to as 'index surfaces'. Whilst some key features are present along these index surfaces such as palaeosols and rhizoliths, implying stabilisation of the dunes, defining these surfaces as supersurfaces at this stage is premature. A regional study encompassing more of the Moab Member and its relative aeolian environments, i.e., erg centre and erg margin, would be beneficial to determine if these index surfaces are traceable throughout the entire system.

Whilst the use of spectral gamma-ray is extensive in outcrop studies, the studies typically describe preserved successions of marine strata or perhaps lacustrine environments (North & Boering 1999, Svendsen & Hartley 2001, Hampson *et al.* 2005). The use of spectral gamma-ray in aeolian systems has previously been thought to be unsuccessful due to the relatively low percentage of clay-bearing minerals that produce the highest signals of potassium, thorium, and occasionally

uranium. Recent studies, including this one, have proven that SGR can work effectively within marginal environments picking up significant stratigraphic surfaces at scale and indicating cyclicity (Pettigrew, 2019).

With the further acquisition of data from similar aeolian-marine margins to cement the relationship between Th/U peaks and the occurrence of aeolian supersurfaces, there would be a strong advantage in using SGR within dry aeolian systems to determine significant stratigraphic surfaces. Supersurfaces within aeolian successions can be caused by changes in sea level (Kocurek 1988), identifying these surfaces in the proximal part of the basin via peak in the spectral gamma-ray, and comparing these peaks with the same analysis in distal counterparts may allow 'events' denoting sea-level change to be correlated basin-wide despite otherwise differing sedimentological evidence. This could provide a basis for sequence stratigraphy within an inland aeolian succession.

8.3.3 A Closer Look at the Summerville Formation

One additional gap in scientific knowledge of stratigraphy in this area is details regarding the Summerville Formation. The cycle of deposits on the Colorado Plateau following the end of the Triassic Period document a regular cycle of marine margins bordered by coeval aeolian systems, i.e., the Carmel Sea and the Page sandstone, Lower Curtis, and Entrada Sandstone, Middle Curtis, and Moab Sandstone. However, the Summerville formation brings an end to this pattern of marine margin and aeolian sand system despite the Curtis Sea lingering and regressing right up until the end of the Jurassic Period. There is a potentially interesting study into the provenance and characteristics of the Summerville sediments that dictated the expansion of this coastal plain as opposed to the extensive aeolian systems of the previous era.

Aside from a distinction between depositional environments, little in-depth analysis has been carried out on this unit. It is one of the few within the surrounding stratigraphic units not to be divided into members despite a clear distinction in characteristics, for example, between the heterogenous mounds of red silts in the proximal part of the basin and the contrasting distinctly bedded successions of silts and very fine-grained sands moving towards the distal part. The broad depositional environment of the Summerville is defined as a 'coastal plain'. However, as identified by this study and others (Sleveland 2016, Zuchuat *et al.*, 2018, 2019), there are further subdivisions of coastal plain environments that present within the Summerville, such as supratidal flat, intertidal mudflat and intertidal mixed flat. Fully describing these subsections would further document sea-level fluctuations in the basin up to the J-5, which separates the Summerville Formation from the overlying Morrison Formation, giving a complete story of sea-level fluctuations in the Jurassic.

In addition to defining the sedimentological boundaries within the Summerville, a continuation of the gamma-ray analysis as outlined in this thesis would be successful in comparing the use of spectral gamma-ray not only between aeolian and coastal plain successions but also further in defining cyclicity within marginal marine sabkhas as opposed to continental sabkhas (Pettigrew, 2019). The Summerville presents a useful intermediary in this case, as the Curtis Sea was an inland sea that flooded northwards across the Entrada Dune fields, the sabkha preserved within the Summerville Formation in the West of the study have elements of both continental and marginal marine sabkhas that could draw some interesting results via spectral gamma-ray analysis.

Chapter 9: References

- Adams, J.A.** and **Weaver, C.E.**, 1958. Thorium-to-uranium ratios as indicators of sedimentary processes: example of concept of geochemical facies. *AAPG Bulletin*, 42(2), pp.387-430.
- Ainsworth, R.B., McArthur, J.B., Lang, S.C.** and **Vonk, A.J.**, 2018. Quantitative sequence stratigraphy. *AAPG Bulletin*, 102(10), pp.1913-1939.
- Allaby, M.** ed., 2013. *A dictionary of geology and earth sciences*. Oxford University Press.
- Allen, J.R.L.** 1970: Physical processes of sedimentation. London: Allen and Unwin.
- Alvarez, W., Staley, E., O'Connor, D.** and **Chan, M.A.**, 1998. Synsedimentary deformation in the Jurassic of south-eastern Utah—A case of impact shaking? *Geology*, 26(7), pp.579-582.
- Anderson, O.J.** and **Lucas, S.G.**, 1992. The Middle Jurassic Summerville Formation, northern New Mexico. *New Mexico Geology*, 14(4), pp.79-92.
- Anderson, O.J.** and **Lucas, S.G.**, 1994. Middle Jurassic stratigraphy, sedimentation and palaeogeography in the southern Colorado Plateau and southern High Plains. Rocky Mountain Section (SEPM).
- Anderson, R.S.**, 1988. The pattern of grainfall deposition in the lee of aeolian dunes. *Sedimentology*, 35(2), pp.175-188.
- Andreason, M.W.**, 1992. Coastal siliciclastic sabkhas and related evaporative environments of the Permian Yates Formation, north Ward-Estes field, Ward County, Texas. *AAPG Bulletin*, 76(11), pp.1735-1759.
- Aranda, J.T.M., Alfaro, D.A.** and **Flores, R.J.**, 2019. Gamma-ray, spectral gamma-ray and optical borehole imager logs applied in the exploration for ore deposits. In *SEG Technical Program Expanded Abstracts 2019* (pp. 2183-2187). Society of Exploration Geophysicists.
- Armstrong, R.L.**, 1968. Sevier orogenic belt in Nevada and Utah. *Geological Society of America Bulletin*, 79(4), pp.429-458.
- Asfahani, J.**, 2014. Statistical factor analysis technique for characterizing basalt through interpreting nuclear and electrical well logging data (case study from Southern Syria). *Applied Radiation and Isotopes*, 84, pp.33-39.
- Baars, D.L.** and **Doelling, H.H.**, 1987. Moab salt-intruded anticline, east-central Utah. *Geological Society of America Centennial Field Guide Rocky Mountain Section*, pp.275-280.
- Bagnold, R.A.**, 1941. The physics of blown sand and desert dunes: New York. *William Morrow & Company*.
- Baker, A.A., Dane, C.H.** and **Reeside Jr, JB**, 1933. Paradox formation of eastern Utah and western Colorado. *AAPG Bulletin*, 17(8), pp.963-980.
- Baker, A.A., Dane, C.H.** and **Reeside, J.B.**, 1936. *Correlation of the Jurassic formations of parts of Utah, Arizona, New Mexico and Colorado* (No. 183-185). US Government Printing Office.
- Baker, A.A., Dobbin, C.E., McKnight, E.T.** and **Reeside Jr, JB**, 1927. Notes on the stratigraphy of the Moab region, Utah. *AAPG Bulletin*, 11(8), pp.785-808.
- Banham, S.G.** and **Mountney, N.P.**, 2013. Controls on fluvial sedimentary architecture and sediment-fill state in salt-walled mini-basins: Triassic Moenkopi Formation, Salt Anticline Region, SE Utah, USA. *Basin Research*, 25(6), pp.709-737.
- Barker, D.C.** and **Bhattacharya, J.P.**, 2018. Sequence stratigraphy on an early wet Mars. *Planetary and Space Science*, 151, pp.97-108.
- Bemis, S.P., Micklethwaite, S., Turner, D., James, M.R., Akciz, S., Thiele, S.T.** and **Bangash, H.A.**, 2014. Ground-based and UAV-Based photogrammetry: A multi-scale, high-resolution mapping tool for structural geology and paleoseismology. *Journal of Structural Geology*, 69, pp.163-178.

- Besly, B., Romain, H.G. and Mountney, N.P.**, 2018. Reconstruction of linear dunes from ancient aeolian successions using subsurface data: Permian Auk Formation, Central North Sea, UK. *Marine and Petroleum Geology*, 91, pp.1-18.
- Bjerrum, C.J. and Dorsey, R.J.**, 1995. Tectonic controls on deposition of Middle Jurassic strata in a retroarc foreland basin, Utah-Idaho trough, western interior, United States. *Tectonics*, 14(4), pp.962-978.
- Blakey, R.C. and Gubitosa, R.**, 1983. Late Triassic palaeogeography and depositional history of the Chinle Formation, southern Utah and northern Arizona. Rocky Mountain Section (SEPM).
- Blakey, R.C. and Ranney, W.**, 2008. *Ancient Landscapes of the Colorado Plateau*. Grand Canyon Assn.
- Blakey, R.C.**, 1994. Paleogeographic and tectonic controls on some Lower and Middle Jurassic erg deposits, Colorado Plateau. Rocky Mountain Section (SEPM).
- Blakey, R.C.**, 2019. Pennsylvanian-Jurassic sedimentary basins of the Colorado Plateau and southern Rocky Mountains. In *The sedimentary basins of the United States and Canada* (pp. 315-367). Elsevier.
- Blakey, R.C., Peterson, F. and Kocurek, G.**, 1988. Synthesis of late Paleozoic and Mesozoic eolian deposits of the Western Interior of the United States. *Sedimentary Geology*, 56(1-4), pp.3-125
- Bristow, C.S. and Williamson, B.J.**, 1998. Spectral gamma-ray logs: core to log calibration, facies analysis and correlation problems in the Southern North Sea. *Geological Society, London, Special Publications*, 136(1), pp.1-7.
- Brown Jr, LF and Fisher, W.L.**, 1977. Seismic-stratigraphic interpretation of depositional systems: examples from Brazilian rift and pull-apart basins: section 2—application of seismic reflection configuration to stratigraphic interpretation.
- Buol, S.W. and Eswaran, H.**, 1999. Oxisols. In *Advances in agronomy* (Vol. 68, pp. 151-195). Academic Press.
- Buol, S.W. and Eswaran, H.**, 1999. Oxisols. In *Advances in agronomy* (Vol. 68, pp. 151-195). Academic Press.
- Cannon, S.**, 2015. *Petrophysics: a practical guide*. John Wiley & Sons.
- Caputo, M.V. and Pryor, W.A.**, 1991. Middle Jurassic tide-and wave-influenced coastal facies and palaeogeography, upper San Rafael Group, east-central Utah.
- Cardenas, B.T., Kocurek, G., Mohrig, D., Swanson, T., Hughes, C.M. and Brothers, S.C.**, 2019. Preservation of Autogenic Processes and Allogenic Forcings in Set-Scale Aeolian Architecture II: The Scour-and-Fill Dominated Jurassic Page Sandstone, Arizona, USA. *Journal of Sedimentary Research*, 89(8), pp.741-760.
- Casella, E., Drechsel, J., Winter, C., Benninghoff, M. and Rovere, A.**, 2020. Accuracy of sand beach topography surveying by drones and photogrammetry. *Geo-Marine Letters*, pp.1-14.
- Catuneanu, O.**, 2017. Sequence stratigraphy: Guidelines for a standard methodology. In *Stratigraphy & Timescales* (Vol. 2, pp. 1-57). Academic Press.
- Catuneanu, O.**, 2019. Model-independent sequence stratigraphy. *Earth-science reviews*, 188, pp.312-388.
- Catuneanu, O.**, 2019. Scale in sequence stratigraphy. *Marine and Petroleum Geology*, 106, pp.128-159.
- Catuneanu, O., Abreu, V., Bhattacharya, J.P., Blum, M.D., Dalrymple, R.W., Eriksson, P.G., Fielding, C.R., Fisher, W.L., Galloway, W.E., Gibling, M.R. and Giles, K.A.**, 2009. Towards the standardisation of sequence stratigraphy. *Earth-Science Reviews*, 92(1-2), pp.1-33.
- Catuneanu, O., Galloway, W.E., Kendall, CGSC, Miall, A.D., Posamentier, H.W., Strasser, A. and Tucker, M.E.**, 2011. Sequence stratigraphy: methodology and nomenclature. *Newsletters on stratigraphy*, 44(3), pp.173-245.

- Clemmensen, L.B., Olsen, H. and Blakey, R.C.**, 1989. Erg-margin deposits in the Lower Jurassic Moenave Formation and Wingate Sandstone, southern Utah. *Geological Society of America Bulletin*, 101(6), pp.759-773.
- Collinson, J.**, 2019. *Sedimentary structures*. Dunedin Academic Press Ltd.
- Collinson, J., Thompson, D.B. and Mountney, N.**, 2006. *Sedimentary Structures*. ed. *Harpenden: Terra Publishing*.
- Condon, S.M.**, 1997. *Geology of the Pennsylvanian and Permian cutler group and Permian Kaibab Limestone in the Paradox Basin, south-eastern Utah and southwestern Colorado* (No. 2000). US Government Printing Office.
- Copeland, P., Currie, C.A., Lawton, T.F. and Murphy, M.A.**, 2017. Location, location, location: The variable lifespan of the Laramide orogeny. *Geology*, 45(3), pp.223-226.
- Cornish, V.**, 1914, *Waves of Sand and Snow*, Fisher-Unwin, London, p. 383.
- Cornwall, C., Bourke, M.C., Jackson, D.W. and Cooper, J.A.G.**, 2018. Aeolian slipface dynamics and grainflow morphologies on Earth and Mars. *Icarus*, 314, pp.311-326.
- Cousins, D.P.**, 2020. *Sediment deposition and preservation in Aeolian Systems: A comparison of contemporary and ancient ergs* (Doctoral dissertation, Keele University).
- Crabaugh, M. and Kocurek, G.**, 1993. Entrada Sandstone: an example of a wet aeolian system. *Geological Society, London, Special Publications*, 72(1), pp.103-126.
- Cracknell, A.P.**, 2017. UAVs: regulations and law enforcement. *International Journal of Remote Sensing*, 38(8-10), pp.3054-3067.
- Craig, L.C., Holmes, C.N., Cadigan, R.A., Freeman, V.L., Mullens, T.E. and Weir, G.W.**, 1951. *Preliminary Report on the Stratigraphy of the Morrison and Related Formations of the Colorado Plateau Region* (Vol. 180). US Department of the Interior, Geological Survey.
- Cripps, A.C. and McCann, D.M.**, 2000. The use of the natural gamma log in engineering geological investigations. *Engineering Geology*, 55(4), pp.313-324.
- Crow, R.S., Howard, K.A., Beard, L.S., Pearthree, P.A., House, P.K., Karlstrom, K.E., Peters, L., McIntosh, W., Cassidy, C., Felger, T.J. and Block, D.**, 2019. Insights into post-Miocene uplift of the western margin of the Colorado Plateau from the stratigraphic record of the lower Colorado River. *Geosphere*, 15(6), pp.1826-1845.
- Danise, S., Price, G.D., Alberti, M. and Holland, S.M.**, 2020. Isotopic evidence for partial geochemical decoupling between a Jurassic epicontinental sea and the open ocean. *Gondwana Research*, 82, pp.97-107.
- Davies, S.L. and Elliot, T.**, 1994. The gamma-ray response of high resolution key surfaces and system tracts; examples from the Upper Carboniferous Clare Basin, western Ireland. In *High resolution sequence stratigraphy: innovations and applications: Abstract volume of the Liverpool sequence stratigraphy conference* (pp. 77-81).
- Davies, S. and Elliot, T.**, 1996. Spectral gamma-ray characteristics of high systems, County Clare, Ireland. *High-Resolution Sequence Stratigraphy: Innovations and Applications*. Geological Society, London, *Special Publications*, 104, pp.25-35.
- Dean, W.E.**, 1975. Shallow-water versus deep-water evaporites: Discussion. *AAPG Bulletin*, 59(3), pp.534-535.
- Dean, W.E., Davis, G.R., and Anderson, R.Y.**, 1975, Sedimentologic significance of nodular and laminated anhydrite: *Geology*, v. 3, p. 367-372.
- DeCelles, P.G. and Coogan, J.C.**, 2006. Regional structure and kinematic history of the Sevier fold-and-thrust belt, central Utah. *Geological Society of America Bulletin*, 118(7-8), pp.841-864.
- Desjardins, P.R., Buatois, L.A. and Mangano, M.G.**, 2012. Tidal flats and subtidal sand bodies. In *Developments in Sedimentology* (Vol. 64, pp. 529-561). Elsevier.

- Dickinson, W.R.** and **Gehrels, G.E.**, 2003. U–Pb ages of detrital zircons from Permian and Jurassic eolian sandstones of the Colorado Plateau, USA: paleogeographic implications. *Sedimentary Geology*, 163(1-2), pp.29-66.
- Dickinson, W.R.**, 2004. Evolution of the North American cordillera. *Annu. Rev. Earth Planet. Sci.*, 32, pp.13-45.
- Dickinson, W.R., Klute, M.A.** and **Swift, P.N.**, 1986. The Bisbee basin and its bearing on late Mesozoic paleogeographic and paleotectonic relations between the Cordilleran and Caribbean regions.
- Doelling, H.H.**, 2001. *Geologic map of the Moab and eastern part of the San Rafael Desert 30'x 60' quadrangles, Grand and Emery Counties, Utah, and Mesa County, Colorado*. Utah Geological Survey.
- Doelling, H.H.**, 2002. *Geologic map of the Moab and eastern part of the San Rafael Desert 30'x 60' quadrangles, Grand and Emery Counties, Utah, and Mesa County, Colorado*. Utah Geological Survey.
- Doelling, H.H., Sprinkel, D.A., Kowallis, B.J.** and **Kuehne, P.A.**, 2013. Temple Cap and Carmel Formations in the Henry Mountains Basin, Wayne and Garfield Counties, Utah. *The San Rafael Swell and Henry Mountains Basin-Geologic Centerpiece of Utah*. Utah Geological Association, pp.279-318.
- Duchaufour, P.**, 1982. Salsodic soils. In *Pedology* (pp. 426-442). Springer, Dordrecht.
- Duchaufour, R.**, 2012. *Pedology: pedogenesis and classification*. Springer Science & Business Media.
- Ducker, K., Yuan, H.** and **Zurek, B.**, 2001. Thick-structured Proterozoic lithosphere of the Rocky Mountain region. *Gsa Today*, 11(12), pp.4-9.
- Durán, O., Andreotti, B., Claudin, P.** 2011. On aeolian transport: grain-scale interactions, dynamical mechanisms and scaling laws. *Aeolian Reservoirs*, 3, pp. 243-270
- Duval, B.C., Cramez, C.** and **Vail, P.R.**, 1998. Stratigraphic cycles and major marine source rocks.
- Ehrenberg, S.N.** and **Svana, T.A.**, 2001. Use of spectral gamma-ray signature to interpret stratigraphic surfaces in carbonate strata: An example from the Finnmark carbonate platform (Carboniferous-Permian), Barents Sea. *AAPG Bulletin*, 85(2), pp.295-308.
- Ellwood, J.M., Evans, P.D.** and **Wilson, I.G.**, 1975. Small scale aeolian bedforms. *Journal of Sedimentary Research*, 45(2), pp.554-561.
- Eltner, A., Kaiser, A., Castillo, C., Rock, G., Neugirg, F.** and **Abellán, A.**, 2016. Image-based surface reconstruction in geomorphometry—merits, limits and developments. *Earth Surface Dynamics*, 4(2), pp.359-389.
- Embry, A.F.** and **Johannessen, E.P.**, 1993. T–R sequence stratigraphy, facies analysis and reservoir distribution in the uppermost Triassic–Lower Jurassic succession, western Sverdrup Basin, Arctic Canada. In *Norwegian Petroleum Society Special Publications* (Vol. 2, pp. 121-146). Elsevier.
- Embry, A.F.** and **Johannessen, E.P.**, 2017. Two approaches to sequence stratigraphy. In *Stratigraphy & Timescales* (Vol. 2, pp. 85-118). Academic Press.
- Embry, A.F.**, 1993. Triassic TR sequence analysis. *Sverdrup Basin, Canada Arctic archipelago: Canadian Society of Petroleum Geologists, Carboniferous to Jurassic Pangea, Program and Abstracts, Calgary, Alberta*, p.89.
- Embry, A.F.**, 1995. Sequence boundaries and sequence hierarchies: problems and proposals. In *Norwegian Petroleum Society Special Publications* (Vol. 5, pp. 1-11). Elsevier.
- Embry, A.F.**, 2002. Transgressive-regressive (TR) sequence stratigraphy. In *Gulf Coast SEPM Conference Proceedings, Houston* (pp. 151-172).
- Fan, D.**, 2012. Open-coast tidal flats. In *Principles of tidal sedimentology* (pp. 187-229). Springer, Dordrecht.

- Ferguson, J. and Skyring, G.W.**, 1995. Redbed-associated sabkhas and tidal flats at Shark Bay, Western Australia: Their significance for genetic models of stratiform Cu-(Pb-Zn) deposits. *Australian Journal of Earth Sciences*, 42(4), pp.321-333.
- Fertl, W.H., Chilingarian, G.V. and Yen, T.F.**, 1982. Use of natural gamma-ray spectral logging in evaluation of clay minerals. *Energy Sources*, 6(4), pp.335-360.
- Fillmore, R.**, 2010. *Geological evolution of the Colorado Plateau of Eastern Utah and Western Colorado, including the San Juan River, Natural Bridges, Canyonlands, Arches, and the Book Cliffs*. University of Utah Press.
- Flemming, B.W.**, 2011. 3.02 Geology, Morphology, and Sedimentology of Estuaries and Coasts. *Treatise on Estuarine and Coastal Science*. Academic Press, Waltham, pp.7-38.
- Foos, A.**, 1999. Geology of the Colorado Plateau. *Geology Field Trip Guides by Anabelle Foos, University of Akron*. Available online at: <http://www2.nature.nps.gov/geology/education>.
- Fossen, H.**, 2010. Deformation bands formed during soft-sediment deformation: observations from SE Utah. *Marine and Petroleum Geology*, 27(1), pp.215-222.
- Frahme, C.W. and Vaughn, E.B.**, 1983. Paleozoic Geology and Seismic Stratigraphy of the Northern Uncompahgre Front, Grand County, Utah.
- Frakes, L. and Bolton, B.R.**, 1992. Effects of ocean chemistry, sea level, and climate on the formation of primary sedimentary manganese ore deposits. *Economic Geology*, 87(5), pp.1207-1217.
- Frazier, D.E.**, 1974. Depositional-episodes: their relationship to the Quaternary stratigraphic framework in the northwestern portion of the Gulf Basin. *Virtual Landscapes of Texas*.
- Freeman, W.E. and Visher, GS**, 1975. Stratigraphic analysis of the Navajo Sandstone. *Journal of Sedimentary Research*, 45(3), pp.651-668.
- Fryberger, S.G. and Schenk, C.J.**, 1988. Pinstripe lamination: a distinctive feature of modern and ancient eolian sediments. *Sedimentary Geology*, 55(1-2), pp.1-15.
- Galloway, W.E.**, 1989. Genetic stratigraphic sequences in basin analysis I: architecture and genesis of flooding-surface bounded depositional units. *AAPG Bulletin*, 73(2), pp.125-142.
- Galloway, W.E. and Hobday, D.K.**, 1996. Eolian systems. In *Terrigenous Clastic Depositional Systems* (pp. 250-269). Springer, Berlin, Heidelberg.
- George, G.T. and Berry, J.K.**, 1993. A new lithostratigraphy and depositional model for the Upper Rotliegend of the UK Sector of the Southern North Sea. *Geological Society, London, Special Publications*, 73(1), pp.291-319.
- George, G.T. and Berry, J.K.**, 1994. A new palaeogeographic and depositional model of the upper Rotliegend, offshore The Netherlands. *First Break*, 12(3).
- Gilluly, J. and Reeside Jr, JB**, 1928. *Sedimentary rocks of the San Rafael Swell and some adjacent areas in eastern Utah* (No. 150-D).
- Ginau, A., Engel, M. and Brückner, H.**, 2012. Holocene chemical precipitates in the continental sabkha of Tayma (NW Saudi Arabia). *Journal of Arid Environments*, 84, pp.26-37.
- Gould, K.M., Piper, D.J., Pe-Piper, G. and MacRae, R.A.**, 2014. Facies, provenance and paleoclimate interpretation using spectral gamma logs: Application to the Lower Cretaceous of the Scotian Basin. *Marine and Petroleum Geology*, 57, pp.445-454.
- Gustavson, T.C., Hovorka, S.D. and Dutton, A.R.**, 1994. Origin of satin spar veins in evaporite basins. *Journal of Sedimentary Research*, 64(1a), pp.88-94.
- Gustavson, T.C., Hovorka, S.D. and Dutton, A.R.**, 1994. Origin of satin spar veins in evaporite basins. *Journal of Sedimentary Research*, 64(1a), pp.88-94.
- Hallam, A.**, 1992. *Phanerozoic sea-level changes*. Columbia University Press.

- Hallam, A.**, 1993. Jurassic climates as inferred from the sedimentary and fossil record. *Philosophical Transactions of the Royal Society of London. Series B: Biological Sciences*, 341(1297), pp.287-296.
- Hallam, A.**, 2001. A review of the broad pattern of Jurassic sea-level changes and their possible causes in the light of current knowledge. *Palaeogeography, Palaeoclimatology, Palaeoecology*, 167(1-2), pp.23-37.
- Hampson, G.J., Davies, W., Davies, S.J., Howell, J.A. and Adamson, K.R.**, 2005. Use of spectral gamma-ray data to refine subsurface fluvial stratigraphy: Late Cretaceous strata in the Book Cliffs, Utah, USA. *Journal of the Geological Society*, 162(4), pp.603-621.
- Handford, C.R.**, 1981. Coastal sabkha and salt pan deposition of the lower Clear Fork Formation (Permian), Texas. *Journal of Sedimentary Research*, 51(3), pp.761-778.
- Handford, C.R.**, 1991. Chapter 1 Marginal Marine Halite: Sabkhas and Salinas. In *Developments in sedimentology* (Vol. 50, pp. 1-66). Elsevier.
- Haq, B.U.**, 2018. Jurassic sea-level variations: a reappraisal. *Gsa Today*, 28(1), pp.4-10.
- Haq, B.U., Hardenbol, J.A.N. and Vail, P.R.**, 1987. Chronology of fluctuating sea levels since the Triassic. *Science*, 235(4793), pp.1156-1167.
- Hassan, M.S., Venetikidis, A., Bryant, G. and Miall, AD**, 2018. The Sedimentology of an ERG Margin: The Kayenta–Navajo Transition (Lower Jurassic), Kanab, Utah, USA. *Journal of Sedimentary Research*, 88(5), pp.613-640.
- Havholm, K.G., Blakey, R.C., Capps, M., Jones, L.S., King, D.D. and Kocurek, G.**, 1993. Aeolian genetic stratigraphy: an example from the Middle Jurassic Page sandstone, Colorado Plateau. *Aeolian Sediments: Ancient and Modern*, pp.85-107.
- Havholm, K.G. and Kocurek, G.**, 1994. Factors controlling aeolian sequence stratigraphy: clues from super bounding surface features in the Middle Jurassic Page Sandstone. *Sedimentology*, 41(5), pp.913-934.
- Helland-Hansen, W. and Gjelberg, J.G.**, 1994. Conceptual basis and variability in sequence stratigraphy: a different perspective. *Sedimentary Geology*, 92(1-2), pp.31-52.
- Hesselbo, S.P. and Parkinson, D.N.**, 1996. Sequence stratigraphy in British geology. *Geological Society, London, Special Publications*, 103(1), pp.1-7.
- Hettinger, R.D. and Kirschbaum, M.A.**, 2002. Stratigraphy of the Upper Cretaceous Mancos Shale (upper part) and Mesaverde Group in the southern part of the Uinta and Piceance basins, Utah, and Colorado.
- Hintze, L.F. and Kowallis, BJ**, 2009. *Geologic history of Utah: Brigham Young University Geology Studies Special Publication 9* (p. 225). Tech. rept. Brigham Young University, Salt Lake City, UT.
- Hooshyari-Far, I., Kepic, A. and Podolska, A.**, 2015. A new approach provides opportunities for spectral gamma analysis in boreholes for mineral exploration. *ASEG Extended Abstracts*, 2015(1), pp.1-4.
- Howell, J. and Mountney, N.**, 1997. Climatic cyclicity and accommodation space in arid to semi-arid depositional systems: an example from the Rotliegend Group of the UK southern North Sea. *Geological Society, London, Special Publications*, 123(1), pp.63-86.
- Hugenholtz, C.H., Levin, N., Barchyn, T.E. and Baddock, M.C.**, 2012. Remote sensing and spatial analysis of aeolian sand dunes: A review and outlook. *Earth-science reviews*, 111(3-4), pp.319-334.
- Hunt, D. and Tucker, M.E.**, 1992. Stranded parasequences and the forced regressive wedge systems tract: deposition during base-level fall. *Sedimentary Geology*, 81(1-2), pp.1-9.
- Hunter, R.E.**, 1977. Basic types of stratification in small eolian dunes. *Sedimentology*, 24(3), pp.361-387.
- Hurst, A. and Milodowski, A.**, 1996. Thorium distribution in some North Sea sandstones; implications for petrophysical evaluation. *Petroleum Geoscience*, 2(1), pp.59-68.

- Hurst, A.**, 1990. Natural gamma-ray spectrometry in hydrocarbon-bearing sandstones from the Norwegian Continental Shelf. *Geological Society, London, Special Publications*, 48(1), pp.211-222.
- Jahnert, R.J. and Collins, L.B.**, 2013. Controls on microbial activity and tidal flat evolution in Shark Bay, Western Australia. *Sedimentology*, 60(4), pp.1071-1099.
- Jefferson, C.W., Thomas, D.J., Gandhi, S.S., Ramaekers, P., Delaney, G., Brisbin, D., Cutts, C., Portella, P. and Olson, R.A.**, 2007. Unconformity-associated uranium deposits of the Athabasca Basin, Saskatchewan and Alberta. *Bulletin-geological survey of Canada*, 588, p.23.
- Johnson, D.W.**, 1916. Plains, Planes, and Peneplanes. *Geographical Review*, 1(6), pp.443-447.
- Jordan, B.R.**, 2015. A bird's-eye view of geology: The use of micro drones/UAVs in geologic fieldwork and education. *GSA today*, 25(7), pp.50-52.
- Keeton, G.I.**, 2012. *Sedimentological and stratigraphic characteristics of fluvial sandstones based on outcrop spectral-gamma-ray data and borehole images, Williams Fork Formation, Piceance Basin, Colorado* (Doctoral dissertation, University of Colorado at Boulder).
- Kenny, R.**, 2010. Continental paleoclimate estimates from the late Mississippian Redwall karst event: northern and north-central Arizona (USA). *Carbonates and Evaporites*, 25(4), pp.297-302.
- Kirby, R.**, 2000. Practical implications of tidal flat shape. *Continental Shelf Research*, 20(10-11), pp.1061-1077.
- Kirkham, A. and Evans, G.**, 2019. Aspects of the Abu Dhabi Sabkha. In *Sabkha ecosystems* (pp. 15-40). Springer, Cham.
- Klaja, J. and Dudek, L.**, 2016. Geological interpretation of spectral gamma ray (SGR) logging in selected boreholes. *Nafta-Gaz*, 72(1), pp.3-14.
- Kocurek, G. and Dott Jr, R.H.**, 1983. Jurassic paleogeography and paleoclimate of the central and southern Rocky Mountains region. Rocky Mountain Section (SEPM).
- Kocurek, G. and Dott, R.H.**, 1981. Distinctions and uses of stratification types in the interpretation of eolian sand. *Journal of Sedimentary Research*, 51(2), pp.579-595.
- Kocurek, G. and Havholm, K.G.**, 1993. Eolian Sequence Stratigraphy--A Conceptual Framework: Chapter 16: Recent Developments in Siliciclastic Sequence Stratigraphy.
- Kocurek, G. and Lancaster, N.**, 1999. Aeolian system sediment state: theory and Mojave Desert Kelso dune field example. *Sedimentology*, 46(3), pp.505-515.
- Kocurek, G. and Nielson, J.**, 1986. Conditions favourable for the formation of warm-climate aeolian sand sheets. *Sedimentology*, 33(6), pp.795-816.
- Kocurek, G.**, 1984. Origin of first-order bounding surfaces in aeolian sandstones. *Sedimentology*, 31(1), pp.125-128.
- Kocurek, G.**, 1988. First-order and super bounding surfaces in eolian sequences—bounding surfaces revisited. *Sedimentary Geology*, 56(1-4), pp.193-206.
- Kocurek, G.**, 1991. Interpretation of ancient eolian sand dunes. *Annual Review of Earth and planetary sciences*, 19(1), pp.43-75.
- Kocurek, G.**, 1999. The aeolian rock record (Yes, Virginia, it exists but it really is rather special to create one). In: *Aeolian Environments Sediments and Landforms* (Eds A.S. Goudie, I. Livingstone, and Stokes), pp. 239-259. John Wiley and Sons Ltd, Chichester
- Kok, J.F., Parteli, E.J., Michaels, T.I. and Karam, D.B.**, 2012. The physics of wind-blown sand and dust. *Reports on Progress in Physics*, 75(10), p.106901.
- Kowallis, B.J., Christiansen, E.H., Deino, A.L., Peterson, F., Turner, C.E., Kunk, M.J., and Obradovich, J.D.**, 1998, The age of the Morrison Formation: *Modern Geology*, v. 22, nos. 1-4, p. 235-260.

- Kraus, M.J.**, 1999. Paleosols in clastic sedimentary rocks: their geologic applications. *Earth-Science Reviews*, 47(1-2), pp.41-70.
- Kreisa, R.D. and Moila, R.J.**, 1986. Sigmoidal tidal bundles and other tide-generated sedimentary structures of the Curtis Formation, Utah. *Geological Society of America Bulletin*, 97(4), pp.381-387.
- Kull, L.A. and Ginaven, R.O.**, 1974. *Guidelines for gamma-ray spectroscopy measurements of 235U enrichment* (Vol. 50414). Brookhaven National Laboratory.
- Kumar, B. and Kishore, M.**, 2006. Electrofacies classification—a critical approach. In *6th international conference and exposition on petroleum geophysics, Kolkata, India* (pp. 822-825).
- Leeder, M.**, 2011. Sedimentology and sedimentary basins: from turbulence to tectonics.
- Logan, B.W. and Cebulski, D.E.**, 1970. Sedimentary environments of Shark Bay, Western Australia.
- Logan, B.W.**, 1974. Inventory of diagenesis in Holocene-recent carbonate sediments, Shark Bay, Western Australia.
- Lokier, S.W.**, 2012. Development and evolution of subaerial halite crust morphologies in a coastal sabkha setting. *Journal of arid environments*, 79, pp.32-47.
- Loope, D.B.**, 1985. Episodic deposition and preservation of eolian sands: A late Paleozoic example from south-eastern Utah. *Geology*, 13(1), pp.73-76.
- Loope, D.B.**, 1988. Rhizoliths in ancient eolianites. *Sedimentary Geology*, 56(1-4), pp.301-314.
- Løvborg, L. and Mose, E.**, 1987. Counting statistics in radioelement assaying with a portable spectrometer. *Geophysics*, 52(4), pp.555-563.
- Lucas, S.G.**, 2014. Lithostratigraphy of the Jurassic San Rafael Group from Bluff to the Abajo Mountains, south-eastern Utah: Stratigraphic relationships of the Bluff Sandstone. *Volumina Jurassica*, 12(2), pp.55-68.
- Luttrell, P.R.**, 1993. Basinwide sedimentation and the continuum of paleoflow in an ancient river system: Kayenta Formation (Lower Jurassic), central portion Colorado Plateau. *Sedimentary Geology*, 85(1-4), pp.411-434.
- Mack, G.H., James, W.C. and Monger, H.C.**, 1993. Classification of paleosols. *Geological Society of America Bulletin*, 105(2), pp.129-136.
- Marshak, S., Domrois, S., Abert, C., Larson, T., Pavlis, G., Hamburger, M., Yang, X., Gilbert, H. and Chen, C.**, 2017. The basement revealed: tectonic insight from a digital elevation model of the Great Unconformity, USA cratonic platform. *Geology*, 45(5), pp.391-394.
- Martinius, A.W., Geel, CR and Arribas, J.**, 2002. Lithofacies characterisation of fluvial sandstones from outcrop gamma-ray logs (Loranca Basin, Spain): the influence of provenance. *Petroleum Geoscience*, 8(1), pp.51-62.
- Massare, J.A., Wahl, W.R., Ross, M. and Connely, M.V.**, 2014. Palaeoecology of the marine reptiles of the Redwater Shale Member of the Sundance Formation (Jurassic) of central Wyoming, USA. *Geological Magazine*, 151(1), pp.167-182.
- McDonald, R.R. and Anderson, R.S.**, 1996. Constraints on eolian grain flow dynamics through laboratory experiments on sand slopes. *Journal of Sedimentary Research*, 66(3), pp.642-653.
- McKee, E.D. and Bigarella, J.J.**, 1979. Sedimentary structures in dunes. *Geological Survey Professional Paper*, 1015, pp.87-134.
- McKee, E.D. and Weir, G.W.**, 1953. Terminology for stratification and cross-stratification in sedimentary rocks. *Geological Society of America Bulletin*, 64(4), pp.381-390.
- McKee, E.D.**, 1979. Introduction to a study of global sand seas. In *A study of global sand seas* (Vol. 1052, pp. 1-19). Professional Paper.
- Miall, A.D.**, 2010. *The geology of stratigraphic sequences*. Springer Science & Business Media.
- Miall, AD**, 1997. *The Geology of Stratigraphic Sequences*. Springer-Verlag, pp. 433

- Mitchum Jr, RM**, 1977. Seismic stratigraphy and global changes of sea level: Part 11. Glossary of terms used in seismic stratigraphy: Section 2. Application of seismic reflection configuration to stratigraphic interpretation.
- Mitchum Jr, RM**, 1977. Seismic stratigraphy and global changes of sea level, Part 6: Stratigraphic interpretation of seismic refraction patterns in depositional sequences. *Seismic stratigraphy-applications to hydrocarbon exploration*, 26, pp.117-133.
- Mountney, N., Howell, J., Flint, S. and Jerram, D.**, 1999. Climate, sediment supply and tectonics as controls on the deposition and preservation of the aeolian-fluvial Etjo Sandstone Formation, Namibia. *Journal of the Geological Society*, 156(4), pp.771-777.
- Mountney, N.P. and Thompson, D.B.**, 2002. Stratigraphic evolution and preservation of aeolian dune and damp/wet interdune strata: an example from the Triassic Helsby Sandstone Formation, Cheshire Basin, UK. *Sedimentology*, 49(4), pp.805-833.
- Mountney, N.P.**, 2012. A stratigraphic model to account for complexity in aeolian dune and interdune successions. *Sedimentology*, 59(3), pp.964-989.
- Nelson, M.E. and Crooks, D.M.**, 1987. Stratigraphy and palaeontology of the Cedar Mountain Formation (Lower Cretaceous), eastern Emery County, Utah.
- Nettleton, W.D., Olson, C.G. and Wysocki, D.A.**, 2000. Paleosol classification: problems and solutions. *Catena*, 41(1-3), pp.61-92.
- Nichols, G.**, 2009. *Sedimentology and stratigraphy*. John Wiley & Sons.
- Nicklning, W.G., Neuman, C.M. and Lancaster, N.**, 2002. Grainfall processes in the lee of transverse dunes, Silver Peak, Nevada. *Sedimentology*, 49(1), pp.191-209.
- Nobre, J.A., Freire, A.F.M., Neto, A.A., dos Santos Martins, M., Silva, C.G. and Vieira, R.**, 2020. Quaternary warming and cooling trends in the Bransfield Basin, Antarctic Peninsula, based on gamma-ray spectrometry. *Geo-Marine Letters*, pp.1-8.
- North, C.P. and Boering, M.**, 1999. Spectral gamma-ray logging for facies discrimination in mixed fluvial-eolian successions: a cautionary tale. *AAPG bulletin*, 83(1), pp.155-169.
- Ohlen, HR and McIntyre, L.B.**, 1965. Stratigraphy and tectonic features of Paradox Basin, Four Corners area. *AAPG Bulletin*, 49(11), pp.2020-2040.
- Olig, S.S., Fenton, C.H., McCleary, J. and Wong, I.G.**, 1996. The earthquake potential of the Moab fault and its relation to salt tectonics in the Paradox Basin, Utah.
- Peterson, F.**, 1988. Pennsylvanian to Jurassic eolian transportation systems in the western United States. *Sedimentary Geology*, 56(1-4), pp.207-260.
- Peterson, F.**, 1988. Stratigraphy and nomenclature of middle and upper Jurassic rocks, Western Colorado Plateau, Utah and Arizona. *US Geological Survey, Bulletin*, pp.13-56.
- Peterson, F.**, 1994. Sand dunes, sabkhas, streams, and shallow seas: Jurassic palaeogeography in the southern part of the Western Interior Basin. Rocky Mountain Section (SEPM).
- Pettigrew, R., Priddy, C., Clarke, S.M. and Richards, P.**, 2019. The Cyclic Preservation of Clastic and Evaporitic Sabkha Sediments: Insights from the Cedar Mesa Sandstone Formation of the Cutler Group, Utah, USA.
- Picard, M.D.**, 1977. Stratigraphic Analysis of the Navajo Sandstone: DISCUSSION. *Journal of Sedimentary Research*, 47(1).
- Plint, A.G. and Nummedal, D.**, 2000. The falling stage systems tract: recognition and importance in sequence stratigraphic analysis. *Geological Society, London, Special Publications*, 172(1), pp.1-17.
- Posamentier, H.W. and Allen, G.P.**, 1999. *Siliciclastic sequence stratigraphy: concepts and applications* (Vol. 7, p. 210). Tulsa, Oklahoma: SEPM (Society for Sedimentary Geology).
- Posamentier, H.W., Jervey, M.T. and Vail, P.R.**, 1988. Eustatic controls on clastic deposition I—conceptual framework.

- Potter P. E.**, 1959, Facies Model Conference: Science, v. 129, p. 1292-1294
- Prade, K., Hagelgans, V. and Schwieger, T.**, 1991. Heavy metal accumulation in the plinthic horizon of a ferric gleysol. *Zeitschrift für Pflanzenernährung und Bodenkunde*, 154(3), pp.227-232.
- Priddy, C.L. and Clarke, S.M.**, 2020. The sedimentology of an ephemeral fluvial–aeolian succession. *Sedimentology*.
- Priddy, C.L., Pringle, J.K., Clarke, S.M. and Pettigrew, R.P.**, 2019. Application of photogrammetry to generate quantitative geobody data in ephemeral fluvial systems. *The Photogrammetric Record*, 34(168), pp.428-444.
- Purvis, K.**, 1991. Stoss-side mud-drapes: deposits of interdune pond margins. *Sedimentology*, 38(1), pp.153-156.
- Pye, K.**, 1993. Late Quaternary development of coastal parabolic megadune complexes in northeastern Australia. In *Aeolian Sediments. Ancient and Modern* (Vol. 16, pp. 23-44). Blackwell Scientific Publications.
- Queney, P.**, 1945, Observations sur les rides formées par le vent à la surface du sable dans les ergs sahariens: *Ann. Geophys.*, v. 1, p. 5--8.
- Raup, O.B. and Hite, R.J.**, 1992. *Lithology of evaporite cycles and cycle boundaries in the upper part of the Paradox Formation of the Hermosa Group of Pennsylvanian age in the Paradox Basin, Utah and Colorado* (No. 2000). US Department of the Interior, US Geological Survey.
- Reineck, H.E. and Singh, I.B.**, 1980. Depositional environments. In *Depositional Sedimentary Environments* (pp. 5-7). Springer, Berlin, Heidelberg.
- Reineck, H.E. and Singh, I.B.**, 1980. Tidal flats. In *Depositional sedimentary environments* (pp. 430-456). Springer, Berlin, Heidelberg.
- Remondino, F., Barazzetti, L., Nex, F., Scaioni, M. and Sarazzi, D.**, 2011. UAV photogrammetry for mapping and 3d modeling—current status and future perspectives. *International archives of the photogrammetry, remote sensing and spatial information sciences*, 38(1), p.C22.
- Rider, MH**, 1990. Gamma-ray log shape used as a facies indicator: critical analysis of an oversimplified methodology (Eds. A. Hurst, M.A., Lovell., A.C., Morton). Geological Society Special Publication No. 48: geological applications of wireline logs, The Geological Society, London, pp. 27-37
- Rider, MH**, 1996. The geological interpretation of well logs. Whittles Publishing, pp.288.
- Ritter, G.W.**, 2018. Lithofacies and Sequence Architecture of the Upper Paradox Formation (Middle Pennsylvanian) in the Subsurface Northern Blanding Subbasin, Paradox Basin, Utah.
- Rodríguez-López, J.P., Clemmensen, L.B., Lancaster, N., Mountney, N.P. and Veiga, G.D.**, 2014. Archean to Recent aeolian sand systems and their sedimentary record: current understanding and future prospects. *Sedimentology*, 61(6), pp.1487-1534.
- Romain, H.G.**, 2014. *Controls on aeolian bed-set architecture and implications for reservoir heterogeneity* (Doctoral dissertation, University of Leeds).
- Romain, H.G. and Mountney, N.P.**, 2014. Reconstruction of three-dimensional eolian dune architecture from one-dimensional core data through adoption of analog data from outcrop. *AAPG Bulletin*, 98(1), pp.1-22.
- Rubin, D.M. and Hunter, R.E.**, 1982. Bedform climbing in theory and nature. *Sedimentology*, 29(1), pp.121-138.
- Ruffell, A. and Worden, R.**, 2000. Palaeoclimate analysis using spectral gamma-ray data from the Aptian (Cretaceous) of southern England and southern France. *Palaeogeography, Palaeoclimatology, Palaeoecology*, 155(3-4), pp.265-283.
- Ruffell, A.H., Worden, R.H. and Evans, R.**, 1999. Palaeoclimate Controls on Spectral Gamma-Ray Radiation from Sandstones. *Clay Mineral Cements in Sandstones*, pp.93-108.

- Sansom, P.J.**, 1992. *Sedimentology of the Navajo Sandstone, Southern Utah, USA* (Doctoral dissertation, University of Oxford).
- Schnyder, J., Ruffell, A., Deconinck, J.F. and Baudin, F.**, 2006. Conjunctive use of spectral gamma-ray logs and clay mineralogy in defining late Jurassic–early Cretaceous palaeoclimate change (Dorset, UK). *Palaeogeography, Palaeoclimatology, Palaeoecology*, 229(4), pp.303-320.
- Scholle, P.A., Bebout, D.G. and Moore, C.H.** eds., 1983. *Carbonate depositional environments: AAPG Memoir 33* (No. 33). AAPG.
- Schweickert, R.A., Bogen, N.L., Girty, G.H., Hanson, R.E. and Merguerian, C.**, 1984. Timing and structural expression of the Nevadan orogeny, Sierra Nevada, California. *Geological Society of America Bulletin*, 95(8), pp.967-979.
- Seppälä, M. and Lindé, K.**, 1978. Wind tunnel studies of ripple formation. *Geografiska Annaler: Series A, Physical Geography*, 60(1-2), pp.29-42.
- Serra, O., Baldwin, J., and Quirein, J.**, 1980. Theory, Interpretation, And Practical Applications Of Natural Gamma-Ray Spectroscopy. In *SPWLA 21st Annual Logging Symposium*. Society of Petrophysicists and Well-Log Analysts
- Serra, O. and Abbot, H. T.**, 1980. The contribution of logging data to sedimentology and stratigraphic, SPE 9270, 55th Annual Fall Technical Conference and Exhibition, Dallas, Texas, 19p
- Serra, O. and Sulpice, L.**, 1975, January. Sedimentological analysis of shale-sand series from well logs. In *SPWLA 16th Annual Logging Symposium*. Society of Petrophysicists and Well-Log Analysts.
- Shanley, K.W. and McCabe, P.J.**, 1994. Perspectives on the sequence stratigraphy of continental strata. *AAPG Bulletin*, 78(4), pp.544-568.
- Shao, Y.**, 2008. *Physics and modelling of wind erosion* (Vol. 37). Springer Science & Business Media.
- Sharpe, R. P.**, 1963, Wind Ripples: *Jour. Geology*, v. 71, p. 617---636
- Sierro, F.J., Ledesma, S., Flores, J.A., Torrecusa, S. and del Olmo, W.M.**, 2000. Sonic and gamma-ray astrochronology: Cycle to cycle calibration of Atlantic climatic records to Mediterranean sapropels and astronomical oscillations. *Geology*, 28(8), pp.695-698.
- Sleveland, A.R.N.**, 2016. *The sedimentology and sequence stratigraphy of the Curtis Formation along the eastern San Rafael Swell, Utah* (Master's thesis).
- Sloss, L.L.**, 1963. Sequences in the cratonic interior of North America. *Geological Society of America Bulletin*, 74(2), pp.93-114.
- Solazzo, D., Sankey, J.B., Sankey, T.T. and Munson, S.M.**, 2018. Mapping and measuring aeolian sand dunes with photogrammetry and LiDAR from unmanned aerial vehicles (UAV) and multispectral satellite imagery on the Paria Plateau, AZ, USA. *Geomorphology*, 319, pp.174-185.
- Spencer, C.J., Cawood, P.A., Hawkesworth, C.J., Prave, A.R., Roberts, N.M., Horstwood, M.S. and Whitehouse, M.J.**, 2015. Generation and preservation of continental crust in the Grenville Orogeny. *Geoscience Frontiers*, 6(3), pp.357-372.
- Sprinkel, D.A., Doelling, H.H., Kowallis, B.J., Waanders, G., Kuehne, P.A., Yonkee, W.A. and Chidsey, T.C.**, 2011. Early results of a study of Middle Jurassic strata in the Sevier fold and thrust belt, Utah. *Sevier Thrust Belt: Northern and Central Utah and Adjacent Areas: Utah Geological Association, Publication*, 40, pp.151-172.
- Sprinkel, D.A., Kowallis, B.J. and Jensen, P.H.**, 2011. Correlation and age of the Nugget Sandstone and Glen Canyon Group, Utah. *Utah Geological Association Publication*, 40, pp.131-149.
- Stewart, J.H., Anderson, T.H., Haxel, G.B., Silver, L.T. and Wright, J.E.**, 1986. Late Triassic palaeogeography of the southern Cordillera: The problem of a source for voluminous volcanic detritus in the Chinle Formation of the Colorado Plateau region. *Geology*, 14(7), pp.567-570.

- Stewart, J.H., Poole, F.G., and Wilson J.F.**, 1972. Stratigraphy and origin of the Chinle Formation and related Upper Triassic strata in the Colorado Plateau region: US Geological Survey, Professional Paper 690, 336 p.
- Stokes, W.L.**, 1976. What is the Wasatch Line?
- Stride, A.H.**, 1982. Ancient offshore tidal deposits. In *Offshore tidal sands* (pp. 172-192). Springer, Dordrecht.
- Svendsen, J.B. and Hartley, N.R.**, 2001. Comparison between outcrop-spectral gamma-ray logging and whole-rock geochemistry: implications for quantitative reservoir characterisation in continental sequences. *Marine and Petroleum Geology*, 18(6), pp.657-670.
- Sweet, M.L., Nielson, J., Havholm, K. and Farrelley, J.**, 1988. Algodones dune field of southeastern California: case history of a migrating modern dune field. *Sedimentology*, 35(6), pp.939-952.
- Sztano, O. and de Boer, P.L.**, 1995. Basin dimensions and morphology as controls on amplification of tidal motions (the Early Miocene North Hungarian Bay). *Sedimentology*, 42(4), pp.665-682.
- Tanner, L.H. and Lucas, S.G.**, 2007. The Moenave Formation: Sedimentologic and stratigraphic context of the Triassic–Jurassic boundary in the Four Corners area, southwestern USA. *Palaeogeography, Palaeoclimatology, Palaeoecology*, 244(1-4), pp.111-125.
- Talbot, M.R.**, 1985. Major bounding surfaces in aeolian sandstones--a climatic model. *Sedimentology*, 32: 257-265.
- Thompson, A.E. and Stokes, W.L.**, 1970. *Stratigraphy of the San Rafael Group, southwest and south-central Utah*. Utah Geological and Mineralogical Survey.
- Thorman, C.H. and Peterson, F.**, 2003, May. The Middle Jurassic Elko Orogeny: A major tectonic event in Nevada-Utah. In *Annual Meeting Expanded Abstracts* (Vol. 12, pp. 169-174). Tulsa, Okla.: Am. Assoc. of Pet. Geol.
- Tobisch, O.T., Paterson, S.R., Longiaru, S. and Bhattacharyya, T.**, 1987. Extent of the Nevadan orogeny, central Sierra Nevada, California. *Geology*, 15(2), pp.132-135.
- Tobisch, O.T., Saleeby, J.B., Renne, P.R., McNulty, B. and Tong, W.**, 1995. Variations in deformation fields during development of a large-volume magmatic arc, central Sierra Nevada, California. *Geological Society of America Bulletin*, 107(2), pp.148-166.
- Trudgill, B.D.**, 2011. Evolution of salt structures in the northern Paradox Basin: Controls on evaporite deposition, salt wall growth and supra-salt stratigraphic architecture. *Basin Research*, 23(2), pp.208-238.
- Uysal, M., Toprak, A.S. and Polat, N.**, 2015. DEM generation with UAV Photogrammetry and accuracy analysis in Sahitler hill. *Measurement*, 73, pp.539-543.
- Vail, P.R.**, 1987. Seismic stratigraphy interpretation using sequence stratigraphy: Part 1: Seismic stratigraphy interpretation procedure.
- Valenza, J.M.**, 2016. Redbeds of the Upper Entrada Sandstone, Central Utah: Facies Analysis and Regional Implications of Interfingered Sabkha and Fluvial Terminal Splay Sediments.
- Van Wagoner, J.C., Mitchum, R.M., Campion, K.M. and Rahmanian, V.D.**, 1990. Siliciclastic sequence stratigraphy in well logs, cores, and outcrops: concepts for high-resolution correlation of time and facies.
- Van Wagoner, J.C., Posamentier, H.W., Mitchum, R.M.J., Vail, P.R., Sarg, J.F., Loutit, T.S. and Hardenbol, J.**, 1988. An overview of the fundamentals of sequence stratigraphy and key definitions.
- Verlander, J.E.**, 1995. The Navajo Sandstone. *Geology Today*, 11(4), pp.143-146.
- Wakefield, O.J.W.**, 2010. *Aeolian, fluvial and shallow marine sedimentary system interactions in the Permian Cutler Group, southeast Utah, USA* (Doctoral dissertation, Keele University).

- Wang, C., Mitchell, R.N., Murphy, J.B., Peng, P. and Spencer, C.J.**, 2021. The role of megacontinents in the supercontinent cycle. *Geology*, 49(4), pp.402-406.
- Warren, J.K.**, 1991. Sulfate Dominated Sea-Marginal and Platform Evaporative Settings:: Sabkhas and Salinas, Mudflats and Salterns. In *Developments in Sedimentology* (Vol. 50, pp. 69-187). Elsevier.
- Warren, J.K.**, 2016. Sabkhas, saline mudflats and pans. In *Evaporites* (pp. 207-301). Springer, Cham.
- Wasson, R.J. and Hyde, R.**, 1983. Factors determining desert dune type. *Nature*, 304(5924), pp.337-339.
- Weimer, R.J. and Tillman, R.W.**, 1982, January. Sandstone reservoirs. In *International Petroleum Exhibition and Technical Symposium*. Society of Petroleum Engineers.
- Wentworth, C.K.**, 1922. A scale of grade and class terms for clastic sediments. *The journal of geology*, 30(5), pp.377-392.
- Wiggs, G.**, 2019. Desert Dunes: Form and Process. *Aeolian Geomorphology: A New Introduction*, pp.133-155.
- Wilcox, W. T., & Currie, B.** (2008). Sequence Stratigraphy of the Jurassic Curtis, Summerville, and Stump Formations, Eastern Utah and Northwest Colorado. In M. W. Longman & C. D. Morgan (Eds.), *Hydrocarbon systems and production in the Uinta Basin, Utah*. Rocky Mountain Association of Geologists and Utah Geological Association Publication, 37, 9– 41.
- Wilson, I.G.**, 1971. Desert sandflow basins and a model for the development of ergs. *Geographical Journal*, pp.180-199.
- Wilson, I.G.**, 1972. Aeolian bedforms-their development and origins. *Sedimentology*, 19, 173-210
- Wilson, M.A., Shahid, S.A., Abdelfattah, M.A., Kelley, J.A., Thomas, J.E.**, 2013. Anhydrite formation on the coastal sabkha of Abu Dhabi, United Arab Emirates. In: *Developments in soil classification, land use planning and policy implications*, pp. 175-2012. Springer, Dordrecht.
- Wright, J.C., Shawe, DR and Lohman, S.W.**, 1962. Definition of members of Jurassic Entrada Sandstone in east-central Utah and west-central Colorado. *AAPG Bulletin*, 46(11), pp.2057-2070.
- Yaalon, D.H.**, 1971. Criteria for the recognition and classification of Paleosols. In *Paleopedology* (pp. 153-158). Israel University Press Jerusalem.
- Yonkee, W.A. and Weil, A.B.**, 2015. Tectonic evolution of the Sevier and Laramide belts within the North American Cordillera orogenic system. *Earth-Science Reviews*, 150, pp.531-593.
- Zuchuat, V., Midtkandal, I., Poyatos-Moré, M., Da Costa, S., Brooks, H.L., Halvorsen, K., Cote, N., Sundal, A. and Braathen, A.**, 2019. Composite and diachronous stratigraphic surfaces in low-gradient, transitional settings: The J-3 “unconformity” and the Curtis Formation, east-central Utah, USA. *Journal of Sedimentary Research*, 89(11), pp.1075-1095.
- Zuchuat, V., Sleveland, A.R., Pettigrew, R.P., Dodd, T.J., Clarke, S.M., Rabbel, O., Braathen, A. and Midtkandal, I.**, 2019. Overprinted allocyclic processes by tidal resonance in an epicontinental basin: The Upper Jurassic Curtis Formation, east-central Utah, USA. *The Depositional Record*
- Zuchuat, V., Sleveland, A.R., Sprinkel, D.A., Rimkus, A., Braathen, A. and Midtkandal, I.**, 2018. New insights on the impact of tidal currents on a low-gradient, semi-enclosed, epicontinental basin—the Curtis Formation, east-central Utah, USA. *Geology of the Intermountain West*, 5, pp.131-165